

**LATE CRETACEOUS  
SEDIMENTATION AND TECTONICS  
OF THE SALINIAN TERRANE,  
WEST-CENTRAL CALIFORNIA**

**A DISSERTATION  
SUBMITTED TO THE DEPARTMENT OF GEOLOGY  
AND THE COMMITTEE ON GRADUATE STUDIES  
OF STANFORD UNIVERSITY  
IN PARTIAL FULFILLMENT OF THE REQUIREMENTS  
FOR THE DEGREE OF  
DOCTOR OF PHILOSOPHY**

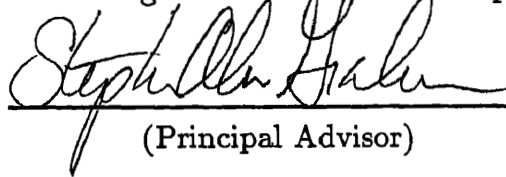
**By  
Karen Grove  
June 1989**

---

©Copyright by Karen Grove 1989  
All Rights Reserved



I certify that I have read this thesis and that in my opinion it is fully adequate, in scope and quality, as a dissertation for the degree of Doctor of Philosophy.

  
(Principal Advisor)

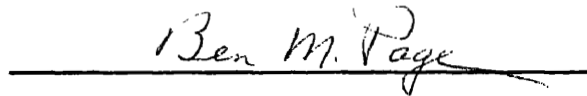
I certify that I have read this thesis and that in my opinion it is fully adequate, in scope and quality, as a dissertation for the degree of Doctor of Philosophy.



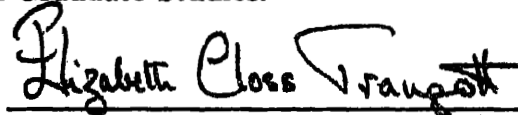
I certify that I have read this thesis and that in my opinion it is fully adequate, in scope and quality, as a dissertation for the degree of Doctor of Philosophy.



I certify that I have read this thesis and that in my opinion it is fully adequate, in scope and quality, as a dissertation for the degree of Doctor of Philosophy.



Approved for the University  
Committee on Graduate Studies:

  
(Dean of Graduate Studies)

## ABSTRACT

Upper Cretaceous strata nonconformably overlie plutonic and high-grade metamorphic rocks of the Salinian terrane, a displaced crustal fragment with a controversial tectonic history. Depositional facies indicate sediment onlap of a basement high toward the northeast and sediment dispersal toward the south and southwest. The preserved sedimentary record consists predominately of coarse-grained detritus that was deposited rapidly within nonmarine to shallow- and deeper-marine portions of a fan-delta complex along a tectonically unstable coast with steep, fault-controlled slopes. Vertical successions record fan-delta progradation and basin filling, followed by a transgressive event that continued into the early Tertiary. Contrary to previous interpretations, the now separated Cretaceous sequences were probably once contiguous parts of the same depositional site. Rapid subsidence within the basin (at least 0.5m/1000yr) was controlled mainly by extension, although transcurrent influences may have been important and probably became more prominent in the early Tertiary.

Upper Cretaceous conglomerate clasts evolved from locally-derived basement types to more distally-derived felsic volcanic types, reflecting the integration of drainages within a maturing topography. Metamorphic, plutonic, and felsic volcanic (112 Ma) clasts, are consistent with derivation from a mature continental arc similar to that which existed in the southern Sierra Nevada and western Mojave regions. Upper Cretaceous sedimentation history of the Salinian terrane can be incorporated into a tectonic model based on restoration to southern California prior to Neogene offset on the San Andreas fault zone. By this model, the Upper Cretaceous Salinian basin was formed as a roughly east-west-trending intra-arc graben, in response to dextral-fault offset within the Sierran magmatic arc. Strike-slip fault(s) accommodated an oblique component of subduction, similar to the present-day Sunda arc in Indonesia and the Kuril arc in southeasternmost Soviet

Union. Extension was facilitated by regional uplift that followed the cessation of magmatism in the arc and induced block faulting. West-vergent thrusting, which accompanied Late Cretaceous acceleration and shallowing of the subducting oceanic slab beneath North America, transported the Salinian terrane to a more outboard position in the Late Cretaceous and/or early Tertiary.

Paleomagnetic data collected from central Salinian Upper Cretaceous strata produced equivocal results because of possible indelible overprinting by the most recent magnetic field directions. Discrepancies between other paleomagnetic data that require megatransport and geologic data that require only minimal tectonic transport, remain unresolved.

## ACKNOWLEDGEMENTS

I especially thank my principal faculty advisor, Steve Graham, for encouragement and assistance during the course of dissertation research. He graciously accepted me as an advisee, and has been a good friend, as well as advisor, since then. I also thank my other research committee members, Jim Ingle, Mike McWilliams, and Ben Page, for their input along the way. The staff in the Geology Department office, Janet Wright and many assistants, made the administrative end of things more manageable. Many new friendships have made my tenure at Stanford a satisfying experience. I particularly thank my office mates of the past three to five years, Mark Rentschler, Roger Block, Alan Carroll, and Ian Moxon, for enlivening the work environment.

I thank David Howell for connecting me with a U.S. Geological Survey graduate internship, which supported my field work and assorted research expenses for four years. I also thank Mary Conger and other staff for their help with the administrative aspects of this appointment. Many geologists at the USGS were helpful. Jack Vedder provided prepublished maps; Victor Seiders provided maps as well as field access assistance. Bill Sliter and Mary McGann processed and analyzed foraminiferal assemblages. Bonnie Murchy looked at some radiolarians from chert clasts. Hugh McLean loaned me his Zodiac motor for Lake Nacimiento field work. I thank Duane Champion for his tutoring in the ways of paleomagnetism and his assistance with data analysis. The planes analysis software provided by the USGS paleomagnetic group was also helpful.

I thank Mike McWilliams and the paleomagnetic group at Stanford for access to the cryogenic magnetometer and field equipment, and for helpful advice. Bill Evitt and John Kokinos processed and analyzed samples for palynomorphs. Lou Ella Saul from the Los Angeles County Museum looked at some turritella assemblages. I thank Jim Wright, who completed isotopic analyses of zircon populations,

and Andy Tomlinson, who has been an amiable instructor (using rock crushers, extracting radiolarians, *finding* radiolarians), and a good friend. Tina Niemi has contributed much to my Stanford experience; I greatly appreciate her friendship, both professionally and personally.

The following people were invaluable field assistants: Greta Miller, Tony Provine, Brian Quinn, Mark Rentschler, and Paul Swenson. I thank the Hunter Liggett Military Reservation for permitting field access within the reservation, and Charlie Berna and the folks at the Santa Margarita Booster Station for kindly granting me access to the north side of Santa Margarita Lake. Other land owners graciously allowed me to roam their property to look at the rocks.

I thank the Geology Department and their contributors for tuition and stipend support during the past five years. Thanks are due to the geologists contributing to the U.S. Geological Survey/ Stanford Alumni Fellowship; being a recipient of this fellowship gave me a much needed respite from teaching assistantship duties. Beside the USGS, research support was provided by Mobil Oil Company (thanks to Dick Moiola), Union Oil Company (thanks to Gregg Blake), and the Shell Oil Company Fund (administered by the Stanford Geology Department), to who I am grateful.

Many people, too numerous to mention, have input stimulating discussions, lectures, and all the ingredients that have made my graduate experience an extremely enriching one. It will always, I'm sure, be a most fond memory. Hopefully, the friendships made during this time will remain for many more years to come. Last, but foremost in importance, I thank Luther and Leona Grove, my parents, for their love and support through the years, and Brian Quinn, my best friend and life's companion, for being there for me.

# Contents

<b>1</b>	<b>Introduction</b>	<b>1</b>
1.1	Geologic Background . . . . .	1
1.2	Previous Work . . . . .	8
1.3	Methods . . . . .	8
<b>2</b>	<b>Depositional Environments of Upper Cretaceous and Lower Tertiary Strata near Lake Nacimiento, Central California Coast Ranges</b>	<b>10</b>
2.1	Introduction . . . . .	10
2.2	Geologic Setting . . . . .	11
2.3	Lake Nacimiento Sequence . . . . .	15
2.3.1	Depositional Facies . . . . .	17
2.3.2	Measured Stratigraphic Sections . . . . .	37
2.3.3	Discussion . . . . .	42
2.4	Hunter Liggett Sequence . . . . .	43
2.4.1	Sequence Description . . . . .	43
2.4.2	Discussion . . . . .	46
2.5	Summary . . . . .	47
<b>3</b>	<b>Paleomagnetic Data From Upper Cretaceous Strata of the Central Salinian Terrane</b>	<b>48</b>
3.1	Introduction . . . . .	48

3.2	Lake Nacimiento Geology . . . . .	49
3.2.1	Sampled Lithology . . . . .	52
3.2.2	Paleontology . . . . .	53
3.2.3	Structure . . . . .	54
3.3	Paleomagnetic Procedures . . . . .	54
3.3.1	Sampling . . . . .	54
3.3.2	Demagnetization Procedures . . . . .	55
3.3.3	Planes Analysis . . . . .	55
3.4	Results and Interpretations . . . . .	58
3.4.1	Geographic Solution . . . . .	58
3.4.2	Stratigraphic Solution . . . . .	60
3.5	Conclusions . . . . .	62
<b>4</b>	<b>Upper Cretaceous Conglomerates From the Salinian and Point Arena Terranes</b>	<b>65</b>
4.1	Introduction . . . . .	65
4.2	Methods . . . . .	66
4.3	Lithologic Classification . . . . .	69
4.3.1	Felsic Plutonic . . . . .	69
4.3.2	Intermediate and Mafic Plutonic . . . . .	69
4.3.3	Felsic Volcanic . . . . .	70
4.3.4	Intermediate and Mafic Volcanic . . . . .	72
4.3.5	Quartzites . . . . .	72
4.3.6	Gneiss, Schist . . . . .	72
4.3.7	Low-grade Metasediment . . . . .	73
4.3.8	Miscellaneous . . . . .	73
4.3.9	Timing of Clast Metamorphism . . . . .	73
4.4	Compositional Clast Counts . . . . .	78

4.4.1	Pozo Grade and American Canyon . . . . .	78
4.4.2	Santa Margarita Lake . . . . .	82
4.4.3	Lake Nacimiento . . . . .	83
4.4.4	Junipero Serra Peak and Big Sur Coast Areas . . . . .	84
4.4.5	Pigeon Point Formation . . . . .	85
4.4.6	Gualala Formation . . . . .	85
4.5	Implications . . . . .	88
4.5.1	Provenance Constraints . . . . .	88
4.5.2	Source Area Evolution . . . . .	94
4.5.3	Stratigraphic Relationships . . . . .	97
4.6	Summary . . . . .	98

## 5 Model For Late Cretaceous Basin Formation Within the Central Salinian Terrane 99

5.1	Introduction . . . . .	99
5.2	Basin Model . . . . .	101
5.3	Upper Cretaceous Salinian Stratigraphy . . . . .	107
5.3.1	General Characteristics . . . . .	107
5.3.2	Santa Margarita Lake Section . . . . .	109
5.3.3	Pozo Grade Section . . . . .	117
5.3.4	Lake Nacimiento Section . . . . .	121
5.3.5	Junipero Serra Section . . . . .	126
5.3.6	Conglomerate and Sandstone Petrography . . . . .	127
5.4	Thermal History . . . . .	132
5.4.1	Sequence Correlations . . . . .	134
5.4.2	Implications for Extensional or Transcurrent Influences . . .	136
5.5	Comparison to Other Late Cretaceous Sequences . . . . .	138
5.5.1	Great Valley Sequence (GVS) . . . . .	138



5.5.2	Southern California . . . . .	139
5.5.3	Sur-Obispo Terrane . . . . .	144
5.5.4	Pigeon Point and Gualala Formations . . . . .	145
5.6	Southern California Reconstruction . . . . .	146
5.6.1	Basement Rocks . . . . .	146
5.6.2	Model for Salinian Reconstruction . . . . .	149
5.7	Modern Analogs . . . . .	156
5.8	Comparison with Paleomagnetic Data . . . . .	157
5.9	Conclusions . . . . .	160
<b>A</b>	<b>Paleontology</b>	<b>165</b>
A.1	Foraminifers . . . . .	165
A.1.1	Faunal lists . . . . .	165
A.1.2	Sample descriptions . . . . .	168
A.2	Palynomorphs . . . . .	171
A.3	Megafossils . . . . .	173
A.3.1	Turritellas . . . . .	173
A.3.2	Ammonites . . . . .	173
<b>B</b>	<b>Paleomagnetic data</b>	<b>176</b>
B.1	Demagnetization measurements . . . . .	176
B.2	Demagnetization planes data . . . . .	194
<b>C</b>	<b>Conglomerate Data</b>	<b>196</b>
<b>D</b>	<b>Vitrinite Reflectance Data</b>	<b>200</b>
D.1	Sample descriptions . . . . .	200
D.2	Discussion . . . . .	202
D.3	Reflectance histograms . . . . .	202

## List of Figures

2.1	Location map for Lake Nacimiento . . . . .	12
2.2	Geologic map of Lake Nacimiento vicinity. . . . .	13
2.3	Rock exposures at Lake Nacimiento . . . . .	14
2.4	High and low water levels at Lake Nacimiento . . . . .	16
2.5	Base map of Lake Nacimiento study area . . . . .	18
2.6	Correlation diagram of measured sections . . . . .	19
2.7	Stratigraphic sections A and B . . . . .	20
2.8	Stratigraphic sections C and D . . . . .	21
2.9	Stratigraphic sections E and F . . . . .	22
2.10	Stratigraphic section G . . . . .	23
2.11	Turbidite-facies beds . . . . .	25
2.12	Submarine-channel-fill deposits . . . . .	27
2.13	Shelf/slope-facies deposits . . . . .	29
2.14	Shelf/slope-facies ichnofossils . . . . .	30
2.15	Shallow-marine-facies deposits . . . . .	32
2.16	Shallow-marine indicators . . . . .	33
2.17	Fan-deltaic sequences . . . . .	35
2.18	Fluvial (lower Tertiary) facies . . . . .	37
2.19	Transgressive sequence at section B . . . . .	39
2.20	Fort Hunter Liggett section . . . . .	45
3.1	Location map . . . . .	50

3.2	Site locations at Lake Nacimiento . . . . .	51
3.3	Susceptibility and intensity curves . . . . .	56
3.4	Orthogonal vector plots . . . . .	57
3.5	Separated demagnetization paths . . . . .	59
3.6	Same site demagnetization paths . . . . .	59
3.7	Planes solution . . . . .	63
4.1	Location map . . . . .	67
4.2	Sampling grid . . . . .	68
4.3	Felsic volcanic clasts1 . . . . .	74
4.4	Felsic volcanic clasts2 . . . . .	75
4.5	Intermediate and mafic volcanic clasts . . . . .	76
4.6	Metamorphic clasts . . . . .	77
4.7	Map and sections of Santa Margarita Lake, Pozo Grade, and Amer- ican Canyon areas . . . . .	80
4.8	Compositional clast count data . . . . .	81
4.9	Schematic Santa Margarita Lake to Pozo Grade cross section . . . . .	83
4.10	Map and sections of Lake Nacimiento area . . . . .	86
4.11	Map and sections near Big Sur Coast . . . . .	87
4.12	Map, section, and conglomerate data from Pigeon Point . . . . .	89
4.13	Map, sections, and conglomerate data from the Point Arena terrane . . . . .	90
4.14	Summary diagram conglomerate data . . . . .	95
4.15	Paleogeographic model for Late Cretaceous basin . . . . .	96
5.1	Central Salinian terrane location map . . . . .	102
5.2	Salinian outcrop map with Tertiary offset removed . . . . .	104
5.3	Fan-delta model for the Late Cretaceous Salinian basin . . . . .	105
5.4	NW-SE basin cross section . . . . .	106

5.5	NE-SW basin cross section . . . . .	107
5.6	Santa Margarita Lake sequence . . . . .	111
5.7	Study area at Santa Margarita Lake and Pozo Grade areas . . . . .	112
5.8	Delta-front deposits . . . . .	114
5.9	Slope-channel deposits . . . . .	115
5.10	Delta-plain deposits . . . . .	116
5.11	Pozo Grade sequence . . . . .	119
5.12	Alluvial deposits from Pozo Grade . . . . .	120
5.13	Lake Nacimiento sequence . . . . .	123
5.14	Study areas near Lake Nacimiento and Fort Hunter Liggett . . . . .	124
5.15	Junipero Serra Sequence . . . . .	128
5.16	Study area near Junipero Serra Peak . . . . .	129
5.17	Uranium-lead isotopic data curves . . . . .	130
5.18	Uranium-lead isotopic data listing . . . . .	131
5.19	Map of central and southern California . . . . .	140
5.20	Southern San Joaquin Upper Cretaceous isopach map . . . . .	141
5.21	Restoration of Salinian terrane to southern California . . . . .	143
5.22	Model for Late Cretaceous extension . . . . .	150
5.23	Tectonic escape model for westward thrusting . . . . .	153
5.24	Modern analogs: Kuril and Sunda arcs . . . . .	158

# Chapter 1

## Introduction

The Salinian terrane is an allochthonous crustal block located in the southern Coast Ranges of west-central California. Between 15 and 30 Ma, this crustal fragment was detached from the North American plate and transferred to the Pacific plate. Since then, it has moved 300-330 km northward and has been internally segmented as a result of San Andreas fault movements (reviewed in Graham and others, 1989). This Neogene tectonism, however, has obscured older relationships, and the pre-Neogene displacement of the block remains problematic.

The purpose of this dissertation is to shed more light on the poorly understood early history of the Salinian terrane. As such, it is a contribution to the continuing effort to unravel the succession of events that have shaped this crustal fragment into its present configuration. I have focused on the Upper Cretaceous strata, using the principles of sedimentary analysis to interpret the tectonic evolution of the Salinian terrane. Research methods include environmental facies analysis, conglomerate petrology, biostratigraphy, and paleomagnetic analysis.

### 1.1 Geologic Background

The Salinian terrane consists of Cretaceous plutonic and older high-grade metamorphic rocks overlain by Upper Cretaceous to Recent sedimentary rocks. This piece of continental basement is surrounded by oceanic accretionary-complex basement

(Franciscan-type) to the east and west, the boundaries delineated by the San Andreas and Nacimiento faults, respectively. To the south, a Tertiary sedimentary cover obscures basement relationships, and the Big Pine fault rather arbitrarily defines the southern terminus. However, some of the Salinian basement rocks have affinities with basement rocks in southern California, and the southeastern sector has been included with the Tujunga terrane, which extends discontinuously into the San Gabriel and Orocopia-Chocolate Mountains regions (Blake and others, 1982; see Figures 5.1 and 5.19 for geographical localities). To the north, the Salinian terrane trends offshore and the northern terminus is also equivocal. Granitoid basement rocks extend as far north as Bodega Head. Another crustal fragment west of the San Andreas fault lies even farther to the north, but because metabasaltic rocks similar to Franciscan Complex rocks underlie the sedimentary section, it has been separated from the Salinian terrane as the Point Arena terrane (Blake and others, 1982).

The Salinian terrane has been described as a composite terrane (Vedder and others, 1982), because abrupt terminations and sharp contrasts of basement lithologies along faults within the terrane suggest early amalgamation of disparate crustal pieces. Ross (1978) divided the Salinian terrane into four blocks on the basis of these contrasting basement types. The Central block comprises the bulk of the Salinian terrane and consists predominately of granodiorite and quartz monzonite that are "a comagmatic coherent basement framework within which major structural dislocations seem unlikely" (Ross, 1978). Amphibolite- to granulite-grade country rocks in the northern part of the block (named the Sur Series by Trask, 1926) were derived from platform-type sedimentary rocks of uncertain age (Compton, 1966b). The metamorphic rocks are a heterogeneous mix of quartzfeldspathic gneiss, schists, and granofels with local limestone (Ross, 1978). The Sierra de Salinas schist, exposed in the Gabilan Range and along the northeast edge of the Santa

Lucia Mountains is, in contrast, a mass of homogeneous biotite quartzofeldspathic schist that probably originated as a "thick pile of graywacke with shaly interbeds" (Ross, 1976).

The Western block is a thin sliver bounded by the Palo Colorado and Sur-Nacimiento faults that contains distinctive high-grade charnockites (Compton, 1966). Rocks of the Southeastern block (also referred to as the Red Hills/Barrett Ridge slice, Vedder and Howell, 1982) are also distinctive. Exposures at Red Hills, Barrett Ridge, and Mount Pinos-Mount Abel are high-grade gneisses and migmatites that are similar to Precambrian basement rocks in the San Gabriel and San Bernardino Mountains (James and Mattinson, 1988). Gneisses at Mount Pinos-Abel are intruded by Cretaceous plutons and faulted against the Pelona schist to the north (James and Mattinson, 1988). The Southeastern block has been grouped together with rocks in the San Gabriel, Orocopa, and Chocolate Mountains as the Tujunga terrane (Blake and others, 1982; Howell and others, 1987).

Isolated basement outcrops are scattered throughout the Northern block. Basement rocks exposed at Ben Lomond Mountain, Montara Mountain, the Farallon Islands, Point Reyes, and Bodega Head are similar to those of the Central block (Ross, 1978). Removal of 115 km (Graham and Dickinson, 1978) to 150 km (Clarke and others, 1984) of right slip along the San Gregorio-Hosgri fault aligns related rock types at Bodega Head-Ben Lomond and Point Reyes-Monterey (Ross, 1984). At the southern end of the block, unusual quartz and anorthositic gabbro exposed just north of the Zayante-Vergeles fault at Logan may be fragments of ophiolitic ocean crust (Ross, 1970). At the northern end of the block, metabasalts underlying the sedimentary sequence near Point Arena are also unusual and have been variously interpreted as rift basalts developed in granitic basement (Silver and others, 1971) and as Franciscan basement (Wentworth, 1968). This area has been separated as the Point Arena terrane (Blake and others, 1982).

Mattinson and James (1985) and James and Mattinson (1988) summarized the age data for Salinian basement rocks. Plutonic rocks were emplaced between 75–120 Ma and show a general younging trend from northwest to southeast (Mattinson and James, 1985). Younger 60–90 Ma ages are interpreted as cooling ages (Mattinson and James, 1985). There is an inverse relationship between the age of the plutons and the amount of “offset” between emplacement and cooling ages; this suggests shallow emplacement and rapid uplift for the youngest plutons toward the southeast (Mattinson and James, 1985).

Initial  $^{87}\text{Sr}/^{86}\text{Sr}$  ratios greater than .7060 for Salinian granitoids (Kistler and others, 1973; Kistler and Petterman, 1978) attest to the continental character of these rocks. Work on strontium isotopes (Kistler and others, 1973), as well as on inherited zircon populations (Mattinson, 1978; 1986), indicate the involvement of Precambrian continental crustal rocks in magma petrogenesis. Sparse age data from metamorphic country suggest both Paleozoic and 1.6–1.7 Ma Precambrian components (James and Mattinson, 1988). Most recent work suggests a complicated, multistaged history for Salinian basement rocks (Mattinson, 1986).

Numerous workers, based on similarities between basement rocks, overlying fore-arc strata, and structural relationships, have related Salinian rocks to those in the southern Sierra Nevada, Transverse, and Peninsular Ranges, and western Mojave Desert regions, and have developed models that restore the Salinian terrane to southern California prior to about 300–330 km of Neogene dextral displacement along the San Andreas fault (e.g., Hill and Dibblee, 1953; Page, 1966; Weibe, 1970a; Burchfiel and Davis, 1981; James, 1986; Silver and Mattinson, 1986). Although Ross (1977; 1978) pointed to problems with these models based on basement mismatches, he has most recently recanted his earlier stance and elaborated numerous correlations between Salinian and southern Sierra Nevadan basement rocks (Ross, 1984). These correlations are detailed further in Chapter 5.



Still, *unique* correlations between rock types have yet to be established and problems with tectonic reconstructions models persist. For example, Page (1982) emphasized the anomalous thinness of the Salinian arc rocks and their abrupt termination against oceanic rocks of the Sur-Obispo terrane along the Nacimiento fault. Compared to the Sierran arc, the Salinian arc is missing the western flank of the batholith with abundant tonalite, trondhjemite, and gabbro; the foothills belt of accreted island arc assemblages; and extensive forearc basin deposits similar to the Great Valley sequence (Page, 1982; Ross, 1984). Page (1982) proposed two mechanisms for removal: megatransport at the earth's surface by strike-slip faults or destruction by piecemeal subduction prior to amalgamation with the Sur-Obispo terrane.

Because Salinian arc rocks are most similar to the central and eastern parts of the Sierran arc (Ross, 1972), models have been developed to extract the eastern portion of a southern Sierran extension. Dickinson (1983) proposed 560 km of Late Cretaceous sinistral displacement along the Nacimiento fault to expose the eastern flank of the Sierran arc, plus 400-500 km of Cenozoic dextral displacement along the San Andreas to move the Salinian terrane northward to its present position. Silver (1982; 1983) postulated two episodes of west-directed overthrusting to emplace an eastern portion of the batholithic belt across the western batholith and forearc regions. Hall (1988) also described a model based on west-vergent thrusting.

Another problem relates to the northwest extension of Salinian plutonic rocks beyond Sierran basement rocks following removal of 300-330 km of Neogene San Andreas displacement. Johnson and Normark (1974) explained this problem by hypothesizing an additional 200-300 km of dextral offset along other Neogene strike-slip faults. Hall (1988) rotated this extension into place by shearing associated with Neogene wrench tectonics and bending of the southernmost Sierras. And Suppe (1970) suggested a "proto San Andreas fault", operative in the early Tertiary, to

provide an additional several hundred km of displacement.

Discrepancies between the geomagnetic latitudes calculated for Cretaceous-aged Salinian sediments and the expected values based on Cretaceous pole data from cratonal North America suggest, however, that the Salinian terrane may have travelled thousands, rather than hundreds, of km from its place of origin (Champion and others, 1981; 1984). Data from Paleocene strata at Point San Pedro (Champion and others, 1984) and the Upper Cretaceous Pigeon Point Formation (Champion and others, 1981; 1984) give mean paleolatitudes of  $24.5^{\circ}$  and  $21.2^{\circ}$  compared to the expected values of  $43.3^{\circ}$  and  $46.5^{\circ}$ , thus indicating poleward displacements of 2100 and 2800 km, respectively. Because of correlations between the 50 Ma Point of Rocks and Butano sandstones across the San Andreas fault (Nilsen and Clarke, 1975), transport must be accomplished in 20 m.y. or less, implying an absolute rate of 8.5 cm/yr or a relative rate of 10-12 cm/yr between North America and the Salinian terrane (Champion and others, 1984).

Paleomagnetic results from the Point Arena terrane (Kanter, 1983) show progressively less offset for younger units. Indicated poleward displacements are 4100 km for metabasaltic "basement" rocks (about 130 Ma), 1800 km for the Paleocene-Eocene German Rancho Formation, and about 900 km for the Miocene Iverson Basalt (Kanter, 1983). Although the Miocene number seems too high, it falls within the confidence limit of the expected value after subtracting 300 km of San Andreas motion, 100-200 km of outboard (e.g., San Gregorio-Hosgri fault) motion, and 100-200 km of motion along faults within the southwestern Great Basin (Kanter and Debiche, 1985).

McWilliams and Howell (1982) replace the Sur-Obispo terrane to an equatorial position in Jurassic time and to a low latitudinal position ( $21 \pm 7^{\circ}$ ) in Campanian-Maastrichtian time, based on discrepant geomagnetic data from ophiolite at Stanley Mountain and Upper Cretaceous turbidites in the San Rafael Mountains. Fones and

others (in prep.) also obtained low latitude results from Upper Cretaceous rocks located at Point San Luis. Vedder and others (1982), based on the occurrence of granitic detritus in red beds west of the Nacimiento fault, inferred the amalgamation of the Salinian and Sur-Obispo terranes prior to Upper Cretaceous sedimentation. They suggested that the Salinian and Sur-Obispo traveled northward after suturing together at low latitudes. This timing is not certain, however. For example, Page (1981; 1982) favored a middle Tertiary age for terrane amalgamation.

To the south, paleomagnetic data from Cretaceous igneous and sedimentary rocks of the Peninsular Ranges and Continental Borderland of the Baja Peninsula (Hagstrum and others, 1985), from Upper Cretaceous marine strata of the Santa Ana Mountains (Fry and others, 1985), and from Cretaceous intrusive rocks of the Southern California Batholith (Teissere and Beck, 1973) indicate northward translations of between 1200 and 1900 km, implying that the entire area west of the San Andreas fault is an amalgamation of displaced terranes. Beck (1980) suggested that these terranes might have originated near the location of the present-day Middle America Trench off the coast of southern Mexico, where Karig and others (1978) described a truncated continental margin.

The geological and geophysical data described above has led to a controversy between two groups:

1. Those who subscribe to a model that derives the Salinian and related terranes from a position 1000-3000 km south of its present position, based on consistency between the various paleomagnetic data sets.
2. Those who subscribe to a model that derives the Salinian and related terranes from southern California, based on strong similarities of basement rock types.

I decided to study the Upper Cretaceous sediments of the Salinian terrane, because they were deposited during the time of proposed megatransport northward and so

should provide some enlightenment about this poorly understood period. These sedimentary rocks lie nonconformably on Salinian basement rocks and have been as poorly known as the tectonic context that surrounds them.

## 1.2 Previous Work

The Upper Cretaceous strata of the Salinian terrane were originally described as a continuation of the geology observed east of the San Andreas fault within the Great Valley Sequence (Trask, 1926; Reiche, 1937). Taliaferro (1944) named all of the Campanian-Maastrichtian strata west of the San Andreas fault the Asuncion Formation, including the strata west of the Nacimiento fault (the Atascadero Formation of Fairbanks, 1904). This name has since been abandoned, however, because of uncertain relationships between the scattered sedimentary sections.

More recent work has included field mapping by Durham (1965; 1968; 1974), Dibblee (1971; 1972), Compton and Dibblee (1974), Hart (1976), Vedder and others (1986), and Seiders (1989); Master's theses by Ruetz (1976), Blackmur (1978), and Butler (1984); Ph.D theses by McClure (1966), and Chipping (1970). The only recent work that has treated the Upper Cretaceous Salinian strata as a whole and in a sedimentological perspective was a reconnaissance study by Howell and others (1977). My work expands on this study and presents major interpretative differences.

## 1.3 Methods

The subsequent part of this dissertation is divided into four chapters, each of which describes a specific aspect of the Salinian problem. My approach was to use a variety of analytical tools to investigate the characteristics of the Upper Cretaceous sedimentary sections. My goal was to document these characteristics and to relate them to a model that could explain the observations within their regional context.

Chapter 2 is an analysis of the depositional environments of the strata around Lake Nacimiento, accomplished by measured sections, biostratigraphy, and other basin-analysis techniques. The purpose of this study was to understand the style of sedimentation and to infer characteristics of the basinal setting (Grove, 1986).

Chapter 3 is a paleomagnetic analysis of sampled calcareous concretions from around Lake Nacimiento. The purpose was to ascertain any translations or rotations of the Salinian terrane since Late Cretaceous time. Although translation has been inferred because of relationships with other areas, no data have heretofore been published from the main portion (Central block of Ross, 1978) of the Salinian terrane. Unfortunately, the primary magnetization was probably not isolated in this study; nevertheless, the procedures and results are described (Grove, 1987).

Chapter 4 is a conglomerate study aimed at determining lateral and vertical changes in clast compositions within the Upper Cretaceous strata of both the Salinian and Point Arena terranes. Procedures include compositional clast counts, petrographic analyses, and isotopic age dating. Observed variations are used to evaluate the relationships of separated sedimentary sections to one another and to possible source areas (Grove, 1989).

Chapter 5 is a synthesis of Chapters 2–4, plus additional stratigraphic data from sections near the La Panza Range and in the northern Santa Lucia Range. Many aspects of Salinian geology are reviewed and incorporated into two models:

1. A model that explains the formation and development of the Late Cretaceous Salinian basin regardless of its precise geographical position.
2. A model that explains the basin's formation in terms of its regional context.

The geological data presented herein are most consistent with a model based on derivation from southern California. The discrepancy between geological and geophysical data is not understood at this time, but is discussed in Chapter 5. I hope that this study will provide a useful framework for future investigations in the area.

## Chapter 2

# Depositional Environments of Upper Cretaceous and Lower Tertiary Strata near Lake Nacimiento, Central California Coast Ranges

### 2.1 Introduction

Lake Nacimiento, a reservoir on the Nacimiento River, is located 28 km northwest of Paso Robles in the central California Coast Ranges about midway between Highways 101 and 1 (Figures 2.1 and 2.2). Rocks of Late Cretaceous and Tertiary age underlie the area and are well exposed around the lake's perimeter at low water levels. Figure 2.3 shows the contrast between the excellent water-washed exposures that are normally below the lake surface and the very poor exposures typically encountered in the densely vegetated hills of the area. The Upper Cretaceous sediments around the lake are unconformably overlain by the Vaqueros Formation (Oligocene to Miocene) and strata of an uncertain, lower Tertiary, age.

This chapter describes a stratigraphic and facies analysis of the Upper Cretaceous and lower Tertiary strata around Lake Nacimiento that was completed during the summer and fall of 1985, an atypical year during which the lake level dropped more than 100 feet below the normal (brimful) level (Figure 2.4). The purpose of this study is to document the structural, stratigraphic, and facies relationships of

Upper Cretaceous and lower Tertiary strata at a locality where, at least on certain occasions, the rocks are well exposed.

## 2.2 Geologic Setting

The Upper Cretaceous strata in the central California Coast Ranges have been previously referred to as the Atascadero Formation by Fairbanks (1904), the Ascuncion Formation by Taliaferro (1944), and the unnamed formation by Dibblee (1971) and Durham (1974). The sediments are herein referred to in a genetic sense, simply as Upper Cretaceous strata, to avoid possible confusion resulting from associations with other names.

Although Upper Cretaceous rocks in the vicinity of Lake Nacimiento were mapped by summer field students from the University of California at Berkeley (summarized by Taliaferro, 1944), and by Durham (1968) and Dibblee (1971), the only sedimentologic investigations conducted heretofore were a reconnaissance study for a volume on the Cretaceous geology west of the San Andreas fault (Howell and others, 1977), and a Master's study of the deep-sea turbidites west of Lake Nacimiento (Butler, 1984). Howell and others (1977) observed a wide range of depositional environments and, based mainly on lithofacies relationships, postulated a regressive sequence around Lake Nacimiento and a borderland-type depositional setting dominated by wrench-fault tectonics (Howell and Vedder, 1978). The study described herein expands on these earlier works by providing a more detailed account of the sedimentologic features observed in the area.

The Salinian terrane is bounded to the east and west by the San Andreas and Sur-Nacimiento faults (Figure 2.1), both of which separate Salinian granitic and metamorphic basement from adjacent Franciscan-type basement. Although Upper Cretaceous sections to the north near Junipero Serra Peak (Ruetz, 1976) and to the south in the La Panza Range (Howell and others, 1977) rest depositionally on

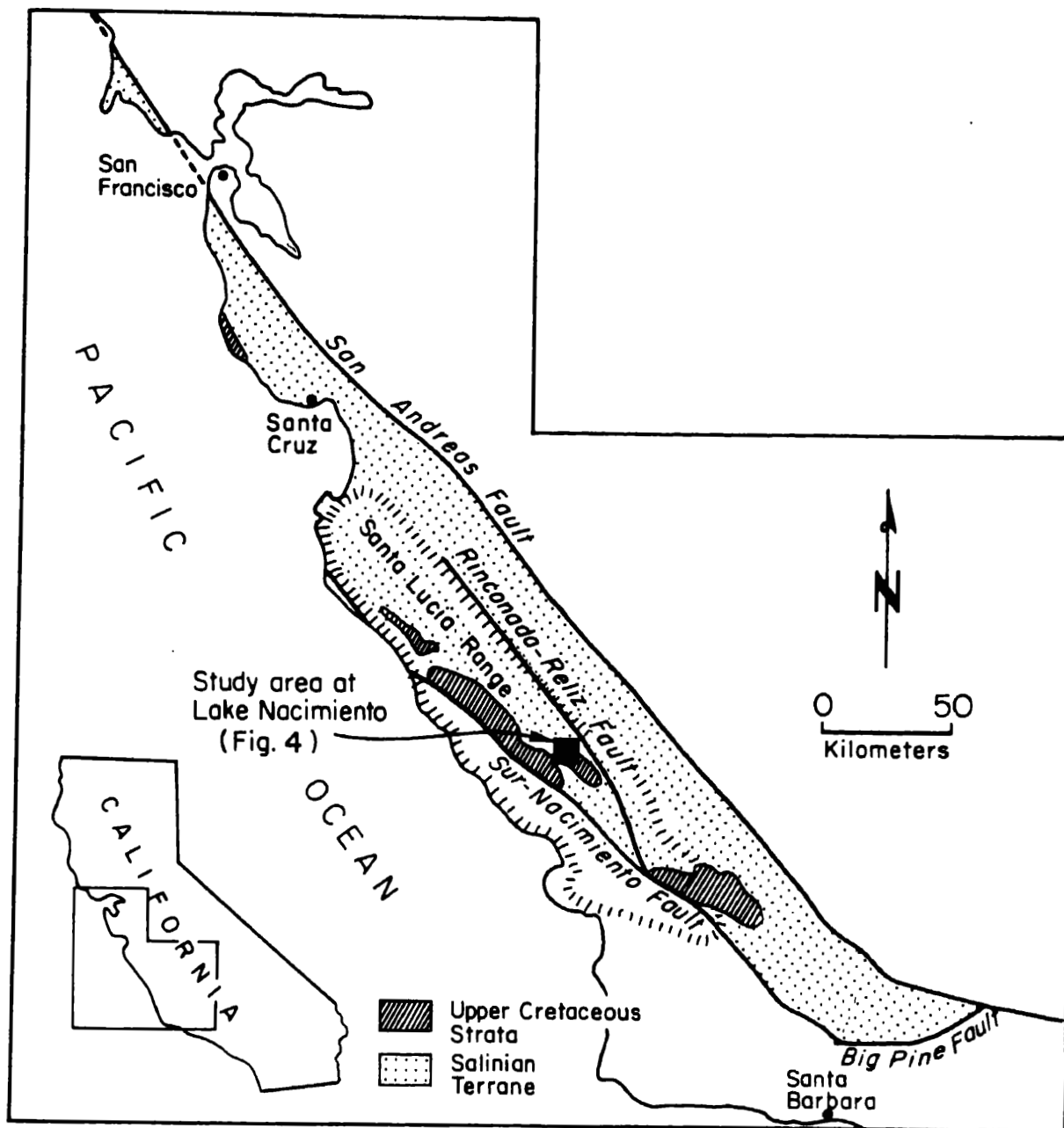


Figure 2.1: Index map of the study area.



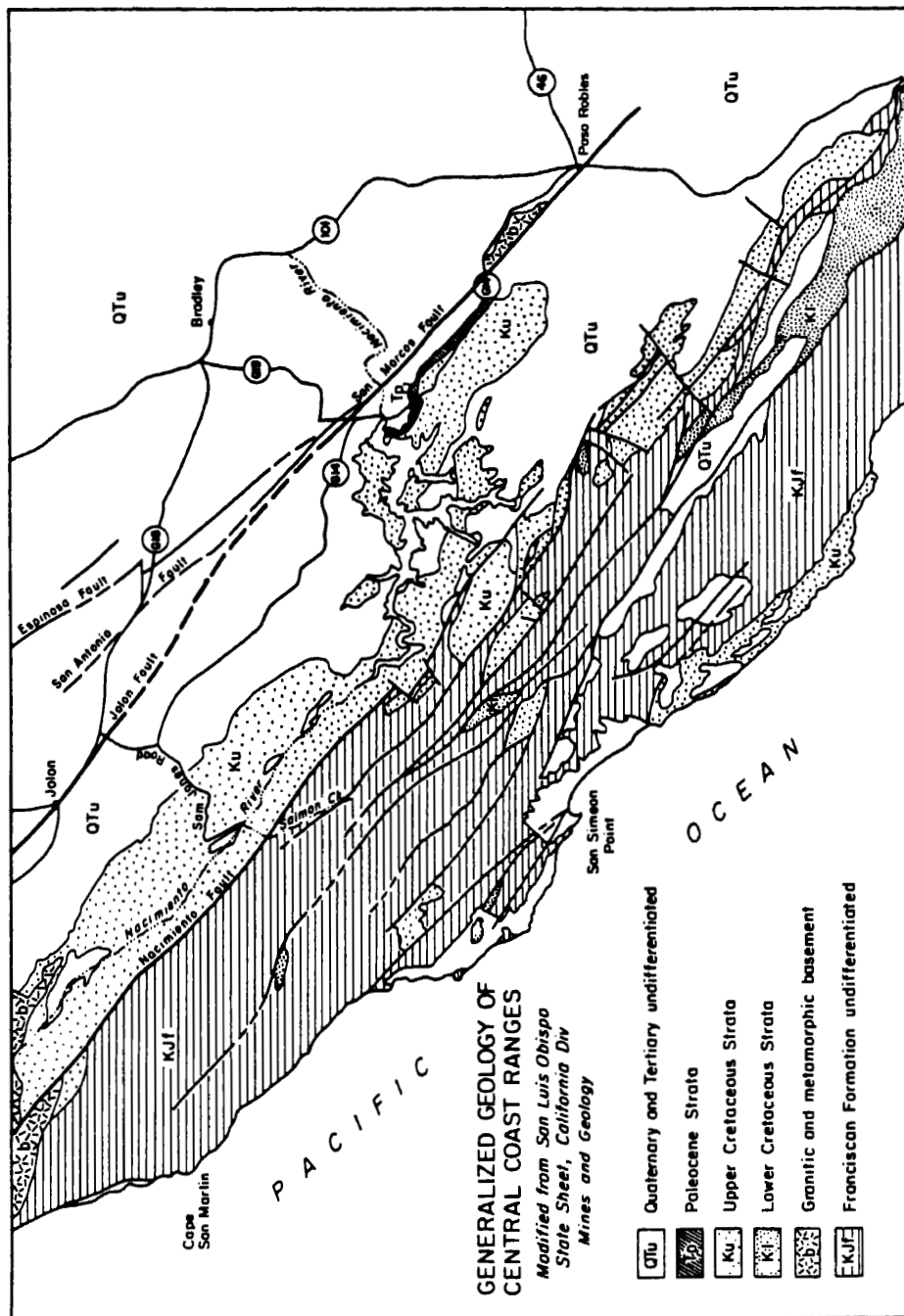


Figure 2.2: Geologic map of Lake Nacimiento vicinity.

Salinian basement rocks, the base of the section near Lake Nacimiento is truncated by the Nacimiento fault (Figure 2.2). A small fragment of granitoid basement rock is exposed between the lake and the town of Paso Robles (Figure 2.2).

The section around Lake Nacimiento dips gently toward the southeast and ranges in age from mid Maastrichtian to Paleocene (Thanetian?) (Saul, 1983; 1986; Sliter, 1986). Although the section is generally considered to be as the Paleocene Dip Creek Formation, it is not clear that these rocks are all Cretaceous in age. The poor exposures to the eastern edge of the outcrop belt of these sediments is hampered by poor exposures.

Upper Cretaceous Hunter Liggett Member is a thin, poorly dated, and separated from the underlying rocks, may be partly coeval with the Lake Nacimiento sequence, but is older at the base. The Hunter Liggett section are poorly exposed. The main emphasis here is on the better exposures of the Hunter Liggett sequence, because of its proximity to the Nacimiento fault, is structurally more complicated.

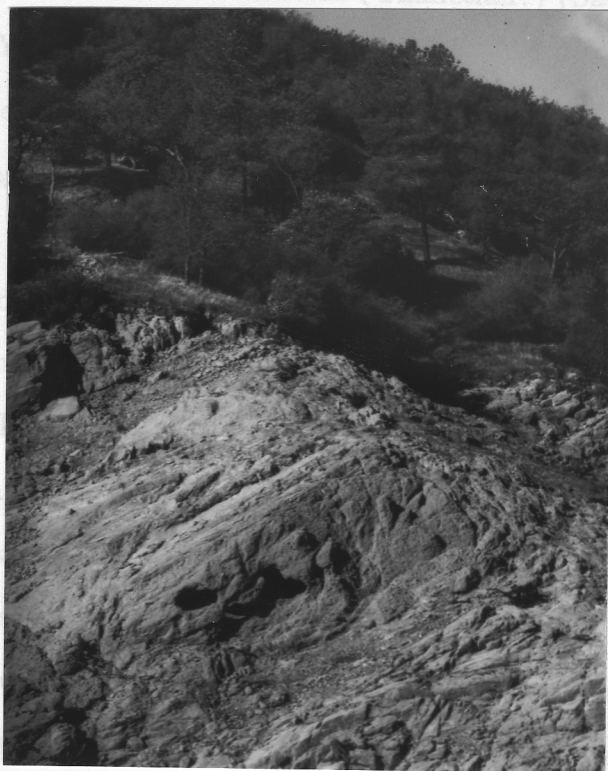


Figure 2.3: Contrast between the water-washed exposures at the edge of Lake Nacimiento during low lake levels, and the poor exposures (vegetated slope above the water line) that are typically encountered in the area (fan-delta facies of section G).

The Lake Nacimiento sequence, although disrupted somewhat by minor faulting and folding, generally crops out on a southeast-dipping homocline (Figure 2.5). The largest obstacle to field investigations is the restricted nature of exposures, which are limited to a "bath-tub ring" between young valley-fill terrace deposits or lake water below and vegetated hillslopes above. Nevertheless, it was possible to construct a series of measured stratigraphic sections (Figure 2.6). These sections

Salinian basement rocks, the base of the section near Lake Nacimiento is truncated by the Nacimiento fault (Figure 2.2). A small fragment of granitoid basement rock is exposed between the lake and the town of Paso Robles (Figure 2.2).

The section around Lake Nacimiento dips gently toward the southeast and ranges in age from mid Maastrichtian to Paleocene (Thanetian?) (Saul, 1983; 1986; Sliter, 1986). Although Taliaferro (1944) separated part of the sequence as the Paleocene Dip Creek Formation, subsequent work by Saul (1983) suggests that these rocks are all Cretaceous in age and that Paleocene strata are restricted to the eastern edge of the outcrop belt (Figure 2.2). In general, the biostratigraphy of these sediments is hampered by poor fossil preservation.

Upper Cretaceous sediments are poorly exposed in a 60-km swath through Hunter Liggett Military Reservation. The Hunter Liggett section, poorly dated and separated from the Lake Nacimiento section by Tertiary strata, may be partly coeval with the Lake Nacimiento section, although it is probably older at the base (Saul, 1986; Seiders, 1986; Sliter, 1986). Sedimentological aspects of the Hunter Liggett section are dealt with briefly in this article, but the main emphasis here is on the better exposures around Lake Nacimiento. The Hunter Liggett sequence, because of its proximity to the Nacimiento fault, is structurally more complicated (Seiders, 1986).

## 2.3 Lake Nacimiento Sequence

The Lake Nacimiento sequence, although disrupted somewhat by minor faulting and folding, generally crops out on a southeast-dipping homocline (Figure 2.5). The largest obstacle to field investigations is the restricted nature of exposures, which are limited to a “bath-tub ring” between young valley-fill terrace deposits or lake water below and vegetated hillslopes above. Nevertheless, it was possible to construct a series of measured stratigraphic sections (Figure 2.6). These sections

were constructed perpendicular to strike and to the postulated paleoshoreline; they are illustrated in Figures 2.7-2.10 and keyed to a study area base map (Figure 2.5).

Section A  
cause indi  
and because  
fannal zon  
however, con  
sistent with  
restriction  
at the base  
mm.; Saul,  
1984; Slite  
are shown  
on the in  
descriptions,  
and locati  
Five m  
ure 2.6).  
individual



sections, and implications for the overall depositional setting of the basin.  
2.3.1  
Deep-wat  
Recent stu  
considerati  
the difficul  
on limited  
exposure i  
classic "m  
important  
les and 2)  
em based  
extensive  
from the  
n a single



Figure 2.4: Contrast between high and low water levels at Lake Nacimiento: A) The lake at brim-full level (June 1986); B) The lake at about 120 feet below brim-full level (October 1985).

sediments are discussed in more general terms, emphasizing the features relevant to a paleogeographic reconstruction.

were constructed perpendicular to strike and to the postulated paleoshoreline; they are illustrated in Figures 2.7–2.10 and keyed to a study area base map (Figure 2.5).

Section correlations were accomplished mainly by extrapolating along strike, because individual beds could not be followed from one section to another and because faunal zonations are rarely better than stage level. The fossil data are, however, consistent with the correlations shown and indicate a range from middle Maastrichtian at the base to latest Late Maastrichtian at the top (W. R. Evitt, pers. comm.; Saul, 1986; Sliter, 1986). Fossil localities, as well as paleocurrent information, are shown on the individual measured sections (Figures 2.7–2.10) Faunal lists, descriptions, and location maps are in Appendix A.

Five major depositional facies were identified around Lake Nacimiento (Figure 2.6). The following text describes these facies, their occurrence in the individual sections, and implications for the overall depositional setting of the basin.

### **2.3.1 Depositional Facies**

#### **Deep-water-turbidite facies**

Recent studies of deep-marine basin-fill systems have emphasized two important considerations: 1) the large amount of variability found in modern examples and 2) the difficulty associated with assessing characteristics of an ancient system based on limited outcrop exposures (Bouma and others, 1985). For example, extensive exposure is required for discerning system geometry, which often varies from the classic “radial-fan” shape, and type of feeder system, which can range from a single canyon source to a series of slope gullies. It is therefore considered inappropriate, in light of the limited lateral and vertical exposure, to fit the deep-marine sediments seen around Lake Nacimiento into an idealized submarine fan model. Rather, the sediments are discussed in more general terms, emphasizing the features relevant to a paleogeographic reconstruction.

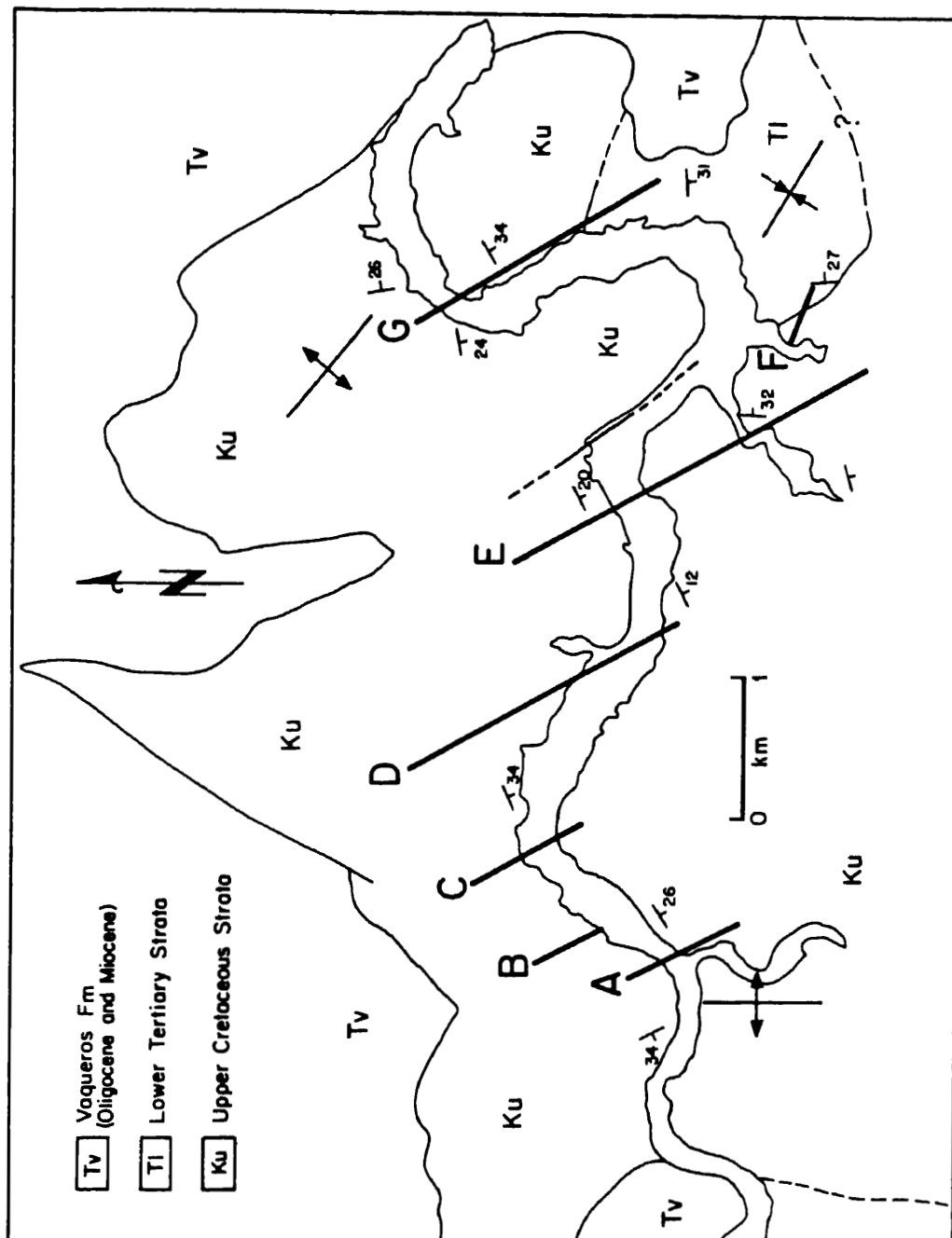


Figure 2.5: Base map of the study area at Lake Nacimiento. Letters A–G correspond to measured stratigraphic sections (Figures 2.6–2.10). The lake is outlined by the 700' contour (brim-full level is at 800').



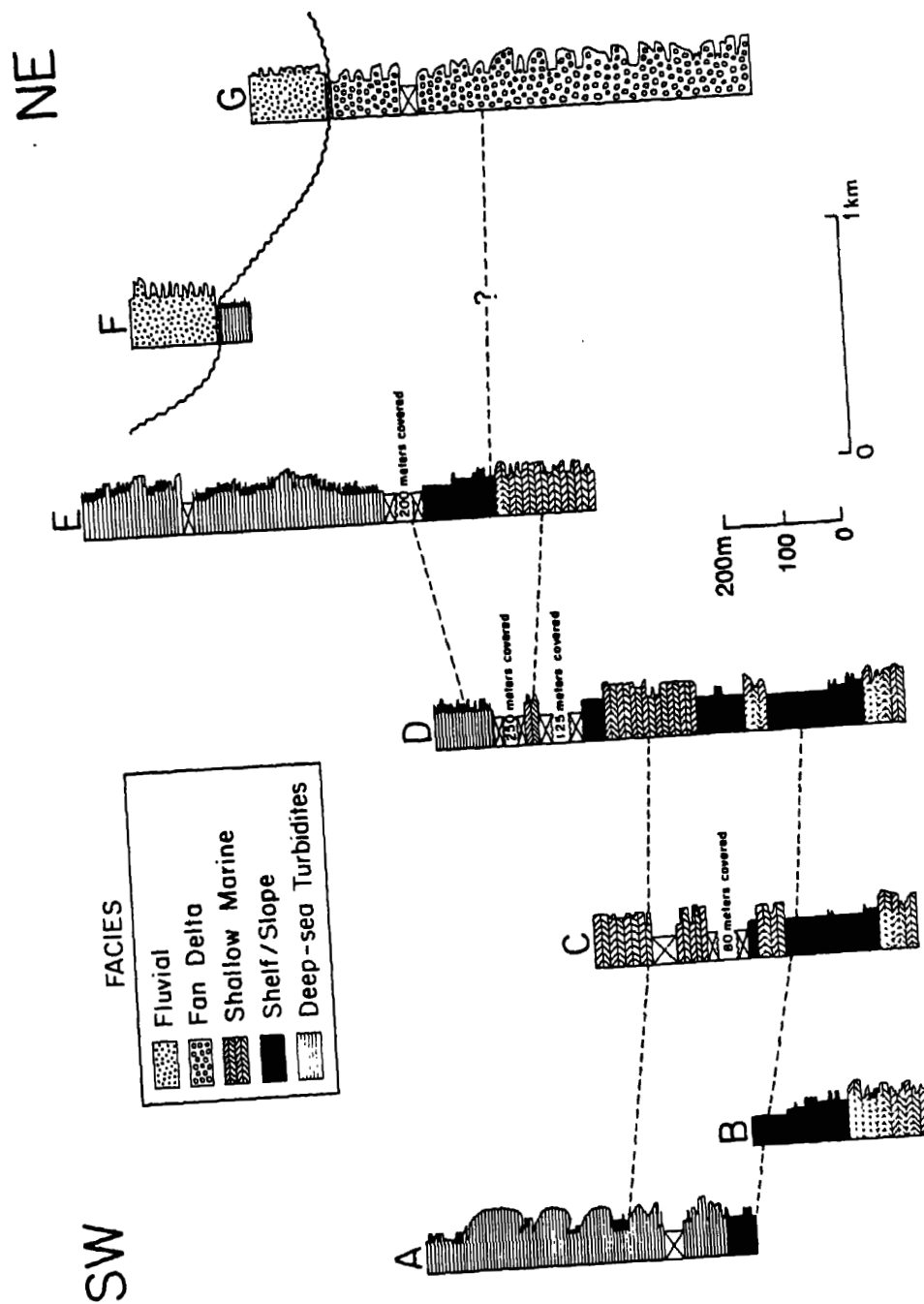


Figure 2.6: Correlation diagram of measured stratigraphic sections A-G. Note the vertical compression in sections C-E. Correlations are based on extrapolation along strike. The correlation between section G and the other sections is queried because of a fault located west of section G.

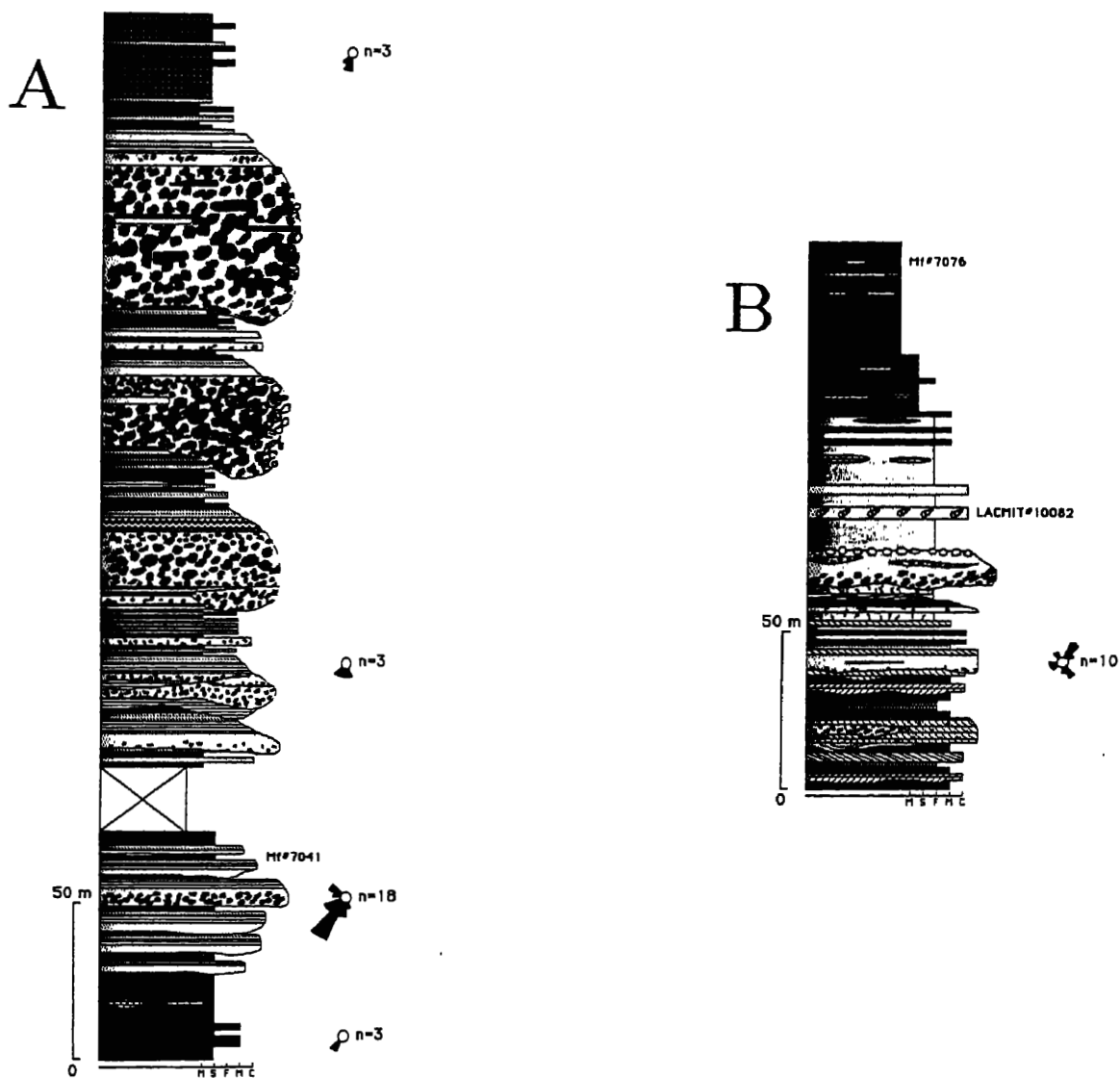


Figure 2.7: Measured stratigraphic sections A and B.



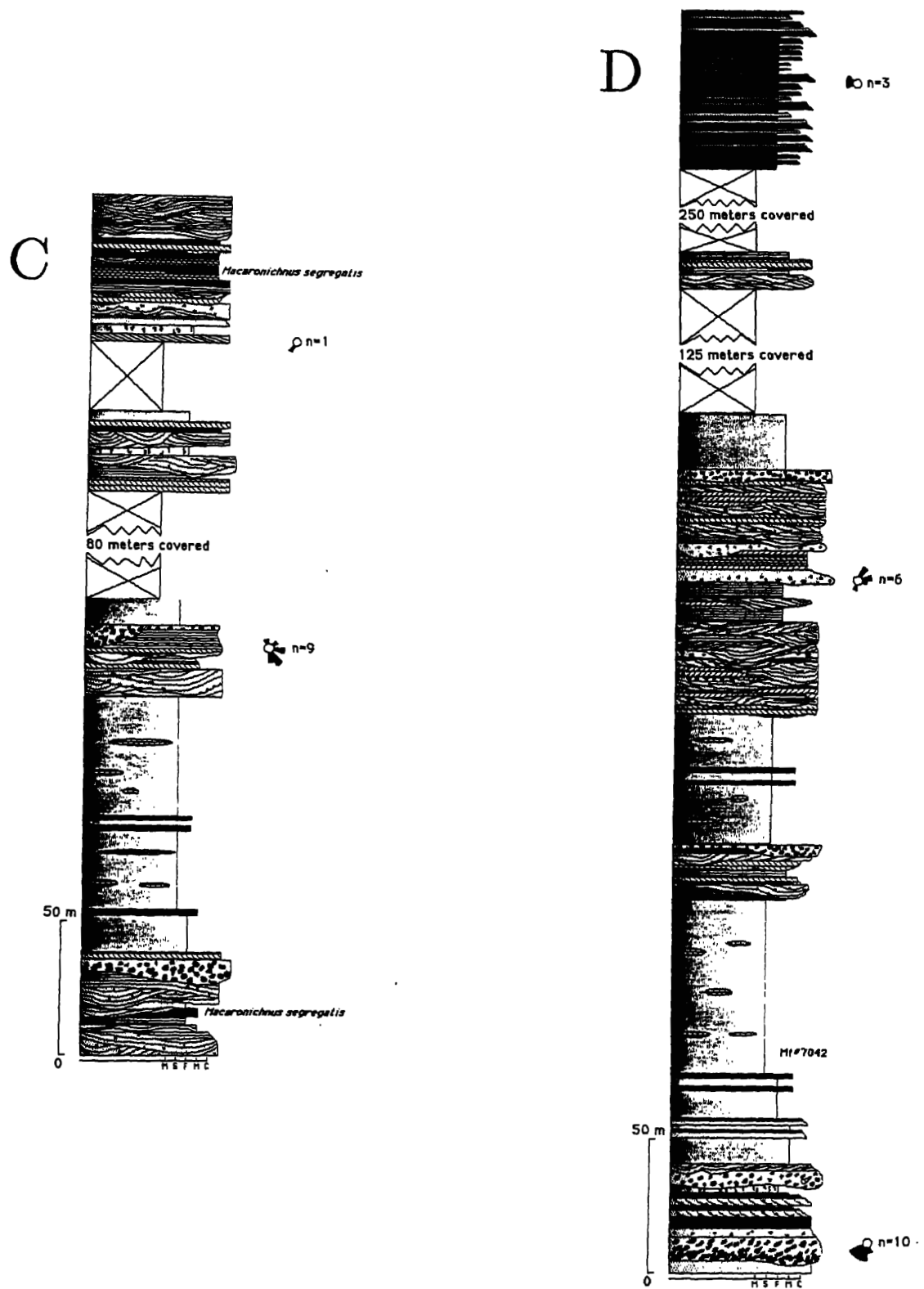


Figure 2.8: Measured stratigraphic sections C and D. Note vertical compression.

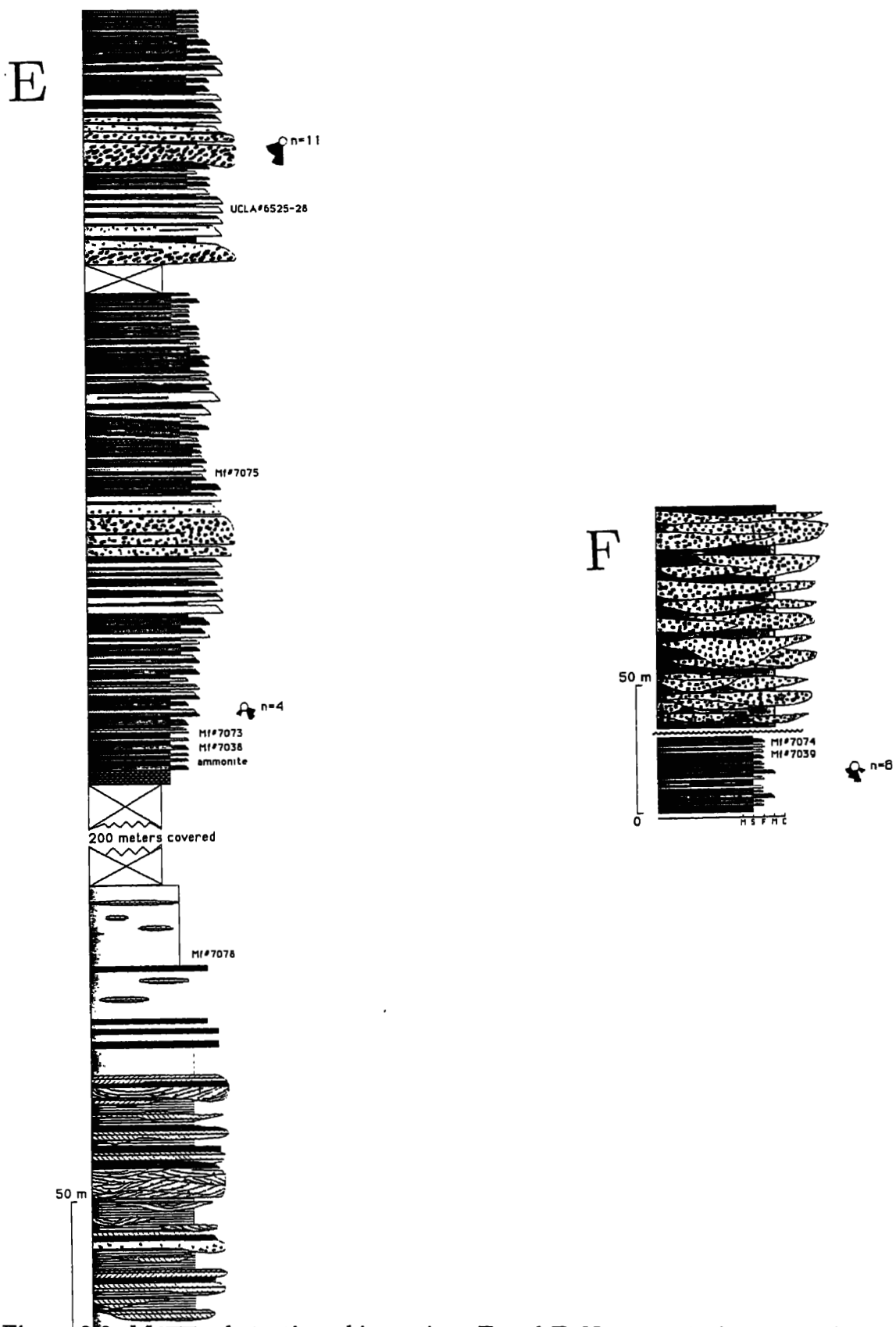


Figure 2.9: Measured stratigraphic sections E and F. Note vertical compression.

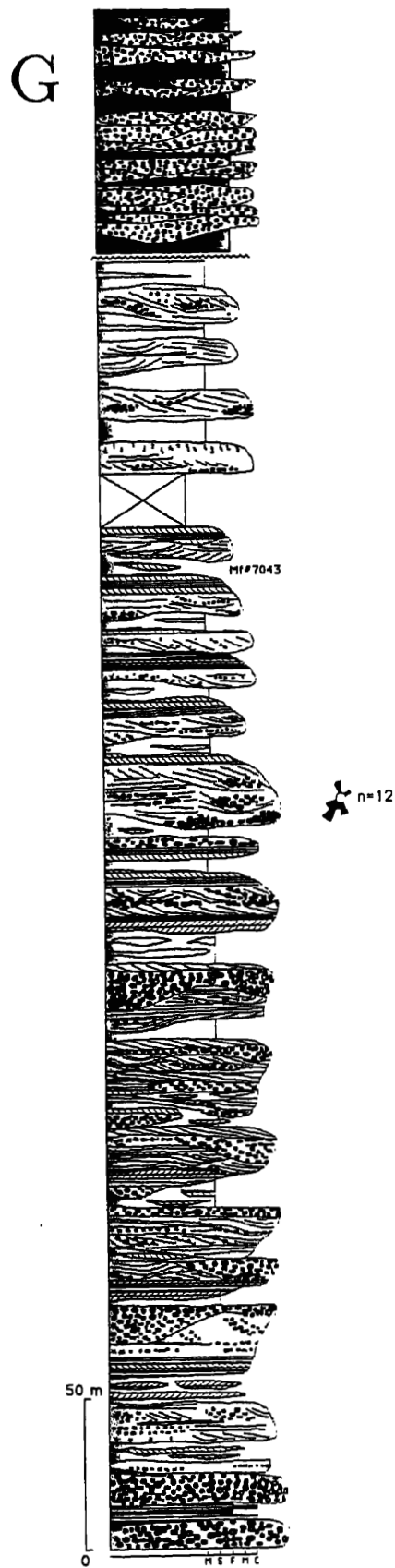


Figure 2.10: Measured stratigraphic section G.

Deep-water turbidites are found toward the top of the sedimentary sections and in the westernmost section (Figure 2.6), indicating a transgressive system and an offshore direction toward the west. This is consistent with paleocurrent indicators, gleaned mainly from pebble imbrications, current lineations, and ripple-crest orientations, that suggest a sediment transport direction from north-northeast to south-southwest (Figures 2.7–2.10).

In general, the turbidite sections were deposited in the proximal to medial parts of a submarine fan system. Upward-thinning and -fining sequences composed of Facies B and C turbidites encased in thin-bedded Facies D and E beds (Mutti and Ricci Lucchi, 1975) indicate a channelized position for these deposits (Figure 2.11). Rare upward-thickening and -coarsening sequences are also found, however, and suggest that the channels had an aggradational rather than an erosional character; progradational lobes may have built up into aggradational channel complexes. The channelized sequences typically have massive and laminated beds of angular granules (grit) and/or weakly imbricated conglomerates with a grit matrix at the base, and become progressively thinner-bedded and finer-grained upward into rippled and laminated fine-sand beds. Flute marks and siltstone intraclasts are occasionally found.

Beds that are interpreted as overbank (levee) or interchannel deposits consist of Bouma sequences with laminated b or rippled c divisions at the base. Angular discordances in bedding (Figure 2.11) and paleocurrent orientations that are often perpendicular to those in the channelized sequences (Figures 2.7–2.9) support the overbank interpretation. Other sequences of thinner-bedded turbidites are tabular and were probably deposited beyond the influence of any channels.

Conglomerate beds are prevalent in the proximal slope-channel (submarine-canyon) deposit shown in Section A (Figure 2.7). The clasts are usually disorganized and sometimes boulder-sized; the channel was probably incised into the



Figure 2.11: Turbidite-facies beds from the top of section E. A) Upward-thinning and -fining sequence interpreted as a channel-fill deposit. Circled day-pack for scale. B) Bedding angularity in thin-bedded turbidites that are interpreted as a channel-levee deposit.

shelf and slope and thus able to tap sediments from the nearshore environment. Large granite boulders in this section suggest basement exposure on the slope and may indicate an active fault scarp. Beds in this section are more disrupted than in the other turbidite sections and contain more basal scours, ripped-up intraclasts, convolutions, and orientation discordances (Figure 2.12). This presumably resulted from a steep depositional slope in a proximal fan position.

Foraminiferal assemblages collected from this facies indicate a mid-bathyal to bathyal depositional depth (Sliter, 1986). However, because the basin was constructed on continental basement, it probably did not attain depths greater than 2,000 meters. Megafossils are primarily turritella tests found in conglomerate or grit beds that were transported from more shallow depths prior to deposition. Trace fossils are typically horizontal unbranched forms of *planolites* type.

### **Shelf/slope facies**

Although some of the sediments within this facies are unequivocally shelf and others slope, it was not possible to delineate the position of the shelf/slope break, if in fact such a distinct break was a part of the basin. The shelf rocks are massive, grey, fine-grained sandstones to mudstones with intercalated fine- to coarse-grained sandstone beds that are sometimes storm-lags containing current-aligned fossil shells (Figure 2.13) and that are sometimes thin turbidite beds containing a laminated or rippled base. Slope sediments are black mudstones with a fauna indicative of low-oxygen, mid-bathyal conditions (Sliter, 1986). Calcareous concretions are common throughout the shelf/slope facies and tend to be aligned along bedding planes (Figure 2.13). Laminations are sometimes visible within the calcareous concretions, but bedding in both the concretions and the grey to black mudstone is generally obscured by pervasive bioturbation. Individual burrows are most often visible within the calcareous concretions and are forms typical of the *Cruziana*



and *Nereites* ichnofacies (Figure 2.14). The intercalated thin-bedded turbidites are sometimes convoluted and suggest slumping on a south- to west-oriented slope.

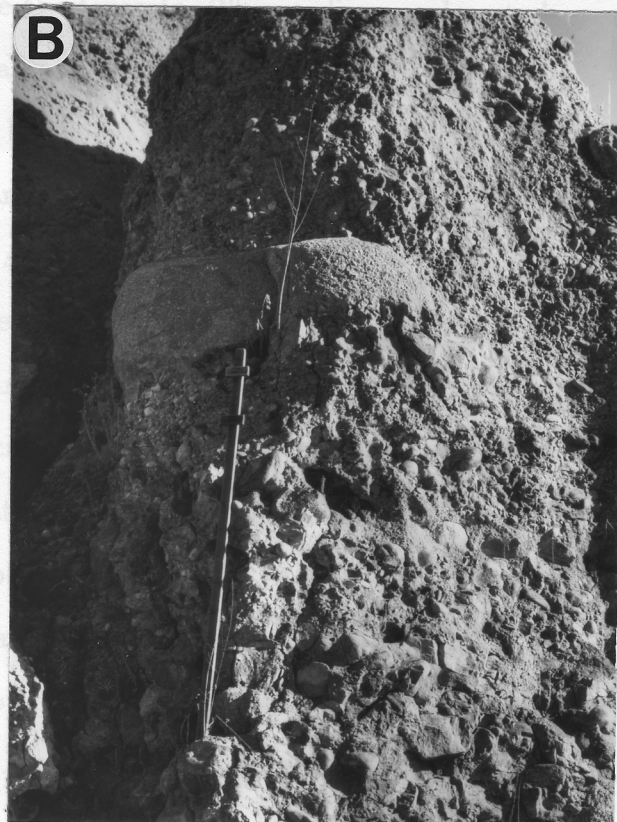


Figure 2.12: Beds of the submarine-channel deposit at the top of section A. A) Graded bed containing mudstone intraclasts at the top. B) Large angular granitic clast in conglomerate (staff height equals 1.5 meters).

and *Nereites* ichnofacies (Figure 2.14). The intercalated thin-bedded turbidites are sometimes convoluted and suggest slumping on a south- to west-oriented slope.

### Shallow-marine facies

Many subenvironments are discernible within the shallow-marine facies. Features indicative of the nearshore environment include the association of plane-laminated sandstone (sometimes with heavy mineral concentrations), northeast-, or landward-directed trough cross-bedding, and sparse vertical burrows of the *Skolithos* ichnofacies (Figure 2.15). Large-scale southeast-, or longshore-directed cross bedding occurs infrequently and may result from longshore bar development (Clifton, 1981). Medium-scale trough cross beds of coarse-grained sandstone are prevalent, and pebbles sometimes line the foresets. The medium-scale sets have diverse orientations, although a southeast direction predominates; they were deposited by megaripple migration induced by shoaling waves or by rip or longshore currents in nearshore channels (Clifton and others, 1971; Kumar and Sanders, 1976).

*Macaronichnus segregatis* trace fossils occur frequently and are good indicators of very shallow-marine deposition (Clifton and Thompson, 1978). The traces are found in mica-rich medium- to coarse-grained sandstone and are sometimes associated with bidirectional cross-bedding (Figure 2.16). Body fossils are rare and generally restricted to concentrated storm lags. Many sandstone beds are well cemented with calcite that was probably supplied by shell dissolution.

Conglomerates are common, and occur either as discrete layers, scattered pebbles, or lenses up to several meters thick. Planar, single layers that alternate with sandstone (Figure 2.15) formed during storm events as receding large waves spread a conglomeratic "storm lag" over the sea bottom; subsequently, sandstone was deposited during post-storm conditions (Kumar and Sanders, 1976; Howard and Reineck, 1981). The lenticular conglomerates were probably deposited in nearshore





Figure 2.13: Features of shelf/slope-facies beds. A) Current-aligned turrilella tests in sandstone bed. B) Calcareous concretion within black mudstone—note compaction of mudstone around concretion.

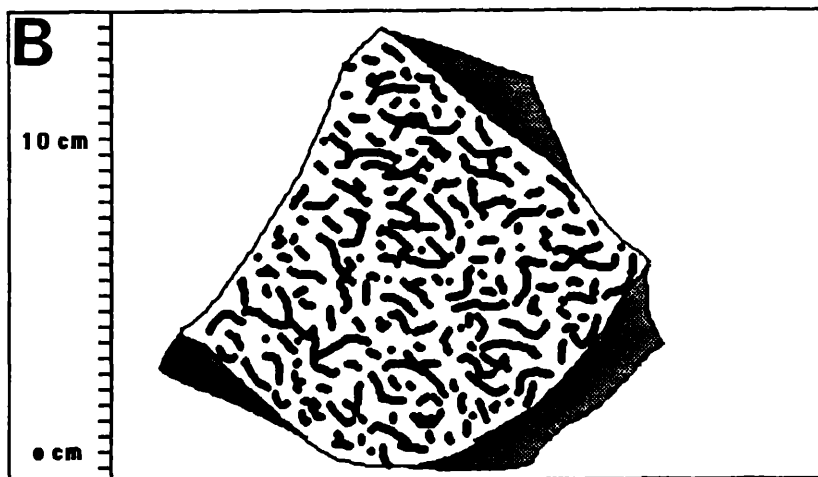
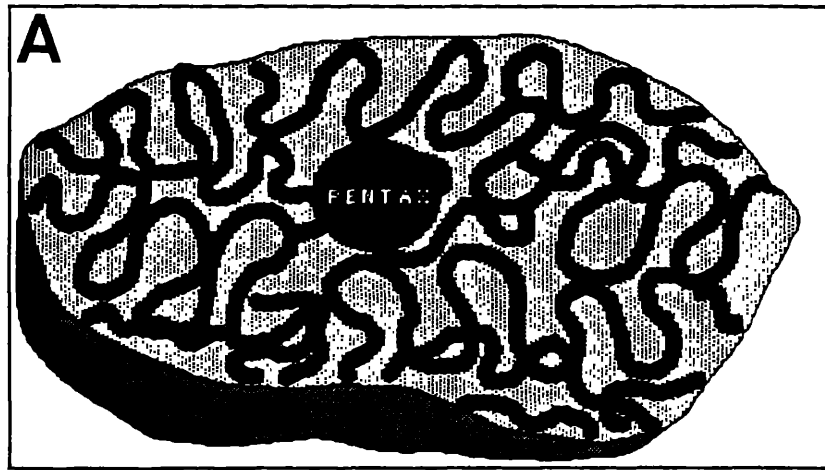


Figure 2.14: Sketches of ichnofossils on bedding planes within the shelf/slope facies. A) *Cruziana* ichnofossils. B) *Nereites* ichnofossils (*Helminthopsis*).

channels by rip or longshore currents. Graded beds that look like turbidity-current deposits are sometimes found within the shallow-marine sequences; this, combined with frequent conglomerate occurrences, suggests a high-relief, tectonically active coastal area.

Deposits of the transitional to offshore environment exhibit a coupling of sandstone beds with planar laminations, hummocky bedforms or, rarely, cross bedding, and siltstone beds that are intensively bioturbated. This association results from a combination of storm and fair weather deposition (Kumar and Sanders, 1976; Howard and Reineck, 1981).

The shallow-marine sequences typically contain many amalgamation surfaces and very thick sandstone beds are thus often found in rocks of this facies. The amalgamation surfaces sometimes preserve remnants of fine-grained beds and are sometimes erosional surfaces with overlying thin conglomerate layers that are similar in appearance to what Clifton (1981) described as transgressive gravel lags. Clearly, much of the sedimentary record has been destroyed by post-depositional erosion.

### **Fan-delta facies**

Sediments of the fan-delta facies reflect a complex interplay between marine and nonmarine processes. A large variety of subenvironments are represented; however, a detailed analysis of these subfacies is beyond the scope of the present study. In general, the fan-delta sequences consist of progradational upward-coarsening packages of sandstone and conglomerate, with thicknesses on the order of several tens of meters (Figure 2.17). Sandwiched between these packages are massive, grey, very fine-grained sandstones to mudstones that commonly contain lenses of coarse sandstone. Remnants of fine-grained sediments are also preserved beneath scoured surfaces within the coarse-grained sequences. These sequences are therefore often amalgamations of successive progradational events. Upward-fining subpackages also



Figure 2.15: Shallow-marine-facies deposits. A) Beach facies: Trough-cross beds formed by shoaling waves scour into plane-laminated beds formed within the swash zone. Cross beds are dipping toward the northeast (landward). Circled lens cap for scale. B) Alternating sandstone and conglomerate layers formed in the nearshore environment.



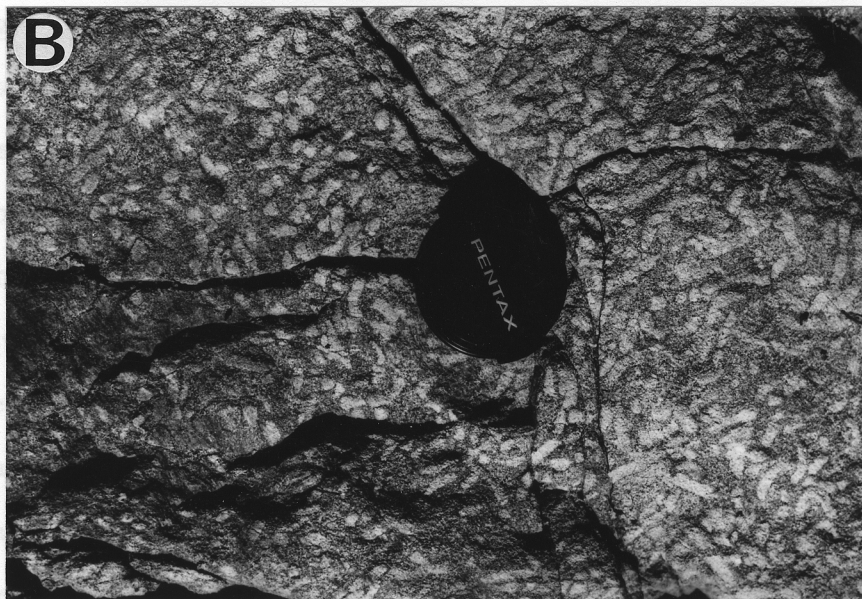


Figure 2.16: Features of shallow-marine facies beds. A) Bidirectional crossbedding with heavy-mineral laminations. B) *Macaronichnus segregatis* trace fossils.

occur and usually grade into massive grey intervals.

Conglomerates are common throughout the fan-delta sections and exhibit a full spectrum of bedding styles, ranging from scattered pebbles to very thick massive beds of cobbles and small boulders. The latter bedding type is consistent with high sediment-concentration flows and mass-emplacement processes operating along a steep coastline, a common situation in the fan-delta setting (Ethridge and Wescott, 1984). Cross-bedded conglomerates occur frequently, and may form in fluvial or foreshore channels or in channel mouth bars (Kleinspehn and others, 1984). Plane-bedded conglomerates and cross-bedded sandstones with pebble-lined foresets are identical to the nearshore deposits of the shallow-marine facies.

The foreshore association of plane-laminated and trough cross-bedded medium- to coarse-grained sandstones is also found within the fan-delta sequences, although not in great abundance. These beds typically grade upward into grey fine-grained intervals that are terminated abruptly by conglomerate beds with erosional bases. The conglomerates are often topped by trough cross-beds of coarse sand to grit with southwest- (offshore) dipping foresets that probably formed by wave reworking in the nearshore environment (Figure 2.17).

Although some of the fan-delta sediments are unequivocally nonmarine (for example, thick gravel beds and associated paleosols at the base of section G) and some are unequivocally marine (for example, plane-laminated and trough cross-bedded foreshore deposits), others are less clearcut and could be fit into either category. Unfortunately, as in the shallow-marine facies, body fossils are rarely preserved; this situation hampers environmental interpretations. The only fossils recovered to date are echonoid debris and trace fossils of *Skolithos* type. Shallow-marine and fan-delta facies share many common features and some of the shallow-marine deposits are probably distal edges of the fan-delta complex.

The facies relationships of fan-delta deposits are often complex, because they are



Figure 2.17: Photo mosaic of fan-deltaic sequences in section G. Visible outcrop is about 30 meters high. Some scoured bases, conglomerates, sand-wave deposits, and lenticular sandstone beds are highlighted. Right edge of B is continuous with left edge of A.



responses to a large variety of both intra- and extra-basinal controls (Kleinspehn and others, 1984). Clearly, the basin must be subsiding in order to accumulate hundreds of meters of shoreline sediments (see section G, Figure 2.10). The upward-coarsening packages result from progradational events induced by tectonic activity near the coastal area and/or eustatic effects. The situation is probably similar to the modern Copper River fan delta that is prograding into the tectonically active shelf of the Gulf of Alaska (Galloway, 1976). Sporadic uplifts related to faulting and earthquakes in the area punctuate a gradual subsidence that is occurring at a rate of about 3 cm/yr (Galloway, 1976).

Superimposed on the large-scale basinal controls are the effects of smaller-scale processes such as lateral migration of subenvironments within the fan-delta system. The fine-grained subfacies of the Nacimiento fan delta was probably deposited at the edges of the complex, with the sandstone lenses representing the distal portions of distributary channels. Avulsion and rapid sediment input emplaced more proximal (conglomeratic) portions of channels over the fine-grained sediments. Upward-fining sequences then developed as the channels were abandoned and diverted to new localities (Kleinspehn and others, 1984). Considerable erosion can occur during channel progradation and by reworking in the shallow marine environment (Galloway, 1976).

The type of sequence that develops depends on the interplay of these various controls and on which control is dominant at a particular time (Kleinspehn and others, 1984). The great variety of subfacies encountered within the Nacimiento fan-delta sequences attests to the complicated nature of this interplay. The sequences contain many erosional surfaces and indicate a system that was very active both in terms of its intra- and extra-basinal controls.



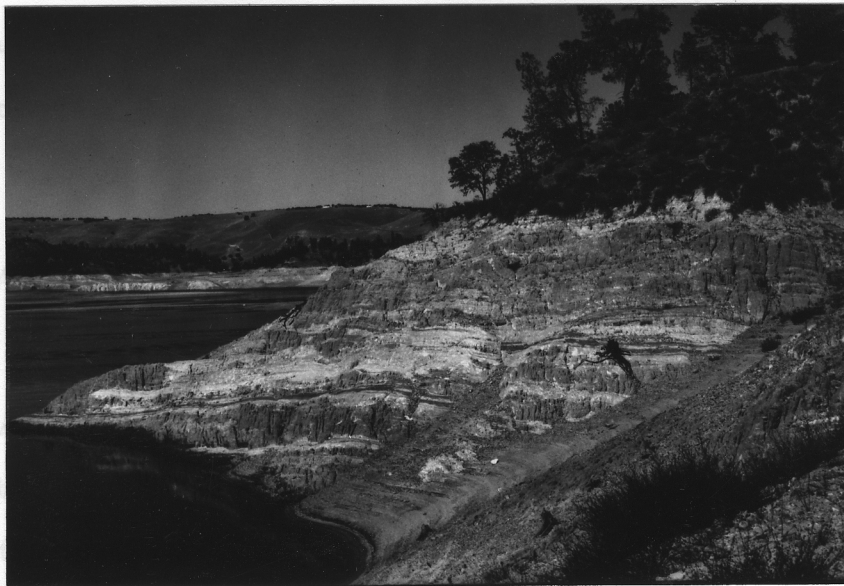


Figure 2.18: Fluvial facies sequence in lower Tertiary beds at the top of sections F and G. Note lenticular conglomerate beds encased in finer-grained sediment. Height of exposure is about 30 meters.

### Fluvial facies

The fluvial facies occurs only in the localized lower Tertiary deposits (Figures 2.5, 2.6). They are distinguished from the fan-delta sediments because they lack a demonstrable marine influence and commonly contain red beds. In addition, the conglomeratic channels are more lenticular, and contain many clasts of Cretaceous sandstone. The beds are not organized in upward-coarsening or -fining packages; rather, the conglomerates are nested within fine-grained sandstone to mudstone of probable overbank origin (Figure 2.18). This depositional style suggests a braided stream environment with highly anastomosing channels. Some of the red beds have the appearance of paleosols. No fossils of any kind have been recovered from this facies.

### 2.3.2 Measured Stratigraphic Sections

Refer to Figures 2.7–2.10 for illustrations of the measured sections and to Figure 2.6 for a correlation diagram of these sections. Notice that paleocurrent directions

indicate a paleoshoreline that was oriented roughly northwest to southeast. The sections are herein described from southwest to northeast, in a direction of increasing proximity to the Late Cretaceous landmass.

### Section A

Section A (Figure 2.7) is interpreted as a slope-channel deposit and consists mainly of Facies A and B conglomerates and sandstones (Mutti and Ricci Lucchi, 1975). Beds are typically lenticular with scoured bases; they frequently contain convolutions, pelitic intraclasts, and are, in general, highly disrupted.  $T_a$  Bouma sequence divisions are prevalent, but  $T_b$  and  $T_c$  divisions are also common, particularly in the finer grained intervals. The channel complex is over 200 m thick and continues on both sides of the lake. Conglomerate beds are thickest and coarsest grained toward the top of the section. At the top, the conglomerates abruptly give way to thin-bedded turbidites that are similar to the deposits of Sections D, E, and F.

### Section B

Section B is a transgressive sequence (Figure 2.7) has shallow-marine deposits at the base and is progressively thinner-bedded and finer-grained upward into black slope mudstones. Figure 2.19 shows this section.

### Section C

Section C (Figure 2.8) is also transgressive, but is punctuated upsection by progradational wedges of shallow-marine deposits. The shelf/slope facies sediments in this section are probably not as deep as in section B (they are not black or as fine grained), but benthic foraminiferal assemblages still suggest water depths of at least several hundred meters (Sliter, 1986). The presence of shallow-marine sediments within this facies therefore requires that basin subsidence be interrupted by peri-



Figure 2.19: Photograph of section B looking upsection (southeast) from shallow-marine facies rocks to black slope mudstones.

ods of uplift. The covered intervals in this section are obscured by lake water and terrace sediments.

### Section D

The bottom part of Section D (on the north side of the lake; Figure 2.8) is very similar to Section C; however, an upsection deepening is indicated by the presence of deep-water turbidites at the top of Section D. These turbidites are exposed along the south side of the lake, but only at very low lake levels. Notice that large intervals in this section are covered by lake water and terrace sediments.

### Section E

Section E (Figure 2.9) is a transgressive sequence with shallow-marine sediments at the base and deep-water turbidites at the top. Bedding orientations along the

southeast side of the lake in the vicinity of Dip and Snake Creeks depart somewhat from a southeast-dipping homocline, and the turbidite sequence at the top of Section E is a composite of this area (Figure 2.5). A large covered interval precludes definite connection of the turbidite section with the sequence at the base. Faunal data (W. R. Evitt, pers. comm.; Saul, 1986; Sliter, 1986) show, however, that the turbidites are younger than the sediments at the base, and the deepening upward exhibited here is consistent with the relationships seen in other sections where there are more visible connections between parts (for example, Section A).

## **Section F**

The fluvial sediments at the top of Section F (Figure 2.9) are restricted to the center of the syncline shown on the base map (Figure 2.5) and lie disconformably on thin-bedded turbidites. The contact between the two facies can be located within a few meters. Although bedding is difficult to measure in the lenticular conglomerate beds, there is apparently little angular discordance between the turbidites and the fluvial sediments. A fault along the north side of the lake trends into the syncline containing these rocks (Figure 2.5). It seems likely, therefore, that these sediments were deposited in a localized (probably transcurrent) fault basin analogous to the situation envisioned by Seiders (1986) for the Tertiary deposits at the Palisades in the Burnett Peak Quadrangle not far northwest of Lake Nacimiento. Unfortunately, no fossils of any kind have been recovered from the fluvial facies. The presence of Cretaceous sandstone clasts in the conglomerates suggests an Oligocene age, because this is the time of Cretaceous unroofing in other parts of the Coast Range (Sespe Formation, for example), and because the nonmarine Lospe Formation unconformably overlies Cretaceous strata 25 km to the southwest (Hall and others, 1979). A Paleocene or Eocene age cannot be ruled out, however.

## Section G

Section G (Figure 2.10) consists of about 500 meters of fan-delta sediments. The section is most nonmarine in character at the base (with paleosols and very thick gravel beds) and appears to deepen upward somewhat: conglomerates are less common and fine-grained beds are more common toward the top of the section. Fan-deltaic sediments along the south side of the lake are truncated by a disconformity and overlying lower Tertiary deposits. Section G is schematized somewhat in order to illustrate these relationships.

The fan-deltaic sediments are truncated by a northwest-trending fault, which juxtaposes rocks of the shelf/slope facies (Figure 2.5). Thus, the fan-delta sections are disconnected from the other sections, and the correlations here are somewhat tenuous. In addition, the lower Tertiary deposits unconformably overlie deep-water turbidites on the west limb of the syncline and fan-delta sediments on the east limb (Figures 2.5 and 2.6). This syncline lines up with the trace of the fault on the north side of the lake and it seems likely that the fluvial sediments were deposited in a fault-related basin that has been subsequently folded. The fault is vertical where visible along the north side of the lake, and it may be a transcurrent fault similar in style to the Piedras Altas fault described by Seiders (1986).

The position of Section G on the correlation diagram (Figure 2.6) is consistent with paleocurrent indicators and lithofacies relationships in the other sections that predict more proximal facies to the north or northeast. It is likely, though, that Section G is not palinspastically correct. However, if the aforementioned fault is transcurrent, it probably does not separate rocks of very different ages. If anything, the section is probably a little older than shown on the correlation diagram. Similar rocks are poorly exposed in the hills north of the lake (just below, and thus slightly older than, the base of the measured sections). A slightly older age would still be consistent with the relationships observed in the other sections. Alternatively,

depending on the type of past fault motion, section G could be Paleocene and younger than the other sections. Faunal data from Section G are required in order to satisfactorily resolve this problem.

### 2.3.3 Discussion

According to the turritella zonation of Saul (1983; 1986), the entire Nacimiento section was deposited during the mid to late Maastrichtian stage. The top of the Nacimiento sequence (in Section E) is apparently very latest Maastrichtian, although some of the fauna are very similar to Danian forms (Saul, 1986). A dinoflagellate assemblage from the top of the sequence corroborates the very Late Cretaceous designation, and also contains forms found only in the Danian on the east side of the San Andreas fault (W. R. Evitt, per. comm.). Ammonite localities indicate a Cretaceous age, but the top of Section E is very close to straddling the Cretaceous/Tertiary boundary. Further to the southeast, a locality along Godfrey Road is assigned a definite Paleocene age (Saul, 1983; 1986), but the exposures between this locality and the lake are very poor and the stratigraphy unresolved. Residual foraminiferal assemblages of mostly benthonic species that were collected from the Nacimiento Lake sections are not sufficient for resolving fine-scale correlations, but are consistent with the data from other fossil types (Sliter, 1986).

The Lake Nacimiento sequence was therefore deposited within a space of several million years, requiring average sediment accumulation rates on the order of 0.5m/1000yr. Apparently, the basin was subsiding faster than sediments were accumulating, because a transgressive sequence was produced. Sea-level curves (Vail, 1977) indicate a relatively stable sea level at the end of the Cretaceous, so the basin must have been subsiding at rates greater than 0.5m/1000yr. Higher subsidence rates may be required during some intervals, in order to compensate for the periods of uplift indicated by the presence of shallow-marine sediments within the



shelf/slope facies.

Tectonically active settings can produce basins wherein rapid subsidence is punctuated by periods of abrupt uplift; analogs include the modern Gulf of Alaska forearc basin (Galloway, 1976) and late Tertiary basins of the southern California Continental Borderland (Howell and Vedder, 1981). Transform-margin basins are particularly likely settings, because these areas are often subjected to alternating periods of transtension and transpression (Crowell, 1974), and because very rapid rates of both subsidence and uplift are common (Lajoie and others, 1976, document uplift rates exceeding 10m/1000yr).

The facies changes shown in the correlation diagram (Figure 2.6), particularly between the fan-delta sediments of Section G and the shelf/slope sediments of Section E, indicate a steep depositional slope on the order of 15°–20°. This is not unreasonable when compared to modern settings such as the transtensional Dead Sea basin, where depths of 700 meters are attained within 2 km of the shoreline (Manspeizer, 1985; slope equals about 19°), and the transform margin basins in the California borderland, where slopes of 25° are documented (Junger, 1976). Also, if Section G is, in fact, a bit older or younger than assumed, somewhat less steep slopes would be required. Nevertheless, facies changes within the basin occurred rapidly both laterally and vertically, probably reflecting steep depositional slopes, as well as rapid vertical tectonic movements within the basin.

## 2.4 Hunter Liggett Sequence

### 2.4.1 Sequence Description

The Upper Cretaceous sediments west of Lake Nacimiento are generally deep-water turbidites that are poorly exposed and not easily accessible. Consequently, this study focused on the better exposures to the east. Nevertheless, one generalized stratigraphic section of the Upper Cretaceous sequence visible along a dirt road cut

within the Hunter Liggett Military Reservation was constructed (Figure 2.20). The units in this section follow the nomenclature of Seiders (1986).

### **Unit A**

Unit A is at the base of the sequence, adjacent to the Nacimiento fault. It consists of pebbly mudstone to conglomerate with intercalated sandstone turbidite beds. The unit is very thin in this area, but elsewhere it consists of very thick conglomeratic sequences (V.M. Siders, pers. comm.).

### **Unit B**

Unit B lies stratigraphically above Unit A and consists of very thick-bedded Facies A turbidites with intercalated thin-bedded Facies C and D turbidites. The thick beds reflect the deposition of high density flows; they sometimes contain thin inversely graded "traction carpet" layers at the base, but consist predominately of massive grit that is graded toward the top of the beds. Conglomerate is absent in this unit, although small scattered pebbles often occur within the granular beds. Grain sizes within the thin beds range from fine to coarse sand; they are sometimes intensively bioturbated.

The beds in Unit B are sometimes organized in crude upward-thickening packages, but rare upward-thinning sequences are also found. Beds are tabular over the space of an outcrop, but the limited exposures preclude tracing over much lateral distance. Amalgamation surfaces are common, and beds are frequently up to tens of meters thick.

### **Unit C**

Conglomerate is the dominant lithology of Unit C, but sandstone and mudstone are also common (Seider, 1989). Although only poorly exposed along the road in the



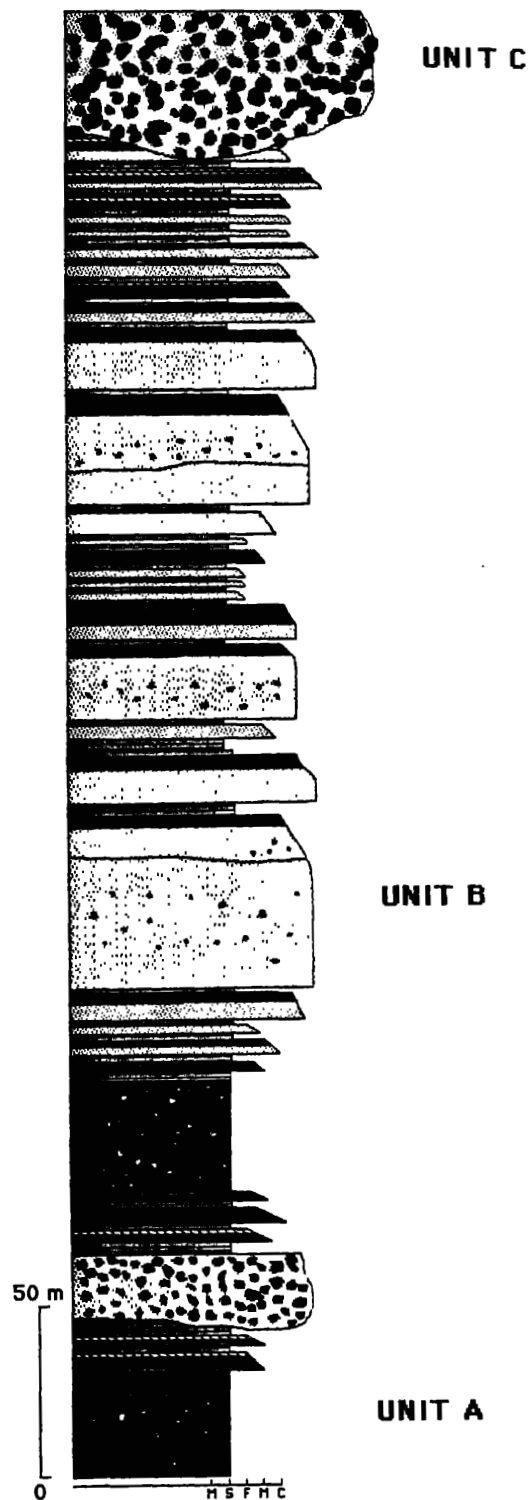


Figure 2.20: Generalized stratigraphic section of Upper Cretaceous sedimentary rocks east of the Naciminto fault in the Hunter Liggett Military Reservation. Section nomenclature from Seiders (1986). Seiders (1989) applied formational names to these units.

Military Reservation, large, massive, conglomeratic beds crop out about 12 km to the south along the Nacimiento River. The conglomerate beds have scoured bases and overlie thin-bedded turbidites of Unit B.

## 2.4.2 Discussion

The Upper Cretaceous strata west of Lake Nacimiento were not analyzed in any detail as part of the present study. However, a reconnaissance study by the author, mapping by Seiders (1989), and a Master's study by Butler (1984), indicate the dominance of deep-water turbidites in the area. This is consistent with data collected from the Lake Nacimiento sections, which predict the occurrence of deeper-water sediments in a westward direction.

Samples collected by V.M. Seiders (1986, 1989) from Units B–D have yielded Maastrichtian foraminiferal assemblages that are similar to assemblages recovered from the Lake Nacimiento sections. This suggests that the sequence to the west is at least partly coeval with the lake sequence. It may also imply an environmental similarity. The assemblages generally consist of agglutinated, benthic forms that are better for environmental than age determinations.

Unit B, lacking conglomerate lithologies, may have been deposited on more distal portions of the submarine fan than the channel deposits seen at Lake Nacimiento. Unit B is enveloped by the conglomeratic Units A and C, however. This is consistent with the conclusion that vertical movements were occurring within the basin. Alternatively, the lack of conglomerates in Unit B could result from a changing source area. Upper Cretaceous sandstones (up to granule size) are arkosic and reflect unroofing of the granitic basement. The conglomerate clasts, on the other hand, are predominately volcanic lithologies that are not found within basement rocks of the Salinian terrane and are of unknown origin. If the Upper Cretaceous basin was located within a transform margin setting, it could have been carried, conveyor-belt

fashion, past localities that were draining different source areas.

## 2.5 Summary

A facies and stratigraphic analysis of Upper Cretaceous strata near Lake Nacimiento shows a progressive deepening of the basin throughout the Late Maastrichtian stage. This upward deepening is corroborated by benthic foraminiferal assemblages (Sliter, 1986). Shallow-marine strata within deeper-water sequences indicate, however, that periods of uplift punctuated the overall basinal subsidence. Paleocurrent indicators and facies relationships show a sediment transport direction within the basin from north to south. This direction is in terms of present-day geographic coordinates and ignores possible, but unsubstantiated, rotation resulting from tectonic transport.

Various lines of evidence indicate that the Late Cretaceous basin was located within a tectonically active setting: 1) presence of a conglomerate-rich fan-delta system, 2) steep slopes with basement exposed, 3) rapid basinal subsidence, 4) high sediment input, and 5) rapid vertical and lateral facies changes.

Although the exact location of the Salinian terrane is uncertain, it was no doubt located somewhere within the western Cordillera of North or Central America. The Late Cretaceous basin was probably located within a forearc or transform margin setting along this convergent coast. Many of the sedimentological characteristics suggest a transform-margin setting, but a subduction-related forearc with an oblique component of convergence is just as likely. The Upper Cretaceous sedimentary rocks record the history of the Salinian terrane during a critical time within which there were probably major changes in the relative motions of the lithospheric plates (Page and Engebretson, 1984). Thus, studies of this area have important implications for the tectonic evolution of the eastern Pacific region in general.

## Chapter 3

# Paleomagnetic Data From Upper Cretaceous Strata of the Central Salinian Terrane

### 3.1 Introduction

Discrepancies between the geomagnetic latitudes calculated from Cretaceous and early Tertiary strata and the expected values based on paleomagnetic pole data from cratonal North America suggest that the Salinian terrane has been translated thousands of kilometers northward from its original location. Champion and others (1981; 1984) obtained paleolatitudes of  $24.5^{\circ}$  and  $21.2^{\circ}$  from the Upper Cretaceous Pigeon Point Formation and Paleocene strata at Point San Pedro (Figure 3.1), suggesting northward displacements of 2100 and 2800 km, respectively. Similarly, results from the Paleocene to Eocene German Rancho Formation near Gualala in the Point Arena terrane (Figure 3.1) show 1800 km of northward displacement (Kanter, 1983).

Paleomagnetic data from the Sur-Obispo terrane also indicate large-magnitude northward translations. McWilliams and Howell (1982) obtained a paleolatitude of  $21^{\circ}$  from Upper Cretaceous strata in the San Rafael Mountains. Data collected from Upper Cretaceous turbidites along the coast at Point San Luis yield a mean paleolatitude of  $20^{\circ}$  (Fones and others, in prep.). A fluvial-deltaic sequence located in the

San Rafael Mountains contains clasts of granite, a lithology not found west of the Nacimiento fault (Vedder and others, 1980). Vedder and others (1982) postulated a Salinian source for the granite clasts and suggested that the Salinian and Sur-Obispo terranes were sutured together by Late Cretaceous time, and transported northward with the Tijunga terrane as a single block, the Santa Lucia-Orocopia allochthon. Page (1982) favored a middle Tertiary age for terrane amalgamation, however, and the Sur-Obispo data may not be applicable to Salinian history. Furthermore, the Point Arena terrane and the Pigeon Point locality, because of uncertain basement types, have an uncertain relationship to the main portion of the Salinian terrane. The strata at Point San Pedro, however, rest on bona fide Salinian-type quartz diorite basement rocks, and these data are more difficult to dismiss.

Because no data were available from the main, central portion of the Salinian terrane, paleomagnetic samples were collected in the fall of 1986 from Upper Cretaceous sedimentary rocks exposed along the south shore of Lake Nacimiento, a reservoir located in the central California Coast Ranges about 250 km south of San Francisco and 35 km inland from the coast (Figures 3.1 and 3.2). Unfortunately, it was not possible to isolate the primary component from these samples; however, the results and procedures are herein described.

## 3.2 Lake Nacimiento Geology

Although rocks in around Lake Nacimiento are obscured by soil and thick vegetation, good water-washed exposures are often visible around the lake's circumference after summer draining of the reservoir. An exceptionally low lake level in the summer and fall of 1985 facilitated a detailed sedimentological analysis of the 2000 meter-thick Upper Cretaceous sequence (Grove, 1986). The retrogradational sequence exposed around the lake's edge records deposition within a rapidly subsiding basin along a tectonically active coastline. Paleocurrent data and facies

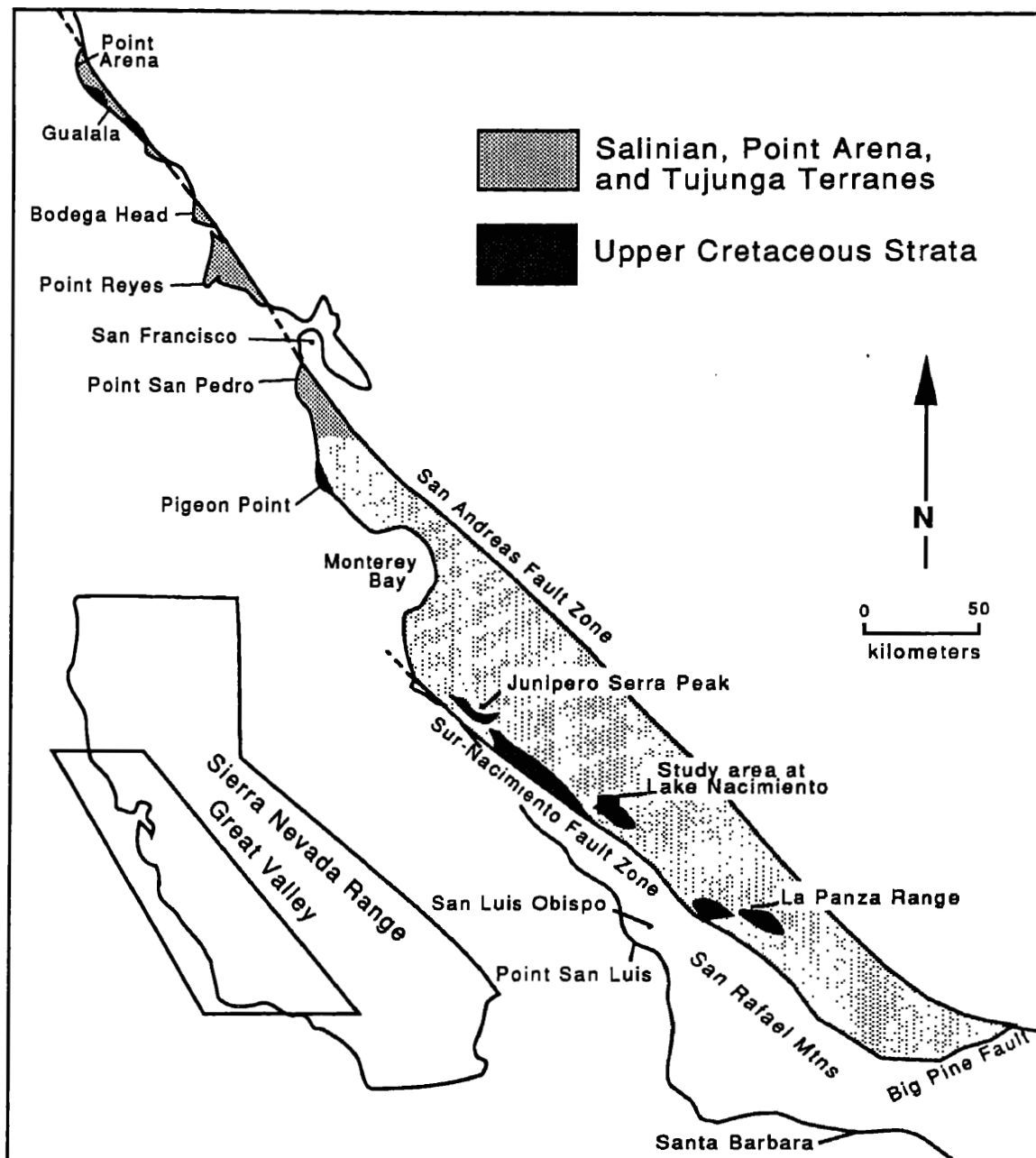


Figure 3.1: Location map of study area.

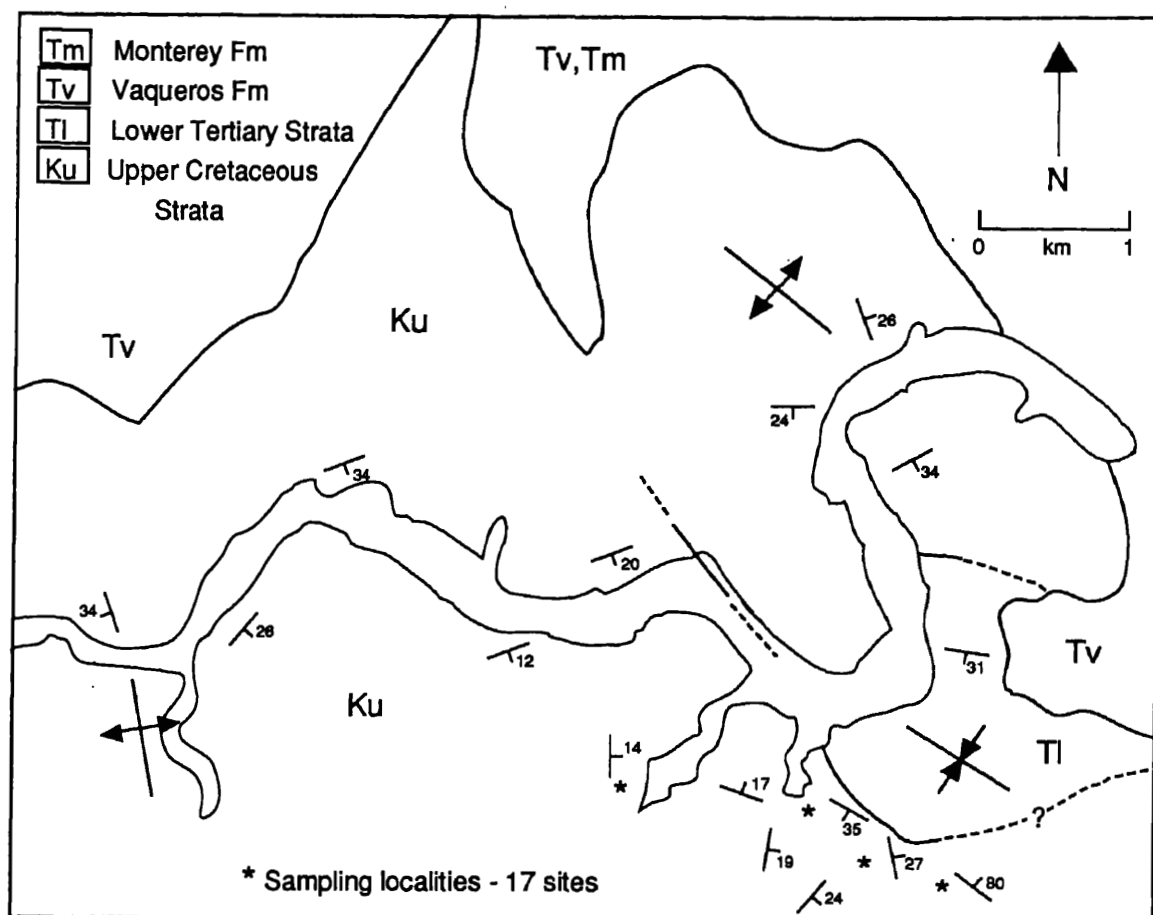


Figure 3.2: Study area at Lake Nacimiento. Geology modified from Dibblee (1970). 700' elevation contour of the lake shown; brim-full level is at 800'.

relationships indicate an offshore direction to the southwest, in terms of present-day coordinates. Depositional facies vary from shallow- to deep-water marine from northeast to southwest and from lower to higher within the sedimentary section.

### 3.2.1 Sampled Lithology

Paleomagnetic cores were collected from calcareous concretions found within the slope facies association of mudstone and thin-bedded turbidites. The .05-.5 meter-thick concretions occur as discontinuous lenses aligned along bedding planes. Deflection of shale layers around the lenses shows that the concretions formed soon after deposition, before the sediments were thoroughly compacted. Thus, the ambient magnetization should have been preserved in aligned detrital magnetite grains at this time. The slope facies rocks at Lake Nacimiento are similar to descriptions of the Holz Shale (Buck and Bottjer, 1985), an Upper Cretaceous member of the Ladd Formation found in the Santa Ana Mountains of southern California. The calcareous concretions in the Holz Shale have also been interpreted as early-formed diagenetic features (Buck and Bottjer, 1984). Hornafius (1984), in his study of magnetism within calcareous concretions of the Monterey Formation in southern California, was able to establish a close enough correlation between the diatom biostratigraphy and the magnetic polarity sequence to suggest that the primary magnetization within the concretions was acquired less than a few meters below the seafloor. He interpreted this as a post-depositional remanent magnetization (pDRM) acquired during compaction and dewatering of the sediment, even before carbonate cementation had occurred.

Grain sizes within the concretions vary from mud to medium-sand size, depending on whether they occur in mudstone or sandstone layers. Many of the sampled concretions contain a high percentage of quartz silt and fine-grained sand; they often exhibit magnetically more stable behavior than do the samples that contain



a higher percentage of mud-sized grains. A finely crystalline calcite cement welds the grains together to form an extremely durable rock. Although the concretions frequently have a weathered brown exterior rind about 1 cm thick, they appear more fresh and grey in their interiors. In thin section, however, the samples show some evidence of goethite formation. Laminated or rippled bedding is sometimes visible within the concretions, but more often, the bedding has been obliterated by extensive bioturbation.

### 3.2.2 Paleontology

Foraminifers collected from mudstone layers close to the sampled sites confirm a lower slope environmental interpretation; they suggest deposition in low-oxygen bathyal water depths probably not exceeding 900-1000 m (Sliter,1986). The residual assemblages of mostly agglutinated benthic forms range from Late Campanian to Paleocene, but contain several species exclusive to the Maastrichtian stage. According to Sliter (1986), the Lake Nacimiento faunas resemble those from the Rosario Group of southern California and northern Baja California more than those from the Great Valley Sequence exposed east of the San Andreas fault. This observation is not surprising in light of the paleomagnetic data, which suggests similar low paleolatitudes for the three areas during the Late Cretaceous (Champion,1984; 1986; Fry and others,1985; Hagstrum and others,1985).

Mollusk (Saul,1986) and palynomorph (W.R. Evitt, pers. comm., 1986) assemblages indicate a latest Maastrichtian age for the paleomagnetic sampling sites. Some of the forms in both assemblages are limited to the early Paleocene (Danian stage) at localities east of the San Andreas fault. However, ammonites show that deposition was still within the Cretaceous (Taliaferro,1943; Grove,1986).

### 3.2.3 Structure

The Cretaceous sequence around Lake Nacimientito extends discontinuously to the west, where it is truncated by the Nacimientito fault zone. Except for a small sliver of granite outcrop located about 20 km south of the lake, basement rocks are not exposed at this latitude. However, similar Cretaceous-aged sediments lie depositionally on plutonic and metamorphic rocks both to the north near Junipero Serra Peak and to the south in the La Panza Range, and this basement type is also assumed to underlie the Lake Nacimientito area.

Structurally, the sequence is tilted to the southeast, with dips rarely exceeding 30°. Broad folds interrupt the mainly homoclinal sequence, creating a diversity of structural orientations at the sampling sites (Figure 3.2). There is little discernible angular discordance between the Cretaceous rocks and the overlying Tertiary sequence around Lake Nacimientito, although some angularity is observed at other localities. In a deformational analysis in the Santa Lucia Range about 70 km to the north, Compton (1966) showed that folds with orientations similar to those near Lake Nacimientito formed during the recent Plio-Pleistocene event and involved basement as well as the overlying sedimentary rocks.

## 3.3 Paleomagnetic Procedures

### 3.3.1 Sampling

2.5 cm-diameter samples were cored from calcareous concretions and oriented with a magnetic compass before extraction. In total, 104 samples were collected from 17 sites. Rock exposures are limited to a narrow strip around the lake and, because the sampled lithologies are widely spaced, it was not possible to obtain cores from complete rock sequences. Instead, cores were collected from isolated beds containing one or several concretions; each of these areas was treated as a site. There are a variety of structural attitudes, but no discrete folds were found that could be

sampled on both limbs. Several small-scale folds with horizontal fold axes were observed, suggesting that a simple bedding correction around a horizontal axis is a sufficient structural correction for the sites.

### 3.3.2 Demagnetization Procedures

Sample cores were cut into 2.2 cm-length specimens whose magnetic directions and intensities were measured on the cryogenic magnetometer in the Stanford University's paleomagnetic laboratory. Initially, two specimens from the same sample were demagnetized, one by stepwise alternating magnetic fields and the other by incremental heating. These experiments showed that thermal demagnetizations more effectively removed the overprinting direction, so this method was used on the remaining specimens. Weak NRM intensities ranging from  $5.42 \times 10^{-7}$  A/m to  $4.54 \times 10^{-6}$  A/m decreased rapidly, without reaching stable endpoints. Measurements lost directional coherence and began behaving erratically in the 250° to 350° range. A concurrent increase in susceptibility suggests the manufacture of new mineralogies, probably magnetite, during the heating process (Figure 3.3). Specimens were thermally demagnetized by increments of 25° to maximize the information obtained before instability occurred.

### 3.3.3 Planes Analysis

Zijderveld (1967) vector component diagrams show demagnetization paths that head toward the origin as long as directional stability is maintained (Figure 3.4). Although not reaching stable endpoints, the magnetic vectors frequently move away from a northerly- and downward-directed component toward a southerly- and upward-directed component in uncorrected space. If two components with overlapping coercivities are removed simultaneously, the sample demagnetization path, as plotted on a unit sphere, will lie along a great circle. These demagnetization circles will show convergence if the two components have a large angle one to the

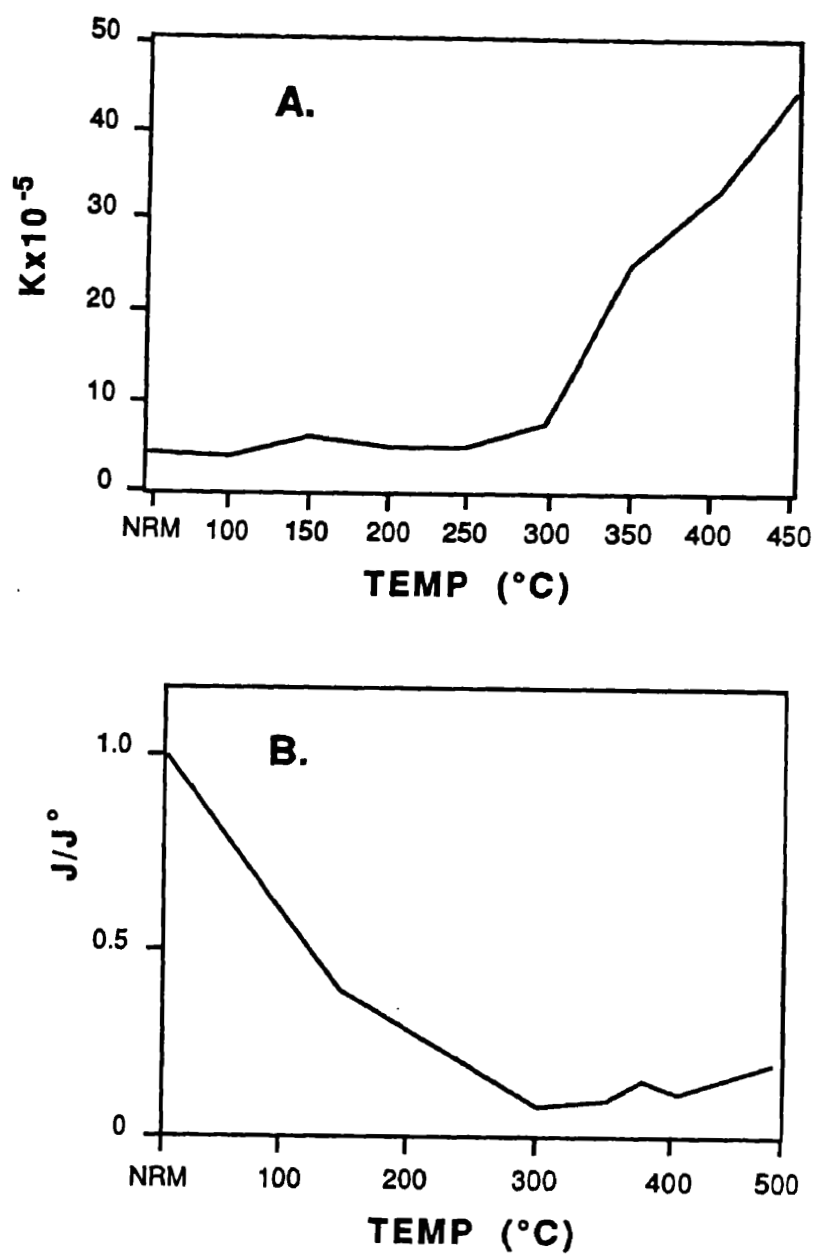


Figure 3.3: Data for sample S35-5. A) Susceptibility versus temperature. B) Normalized intensity versus temperature. Susceptibility and intensity increases above 300 $^{\circ}\text{C}$  are concurrent with the beginning of erratic demagnetization behavior.

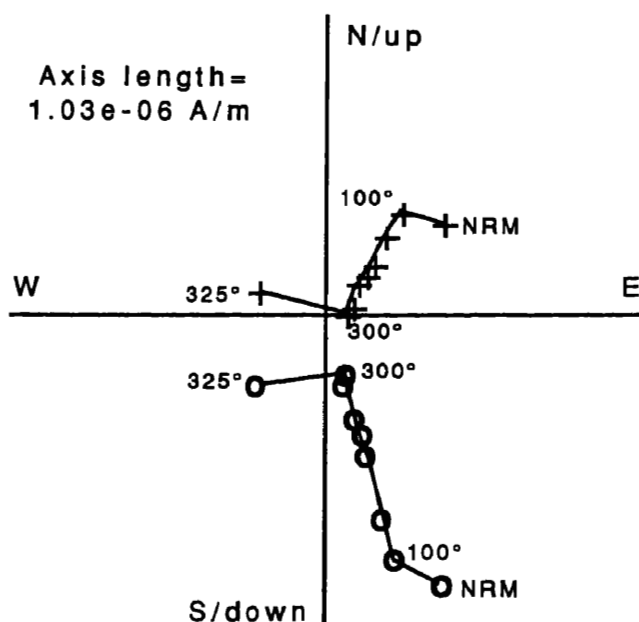


Figure 3.4: Orthogonal projection of remanent magnetic vectors for sample S32-3a. Pluses show horizontal projection; open circles show vertical projection. Sample loses directional stability above 300 C.

other. If primary and secondary magnetization directions have been dispersed by an intervening folding event, the directions of both components can be obtained from the intersections of the demagnetization circles in structurally corrected and uncorrected coordinates (Halls,1976). Planes are fit to the vectors that define the demagnetization circles by a least squares method (Halls,1976; Kirschvink,1980). The poles to these planes should lie along a great circle whose pole is the best estimate of component direction. Although planes solutions have an inherent polarity ambiguity, the correct polarity is typically ascertained from the directional sense of the demagnetization paths.

The two main components observed in the Lake Nacimiento specimens are sufficiently separate to produce converging demagnetization circles (Figure 3.5). However, it does not appear that the dispersion is caused by folding alone. If folding is the sole cause, the demagnetization vectors of samples obtained from beds with similar structural orientations should follow similar paths. This is not necessarily

the case, however, and even samples from the same bed may exhibit different paths (Figure 3.6). It seems likely that much of the dispersion is caused by the essentially antipolar nature of the two components. A small change in the orientation of the NRM direction is enough to change the direction of the shortest path to the reversed polarity component. The affect of the reversed component's antipodal position is to obscure the dispersion that might have been caused by folding, and therefore, to invalidate the fold test in this situation.

The vectors that define each specimen's demagnetization path were plotted by hand on a stereonet for visual determination of their behavior. Sixty-one of 88 measured specimens were judged to have two-component great circle paths amenable to planes analysis. Rejected specimens were indelibly overprinted with the present-day field or were magnetically unstable even at low temperatures. A low coercivity VRM component, probably associated with drilling operations, was easily removed by the 100° thermal step (Figure 3.4). Consequently, great circle paths began at 100° for these samples. Demagnetization circles for the 61 analyzed specimens range from 7°-94° in arc length, with a mean arc length of 26°.

Planes orientations were calculated as least squares fits to the demagnetization vectors that approximate great circle paths (Halls,1976; Kirschvink,1980). The poles to these planes fell along a great circle whose pole was calculated as the best estimate of component direction. This procedure was carried out both in structurally uncorrected (geographic) and in structurally corrected (stratigraphic) coordinates.

## 3.4 Results and Interpretations

### 3.4.1 Geographic Solution

The geographic solution,  $D=10$ ;  $I=+60$  (Figure 3.7), is statistically indistinguishable from the Bruhnes axial dipole field direction associated with the site. This

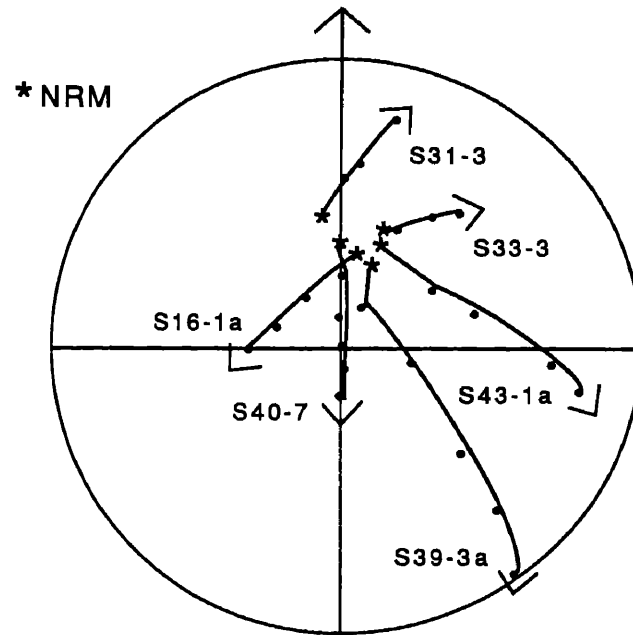


Figure 3.5: Example demagnetization paths showing component dispersion.

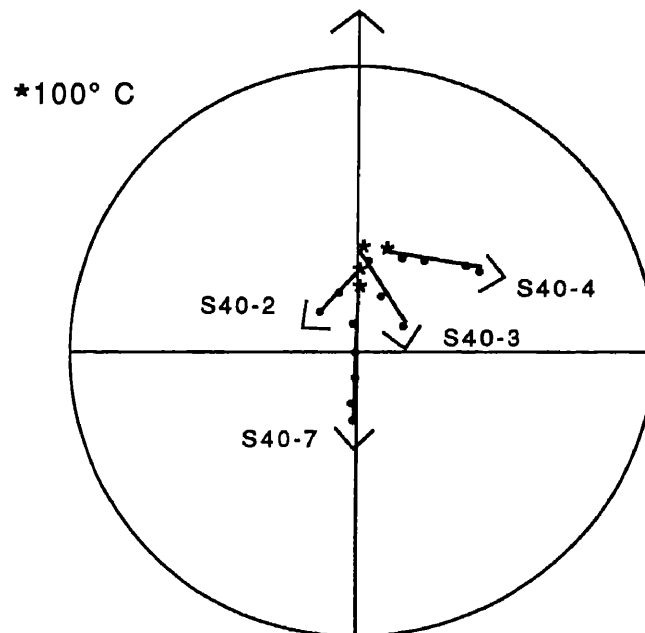


Figure 3.6: Example demagnetization paths for samples from site S40. All samples are from beds with a similar structural orientation.

direction therefore represents a Bruhnes field overprint that is probably a CRM resulting from weathering and goethite formation.

### 3.4.2 Stratigraphic Solution

The stratigraphic solution,  $D=210$ ;  $I=-60$  (Figure 3.7), is statistically less precise than the geographic solution. This is not surprising, because stable endpoints are not reached in any of the samples and cleaning paths were well short of the reversed convergence. A reversed polarity was chosen for this component based on the directional sense of demagnetization paths (Figure 3.5). As discussed previously, the antipolarity of the two components renders a fold test difficult to perform. Planes convergence suggests some coherence in the unfolded state. However, specimens with similar structural orientations do not necessarily follow similar demagnetization paths, implying that component dispersion is not caused by folding alone. Without structurally-controlled dispersion, the primary component cannot be isolated. Because the timing of magnetization relative to folding is uncertain, the interpretation of the reversed component is ambiguous when compared to the expected reversed direction for the sampled locality, assuming contiguous motion with North America.

If the stratigraphic solution is a prefolding, primary direction, the Salinian terrane has undergone  $38^\circ$  of clockwise rotation and minimal northward translation since Late Cretaceous time (Figure 3.7). However, geological considerations make such large magnitude rotations unlikely. Paleocurrent directions in the sampled locality would rotate from westerly and southerly directions (Grove, 1986) to more southerly and even easterly directions, requiring an improbable paleogeographic position. A clockwise rotation is consistent, though, with bending in the southern Sierras (Kanter and McWilliams, 1982). Paleomagnetic results from granitic basement rocks and Miocene sediments in the southern Sierras only constrain the bend-



ing to 80-16 Ma (Kanter and McWilliams,1982; McWilliams and Li,1985). Better constraints are suggested by preliminary data from 20-25 Ma Tehachapi Mountain basalts that show considerable rotation (Plescia and Calderone,1986; S.A. Graham, pers. comm., 1988) and imply a 25-16 Ma rotational event. However, Tertiary (Monterey Formation) rocks of similar age from the Santa Lucia Mountains show no rotation (Khan and Coe,1987). If the young bending age is correct, any rotation seen in Late Cretaceous-aged rocks of the Salinian terrane should also be reflected in middle Tertiary-aged rocks.

The Late Cretaceous is a frustrating time period for paleomagnetic analysis at the latitude of central California because the "expected" magnetic direction is similar to the present-day magnetic field direction. Consequently, lacking supporting evidence, an "expected" solution can be interpreted either as a primary Cretaceous component or as a present-day overprint. In this analysis, demagnetization paths are observed to move away from a present-day normal overprint toward a reversed direction. However, they could be moving toward a Matuyama field direction, acquired during the most recent reversed epoch that lasted from 2.5-.7 Ma. The sampled sequence was probably being folded and exposed to weathering during this period, so a chemical overprint could have occurred. Although the acquisition of two such closely spaced remagnetizations is not a common occurrence, Hornafius (1984) reported both a reversed and a normal polarity direction in a calcareous concretion of the Monterey Formation, which he interpreted as both Matuyama and Bruhnes epoch overprints.

The stratigraphic solution is distinct from the Matuyama field, but if the Matuyama direction is corrected by the same structural flattening that was applied to the planes orientations, it rotates to a position statistically indistinguishable from the planes solution (Figure 3.7). Thus, the solution could be a reversed magnetic component in the direction of the Matuyama field that is only apparently rotated

as an artifact of structural correction. With a post-folding interpretation, however, identification of this component is uncertain.

### 3.5 Conclusions

This paleomagnetic analysis is confounded by various difficulties. The expected magnetic direction is similar to the present-day magnetic direction so that primary and overprinting directions are not easily discriminated. The rocks contain weak pDRMs that decrease rapidly, without reaching stable endpoints. Conventional fold tests are not applicable to planes analysis in this instance, where the two components are nearly antipolar.

The secondary component in each specimen is easily isolated and identified as a Bruhnes field overprint. It was probably caused by a weathering-associated CRM. Demagnetization paths move away from the secondary component along great circle trajectories, implying the simultaneous removal of two components with overlapping coercivities. Isolation of the primary component, however, is more difficult.

Specimens with similar structural attitudes do not necessarily exhibit similarly oriented demagnetization paths, suggesting that folding was not the sole cause of component separation. Demagnetization paths apparently head from the NRM direction to its antipode, so many paths are possible as the shortest distance between the points. This might contribute to the observed dispersion and the ‘primary’ component might be a post-folding, reversed-polarity overprint. Since the Salinian terrane experienced a Plio-Pleistocene deformational event, the Lake Nacimiento sedimentary sequence could have been exposed to weathering during the most recent reversed (Matuyama) epoch. The assessment of this component is tenuous however, if the magnetization is post folding. With certainty, one can only say that the demagnetization paths appear to be purposefully headed toward some reversed direction, probably with a southerly declination.

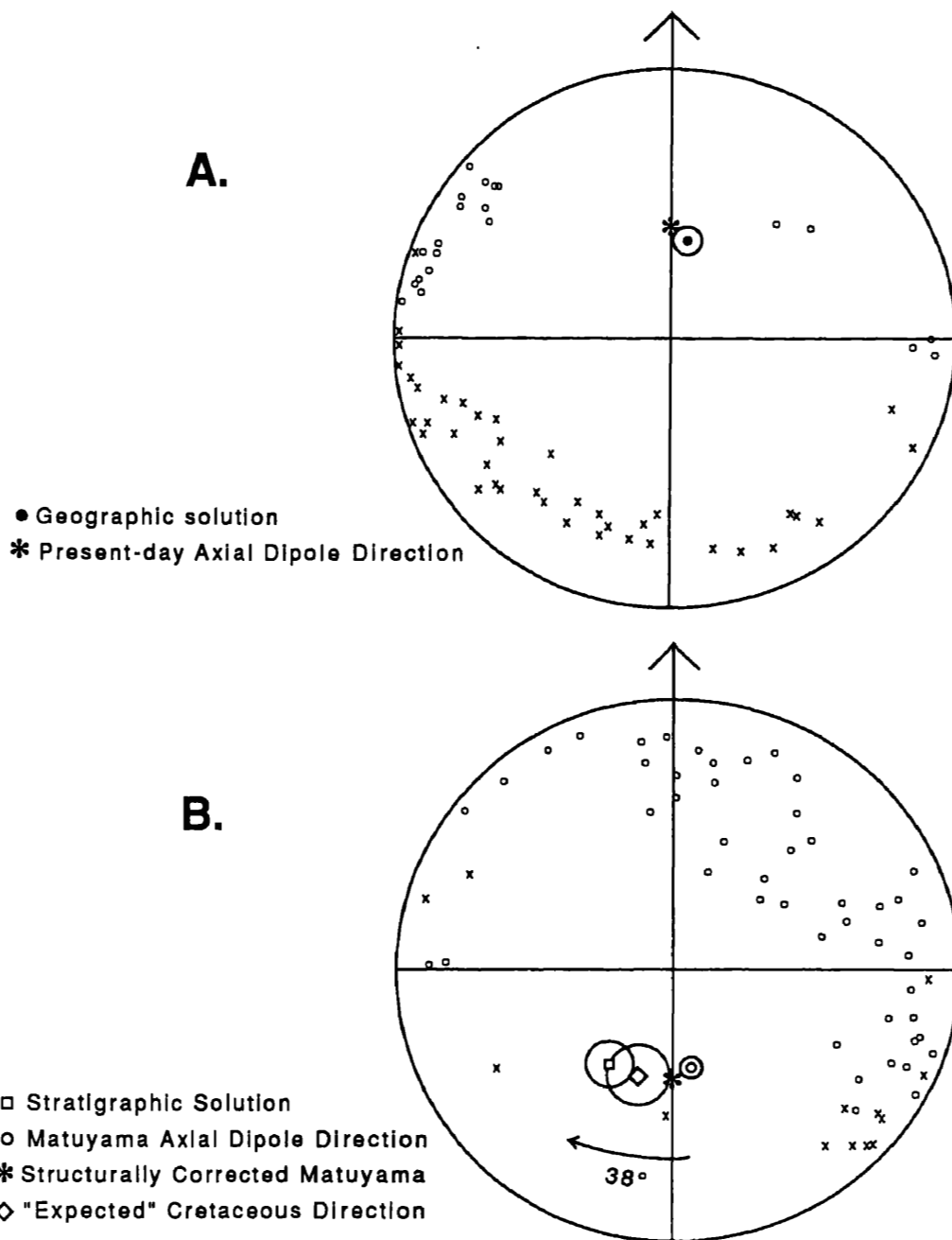


Figure 3.7: A.) Geographic planes solution ( $\alpha_{95} = 3.4$ ) with associated confidence circles. B.) Stratigraphic planes solutions ( $\alpha_{95} = 6.7$ ), expected Upper Cretaceous/Paleocene direction ( $\alpha_{95} = 2.2$ ), and structurally corrected Matuyama direction ( $\alpha_{95} = 8.9$ ) with associated confidence circles. Solutions are the pole to the plane of poles to demagnetization planes in geographic (structurally uncorrected) coordinates. Poles to the sample demagnetization planes are shown: crosses are lower hemisphere poles; open circles are upper hemisphere poles.

Alternatively, the second component could be a primary, Late Cretaceous to Paleocene direction that has experienced clockwise rotation. The sampled sequence has a Latest Cretaceous or an earliest Paleocene age, and a reversed polarity is possible for this time period (Harland et.al.,1982). Nevertheless, the lack of a stringent fold test, the unlikelyhood of large rotations, and the presence of strongly overprinting directions in these rocks urge caution for this interpretation.

The Salinian terrane is, for the most part, situated inland where fresh rock exposures are rare. The problems encountered in this study are typical of rocks from this area and the ambiguity inherent in the paleomagnetic results is not easily resolvable. In the case of this study, sediments that have a grey, pristine appearance nevertheless turn out to be strongly overprinted. In thin section, these rocks do not appear so fresh and show evidence of extensive goethite formation. Although calcareous concretions have been used successfully in the past to obtain primary magnetizations (Hornafius,1985), the particular geologic history of the Lake Nacimiento rocks seems to have rendered them with indelible magnetic overprints. Because the paleomagnetic data are ambiguous, additional geologic information is required for answering questions relating to tectonic reconstructions.

## Chapter 4

# Upper Cretaceous Conglomerates From the Salinian and Point Arena Terranes

### 4.1 Introduction

Conglomeratic sediments are widespread throughout the various Upper Cretaceous sections of the Salinian terrane. Because conglomerate clasts are whole-rock samples of the sediment source area(s), they are excellent provenance indicators and can place important constraints on tectonic reconstructions. Although similar conglomerate populations have been used elsewhere to elucidate sediment provenance and to suggest tectonic models (e.g., Carey and Colburn, 1978; Kies and Abbott, 1983), the Salinian clasts have, for the most part, received only a cursory examination. Seiders and Blome (1988) did use similarities between Mesozoic conglomerates from the Nacimiento block (Sur-Obispo terrane, Figure 4.1) and from coeval strata east of the San Andreas fault to infer that these areas (including the Salinian terrane) were in close proximity during the Mesozoic era.

This chapter describes a conglomerate study that had a twofold goal: 1) to analyze clast compositions for constraining sediment provenance, and 2) to analyze lateral and vertical variations in clast compositions for assessing provenance changes and for correlating separated stratigraphic sections. A new correlation tool was desired because biostratigraphic information from the Upper Cretaceous sec-

tions is very limited and rarely provides a zonation more detailed than stage level. Conglomerate clasts were also sampled from Upper Cretaceous strata of the Point Arena terrane for comparison with the Salinian conglomerates. The studied sections are all Upper Campanian to Maastrichtian at the base, and, except the Pigeon Point Formation, continue upward into strata of Paleocene age.

## 4.2 Methods

Data for the conglomerate study were obtained from compositional clast counts and from petrographic analyses. The clast counts were completed in situ at the outcrop, because the cobble to boulder size of the conglomerates made collection and transport to the laboratory unwieldy, and a systematic sampling bias could result from selectively extracting only the smaller clast sizes. To obtain a random sampling of clasts in the outcrop, each conglomerate bed was treated as a thin-section point count. I constructed a grid with 10 cm-spaced nodes and stretched it across the outcrop, choosing the clast beneath each node, and tallying its lithology (Figure 4.2). I counted one hundred clasts per sample, treating each conglomerate bed as one sample. To aid lithologic identifications, clasts were extracted from the outcrop and cracked open to expose the fresh surface. Sometimes, though, rock textures were most visible on the weathered surfaces. A spray bottle filled with water was found to be an indispensable field tool for highlighting the textures and the mineralogies.

In general, the vertical spacing between samples was about several hundred meters. Equal spacings were impossible because of limited exposure, limited field access, and unavailability of conglomeratic sediment types. Individual conglomerate beds were selected to maximize: accessibility of the stratum; flat surfaces suitable for grid layout; sufficient density of clasts; clast sizes in a range generally not exceeding 10 cm (to avoid counting the same clast more than once); clast surfaces not heavily

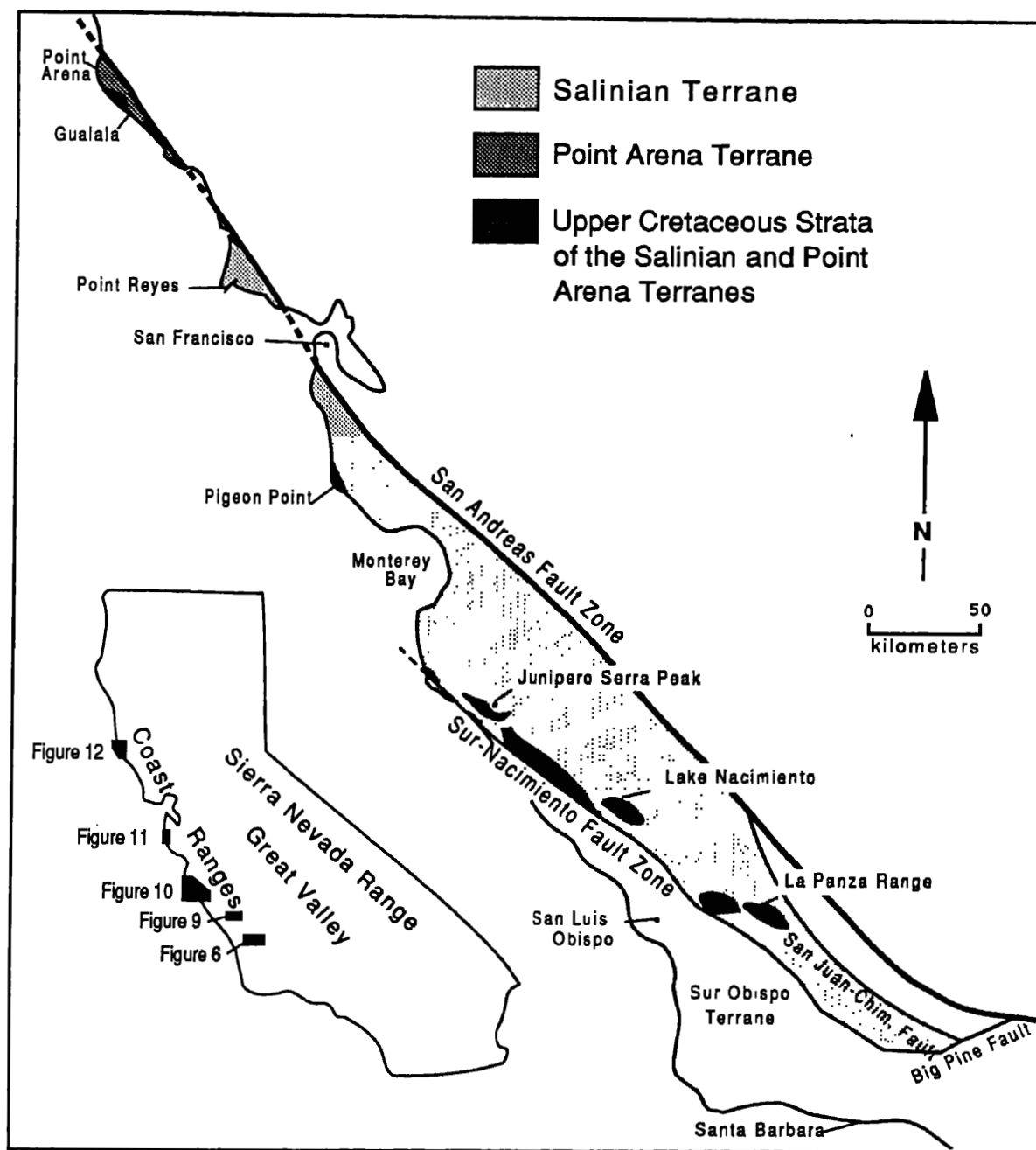


Figure 4.1: Location map of study areas. Figure numbers refer to larger-scale maps of each study area.

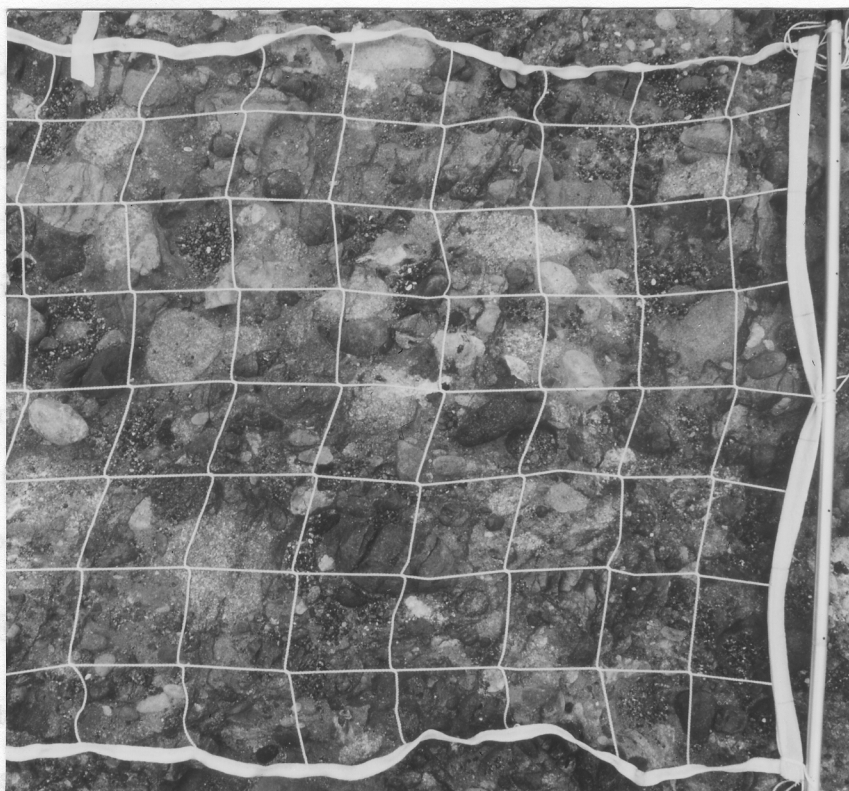


Figure 4.2: Grid used for compositional clast counts. Grid spacing between nodes is 10 cm.

weathered. Clasts with diameters less than 1 cm were classified as matrix because they were too small to identify reliably.

Fifty compositional clast counts were completed throughout the Upper Cretaceous sedimentary sections of the Salinian and Point Arena terranes. To aid field identification, a representative clast suite was collected and examined petrographically before conducting the counts. Additional samples were collected during the field counts. In all, 112 samples were thin sectioned and examined: 12 from the Gualala Formation; 20 from the Pigeon Point Formation; and 80 from the unnamed Upper Cretaceous strata—4 in the Sur Coast/Junipero Serra Peak area, 24 in the Lake Nacimiento/Hunter-Liggett Military Reservation area, 17 around Santa Margarita Lake, and 35 in the La Panza Range along Pozo Grade and in American Canyon. In most cases, thin section analyses of sampled clasts agreed with the lithologic determinations made in the field.



## 4.3 Lithologic Classification

For the field conglomerate counts, clast compositions were divided into many, specific categories in order to preserve as much information as possible about the range of lithologies. Much of this detail is documented in the Appendix C by compositional lists for each studied section. These specific categories were later grouped into more generalized categories to aid interpretation, comparison, and display. The criteria used to distinguish each general category, as well as its constituent categories, are described below.

### 4.3.1 Felsic Plutonic

These clasts are medium- to coarse-grained intrusive igneous lithologies with granular textures and a compositional range from granitic to granodioritic. This category also includes granitic porphyries, wherein feldspar phenocrysts are enclosed in a fine-grained quartz and feldspar groundmass, and aplites. The latter two types are sometimes difficult to distinguish from crystal-rich felsic volcanic clasts, but they make up only a small percentage of the total category population.

### 4.3.2 Intermediate and Mafic Plutonic

This category consists of medium- to coarse-grained intermediate and mafic plutonic rocks that include diorites, diabases, and gabbros. Most of the clasts in this category are intermediate in composition, except in the Gualala section, where gabbroic clasts dominate some of the clast populations. Most of these rocks show evidence of low-temperature metamorphism, probably of a liquid-rich metasomatic variety. Common minerals are the lower greenschist facies association of albite, epidote, chlorite, actinolite, and calcite. No metamorphic fabric is observed in these rocks and the original textures are often preserved. Sometimes, however, the alteration is so severe that the textures are obliterated. Granular and ophitic to subophitic

textures are common. Rarely, crystal-rich intermediate-composition tuffs might be confused with these clast types.

### 4.3.3 Felsic Volcanic

The felsic volcanic clasts range from rhyolitic to dacitic in composition. This category is divided into light-colored and dark-colored varieties. While this division does not precisely separate more felsic from more intermediate varieties, thin-section analyses show a tendency for the light-colored varieties to have rhyolitic to rhyodacitic compositions and the dark-colored varieties to have rhyodacitic to dacitic compositions. Because it was not possible to determine the exact composition of these clasts in the field, the color division was pragmatically chosen as the most consistent and the most reproducible. Many of the dark-colored clasts are green, because the mafic minerals are altered to chlorite and, sometimes, epidote or pumpellyite. Clast colors cover a wide range, from white, pinks, greys, and tans, to purples, greens, and black.

The felsic volcanic category consists of a large variety of volcanoclastic and lava flow rocks. All volcanic glass has been devitrified, and most of the clasts have been subsequently recrystallized, as shown by prevalent granophyric textures, which often obscure the original volcanic textures. Recrystallization has made these clasts into dense, resistant varieties that are highly preservable in the sedimentary record. This category is subdivided by texture, as well as color, into aphanites, tuffs, and porphyries. Aphanites are aphyric volcanoclastic or lava flow rocks, and volcanic rocks wherein volcanoclasts and phenocrysts are indistinguishable within the recrystallized groundmass. Recrystallization often gives these clasts a chert-like appearance.

Despite recrystallization, original volcanic textures are often discernible. Volcanoclastic textures are particularly common, indicating a dominance within this category of volcanoclastic varieties. This subcategory is referred to as tuffs, imply-

ing a pyroclastic origin, but epiclastic types are also certainly present. Because the original field relationships are not obtainable from isolated clasts, however, the specific genesis of these volcanoclastic rocks generally cannot be determined. The term "tuff" was chosen for ease of reference, but volcanoclastic rocks of all types are probably represented.

The tuffaceous clasts contain crystals, lithic fragments, and juvenile fragments such as pumice pieces. The crystals are quartz, feldspar, and sometimes biotite and hornblende minerals that are often fragmental and sometimes highly embayed (Figure 4.3A). Lithic fragments, usually volcanic types, are commonly represented (Figure 4.3A and B). Although the tuffs are totally crystalline, devitrified varieties, the original glassy textures are frequently visible. For example, one can find axiolitic textures, wherein crystals fibers are oriented perpendicular to the walls of replaced glass shards or pumice fragments, and welded textures, wherein pumice pieces are flattened by compaction (Figures 4.3B, 4.4C). The tuffaceous groundmass is usually a network of minute fibrous crystals that result from the devitrification of ash-sized glass pieces and granophyric-textured crystals that result from recrystallization. Lapilli as well as ash tuffs are represented.

The porphyritic felsic volcanics have an aphanitic groundmass containing phenocrysts of quartz and plagioclase in the more siliceous varieties, and of plagioclase plus biotite and/or hornblende in the more intermediate varieties. Perlitic textures, resulting from glass hydration, are sometimes visible (Figure 4.4D). The porphyritic rocks formed as lava flows or as shallow intrusions. They grade into granite porphyries of the felsic plutonic category. Criteria that were used in the field to distinguish tuffs from porphyries were the presence in tuffs of: 1) pumice and lithic fragments, 2) fragmental crystals and 3) glassy, welded textures. Some of the clasts designated as porphyries are certainly tuffs, but recrystallization has sometimes obscured the tuffaceous textures.

#### **4.3.4 Intermediate and Mafic Volcanic**

This category includes fine-grained and porphyritic volcanics such as basalts and andesites. Diabases might also be counted here if they were perceived as fine grained. Like the intermediate and mafic plutonics, these lithologies typically exhibit a low-temperature greenschist facies mineral assemblage. Andesites have the appearance of propylites, with plagioclase altered to albite and epidote, and mafics altered to chlorite, calcite, and iron oxides. Basalts usually contain the “spilitic” assemblage of epidote, chlorite, calcite, iron oxides, and may have quartz-filled amygdules (Figure 4.5A). Intersertal, trachytic, and subophitic textures are common (Figure 4.5B). Although textures are often visible in thin section, extensive alteration has obliterated much of the original mineralogy and texture, particularly when viewed in hand sample. These “greenstones” were the nemesis of this geologist, being the most difficult lithologies to distinguish in the field clast counts.

#### **4.3.5 Quartzites**

The quartzite category includes vein quartz and a spectrum of metaquartzites that range from pure quartz varieties (the most common types) to varieties containing significant percentages of feldspar and clay minerals. Other minerals include zircons, graphite, iron oxides, and iron sulfides that are sometimes concentrated in bands that reflect original bedding and that are sometimes widely disseminated, probably reflecting post-depositional enrichment. Original clastic textures are frequently visible; metaconglomerates are infrequent components. Colors from white to grey to green to purple to black are represented.

#### **4.3.6 Gneiss, Schist**

Schists are mainly biotite quartzo-feldspathic varieties. Gneisses include both orthogneisses that contain mineral assemblages of quartz, microcline, plagioclase,

hornblende, apatite, and sphene, and paragneisses that contain quartz, feldspar, and biotite. Some of the gneissic clasts have a mylonitic appearance (Figure 4.6A). The presence of epidote, chlorite, and sericite in some of the clasts suggests a retrograde metamorphic event.

#### **4.3.7 Low-grade Metasediment**

This category includes metapelites (Figure 4.6B) and metasandstones that are tan to green in color and weakly to nonfoliated. The sandstones are feldspathic arenites to lithic packstones, although the original mineralogy has been somewhat altered. Lithic clasts and matrix materials are often recrystallized to phyllosilicates and clays, imparting a green color to most of the metasandstones.

#### **4.3.8 Miscellaneous**

This category consists of intraclasts of mudstone and siltstone, and clasts that are too weathered to identify because they are totally altered to clay minerals. This category does not exceed a few percent of the total clast population, and so does not significantly bias the compositional counts.

#### **4.3.9 Timing of Clast Metamorphism**

The high-grade metamorphic clast types—gneisses, schists, quartzites—were certainly metamorphosed prior to deposition within conglomerate layers. However, the timing of metamorphism in the lower-grade clast types is less clear. None of the 112 clasts examined in thin section have escaped alteration. The intermediate to mafic igneous lithologies usually contain sub- to lower greenschist facies mineral assemblages. And while these assemblages are less evident in the felsic igneous lithologies, the feldspars are typically altered to turbid-looking albite, sericite, or epidote, and mafic minerals such as biotite and hornblende are altered to chlorite. Pumpellyite is also occasionally found. Quartz and feldspar minerals are frequently

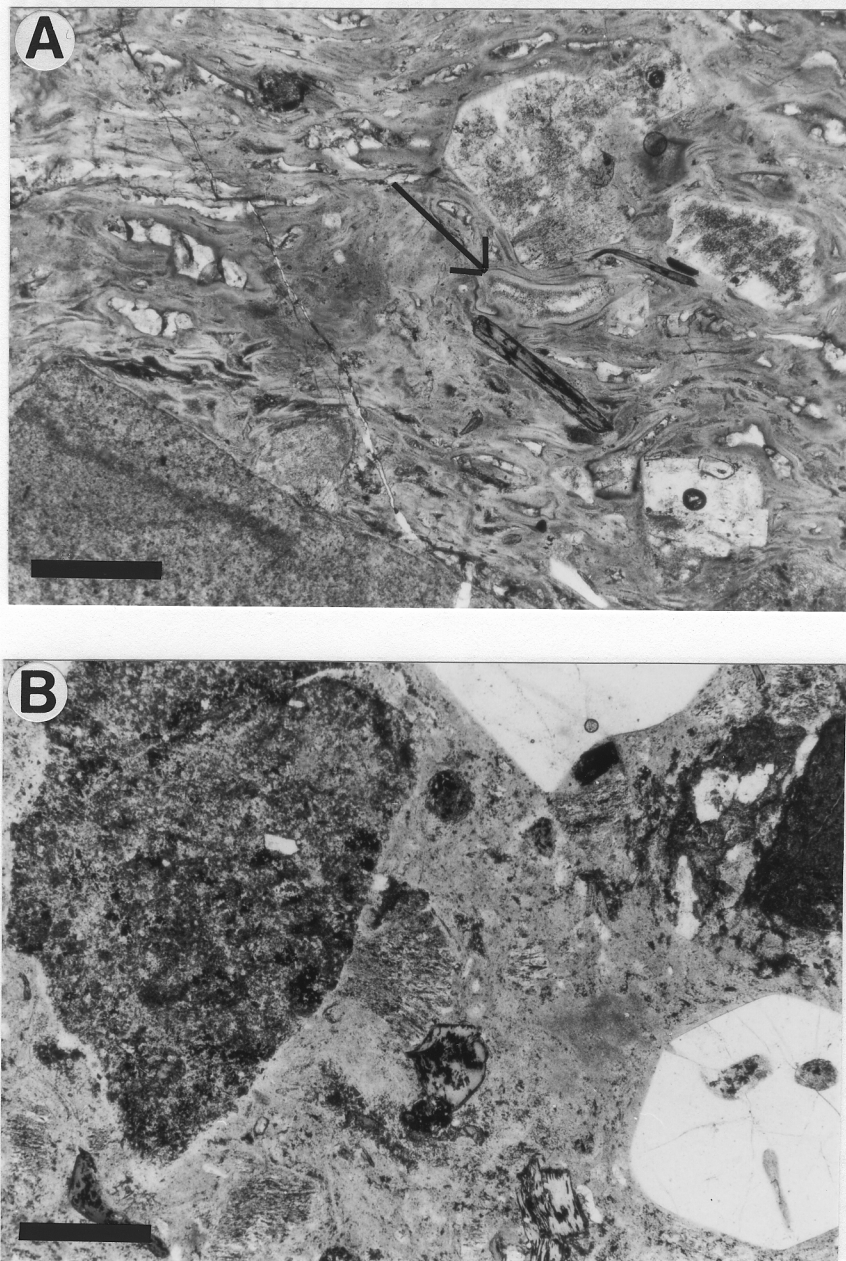


Figure 4.3: Photomicrographs of felsic volcanic clasts. Bar scale=0.5 mm. A) Volcaniclastic clast under plain light, showing axialitic texture of crystal fibers that have replaced glass shards (arrow), crystal pieces, and igneous lithic fragments (lower left corner). B) Volcaniclastic clast under plain light, showing embayed quartz crystals, lithic pieces (upper left corner), and fragmental texture. Biotite in center is altered to chlorite.



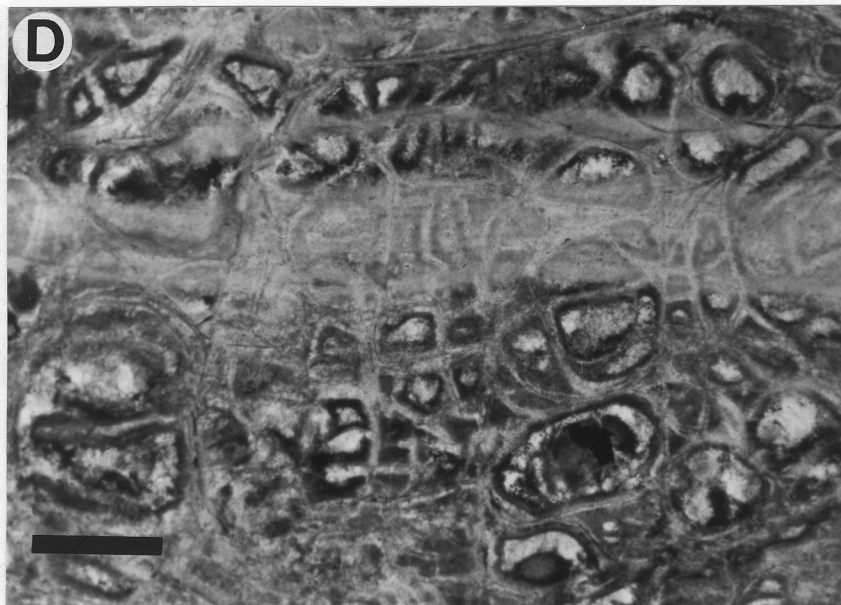


Figure 4.4: Photomicrographs of felsic volcanic clasts. Bar scale=0.5 mm. C) Welded tuff clast under crossed nichols, showing devitrified pumice fragments that are flattened and deflected around rigid lithics. D) Dacitic lava flow clast under plain light, showing perlitic cracks that result from glass hydration (glass is now devitrified), and flow banding.

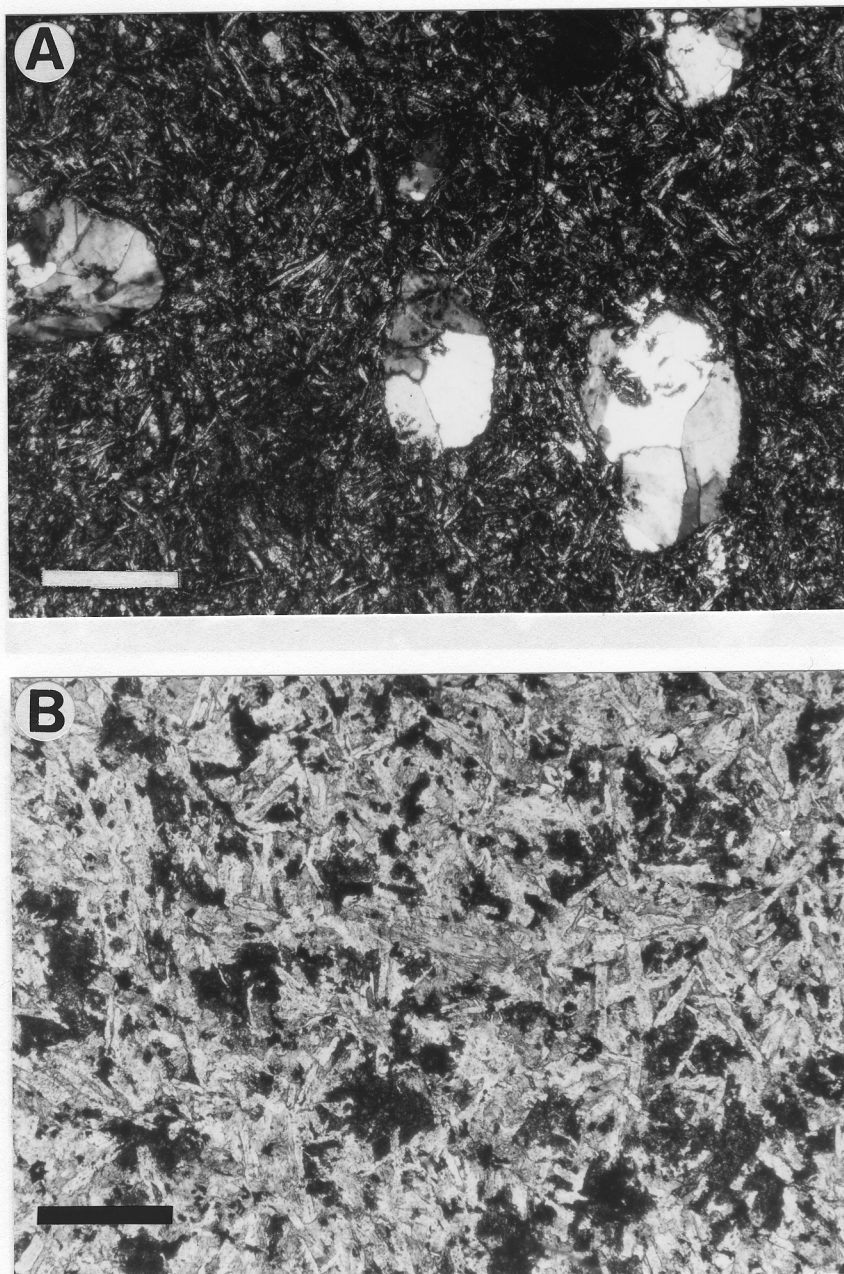


Figure 4.5: Photomicrographs of intermediate and mafic volcanic clasts. Bar scale=0.5 mm. A) Basaltic clast under crossed nichols, showing intersertal texture and quartz-filled amygdules. B) Basaltic-andesite clast under plain light, showing intersertal texture of feldspar laths and interstitial epidote (high relief mineral) and chlorite.



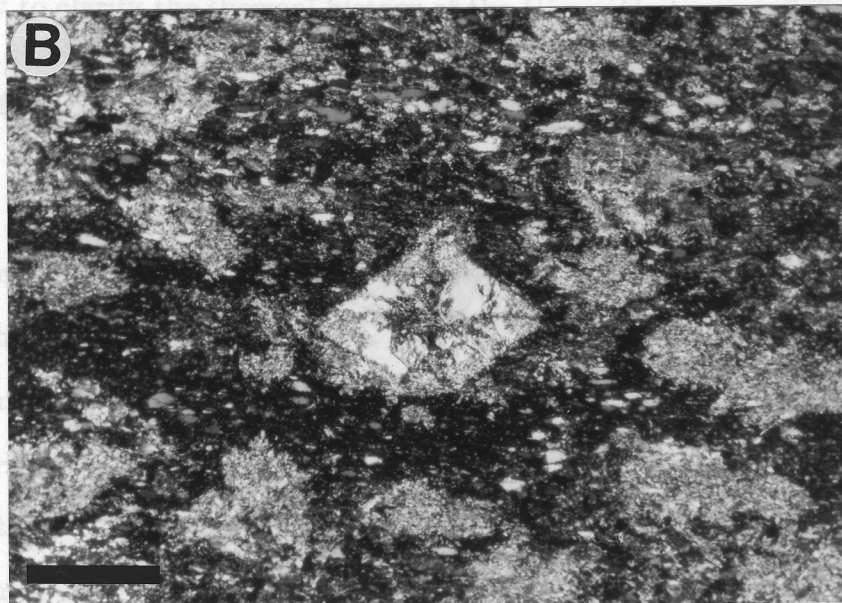


Figure 4.6: Photomicrographs of metamorphic clasts. Bar scale=0.5 mm. A) Gneiss clast under crossed nicols, showing incipient mylonitization. Quartz, feldspar, and biotite minerals are visible. B) Metapelite clast under crossed nicols, showing an andalusite crystal that is partially sericitized from retrograde metamorphism.

recrystallized and clasts have sometimes been infused by iron-rich fluids. The high-grade metamorphic clasts commonly contain epidote, chlorite, and sericite, and contain textural evidence of a retrograde metamorphic event.

Of course, the alterations described above could have occurred in the source region as a result of hydrothermal or deuteric fluids. But it seems a large coincidence that *all* of the clasts have been altered. In addition, the matrix of sandstone sediments in the Upper Cretaceous strata appear to be recrystallized to a sub-greenschist assemblage of clay minerals, and sometimes epidote, pumpellyite, and chlorite. However, many of the sandstones are feldspathic arenites, and do not contain the requisite composition for developing the low temperature metamorphic phases. Also, many of the metamorphic minerals in the sandstones may be detrital. Analyses of the mudstone/shale portion of the sedimentary package are currently underway to clarify the thermal history of the Upper Cretaceous Salinian sequence.

## 4.4 Compositional Clast Counts

### 4.4.1 Pozo Grade and American Canyon

Conglomerate clast data were collected from two sections in the La Panza Range east of the La Panza fault in the southern portion of the Salinian terrane (Figures 4.1 and 4.7). Both sections nonconformably overlie basement rocks, which are granodioritic at Pozo Grade and gneissic at American Canyon (Blackmur, 1978). Both sections are nonmarine at the base and grade upward into nearshore and offshore marine facies rocks, recording the deposition of a transgressing fan-delta system (Figure 4.7). Paleocurrent indicators show an offshore direction toward the south or southwest. Although the American Canyon sequence is located about 7 km south (in the offshore direction) of the Pozo Grade sequence, no faults are evident between the two sections, and the American Canyon area was probably an offshore basement high associated with a rugged topography (Blackmur, 1978). The Upper

Cretaceous strata are continuous to the south into Paleocene and Eocene strata that are predominately deep-water turbidites (Chipping, 1972).

The Pozo Grade and American Canyon sections contain different clast populations, apparently reflecting the different basement lithologies at the two localities (Figure 4.8). The Pozo Grade section has a higher percentage of plutonic clasts, whereas the American Canyon section has a higher percentage of metamorphic clasts. At Pozo Grade, the section loses plutonics and gains felsic volcanics upward, whereas at American Canyon, the percentage of metamorphics remains relatively constant. There is an increase in quartzites relative to gneisses and schists, which probably correlates with the quartzite increase seen in the middle of the Pozo Grade section. It was not possible to sample very far stratigraphically upsection in the American Canyon, but float rocks in the canyon, which upstream drains only basement and Upper Cretaceous rocks, contain numerous felsic volcanic clasts, and this section also probably gains volcanics upward.

The quartzite clasts here are notable because they constitute a large percentage of the total clast population, and include a wide range of types, including white, pink, purple, green, dark grey, and banded varieties. The gneissic clasts, which include both ortho- and paragneisses are also more abundant here than elsewhere in the Salinian terrane, presumably because of the metamorphic basement rocks located nearby. Granodiorites and diorites are common in the Pozo Grade section; chlorite and epidote in clasts suggest metasomatic alteration of these rocks. Andesites and basalts (greenstones) are also represented and are altered. Low-grade metasediments are phyllites, and sandstones that range from feldspathic arenites to lithic packstones. The lithic sandstones comprise green clasts that are difficult to distinguish from greenstones.

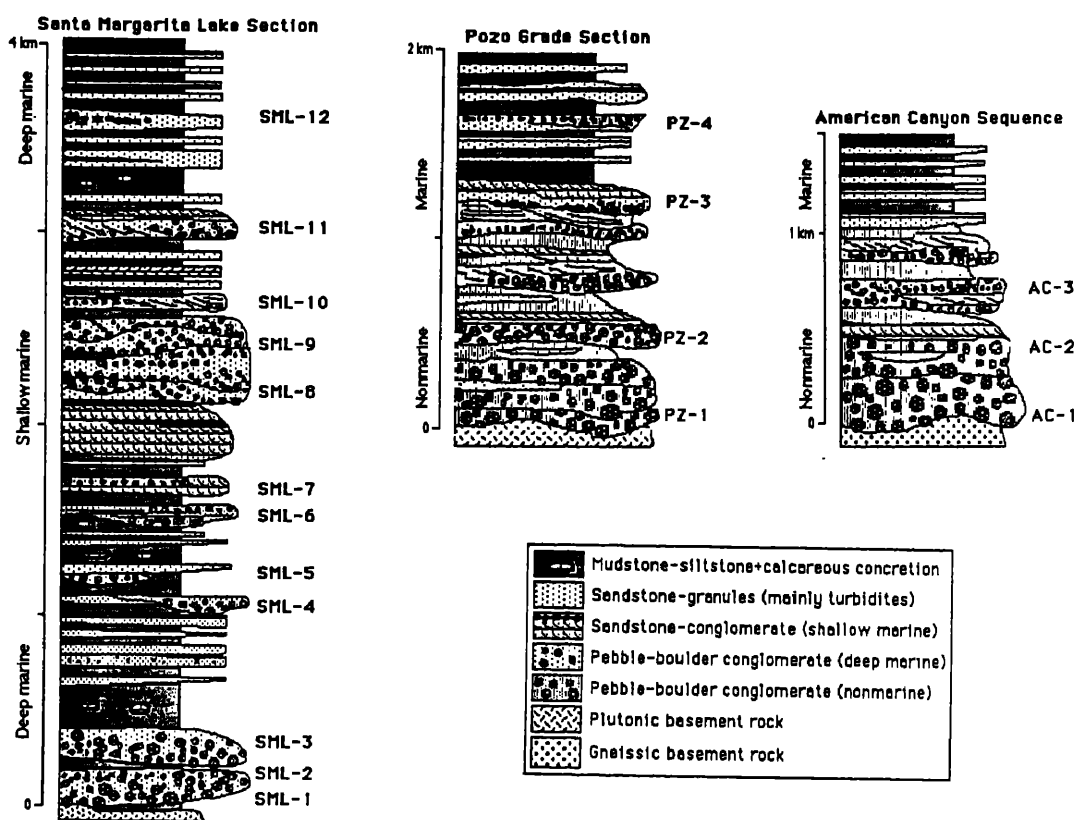
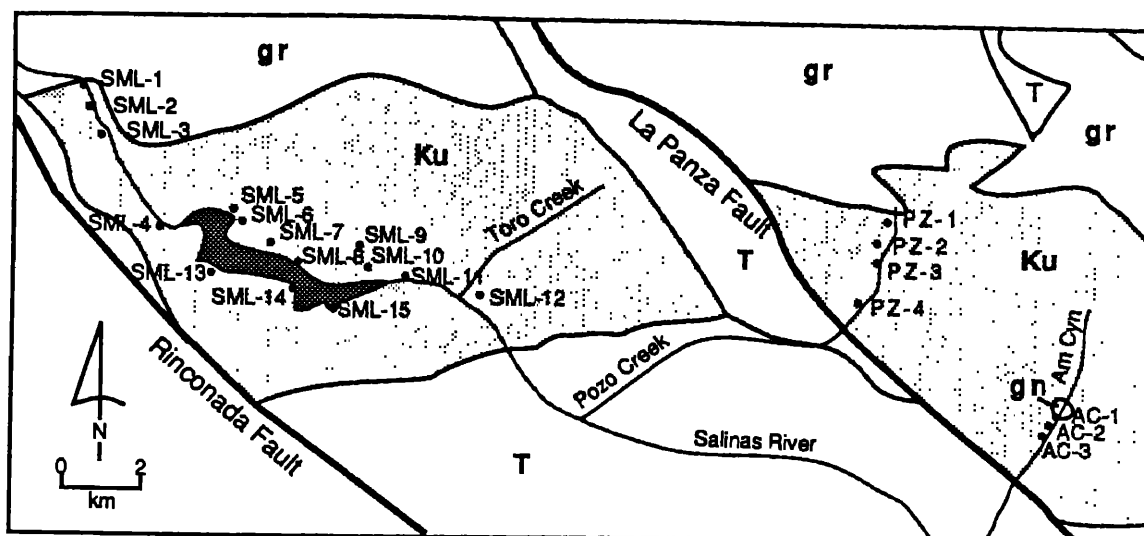


Figure 4.7: Map and generalized stratigraphic sections of Santa Margarita Lake (SML), Pozo Grade (PZ), and American Canyon (AC) areas, showing locations of conglomerate clast counts. See Figure 4.1 for location within the Salinian terrane. Geology on map is simplified from Geologic Map of California, San Luis Obispo sheet; Vedder and others (1986). gr=granitic basement; gn=gneissic basement; Ku=unnamed Upper Cretaceous strata; T=undifferentiated Tertiary strata.

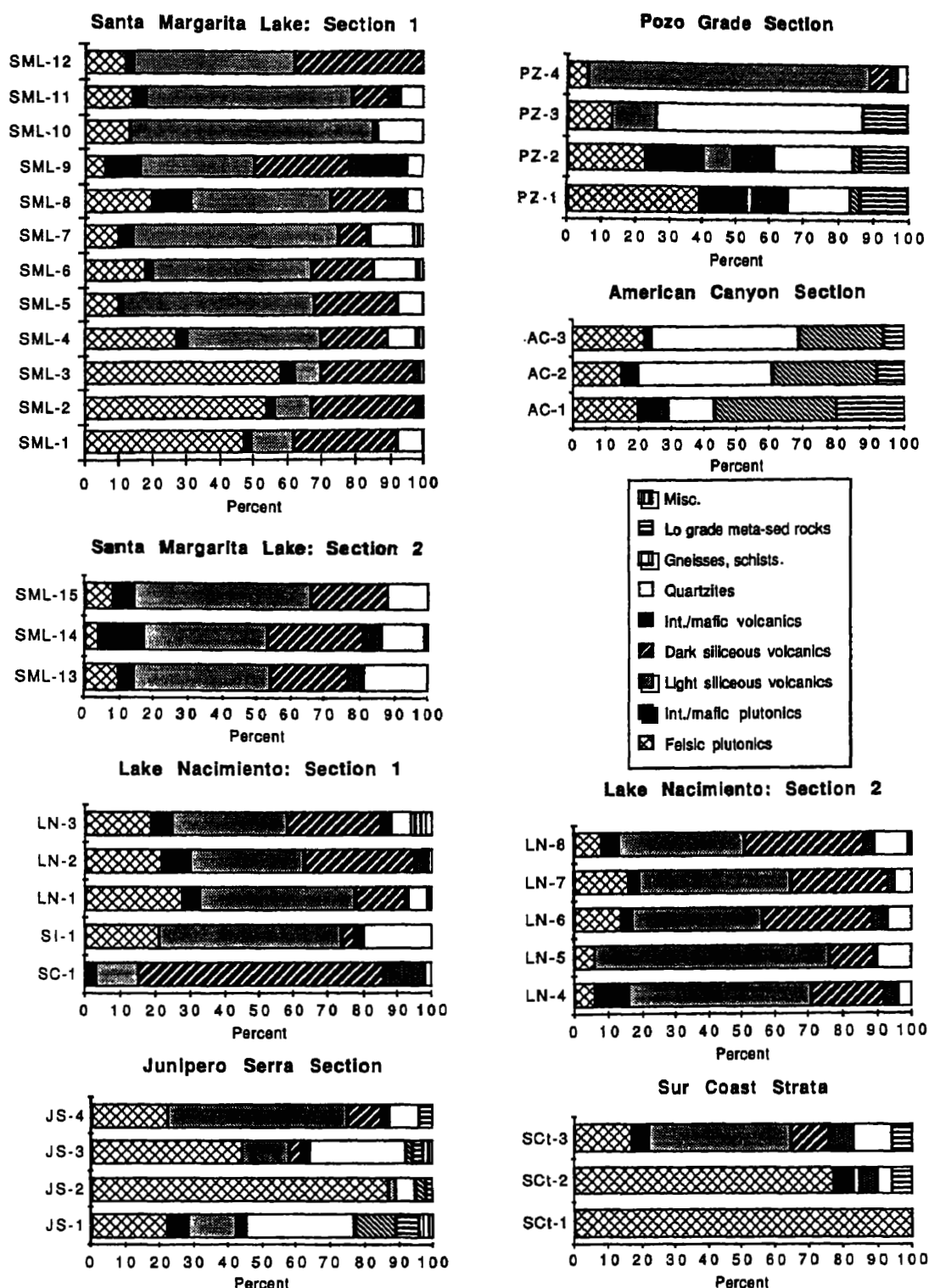


Figure 4.8: Compositional conglomerate clast data for sections from the main portion of the Salinian terrane. Note: Lake Nacimiento, Section 1—SC-1 and SC-2 are not continuous with LN-1 to 3 (see Figure 4.10); Sur Coast Strata—these counts are from isolated outcrops with uncertain time relationships (see Figure 4.11).

#### 4.4.2 Santa Margarita Lake

The Santa Margarita Lake section is west of the La Panza fault and lies nonconformably on a plutonic basement of granodiorite and quartz monzonite (Figure 4.7; Hart, 1976). The section consists at the base of deep-water clastic rocks deposited by sediment-gravity flows, overlain by shoaling shallow-marine sandstones and conglomerates deposited mainly by tractive flow mechanisms. These in turn are overlain by turbidites, which extend across the Cretaceous-Tertiary boundary (Figure 4.7). The offshore direction is toward the south-southwest.

The clast populations at SML-1 to SML-3 at the base of the section are dominated by felsic plutonics and dark green volcanics of intermediate compositions (Figure 4.8). The plutonic clasts are frequently boulders with diameters up to 1 or 2 meters. Their large percentage and size probably reflects a proximal derivation from basement that was exposed on steep, submarine slopes. Plutonics become less frequent upsection and the volcanic clast populations become dominated by light-colored varieties. The dark-colored varieties are more likely to be grey or black and more siliceous than the types at the base. Several counts were completed on the south side of Santa Margarita Lake to test for any major lateral variations, but none were found (Figure 4.8).

The sedimentary sequences are distinctly different on the east and west sides of the La Panza fault, which has been most recently active as a northeast-side-up thrust fault (Figure 4.7; Dibblee, 1971). Similar basement lithologies across the fault (Ross, 1972) negate the existence of large horizontal displacements. Figure 4.9 presents a possible scenario to explain the observed lack of a deep-water basal sequence on the east side of the La Panza fault. Sediments onlap a basement high from the southwest, and are overlain by a progradational-retrogradational sedimentary wedge, thus producing a regressive-transgressive sequence at the Santa Margarita Lake locality and just a transgressive sequence at the Pozo Grade/American

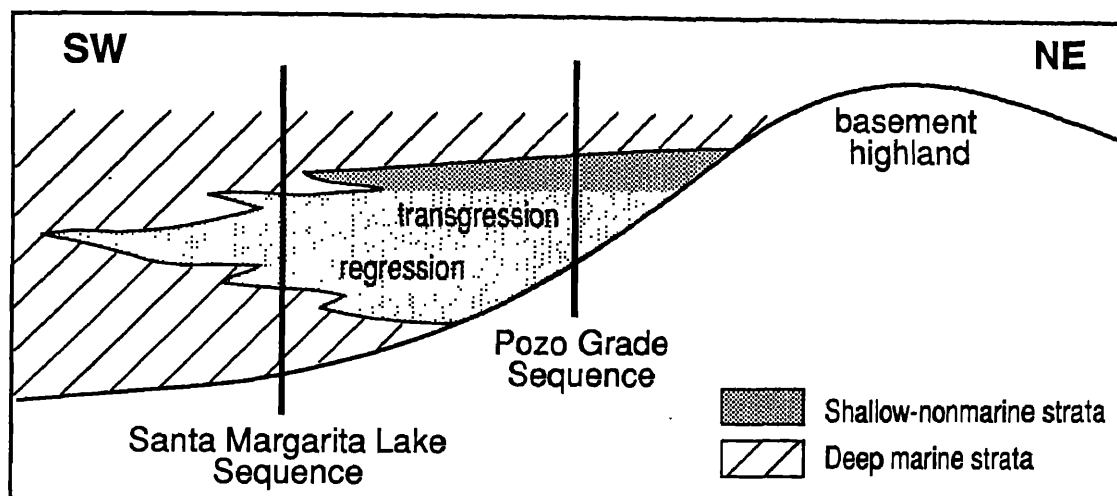


Figure 4.9: Scenario to explain the different sequences seen on opposite sides of the La Panza fault (see Figure 4.7). Onlap of a basement high toward the northeast is followed by a regressive-transgressive couplet, thus producing a deep-shallow-deep sequence at Santa Margarita Lake and a shallow-deep sequence at Pozo Grade. This interpretation is supported by sediment thinning toward the northeast, paleocurrent directions toward the southwest, and similar conglomerate populations from the midsection counts at Santa Margarita Lake and from the basal counts at Pozo Grade.

Canyon localities. This interpretation is supported by conglomerate data and by paleocurrent indicators that predict more offshore facies toward the west-southwest. According to the scenario in Figure 4.9, the nonmarine base at Pozo Grade should correlate with the shallow-marine midsection at Santa Margarita Lake. SML-8 and 9 are counts from the midsection conglomerates (Figure 4.7). They show an influx of intermediate to mafic plutonic and volcanic clasts that are similar to clast types found at the base of the Pozo Grade section (Figure 4.8). This occurrence is consistent with at least a partially shared source area at this time.

#### 4.4.3 Lake Nacimiento

Basement rocks are not exposed at the latitude of Lake Nacimiento, which is located about 60 km northeast of Santa Margarita Lake (Figure 4.1). The base of the Upper Cretaceous section is truncated by faulting and the top is disconformably overlain by Tertiary strata (Figure 4.10; Dibblee, 1972). The section is shallow marine at the

base and is transgressive upward into deep-water turbidites. Facies relationships and paleocurrent directions indicate an offshore direction toward the southwest. Additional Upper Cretaceous sediments to the west in the Hunter-Liggett Military Reservation are truncated at the base by the Nacimiento fault (Figure 4.10). This section is probably slightly older than the one around Lake Nacimiento and consists of deep-water turbidites.

The conglomerate count from the base of the section in the Hunter-Liggett Military Reservation is dominated by dark green tuffs and intermediate volcanics. The other Hunter-Liggett sample, as well as the samples from around Lake Nacimiento, is dominated by felsic volcanics. Signification percentages of felsic plutonics and quartzites are also represented (Figure 4.8).

#### **4.4.4 Junipero Serra Peak and Big Sur Coast Areas**

An Upper Cretaceous section west of Junipero Serra Peak, about 60 km northeast of Lake Nacimiento, lies nonconformably on a heterogeneous plutonic and metamorphic basement and is overlain by Paleocene and younger Tertiary rocks (Figures 4.1 and 4.11; Compton, 1966). The rocks are poorly exposed and inaccessible, so the composite section (Figure 4.11) is somewhat speculative. Ruetz (1976) listed metamorphic and plutonic lithologies as the dominant clast types in both the Paleocene and Upper Cretaceous conglomerates. But although gneisses and schists were found in this study, particularly at the base of the section, they were not found in the amounts previously described (Figure 4.8). The count at the top of the Upper Cretaceous section is dominated by felsic volcanic clasts and is a population similar to those from around Nacimiento and Santa Margarita Lakes.

One count is dominated by felsic plutonic clasts and is similar to two counts located along the coast (SCt-1 and 2 in Figure 4.8). These conglomerates occur in thick, disorganized beds and may be parts of the same slope-channel deposit



that has been dismembered by Tertiary faulting and folding. The Sur Coast Upper Cretaceous strata occur in fault-bounded slices as incomplete sections (Figure 4.11). SCt-3 contains the usual felsic volcanic-dominated clasts. It was placed above the other counts because this relationship is consistent with that seen at other localities—younger parts of sections are generally dominated by these volcanics.

#### **4.4.5 Pigeon Point Formation**

The Pigeon Point Formation is an Upper Cretaceous sequence located about 50 km south of San Francisco, west of the San Gregorio fault (Figures 4.1 and 4.12). The section structurally overlies and is disconformably overlain by younger Tertiary units. Most of the sediments are deep-sea turbidites, although shallow-marine rocks occur at the top of the section (Figure 4.12; Lowe, 1979).

Clast populations at Pigeon Point differ somewhat from those to the south in the main part of the Salinian terrane. "Greenstones" and low-grade metasandstones make up a large percentage of the total clast population, although these lithologies decrease somewhat upsection (Figure 4.12). Siliceous volcanics are abundant, but dark-colored varieties are more common than in the previously discussed sections. In addition, quartzites are less common, and intermediate and even some mafic plutonic lithologies are well represented. Although chert has been described elsewhere as a prevalent lithology (Hall and others, 1959), most of the red and black chert-like clasts are volcanic aphanites or sparse porphyries. Several green and red chert clasts were found, although not in quantities sufficient to appear in the clast count data. Two clasts contain radiolarians that are Late Jurassic in age (Bonnie Murchy, pers. comm.).

#### **4.4.6 Gualala Formation**

The Gualala Formation is an Upper Cretaceous section located in the Point Arena terrane, an enigmatic locality because the sedimentary sequence structurally overlies

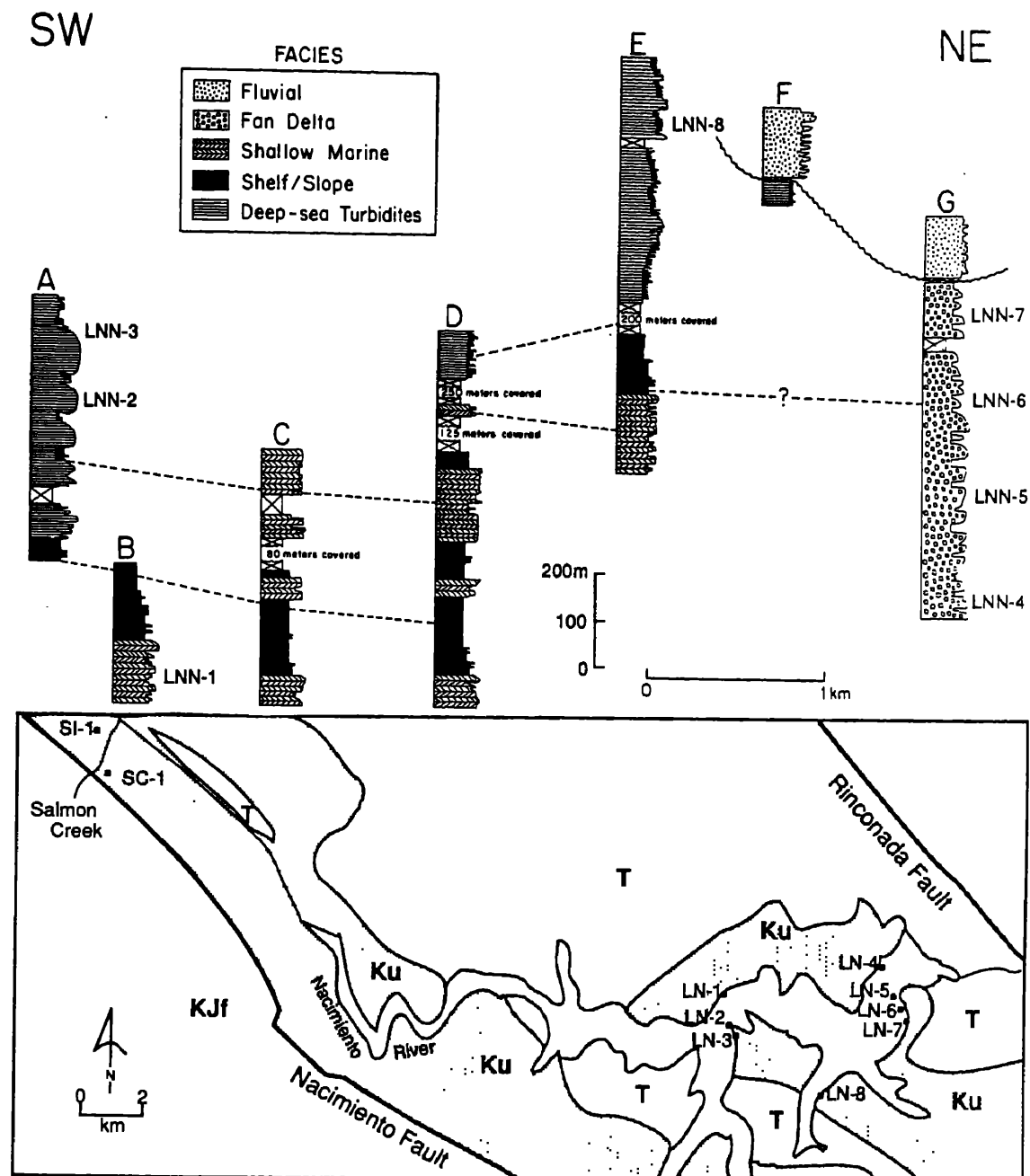


Figure 4.10: Location map and stratigraphic sections of Lake Nacimiento (LN) area, showing locations of the conglomerate clast counts. See Figure 4.1 for location within the Salinian terrane. Geology on map simplified from the Geological Map of California, San Luis Obispo sheet. Stratigraphy from Grove (1986). KJf=Franciscan Complex; Ku=unnamed Upper Cretaceous strata; T=undifferentiated Tertiary strata; SC=Steve Creek Fm and SI=Shut-In Fm (Seiders, 1989).

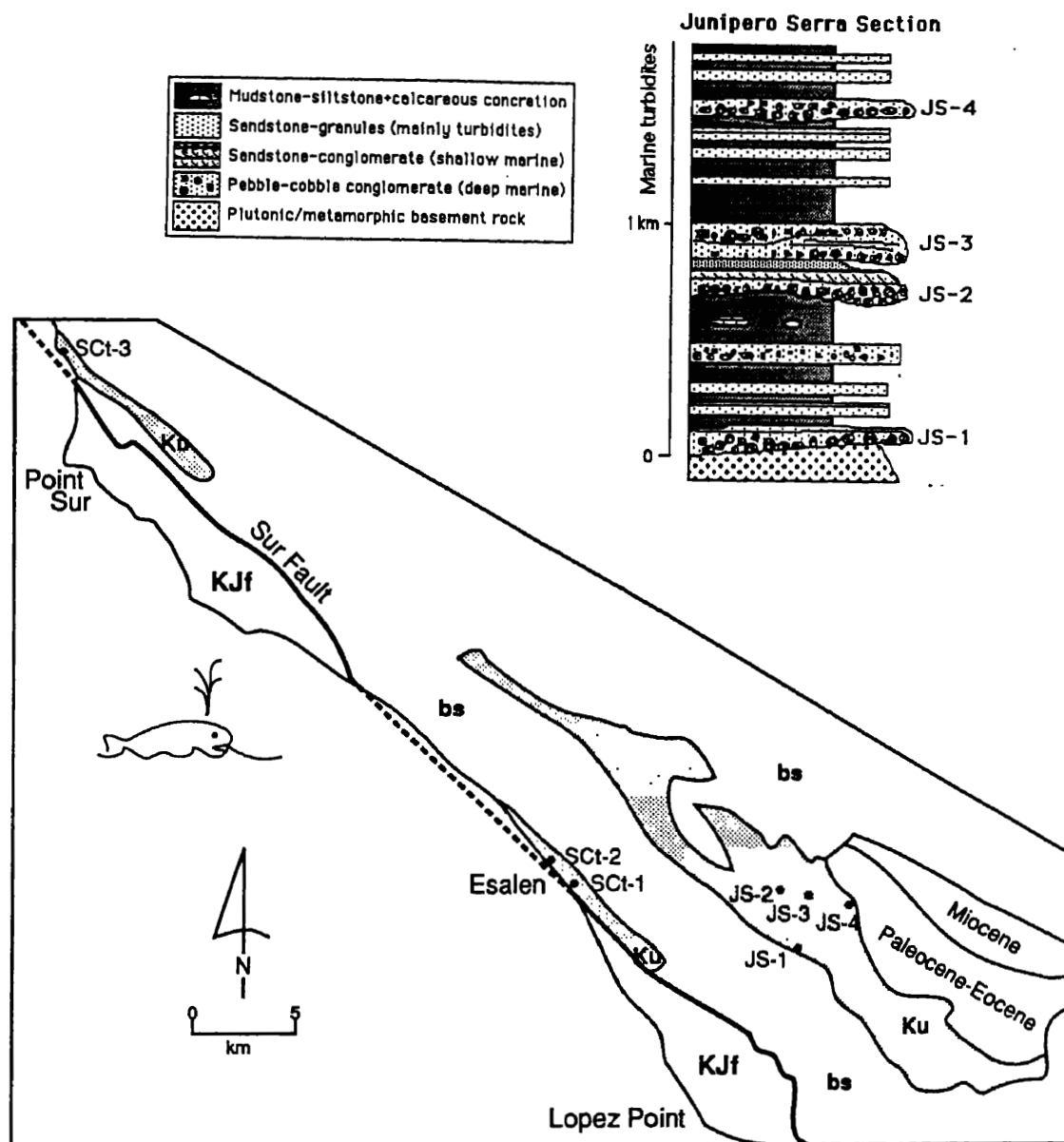


Figure 4.11: Map and generalized stratigraphic section of Big Sur Coast (SCt) and area west of Junipero Serra Peak (JS) in the Ventana Wilderness, showing conglomerate localities. See Figure 4.1 for location within the Salinian terrane. Geology on map simplified from the Geological Map of California, Santa Cruz sheet. KJf=Franciscan Complex; bs=plutonic/metamorphic basement complex; Ku=unnamed Upper Cretaceous strata.

metabasaltic and metadiabasic rocks (so called "spilites") that, although located west of the San Andreas fault, have a greater affinity to the Franciscan assemblage than to the basement rocks of the Salinian terrane (Wentworth, 1966; Figures 4.1 and GF). The Gualala Formation is disconformably overlain by younger Tertiary strata. The Upper Cretaceous sedimentary sections and correlations (Figure 4.13) that form the framework for the conglomerate data are adapted from Wentworth (1966). However, sections are highly disrupted by faults and the biostratigraphy is practically nonexistent. A reconnaissance survey of these rocks for the present study suggests that the available correlations are probably not entirely accurate, but considerable work is required for their improvement.

The Gualala Formation clasts more closely resemble the Pigeon Point clasts than populations in other parts of the Salinian terrane (Figure 4.13). "Greenstones" and low-grade metasediments are prevalent. In the Anchor Bay Member, metagabbros and metabasalts predominate. They contain the usual greenschist mineral assemblage. Although Wentworth (1966) found no clasts similar to the underlying metabasaltic rocks, some of the clasts sampled in this study from the Anchor Bay Member are similar, both in hand specimen and thin sections. Populations from the Stewart's Point Member contain numerous felsic volcanic clasts and are similar to the Salinian terrane clasts.

## 4.5 Implications

### 4.5.1 Provenance Constraints

The Upper Cretaceous conglomerate clasts were derived from a magmatic arc terrane that included plutonic, volcanic, and metamorphic lithologies. Felsic to intermediate plutonic clasts are similar to Salinian basement rocks, which were rapidly uplifted during the Campanian stage (Mattinson and James, 1985) and exposed to erosion. Metamorphic clasts are especially prevalent in the southeasternmost sec-

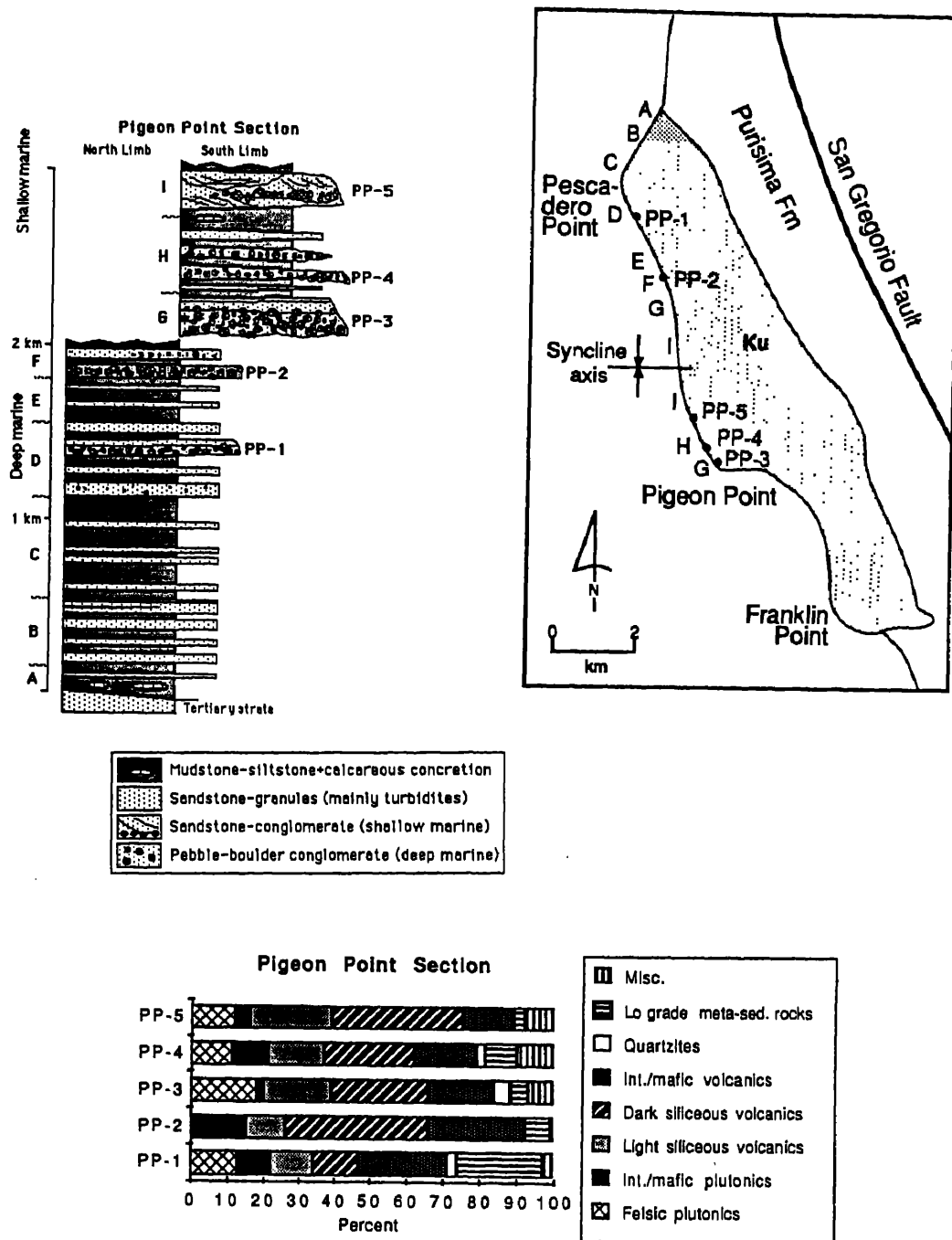


Figure 4.12: Map, generalized stratigraphic section, and conglomerate count data from the Pigeon Point (PP) area along the San Mateo County coast, showing conglomerate localities. See Figure 4.1 for location within the Salinian terrane. Geology on map simplified from the Geologic Map of California, San Francisco sheet. Ku=Pigeon Point Formation (Upper Cretaceous). Stratigraphy modified from Lowe (1979). Letters A-I refer to Lowe's (1979) subdivisions.

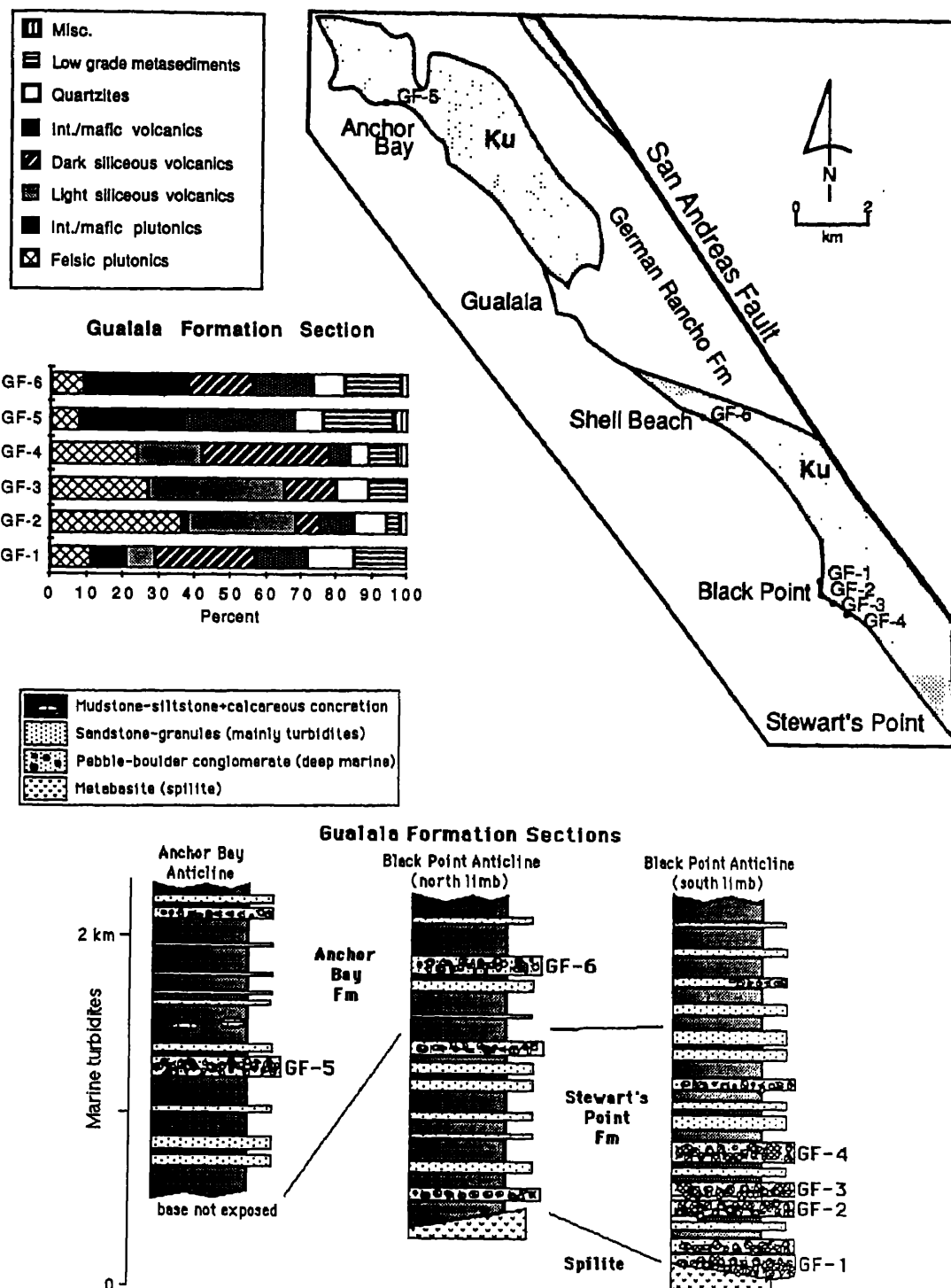


Figure 4.13: Map, generalized stratigraphic sections, and conglomerate count data from the Point Arena terrane. See Figure 4.1 for location. Geology on map simplified from the Geologic Map of the Santa Rosa Quadrangle (Cal. Div. of Mines and Geology). KJf=Franciscan Complex; Ku=Gualala Formation (Upper Cretaceous); GF=Gualala Formation. Stratigraphy modified from Wentworth (1966). Note, however, that the correlations are poorly constrained.

tions located at Pozo Grade and American Canyon. Gneissic basement is exposed at American Canyon and west of the San Juan-Chimeneas fault (Figure 4.1) in the Barrett Ridge slice (Ross, 1972), a block that has been associated with other crustal fragments in southern California as part of the Tujunga terrane (Blake and others, 1982). These basement rocks provide a likely source for the gneissic and schistose clasts. Quartzite lithologies, however, are not widely represented in nearby basement rocks, and the great quantity of quartzite clasts found in the southeast sections remains enigmatic. Quartzite clasts are also represented in the other conglomerate populations sampled, but in lesser amounts. These clasts are extremely durable rocks, and their percentages in the clast populations are probably overrepresentations of their percentages in the source region. For example, Abbott and Peterson (1978) experimentally showed that highly resistant clasts, such as quartzites and felsic volcanics, abrade less resistant rocks types, thus greatly reducing their numbers in the sedimentary record.

Metamorphic basement rocks are extensively exposed in the northern Santa Lucia Range near Junipero Serra Peak, and these lithologies are present in the local clast populations, particularly at the base of the section. Compton (1966) and Weibe (1970) describe zircon-rich and graphite- and pyrite-bearing quartzites in the northern Santa Lucia Range that sound similar to the Salinian quartzite clasts.

The felsic volcanic clasts, because of their absence in the basement rocks of the Salinian terrane and because they are very hard, durable rocks, have been previously described as "exotic" clasts with a multicyclic history (Howell and Vedder, 1978; Vedder and others, 1982). However, U/Pb age data obtained from two zircon populations extracted from a rhyodacitic boulder sampled at Lake Nacimiento show a volcanic age of 112 Ma, and a xenocrystic age of 1.6 Ga (see Chapter 5). These ages are similar to ages from Salinian plutonic basement rocks (Mattinson and James, 1985) and do not require an exotic source area. It is possible, of course, that

the volcanic clasts were derived from multiple sources. But the common occurrence of felsic components such as quartz, biotite, and hornblende phenocrysts in the volcanics does require that the source be a mature continental arc. In addition to the felsic volcanics, there are intermediate to mafic varieties that are much less resistant and therefore more difficult to recycle.

The clast populations in the Pigeon Point and Gualala Formations contain lithologies similar to the other Salinian terrane populations, but they have greater percentages of intermediate to mafic volcanic and plutonic clasts. Lee-Wong and Howell (1977) also described differences in the sandstone petrology of Pigeon Point sediments compared to those from other parts of the Salinian terrane.

Although the Pigeon Point conglomerates include some chert clasts, these cherts do not contain radiolarians that are similar to radiolarians derived from Franciscan assemblage cherts (Bonnie Murchy, pers. comm.). A gabbroic clast from the Gualala Formation has a minimum Jurassic age of 161 to 163 Ma (James and others, 1986). These data are consistent with derivation from Jurassic island arc terranes similar to those found in the foothills belt along the western edge of the Sierra Nevada Range. Some of the clasts from the Anchor Bay Member of the Gualala Formation are similar to metabasaltic rocks that are exposed in the Point Arena terrane, but whose origin is still poorly understood.

If 115 km (Graham and Dickinson, 1978) to 150 km (Clark and others, 1984) of right-lateral offset is restored across the San Gregorio fault (Figures 4.1 and 4.12), the Pigeon Point Formation returns to a position west of the Nacimiento fault zone, where some of the Upper Cretaceous conglomerates are described as containing numerous "greenstone" lithologies that sound similar to the Pigeon Point and Gualala Formation clasts (Hall and others, 1979). The terranes east and west of the Nacimiento fault may have been juxtaposed by Late Cretaceous time (Vedder and others, 1982), but this hypothesis has not been thoroughly tested and remains



tentative. In any case, the Pigeon Point and Gualala Formations seem to bear a closer affinity to the Upper Cretaceous sediments west of the Nacimiento fault (Sur-Obispo terrane) than to those east of the fault in the Salinian terrane.

The clast data reviewed here are compatible with a Sierra Nevada arc source, assuming restoration of about 300 km of Neogene offset across the San Andreas fault. The two component—middle Cretaceous and Precambrian—volcanic age data are similar to data obtained from volcanic rocks in southern Sierran roof pendants (Cathy Busby-Spera, pers. comm.). The southern portion of the Sierran batholith was built on continental crust, so the associated volcanic rocks are predominately felsic varieties similar to the Salinian clasts. Metamorphic rocks, including quartzites, are available in the San Bernardino Mountains and Mojave Desert region (Burchfiel and Davis, 1981), and the Sierran foothills belt was once probably continuous to the south (Sams and Saleeby, 1988), providing a source for the intermediate to mafic clasts.

It is more difficult though, to make comparisons in southern Mexico, where paleomagnetic data suggest that similarities should be found. Precambrian metamorphic rocks occur in the Oaxacan terrane and Mesozoic arc rocks occur in the Guerrero terrane (Ruiz and others, 1988). The arc rocks are poorly dated, however, and although only Jurassic ages have been obtained so far, Cretaceous ages cannot be ruled out (Joaquin Ruiz, pers. comm.). Thus, more data are required from this area before its potential as a source for Salinian conglomerates can be properly evaluated.

Locating the specific source area is complicated by the existence of Cretaceous magmatic arcs along much of the western margin of North America. For example, Dickinson (1982) showed that sandstones exposed within fore-arc regions of the circum-Pacific region have similar compositions everywhere. Still, considering the diverse suite of clast types represented in the Salinian conglomerates, future

comparisons should significantly narrow the range of viable source terranes.

#### 4.5.2 Source Area Evolution

The conglomerate data also point to changes in the sediment source area through time. An observation common to the sections (excluding Pigeon Point and Gualala) is that basal clast populations are dominated by a variety of lithologies compatible with basement rock types, whereas younger populations are dominated by felsic volcanic lithologies that are unknown from within the basement complex (Figure 4.8). Consequently, the basal counts from the various sections differ markedly from one another, while the upper counts are similar. Figure 4.14 summarizes the conglomerate data from the Salinian sections, emphasizing the tendency toward dominance by felsic volcanic clast populations in the upper portions of the sections.

This lithologic change probably reflects a change from local to more distant sediment sources as a rugged topography with short drainages evolved into a more mature landscape with integrated drainages. The felsic volcanics (and also the quartzites), being durable rock types, are capable of long distance transport without disintegration. These clasts are generally well rounded and sometimes polished, consistent with prolonged abrasion by stream transport, whereas the plutonic and intermediate to mafic volcanic clasts generally have more angular shapes. Figure 4.5.2 summarizes the hypothesized paleogeographic setting, wherein short drainages supply locally derived sediment to a basin that is newly formed following uplift of Salinian basement rocks. Following basin filling, increased tectonic activity produced renewed conglomerate influx and increased basin subsidence. Throughout this time, drainages became more fully integrated and were thus able to tap more distant sediment sources. A similar evolution from local to distant source areas was hypothesized by investigators of Eocene conglomerates in southern California (Kies and Abbott, 1983).

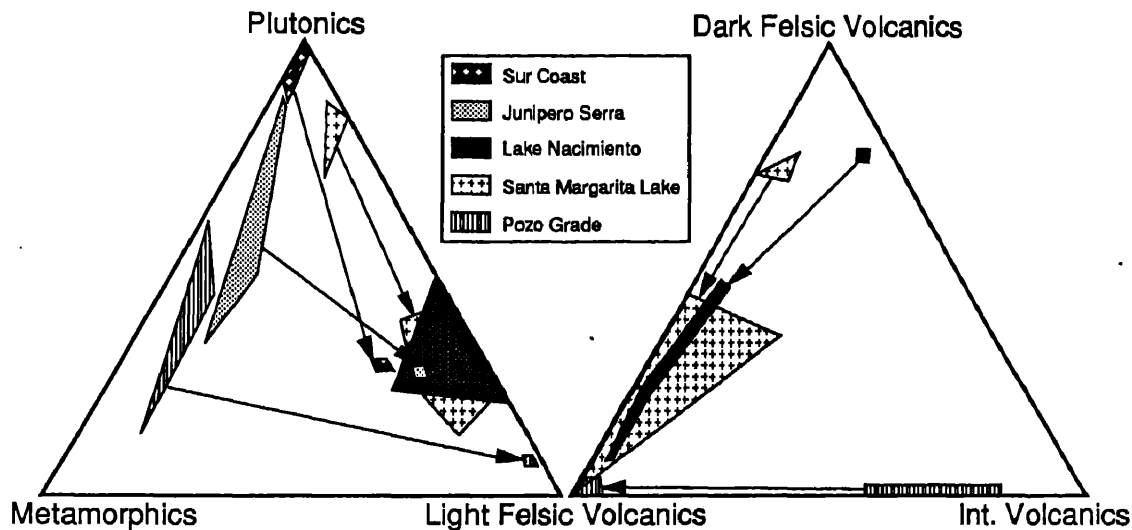


Figure 4.14: Summary diagram of conglomerate data from the main portion of the Salinian terrane. Arrows point from the bottom to the top of the various sections. Outlined areas are fields of data points for each section. Two ternary diagrams are used to show all of the data; the three composition types on each diagram are normalized as a percentage of 100. For unnormalized percentages, see Figure 4.8. Shown here are upsection changes from plutonic and metamorphic to light-colored felsic volcanic clasts and from dark-colored felsic and intermediate volcanic to light-colored felsic volcanic clasts, probably reflecting an evolution from local to more distant sediment source areas. Note that age relationships for the conglomerate localities on the Big Sur coast are unclear.

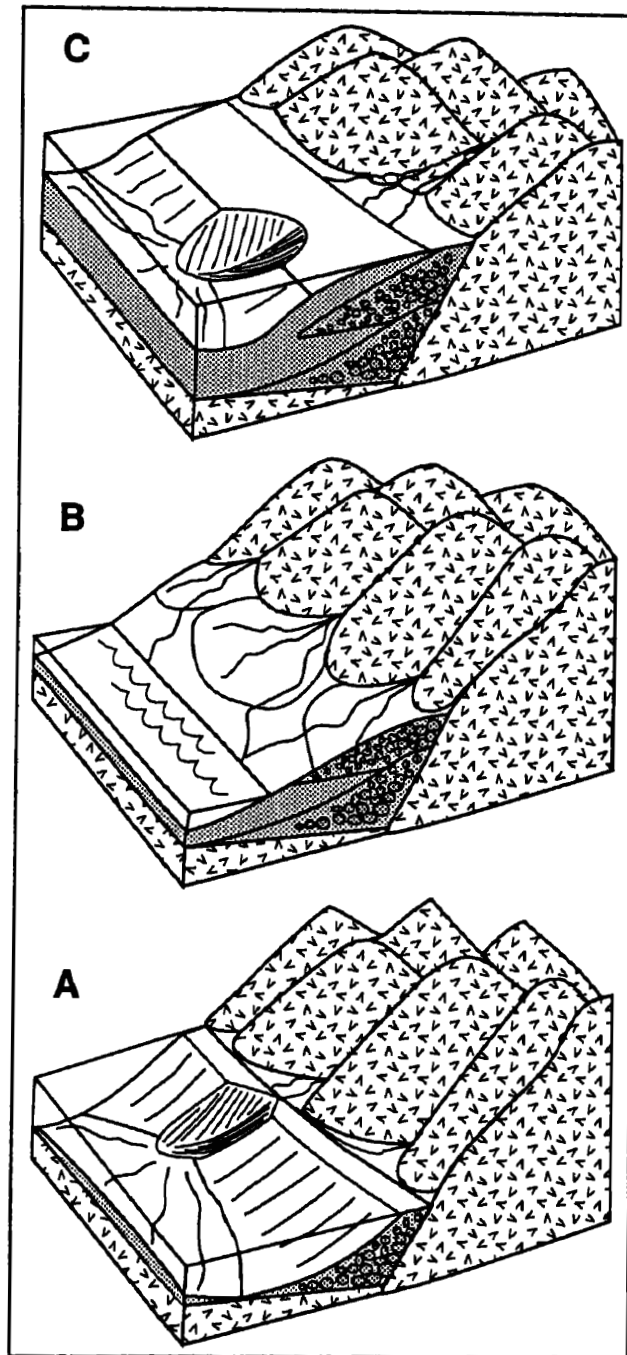


Figure 4.15: Model for Late Cretaceous Salinian basin. A) The basin forms, following uplift of basement rocks. A steep topography associated with a narrow shelf and short drainages typify the setting. Turbidity currents deposit sediments derived from local basement rocks. B) The basin fills, although subsidence continues, accomodating a thick shallow-marine section. Renewed tectonic activity induces a large conglomerate influx and subsidence increases. Drainages become better integrated, and rivers tap sediment from more distant sources. C) Subsidence accelerates and the basin deepens. Deep-sea turbidites are deposited continuously across the Cretaceous/Tertiary boundary. Conglomerate populations are dominated by felsic volcanic clasts brought to the coast by rivers.

### 4.5.3 Stratigraphic Relationships

Biostratigraphic information from the Upper Cretaceous Salinian sediments rarely provide more detail than Upper Campanian to Maastrichtian stage, a range that encompasses the entire stratigraphic column. Unfortunately, the conglomerate composition variations are generally not sufficiently distinctive to augment the biostratigraphy. Investigators of Paleogene conglomerates from the Salinian terrane found clast types that were considered unique enough to correlate between sections (Bachman and Abbott, 1988). No clasts found in this study, however, were felt to be sufficiently unique for this purpose. Nevertheless, variations in clast compositions do support several stratigraphic relationships (Figure 4.8). Similarities between midsection counts at Santa Margarita Lake and basal counts at Pozo Grade support the correlations illustrated in Figure 4.14. Dominance of felsic plutonic clasts in populations from the Junipero Serra section and the Sur Coast strata suggests that these areas were once continuous and that lateral offset along the Coast Range fault between them has been slight. And the dominance of volcanic populations by dark green types, usually tuffs, in the basal counts at both Nacimiento and Santa Margarita Lakes (SC-1 and SML-1 to 3 in Figure 4.8), may support their correlation.

In general, the similar clast populations from the various Salinian sections (Figure 4.8) and the similar evolution within these sections from local to distant sources discussed previously (Figure 4.14), suggest that these sediments were deposited in a single, laterally continuous basin. Although previous descriptions have suggested Late Cretaceous deposition in separate basins within the Salinian terrane (Vedder and others, 1982), it is here proposed that the now separated sections were once part of a continuous, coherent basin and their present outcrop distribution reflects Cenozoic uplift, tectonism, and erosion. The Pigeon Point and Gualala localities may have been separate depositional centers, but the relationship of these areas to

the main portion of the Salinian terrane remains uncertain.

The specific clast compositions vary considerably from bed to bed over short vertical and lateral distances (see Appendix C), a predictable result considering that specific sedimentary facies also vary rapidly. These details suggest an unstable setting, where uplift and faulting were exposing new source areas and producing sporadic episodes of accelerated and decelerated basinal subsidence.

## 4.6 Summary

A wide variety of rock types are represented in the Upper Cretaceous Salinian conglomerate clasts. Compositional and age data from these clasts place constraints on possible source areas and provide a base for future comparison with these areas. The source area must include a mature magmatic arc of Cretaceous age built on Precambrian continental crust (similar to the southern Sierran arc), and metamorphic rocks, notably quartzites and gneisses. At least at Gualala, the source area must include Jurassic-aged magmatic arc rocks, probably with an oceanic affinity.

Upward variations in clast compositions demonstrate an evolution from local to distant sources, probably reflecting the progressive integration of drainages in a maturing topography. Compositional variations also suggest correlations between now separate sedimentary sections and support the interpretation of basin contiguity, at least for the main portion of the Salinian terrane. A tectonically active setting caused rapid variations in specific clast populations over short lateral and vertical distances.

## Chapter 5

# Model For Late Cretaceous Basin Formation Within the Central Salinian Terrane

### 5.1 Introduction

The Upper Cretaceous strata of the Salinian terrane have been previously described as the sedimentary fill of a series of sub-basins formed within a strike-slip dominated tectonic setting similar to the continental borderland that exists off the coast of southern California today (Howell and Vedder, 1978; Vedder and others, 1982). This interpretation provides a mechanism for accomplishing the large amount of post-Cretaceous northward translation that discrepant paleomagnetic data require (Champion and others, 1984; Kanter and Debiche, 1985; Howell and others, 1987). Many geologists question the validity of reconstructions that make the Salinian terrane an exotic, far-travelled crustal fragment, however—primarily because they find many similarities between Salinian and southern Californian basement rocks, respectively west and east of the San Andreas fault zone (Dickinson, 1983; Ross, 1984; Silver and Mattinson, 1986; Hamilton, 1988; James and Mattinson, 1988).

This chapter summarizes an investigation of the Upper Cretaceous strata within the Salinian terrane and reinterprets the Late Cretaceous basin as a single depocenter formed within a transtensional setting during a time of oblique subduction. But

although strike-slip faulting may have been an important part of the general setting, extension-induced normal faulting seems to have been the dominant control on specific basinal development. Furthermore, the specifics of this basin's formation can be incorporated into a model that is consistent with a location in southern California prior to northward translation along the Neogene San Andreas fault zone. The model involves Late Cretaceous dextral offset within the Sierran magmatic arc, producing an east-west trending intra-arc graben south of the present-day Sierra Nevada Range. West-vergent thrusting and regional uplift are also primary players in the tectonic scenario.

I choose the conservative approach of a southern California restoration because:

- 1) data uncovered in the present study do not contradict this reconstruction, and
- 2) the specific geology of southern Mexico and Central America is not yet sufficiently known to allow detailed comparisons in the area where paleomagnetic data suggest derivation. My goal is to develop a working model for generating the Late Cretaceous Salinian basin, regardless of its specific geographic origin, and then to test that model in the readily accessible locality of southern California. It is herein recognized that gross similarities across a fault zone do not necessarily imply unique correlations, because similar tectonic processes were operating for thousands of kilometers along the western coast of North and South America during the Mesozoic Era and producing similar lithologic sequences along this length. Nevertheless, an improved understanding of the Salinian terrane sequence should facilitate future attempts at establishing believably unique correlations across the San Andreas fault zone.

In the following text, I first present a generalized basin model, followed by the stratigraphic and petrographic evidence for the model. I then evaluate the model within a regional context, by comparing the Salinian sedimentary sequences to similar Upper Cretaceous successions located nearby, and by suggesting a scenario



to explain the basin's evolution within the framework of assumed relocation from southern California.

Notice that the information presented herein focuses on the main portion of the Salinian terrane (Figure 5.1), the so-called "central block" of Ross (1978), because this area contains bona fide Salinian plutonic and metamorphic rocks. Other Upper Cretaceous strata within the Salinian terrane are located at Pigeon Point, west of the San Gregorio-Hosgri fault zone. However, the basement lithology is unknown at this locality, and the sequence may have a closer affinity to the Upper Cretaceous strata found within the Sur-Obispo terrane to the south. The Sur-Obispo sequence and Upper Cretaceous rocks to the north within the Point Arena terrane are discussed briefly in a subsequent part of this paper.

## 5.2 Basin Model

The Upper Cretaceous Salinian strata have been previously interpreted as the infilling of separate, transform-margin basins similar to the present-day borderland basins off the coast of southern California (Howell and Vedder, 1978; Howell and others, 1980; Vedder and others, 1982). I suggest, rather, that lithofacies and petrographic relationships (discussed in subsequent sections) are more consistent with deposition within a single, laterally continuous basin which owes its present outcrop pattern to Neogene strike-slip faulting, uplift, and erosion.

Restoration of up to 60 km of right-lateral offset along the Rinconado fault (evidence discussed in Section 5.4.1) produces a northwest-southeast alignment of the Upper Cretaceous strata, which contain paleocurrents directed predominantly toward the southwest (Figure 5.2). I suggest that this alignment reflects a northwest-southeast oriented paleocoastline that was controlled by block faulting, with an uplifted basement block toward the northeast and a steep-sloped, rapidly subsiding basin toward the southwest. Fan deltas built out from a rugged mountainous

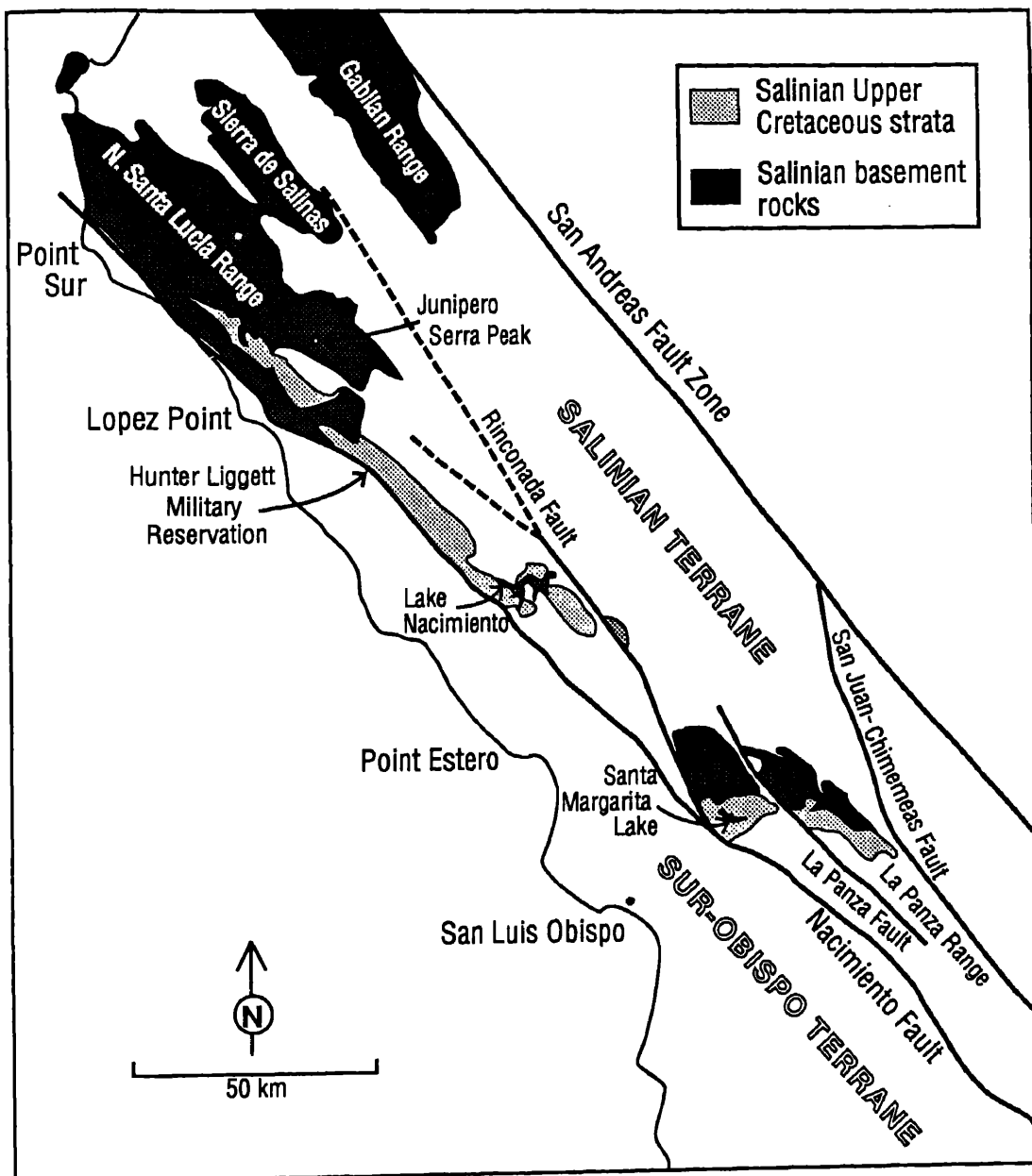


Figure 5.1: Location map for the central Salinian terrane.

terrain, producing thick sequences of coarse-grained, proximal sediments along the mountain front (Figure 5.3). Subordinate southeast- and northwest-directed paleocurrents resulted from longitudinal flow within the basin.

Figure 5.4 is a cross-sectional diagram of the Upper Cretaceous Salinian sections. The northeast sections are thinner than those toward the southwest, perhaps reflecting fault-controlled onlap toward the northeast, as schematized in Figure 5.5. The sedimentary facies record fan-deltaic progradation into deep water, followed by a marine transgression. The entire succession (up to 4 km of strata) was deposited in a short time period, probably not exceeding 10 m.y., and perhaps considerably less. Unfortunately, the biostratigraphy rarely provides more detail than Maastrichtian stage, the time frame during which the entire sequence was deposited. Nevertheless, by assuming deposition of 4 km of section within 8 m.y. and accounting for compaction, we can estimate average sediment accumulation rates in excess of 0.5m/1000 yr. This is within the range of accumulation rates (0.1m to 10m/1000yr) reported for modern active continental margin settings (Stow and others, 1985).

The inferred high subsidence rates imply crustal extension within the Salinian continental crust during Late Cretaceous time. Whether the basin formed as a result of only vertical motions or from a combination of both vertical and lateral motions (transtension) is not entirely clear, particularly because the bounding structures have either been obscured or reactivated by Tertiary tectonic activity. I assert that vertical tectonics were the primary effect, because the sedimentary facies reflect mainly extensional influences, whereas both extensional and compressional influences would be expected within a strike-slip dominated setting (Christie-Blick and Biddle, 1985; Mitchell and Reading, 1986). However, wrench tectonics may have instigated the extensional environment.

It is worth emphasizing that a big improvement in the biostratigraphic resolution is required before this or any other interpretation can be confirmed with a high

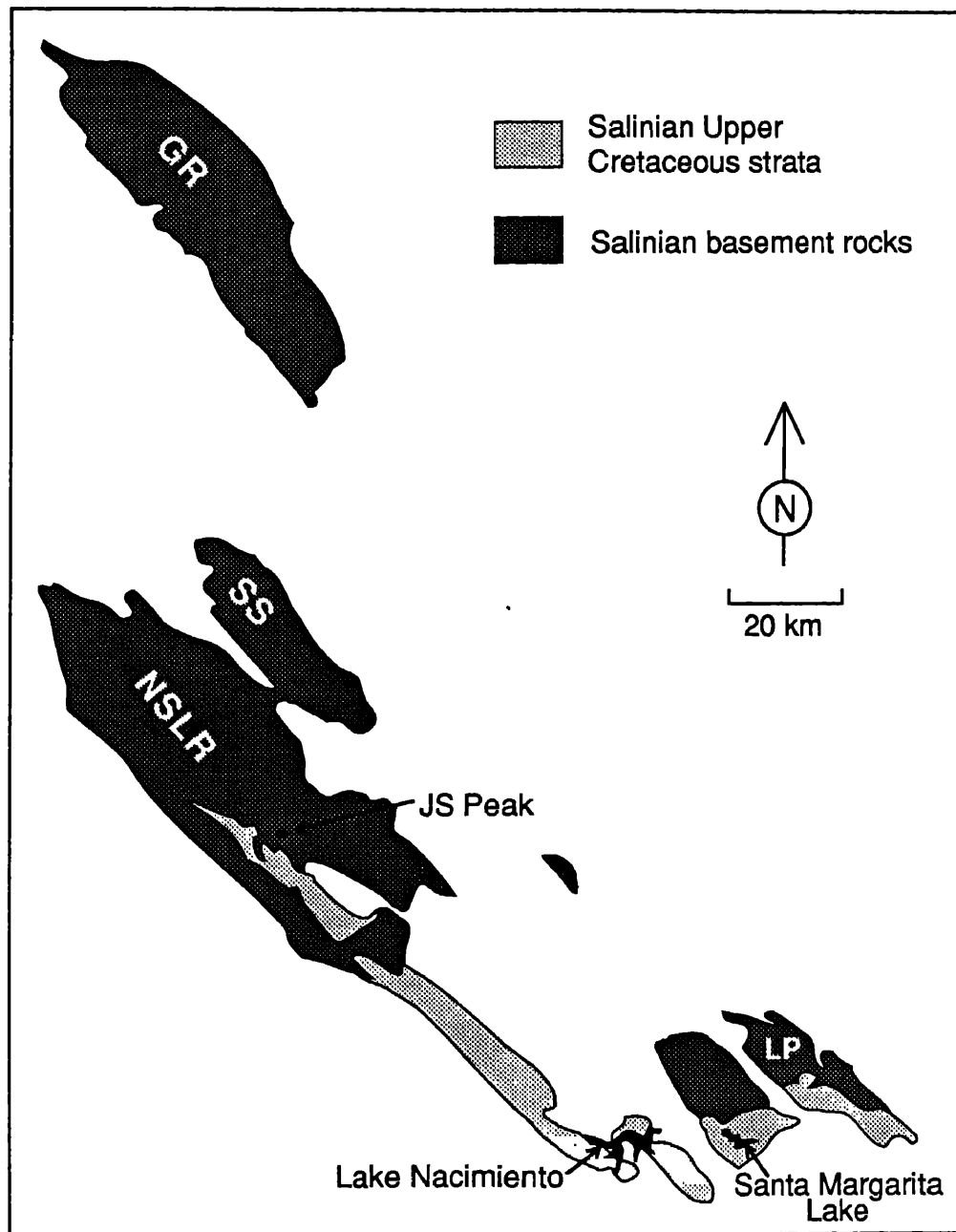


Figure 5.2: Outcrop areas with 60 km and 10 km of right-lateral displacement removed on the Rinconado and La Panza faults, respectively. GR=Gabilan Range; SS=Sierra de Salinas; NSLR=northern Santa Lucia Range; JS=Junipero Serra; LP=La Panza Range.

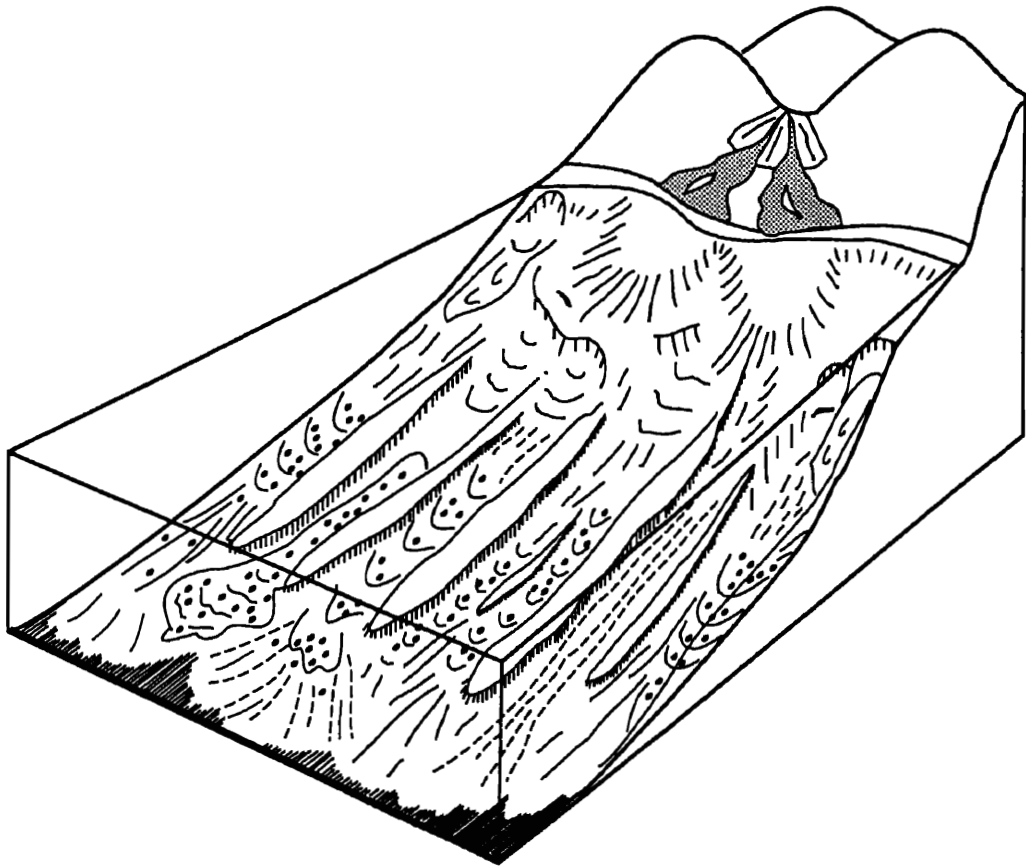


Figure 5.3: Fan-delta model for the Late Cretaceous Salinian basin. Model shows an alluvial fan and braid plain building directly out onto a steep slope where slump failures and sediment-gravity-flow processes dominate. Approximate length of coastline shown: 20 km. Adapted from Postma (1984).

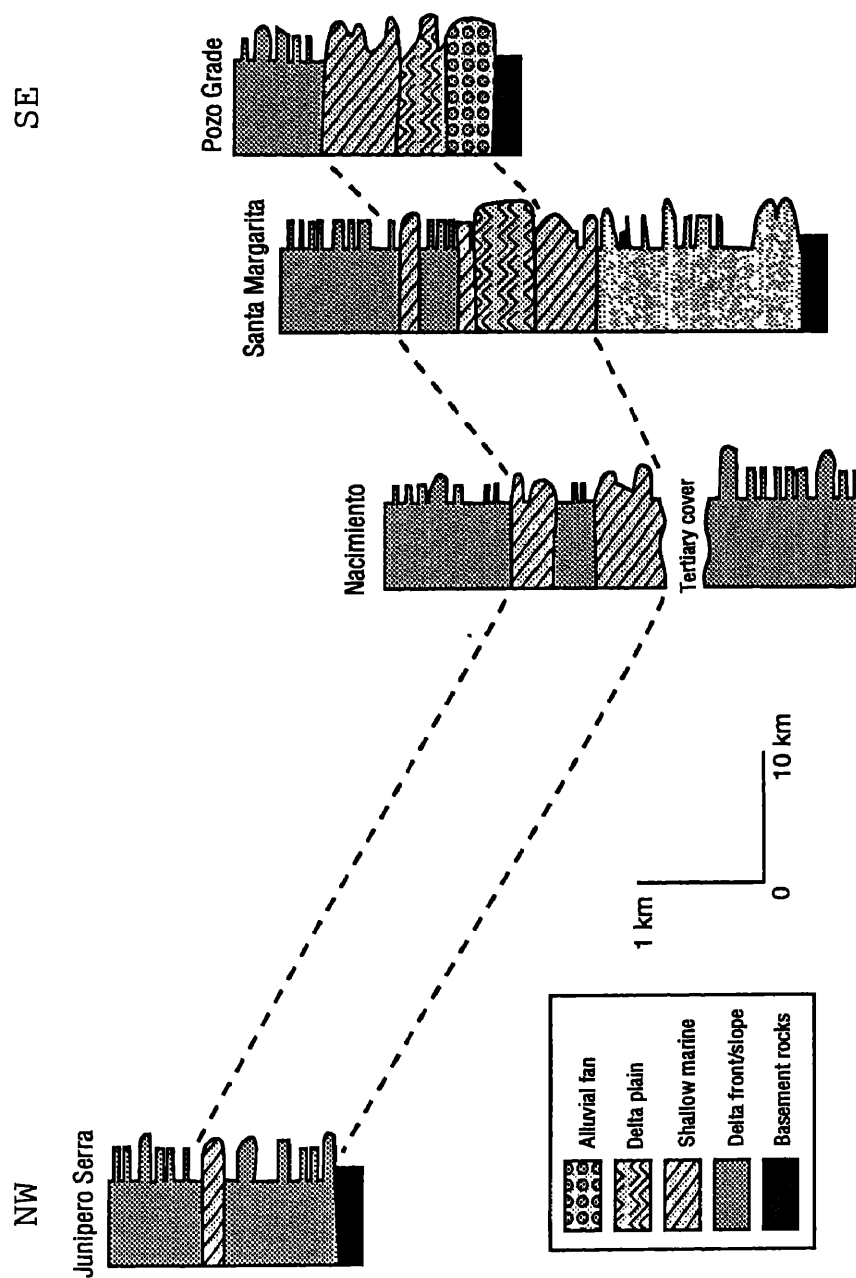


Figure 5.4: Northwest to southeast cross section based on reconstruction in Figure 5.2. Note that these are lithostratigraphic, not biostratigraphic correlations.

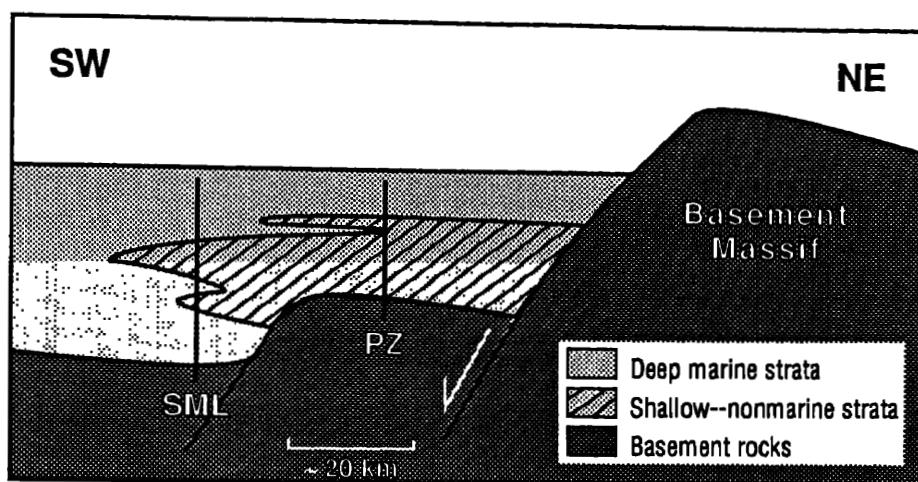


Figure 5.5: Northeast to southwest cross section of the Upper Cretaceous Salinian basin. This scenario explains sediment thinning toward the northeast by onlap of block-faulted basement. The Santa Margarita Lake (SML) and Pozo Grade (PZ) sequences are shown to explain the absence of a deep-water base east of the La Panza fault. This fault may have been a normal fault in the Cretaceous that has been reactivated in the late Tertiary as a thrust fault. Sedimentary facies record fan-deltaic progradation into deep water, followed by a marine transgression.

degree of certainty. Little detailed zonation work has been done on Late Cretaceous to early Tertiary Salinian faunal and floral assemblages. This, combined with poor fossil preservation, has resulted in faunal dates that are long ranging and often conflicting. In addition, sedimentary facies vary considerably over short lateral and vertical distances, and are therefore not useful for correlating between separated sedimentary sections. Distinctive marker beds, such as tuffs or basalt flows, are also lacking. Any interpretation should consequently be viewed with some skepticism.

## 5.3 Upper Cretaceous Salinian Stratigraphy

### 5.3.1 General Characteristics

Salinian Upper Cretaceous sedimentary rocks are characteristically coarse-grained deposits that show evidence of rapid, high-density emplacement. They exhibit a wide range of sedimentary facies that tend to vary rapidly, both vertically and horizontally. They are interesting from a sedimentological perspective because of

the dominance of structures indicative of mass-emplaced sediment-gravity-flow deposits, sometimes intermixed with structures associated with shallow-marine deposition. These characteristics, together with the observed gradation of marine into nonmarine facies, suggest deposition within a fan-delta complex.

Fan-deltaic sequences, both in ancient and modern settings, have been described by numerous authors (e.g., Galloway, 1976; Wescott and Ethridge, 1980; Gloppen and Steel, 1981; Kleinspehn and others, 1984). The essential elements required for building coarse-grained fan deltas, rather than the more common fine-grained deltas, are "high relief adjacent to the coastal zone and high-gradient, bed-load streams that are usually braided to the coast, resulting in a fan-shaped sedimentary deposit comprising subaerial, transitional and subaqueous components" (Ethridge and Wescott, 1984). These sedimentary systems typically develop along fault-controlled coastlines (e.g., Wescott and Ethridge, 1980; Gloppen and Steel, 1981). The observed characteristics inherent to fan-deltaic systems—dominance of coarse-grained, mass-emplaced sediments, high sedimentation rates, and ephemeral, migrating sedimentary environments—develop as a result of the steep topography and vertical and lateral motions associated with active tectonic settings.

Ethridge and Wescott (1984) developed two end-member models for fan-deltaic systems. One is the slope model, wherein fan deltas prograde directly onto a continental or island slope. These fans are truncated by the shelf/slope break, so that coarse-grained sediment-gravity flows are deposited directly seaward of the marine to nonmarine transition zone. The other is the shelf model, wherein fan deltas build out onto a broad shelf, recognized by superior development of nearshore, shoreface, and shelf environments. McPherson and others (1987) restrict the term "fan delta" to situations wherein an alluvial fan directly progrades into water, and choose the term "braid delta" for situations wherein the alluvial fan is located further inland and a braided stream plain feeds into the aqueous environment. By their scheme,



fan deltas and braid deltas are subsets of coarse-grained deltas. In practice, the two end-member models of Ethridge and Wescott (1984) are more straightforward to apply, at least to the ancient Salinian sequence, because the sedimentary record mainly preserves the subaqueous portion of the system.

The Upper Cretaceous Salinian strata resemble the slope fan-delta model most closely (see Figure 5.3). As noted by Howell and others (1980), shelf facies sediments are not well developed within these strata. An analogous situation is probably the Yallah's fan delta in Jamaica, where submarine canyons and valleys head close to the nearshore zone and subareal deposits are fed directly into these canyons (Wescott and Ethridge, 1982, 1980). Sediments are trapped in canyon heads until a critical threshold is reached; the slope then fails and sediments are channelized and funneled downslope by mass-gravity processes. Fault-controlled slopes, affected by high seismic activity and high sedimentation rates, have gradients up to 20°–30° (Wescott and Ethridge, 1982).

### **5.3.2 Santa Margarita Lake Section**

The most complete Upper Cretaceous sequence is located near Santa Margarita Lake (SML), east of the La Panza Range, where about 4 km of strata nonconformably overlie quartz monzonitic and granodioritic basement rocks (Ross, 1972; Figures 5.6 and 5.7). The section dips gently to the southeast and is apparently continuous into Paleocene and Eocene strata to the south (Chipping, 1972; Vedder and others, 1986). The precise location of the Cretaceous/Tertiary boundary is unknown, because different faunal and floral assemblages give conflicting ages, a reality that is characteristic of the Upper Cretaceous strata in general. Vedder and others (1968), Vedder (1977), and Saul (1983) report late Campanian to early Maastrichtian macrofossils; one of these localities is on the south side of the lake near the top of the Upper Cretaceous section along Salsipuedes Creek (Figure 5.7). Alter-

natively, Almgren and Reay (1977) report Maastrichtian microfossils (foraminifera) throughout. They correlate the base of the section with Goudkoff's (1945) D-2 zone and the upper part of the section with Goudkoff's D-1-C zone. W.R. Sliter (pers. comm.; see Appendix A) also reports only Maastrichtian foraminifera, and correlates the middle of the section with the Maastrichtian portion of the Uhalde Formation in the Great Valley Sequence. Many of the reported fossil localities contain assemblages that range from Late Cretaceous to Paleocene, not a very helpful designation. The consistently older ages obtained from the macrofossils may be a result of resedimentation from older deposits; the sample locality at the top of the section is particularly suspect. I have chosen the base of Vedder and others (1986) TKs zone, which contains rare Paleogene sporomorphs and Late Cretaceous to Paleogene foraminifers, as the top of the Cretaceous section.

The stratigraphically lowest several hundred meters of the Santa Margarita Lake section consist of extensive mass-flow emplaced conglomerates that occur within amalgamated beds up to tens of meters thick. This basal sequence is found only in the northwesternmost part of the study area (Figure 5.7), and was probably formed by backfilling of a submarine canyon. Granitic boulders up to 2 meters in diameter suggest local derivation from slope-exposed basement lithologies. A thin mudstone layer at the base of this section contains a foraminiferal assemblage indicative of upper bathyal (upper slope) depths (Almgren and Reay, 1977).

The conglomeratic canyon fill is overlain by a fan-delta front complex that consists of slope mudstones with associated thin-bedded turbidites and calcareous concretions, and slope-channel-fill deposits of mainly sandstone and conglomerate. The mudstones contain bathyal (slope) foraminifera (Almgren and Reay, 1977; W.V. Sliter, pers. comm. and Appendix A). The channel-fill deposits are up to tens of meters thick and were deposited primarily by sediment-gravity-flow mechanisms. They often lack internal structures, and form very thick, massive beds that are

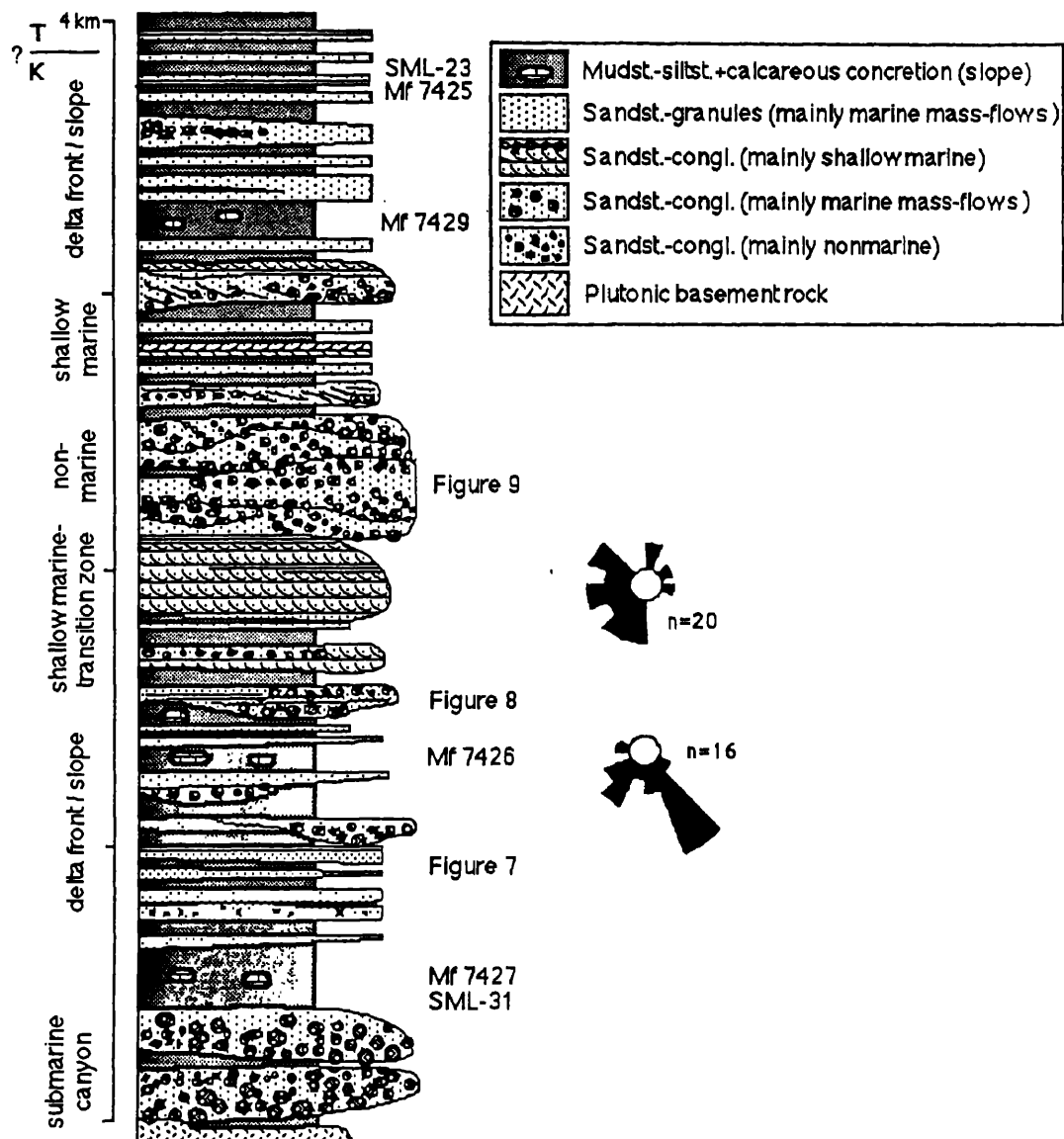


Figure 5.6: Schematic section from the north side of Santa Margarita Lake; see Figures 5.1 and 5.7 for location. Paleocurrents are oriented generally toward the south; shallow-marine strata include north (landward) directions. SML-numbers refer to sample localities for vitronite reflectance (Appendix D) and Mf-numbers refer to microfossil localities (Appendix A). Figure numbers refer to photographs.

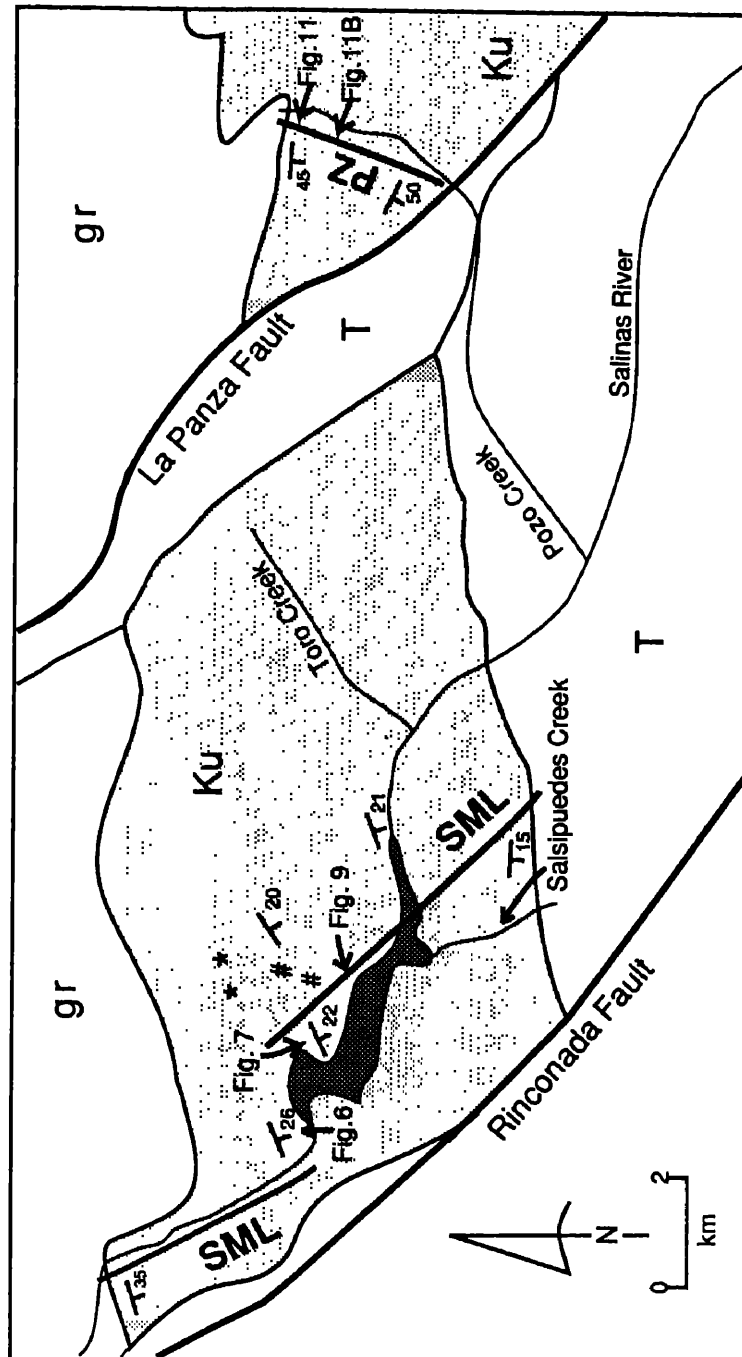


Figure 5.7: Map of study area near Santa Margarita Lake and Pozo Grade. Lines labeled SML and PZ are the approximate locations of the sedimentary sections shown in Figures 5.6 and 5.11. Figures refer to locations of photographs. The lower set of paleocurrent directions in Figure 5.6 are primarily pebble imbrications from near the starred localities; the upper set are diverse cross-bed measurements from near the number-symbol localities. Ku=unnamed Upper Cretaceous strata; T=undifferentiated Tertiary strata; gr=granotoid basement rocks.

frequently amalgamated (Figure 5.8). Conglomerates are poorly sorted and generally lack internal organization. Sandstone beds are sometimes normally graded and may contain tractive-flow structures, such as plane laminations and ripples, in their upper parts. These beds correspond to Mutti and Ricci Lucchi's (1975) Facies A and B turbidites, and were deposited by high-density sediment-gravity flows, as described by Lowe (1982).

The slope-channel deposits have a lenticular geometry and are encased in slope facies rocks (Figure 5.9). Medium-scale cross beds, like those typically formed by megaripple migration in above-wave-base subaqueous environments, are sometimes interbedded with massive and graded mass-flow beds in the channel fill deposits (Figure 5.8). Thus, currents moved down the channels and reworked the sedimentary package. Upsection, the slope deposits grade directly into nearshore and beach deposits without intervening shelf strata, supporting the idea of nearshore-headed slope valleys and deposition within a fan delta that prograded directly onto the slope.

In contrast to the lower portion of the SML sequence, the middle part consists of sandstones and conglomerates that are well organized and that contain many sedimentary structures indicative of tractive-flow depositional mechanisms (Figures 5.6 and 5.10). Cross beds of many sizes and types, including herringbone, trough, and tabular, are ubiquitous. The shallow-marine facies consist mainly of sandstone, but also contain lenticular conglomerates that were deposited as channel mouth bars, and plane-stratified conglomerates that were deposited by wave action in the nearshore zone. The shallow-marine strata are overlain by a predominately conglomeratic sequence that is interpreted as braided stream deposits on the subareal delta plain. Although braided stream conglomerates look similar to ones of shallow-marine origin, the nonmarine beds tend to be less persistent laterally, to form thicker beds, and to be clast rather than matrix supported (Clifton, 1973;

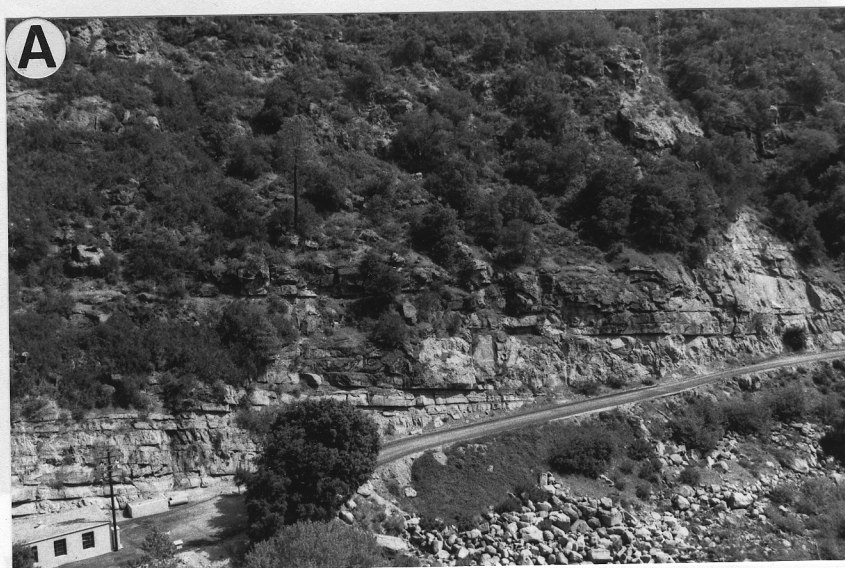


Figure 5.9: slope-facies

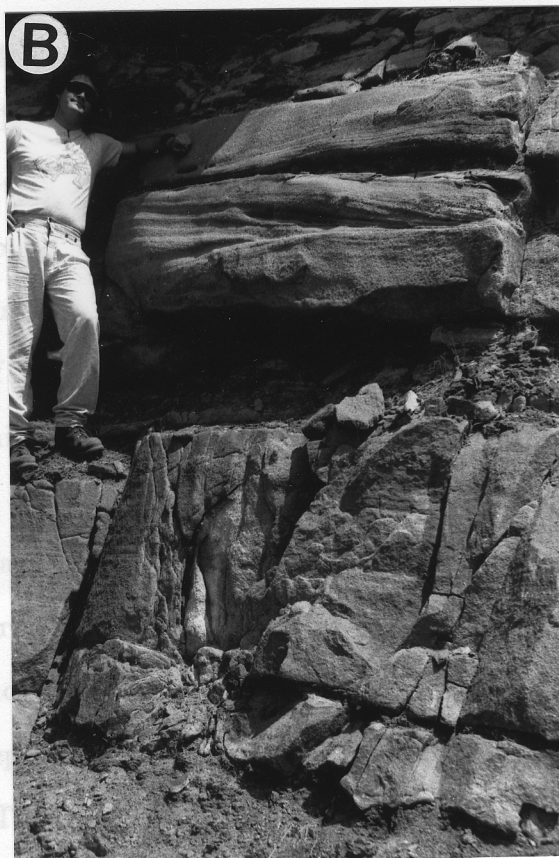


Figure 5.8: Submarine sandstones interpreted as delta-front deposits as in the fan model of Figure 5.3. A) Overview: note broad lenticular geometry of beds. B) Bedding detail: Medium-scale cross beds associated with massive and plane-bedded turbidites.





Figure 5.9: Lenticular sandstone and conglomerate channel deposit encased in slope-facies mudstones.

Nemec and Steel, 1984). On this basis, dominantly shallow-marine strata give way upsection to dominantly nonmarine strata (Figure 5.6). In reality, the coastal plain portion of a fan-delta system is a complex zone of interaction between fluvial and wave processes, and sorting out the specific facies can be difficult (Kleinspehn and others, 1984). Unfortunately, body fossils have not been found, except within calcareous concretions of slope-facies strata. This is probably a result of both high sedimentation rates (high sediment/organism ratio), and post-depositional dissolution.

The nonmarine strata grade upsection into marine rocks, indicating an increase in basinal subsidence relative to sediment supply (Figure 5.6). Shelf-facies strata, consisting of plane- and hummocky-bedded and highly bioturbated sandstones and siltstones, are better represented here, and alternate with shallow-marine sandstones and conglomerates. This alteration reflects an interaction between sedimentary and tectonic processes. For example, Galloway (1976) described the Copper River fan delta, which is prograding into the Gulf of Alaska, wherein episodes of uplift associated with earthquakes, punctuate the more general subsidence of the deltaic

A black and white photograph of a massive, layered rock formation, likely a butte or mesa. The rock face shows distinct horizontal strata. A person is standing at the base of the formation on the left side, providing a sense of scale. Sparse vegetation is visible at the base of the rock.

Figure 5.10: Braided stream deposits of the delta plain.



mass. In addition, deltaic lobes progressively build out and are abandoned.

The top of the section consists of submarine turbidites that become progressively thinner bedded and finer grained upsection (Figure 5.6). The Cretaceous sequence here and at Pozo Grade (next section) is overlain by 2–4 km of Paleogene strata, which are also predominately submarine turbidites (Chipping, 1970). Although there are no apparent unconformities within the section (Chipping, 1972), Vedder and others (1982) suggest a depositional gap in the late Paleocene and/or early Eocene, based on the lack of faunal dates from this time period. These rocks are poorly exposed and not well studied.

As mentioned previously, the Salinian Cretaceous sequence is thickest and most complete near Santa Margarita Lake. A thickness of about 4 km suggests average sediment accumulation and subsidence rates exceeding 0.5m/1000yr. The main control of subsidence in the Upper Cretaceous Salinian basin was probably vertical tectonics. The gross stratigraphic packages of regression followed by transgression have thicknesses on a kilometer scale, too large for eustatic variations (Figure 5.6). The overall large-scale tectonic effect is partitioned into discrete pulses of faulting, producing episodic subsidence. Eustatic variations, rapidly shifting depocenters, and the normal sedimentary processes of progradation and avulsion, are superimposed on the tectonic influences, resulting in a complex array of interfingering sedimentary facies. For example, Gloppen and Steel (1980) observed coarsening- and fining-upward sequences on the scale of several meters up to hundreds of meters in the transtensional Hornelen Basin, reflecting both intra- and extrabasinal controls.

### 5.3.3 Pozo Grade Section

A thinner section of Upper Cretaceous strata is exposed east of the La Panza fault, in the La Panza Range, along Pozo Grade road (Figures 5.11 and 5.7). The top of

the sequence is truncated by the La Panza fault, but is probably close to the Cretaceous/Tertiary boundary (Dibblee, 1972). As usual, however, the precise location of this boundary is equivocal. The only time-diagnostic fossil found in this section is the late Campanian to early Maastrichtian ammonite *Baculites occidentalis* (Vedder, 1977). Its location about 1 km below the top of the section, the possibility of resedimentation from older deposits, and the lack of corroborating dates, however, preclude placing too much confidence in this single date. Late Maastrichtian turritellid mollusks are reported from southeast of Maschesna Mountain and in Deadman Flat further east in the La Panza and Chimeneas Ranch Quadrangles, respectively (Vedder and Brown, 1968; Saul, 1983).

The Pozo Grade sequence is about 2 km thick and records the deposition of a transgressive fan-delta system. Beds at the base of the section, which rest non-conformably on plutonic basement rocks, are very thick, poorly sorted cobble to boulder matrix- and clast-supported conglomerates (Figure 5.12). These beds were deposited within the steep alluvial-fan portion of the fan delta by debris flows. They are interbedded with better sorted cobble conglomerates and sandy red beds that formed as braided stream channel and overbank deposits during fluvial reworking (Figure 5.12). Thin coal beds have also been reported (Blackmur, 1978).

Although specific facies interfinger complexly, the sediments generally fine and become progressively better organized as the delta plain part of the fan delta is encountered upsection. Overlying the delta plain is the transition zone (Ethridge and Wescott, 1984), where stream gravels are input into the shallow marine environment and subjected to wave action. As in the SML section, shelf-facies strata are poorly developed, and shallow-marine strata grade directly into turbidites.

A similar transgressive fan-delta sequence is exposed about 6 km south of Pozo Grade in American Canyon. A small fragment of gneissic basement underlies the Cretaceous section at this locality, which was situated seaward (in Cretaceous time)

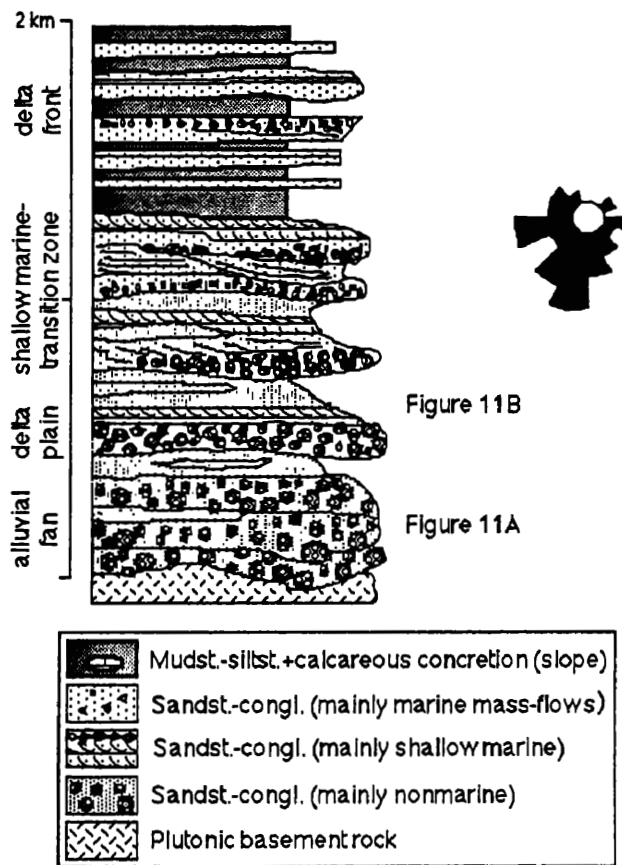


Figure 5.11: Sequence from along Pozo Grade; see Figure 5.7 for location. Paleocurrent directions to the south (from Blackmur, 1978). Figures refer to photographs.

of Pozo Grade, and probably formed near an offshore basement high associated with a rugged topography (Blackmur, 1978).

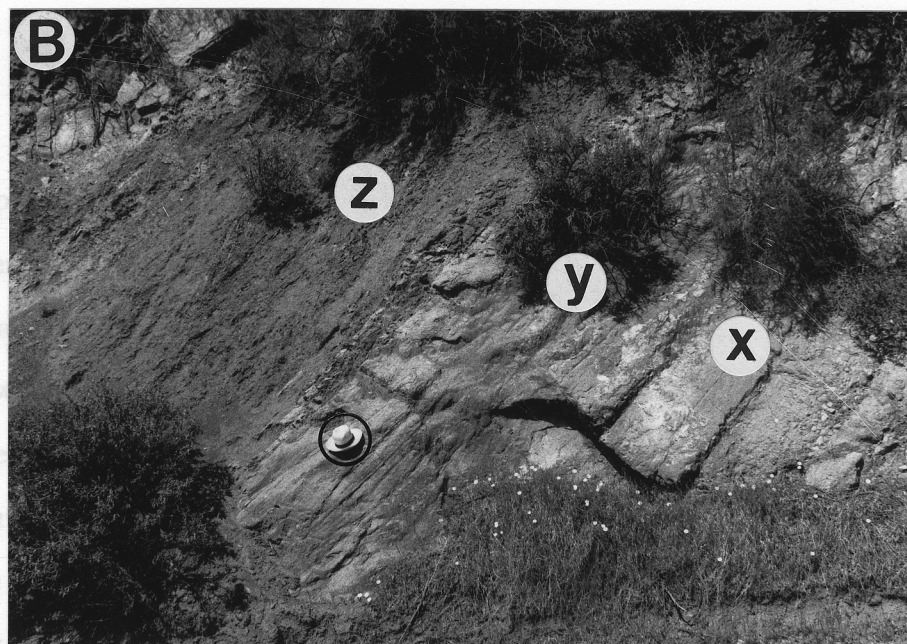
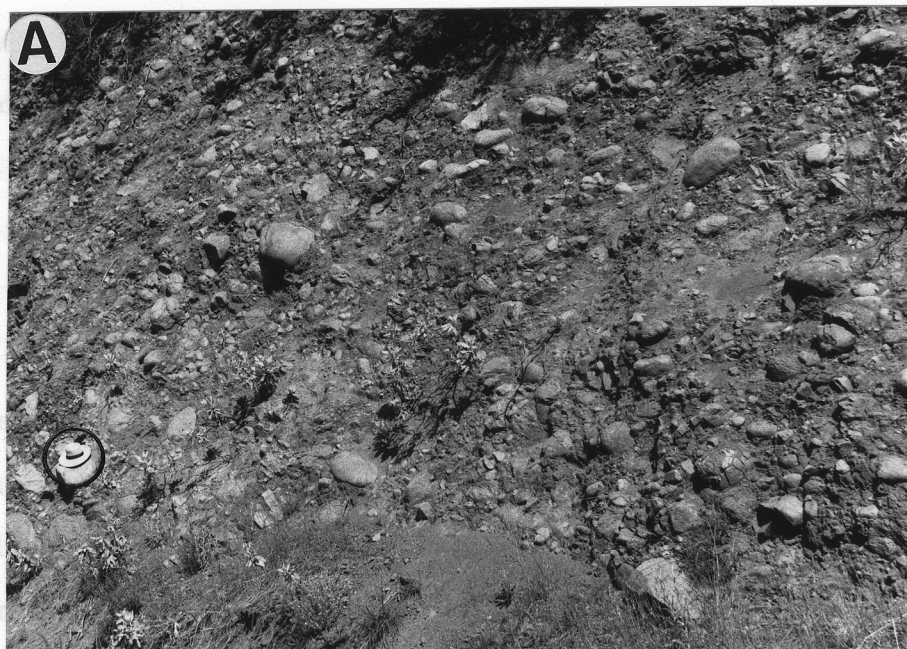


Figure 5.12: Nonmarine deposits from Pozo Grade. A) Poorly sorted, matrix-supported, alluvial-fan debris-flow bed. Largest clasts are quartzites. B) Fining-upward fluvial sequence: conglomerate (X) and sandstone (Y) channel beds with overbank red beds (Z). Circled hat for scale in both photos.

of Pozo Grade, and probably formed near an offshore basement high associated with a rugged topography (Blackmur, 1978).

The similarity of the basement massifs east and west of the La Panza fault precludes the existence of large magnitude strike-slip offset along this fault (Ross, 1972). Ballance and others (1983) suggest 50 km of right-lateral offset on the La Panza fault, but this is based on the tenuous matching of the Simmler Formation to the south with a non-unique source area. I have chosen to use 10 km of right-lateral offset for the Cretaceous reconstruction. This more directly juxtaposes the basement outcrops, and fits the stratigraphic relations observed in the sedimentary sections east and west of the fault, wherein the most proximal facies are found toward the northeast (Figures 5.1 and 5.2). Figure 5.5 summarizes my view of the relationships east and west of the La Panza fault. Perhaps the La Panza fault was a Cretaceous normal fault, which has been reactivated in the Tertiary as a thrust fault.

#### **5.3.4 Lake Nacimiento Section**

The Upper Cretaceous strata near Lake Nacimiento (LN) are described in detail in Chapter 2. The upper portion of the section is exposed around LN and consists of a transgressive sequence that is shallow marine at the base, and that deepens upward into slope mudstones and submarine turbidites that extend across the Cretaceous/Tertiary boundary (Figures 5.13 and 5.14). Facies relationships and paleocurrent indicators show an offshore direction toward the south and southwest.

The Cretaceous strata at LN are generally similar to those near the La Panza Range to the south, except that the nonmarine rocks are not as well expressed. The only nonmarine rocks observed around LN occur in the easternmost section, which consists of stacked fan-deltaic progradational sequences. Even so, marine strata are most prevalent in this section, but nonmarine strata may be more common

in the vegetated hills toward the northeast, where more proximal facies would be predicted.

Although Howell and others (1977) described a regressional sequence at Lake Nacimiento with nonmarine sediments at the top, they apparently misidentified some younger Tertiary deposits as part of the Cretaceous sedimentary section (see Chapter 2). Their assertion (Howell and Vedder, 1978) that the LN and La Panza areas represent the infillings of separate subbasins is based primarily on their observation of a transgressional sequence near La Panza, and a regressional sequence at LN. The present study, however, has shown similar stratigraphic progressions at both localities.

Foraminiferal assemblages support the transgressional aspect of the basinal deposits; they show progressive deepening from neritic at the base of the section to bathyal at the top (Sliter, 1986; see Appendix A for specific collection localities). Foraminifera from the base of the section are Maastrichtian, and correlate with Goudkoff's (1945) D-2 zone, established for the Great Valley Sequence (GVS) east of the San Andreas fault (Almgren and Reay, 1977). Species from the upper half of the section correlate with Goudkoff's C zone and are late Maastrichtian (Sliter, 1986; Appendix A). Some elements of the LN fauna are found only in the Tierra Loma and Marca Shale Members of the Moreno Formation (late Maastrichtian) portion of the GVS. Other elements, however, are found within older Campanian and Maastrichtian strata in the GVS and indicate different stratigraphic ranges for assemblages in the two areas (Sliter, 1986). The LN faunas are more similar to the Rosario Group of southern California and northern Baja California, Mexico (Sliter, 1968), suggesting an environmental similarity between these areas. Uplift of accretionary complex materials had created a bathymetric high at the western edge of the Great Valley forearc basin by the end of the Cretaceous period, causing limited circulation between basinal and open ocean waters (McGuire, 1988). The LN and

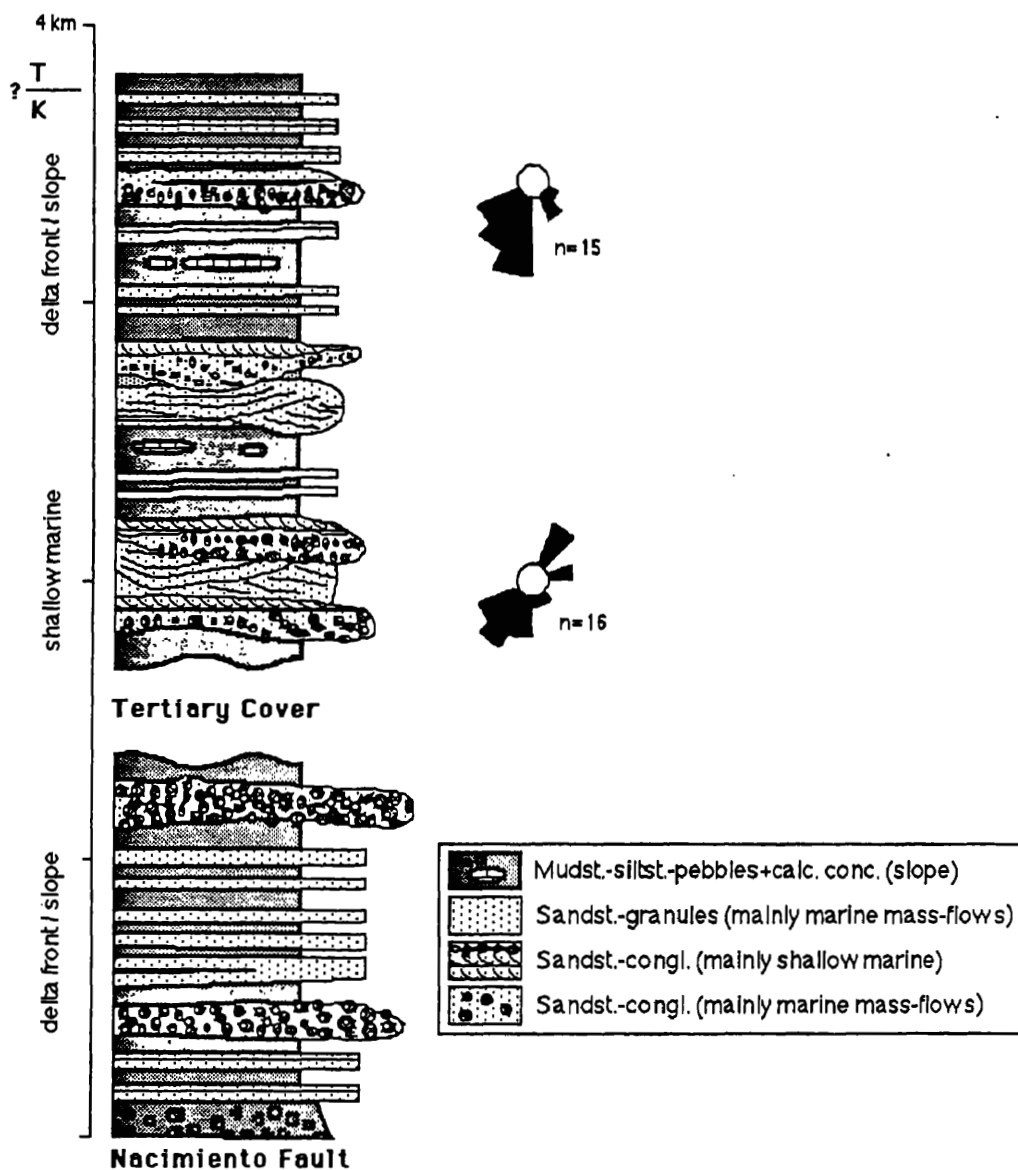


Figure 5.13: Composite Upper Cretaceous sedimentary section from around Lake Nacimiento (LN—the upper part) and in Fort Hunter-Liggett (FHL—the lower part). The two sections are separated by Tertiary cover, and the base of the FHL section is truncated by the Nacimiento fault. (see Figure 5.14 for location). Paleocurrents are toward the south, with subordinate landward (northeast) directions within shallow-marine strata.



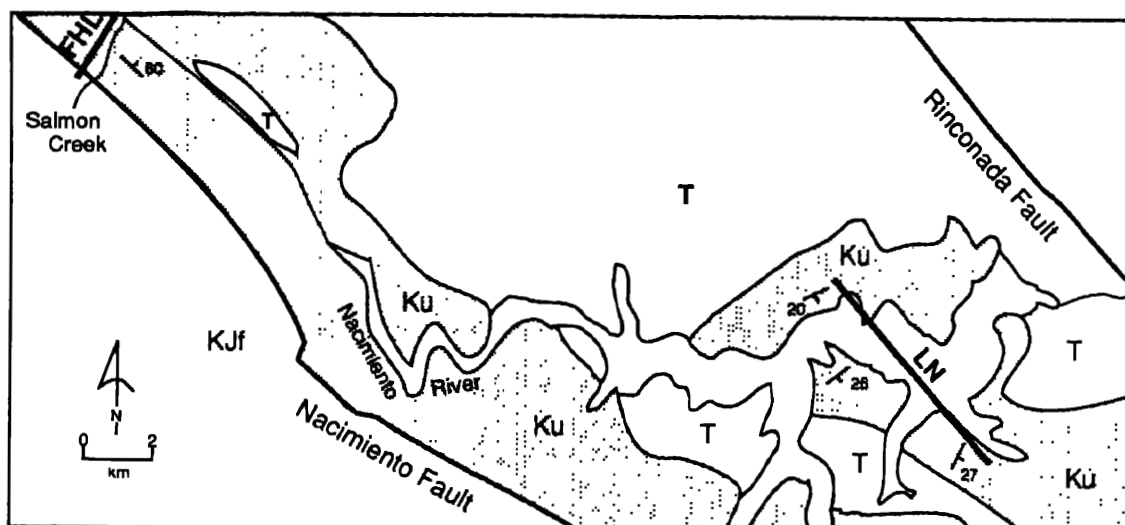


Figure 5.14: Study areas near Lake Nacimiento (LN) and the Hunter Liggett Military Reservation (FLH). The lines refer to the approximate locations of the section depicted in Figure 5.13. Ku=unnamed Upper Cretaceous strata; T=undifferentiated Tertiary strata; KJf=Franciscan Complex.

Rosario Group faunas, alternatively, suggest deposition within a more open-ocean forearc apron (Sliter, 1986).

Saul (1983) has developed a detailed zonation for turrnellid mollusks in California. According to her zonation, the LN section is middle Maastrichtian at the base and latest Maastrichtian at the top (also see Appendix A). Dinoflagellate populations corroborate the latest Maastrichtian age for the top of the section. One assemblage contains forms restricted to the Danian stage of the Paleocene epoch in the GVS (W. R. Evitt, pers. comm., 1986). Ammonites found near this locality, however, indicate a Cretaceous age at LN, again suggesting different stratigraphic ranges for assemblages from the two areas. Paleocene (Thanetian) turrnellas are reported from the eastern edge of Upper Cretaceous outcrop south of Lake Nacimiento (Figure 5.1). Age control between the lake and this sample locality is nonexistent, and some of the outcrop area shown on the map as Cretaceous may actually be Tertiary.

Additional Upper Cretaceous strata (herein referred to as the Fort Hunter



Liggett—FHL—section) to the west are poorly accessible because of their location within the Hunter-Liggett Military Reservation and because of heavy vegetative cover. Some of this area has been recently mapped by Seiders (1989), who describes an east-dipping sequence that is somewhat disrupted by Tertiary faults and broad folds. The base of the section is truncated by the Nacimiento fault, and basement rocks are not exposed. The strata have yielded Maastrichtian foraminifers that may be late Maastrichtian at the eastern edge of the area (Seiders, 1989). Butler (1981) also reported Maastrichtian dinoflagettes and pollen from the upper part of the section further south and directly west of LN. Thus, part of this section (the upper part) may be correlative with the lower portion of the LN section. But based on structural (the entire Upper Cretaceous sequence is dipping, i.e. younging, toward the east and south), and petrographic relationships (Chapter 4), the base of the section is probably older than that around LN. I have shown this portion of the Upper Cretaceous strata as older than the area around LN, because it fits my model of similar sequences here and to the south in the La Panza Range, and the fauna data do not contradict this interpretation (Figure 5.13).

The FHL section consists primarily of sediment-gravity-flow deposits very similar to those at the base of the SML section. Pebbly mudstones adjacent to the Nacimiento fault (Seiders', 1989, Steve Creek Formation) are overlain by granular, massive turbidites (Seiders', 1989, Italian Flat Formation), which are overlain by conglomeratic beds (Seiders', 1989, Shut-In Formation) that have a lenticular geometry and are probably slope channel-fill deposits. The Italian Flat Formation is similar to the conglomerate-sparse, massive sandstones that are found above the submarine canyon fill near the base of the in frequency upsection, where they form lenticular beds of channel-fill origin. Seiders (1989) described large-scale cross beds in the El Piojo Formation, which is east of a strike-slip fault zone and has an uncertain relationship to the FHL section just described. These rocks could be slightly

younger and partially correlative with the shallow-marine facies rocks at the base of LN section. This would produce a similar relationship to SML, wherein turbidites shoal upward into shallow-marine strata (Figure 5.4). The FHL section is not continuous with the LN section to the east; they are separated by overlying middle Tertiary formations.

### 5.3.5 Junipero Serra Section

Upper Cretaceous strata are poorly exposed in the northern part of the central Salinian block west of Junipero Serra Peak in the Ventana Wilderness area (Figures 5.1 and 5.16), where Late Cretaceous mollusks and foraminifera with ranges from Late Cretaceous to Paleocene have been reported (Ruetz, 1976). Ruetz (1976) looked at the southern part of this outcrop belt, which he believed was conformably overlain by Paleocene strata. He described a submarine canyon-fill deposit at the southeastern extremity of the outcrop belt that rests nonconformably on basement rocks (Ruetz, 1976). These rocks contain shallow-water mollusks that are reportedly unreworked. This suggests a submarine canyon that headed close to the nearshore zone, similar to the slope fan-delta model hypothesized for other Upper Cretaceous strata further to the south. Toward the northeast, Paleocene and Eocene strata lie directly on basement with no intervening Cretaceous strata, indicating that progressive onlap to the northeast continued into the early Tertiary (see Graham, 1976).

Figure 5.15 illustrates a composite section, the location of which is shown in Figure 5.16. The element most frequently viewed here is modern vegetation, so the stratigraphic relationships are not entirely clear. Shallow-marine strata overlie slope mudstones near the middle of the section, and the top part consists of sediment-gravity-flow deposits. Styles of sedimentation appear to be quite similar to those seen in other parts of the Salinian terrane. As in the La Panza area, Cretaceous strata are apparently conformably overlain by Paleocene strata (Ruetz,

1976; Compton, 1966), although an angular unconformity occurs between these Paleocene and upper Paleocene to lower Eocene rocks (Graham, 1979). Other Upper Cretaceous strata occur as faulted fragments along the coast north of Lopez Point and north of Point Sur (Figures 5.1 and 5.16).

### 5.3.6 Conglomerate and Sandstone Petrography

A study of Salinian conglomerates is detailed in Chapter 4, but summarized herein. A wide variety of clast types is represented, including basaltic to rhyolitic volcanic rocks, gabbroic to granitic plutonic rocks, low- to high-grade metamorphic rocks, and rare sedimentary rocks. Clast populations at the base of the various Salinian sections are different from one another but become similar upward, generally trending toward dominance by felsic volcanic clasts. This change reflects an evolution from local basement to more distant, fluvially-tapped sediment sources as better integrated drainages developed within a maturing topography. The basement-derived plutonic and metamorphic rocks tend to be somewhat angular and larger in size—boulders are prevalent. The volcanic clasts are usually very well rounded and smaller, reflecting abrasion during prolonged stream transport. Boulders of the volcanic clasts are also found, however.

One rhyodacitic lava boulder, collected from the south shore of Lake Nacimiento, was crushed and the zircon population separated for U/Pb isotopic dating. Figures 5.17 and 5.18 summarize the results of this analysis. Two distinct zircon populations occur in the sample: one is a larger, clear type, and the other is a smaller, reddish type (J.E. Wright, pers. comm., 1988). Three size fractions fall along a discordant line that intersects the radiogenic decay curve (concordia) at  $112 \pm 10$  Ma and  $1613 \pm 380$  Ma. The sample contains low amounts of U, so the discordance is most likely a result of contamination by an older component (the small, reddish grains) rather than lead loss. The 112 Ma date is thus interpreted

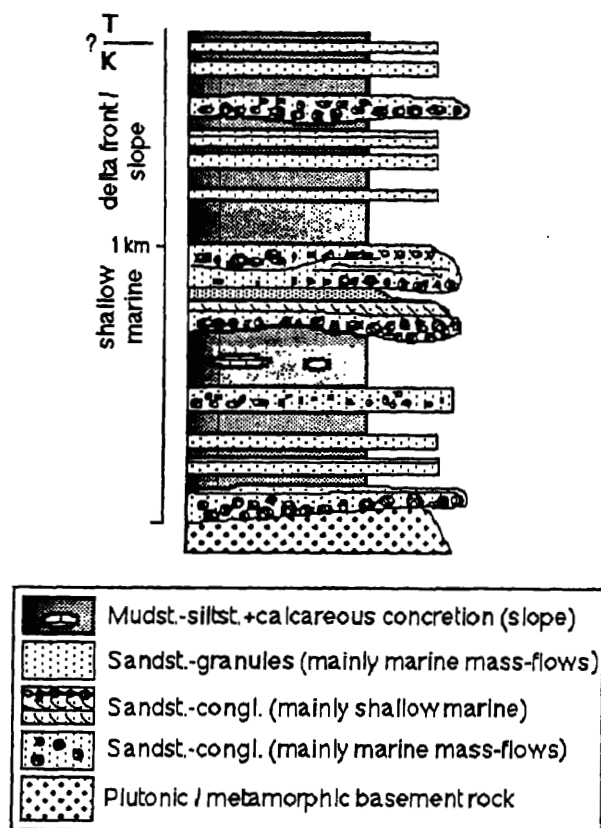


Figure 5.15: Stratigraphic section from west of Junipero Serra Peak; see Figure 5.16 for location. Note that the depicted lithofacies are based on a reconnaissance traverse and are somewhat speculative because of poor exposures.

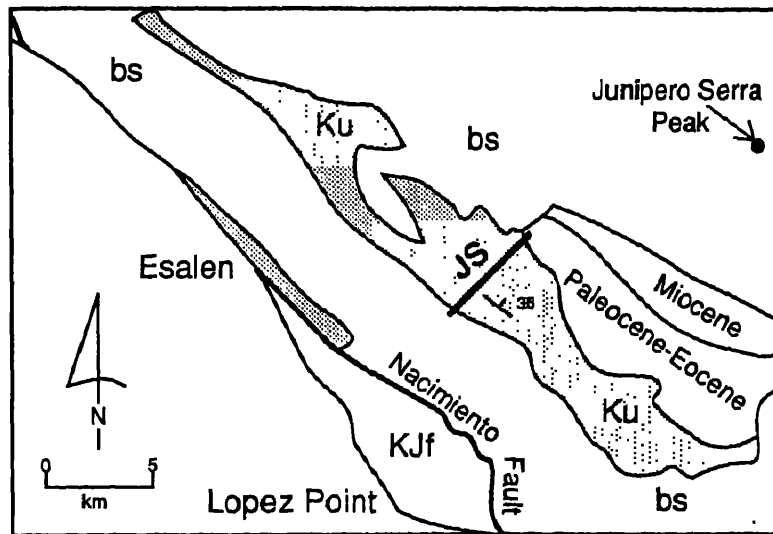


Figure 5.16: Study area west of Junipero Serra Peak in the Ventana Wilderness area. Line refers to approximate location of section depicted in Figure 5.15. Ku=unnamed Upper Cretaceous strata; KJf=Franciscan Complex; bs=plutonic and metamorphic basement complex. Note that the area west of the study area, near the Nacimiento fault, is much more complicated than shown (detailed mapping of Hall, in preparation).

as the igneous cooling age of the volcanic rock and the 1613 Ma date as the age of a xenocrystic component picked up while the molten magma was rising through the crust toward the earth's surface. The 112 Ma age is similar to plutonic ages obtained from basement rocks of the Salinian terrane (Mattinson and James, 1985), and the clasts may be derived from the volcanic cover associated with the plutons' emplacement, but of which there is now no remnant.

The volcanic clasts contain abundant quartz and biotite phenocrysts and are primarily rhyolitic to rhyodacitic in composition. They were therefore associated with a mature magmatic arc that was built on a substantial thickness of continental crust. Although no volcanic cover remains on the Salinian crustal fragment, volcanic rocks in roof pendants of the southern Sierra Nevada Range have similar compositions and ages (Saleeby and Busby-Sperra, 1986). This is, of course, not a unique correlation and does not indicate derivation from the Sierran batholith.

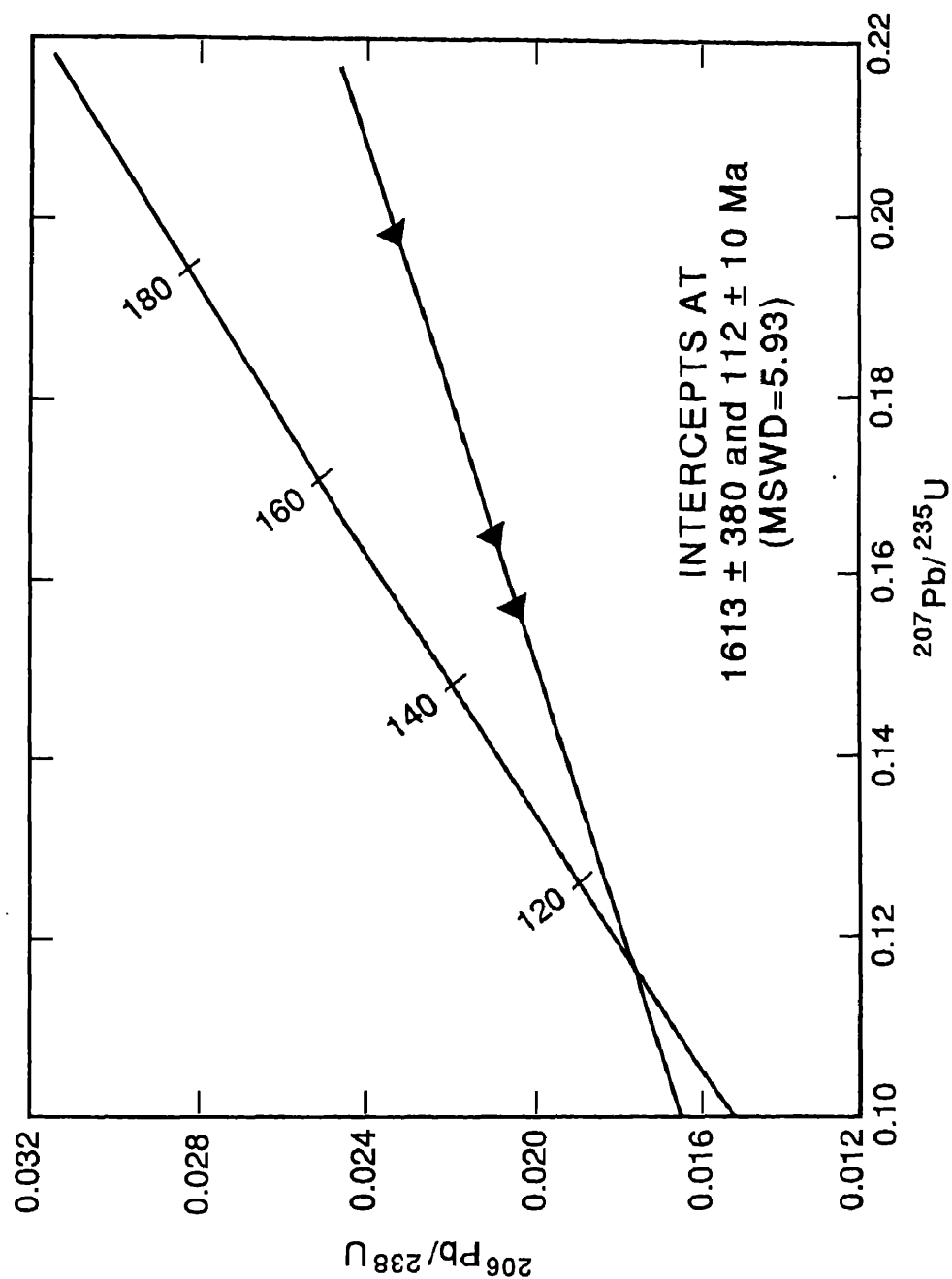


Figure 5.17: Uranium-lead isotopic data from zircon grains extracted from a rhyodacitic lava boulder. See Appendix A for sampling site location.

**TABLE 1. URANIUM-LEAD ISOTOPIC DATA**

Sample	Wt. (mg)	U (ppm)	$^{206}\text{Pb}^*$ (ppm)	Measured ratios**				Atomic ratios				Apparent ages††(m.y.)			
				$^{206}\text{Pb}$	$^{207}\text{Pb}$	$^{208}\text{Pb}$	$^{206}\text{Pb}$	$^{206}\text{Pb}^*$	$^{207}\text{Pb}^*$	$^{207}\text{Pb}^*$	$^{206}\text{Pb}^*$	$^{206}\text{Pb}^*$	$^{207}\text{Pb}^*$	$^{207}\text{Pb}^*$	$^{206}\text{Pb}^*$
				$^{204}\text{Pb}$	$^{206}\text{Pb}$	$^{206}\text{Pb}$	$^{238}\text{U}$	$^{238}\text{U}$	$^{235}\text{U}$	$^{235}\text{U}$	$^{238}\text{U}$	$^{235}\text{U}$	$^{235}\text{U}$	$^{235}\text{U}$	$^{206}\text{Pb}^*$
+200†	17.2	151.9	3.043	304.3	0.46062	0.10919	0.02331	0.19830	0.06170	148.5	183.7	664			
-200C†	22.3	153.1	2.760	648.5	0.41856	0.07940	0.02098	0.16482	0.05698	133.8	154.9	491			
-200F†	18.2	159.2	2.787	281.0	0.49989	0.10769	0.02037	0.15680	0.05582	130.0	147.9	445			

†Numbers refer to size fractions in mesh, C,F are coarsest and finest zircon in a given size fraction

\*Denotes radiogenic Pb, corrected for common Pb using the isotopic composition of  $^{206}\text{Pb}/^{204}\text{Pb}=18.6$  and  $^{207}\text{Pb}/^{204}\text{Pb}=15.6$ . Sample dissolution and ion exchange modified from Krogh (1973).

\*\*Isotopic compositions corrected for a mass fractionation of 0.1%-0.128% per A.M.U. depending upon the mass spectrometer. Uncertainties in the  $^{208}\text{Pb}/^{206}\text{Pb}$  and  $^{207}\text{Pb}/^{206}\text{Pb}$  measured ratios are on the order of 0.03%-0.10%.  $^{206}\text{Pb}/^{204}\text{Pb}$  errors range from about 0.3% to 13% depending upon the ratio (all uncertainties are at the two-sigma level).

††Ages calculated using the following constants: decay constants for  $^{235}\text{U}$  and  $^{238}\text{U}=9.8485\text{E}-10\text{yr}^{-1}$ , respectively;  $^{238}\text{U}/^{235}\text{U}=137.88$ . The two-sigma uncertainties in the  $^{207}\text{Pb}^*/^{206}\text{Pb}^*$  ages were calculated on the combined uncertainties in mass spectrometry and assumed uncertainty of  $\pm 0.1$  in the  $^{206}\text{Pb}/^{204}\text{Pb}$  ratio used for the common Pb correction.

Figure 5.18: Isotopic data

However, none of the Salinian clasts are inconsistent with an original location in southern California. Other clast types have good potential for provenance value. For example, distinctive pink and purple quartzites (meta-quartz-arenites) found in the Pozo Grade sequence and in Upper Cretaceous to Paleocene strata of the Transverse Ranges are similar to Cambrian quartzites located in the Mojave Desert region (I.P. Colburn, pers. comm., 1989). Any believable correlations must ultimately come from a suite of distinctive lithologies.

The similar evolution in clast types seen throughout the various Salinian sections supports the idea of their original contiguity within a single basin. Still, the *specific* clast compositions vary considerably over short vertical and lateral distances. As mentioned previously, the sedimentary facies also vary rapidly. These details suggest an unstable setting, where uplift and faulting were exposing new source areas and producing sporadic episodes of accelerated and decelerated basinal subsidence.

The Upper Cretaceous sandstones are feldspathic arenites that, unlike the conglomerates, are compositionally uniform throughout the central portion of the Salinian terrane (Lee-Wong and Howell, 1977). They are rich in potassium feldspar relative to plagioclase feldspar, reflecting erosion of the plutonic basement following removal of the volcanic cover, similar to the sandstones that occur at the top of the Great Valley Sequence east of the San Andreas fault (Gilbert and Dickinson, 1970). This unroofing sequence is seen in strata of Upper Cretaceous age throughout the western Cordillera (Dickinson, 1982). Consequently, the sandstones are of little value for assessing variations within the sequences or for determining sediment provenance.

## 5.4 Thermal History

Most of the conglomerate clasts within the Upper Cretaceous Salinian sections are altered to some extent (Chapter 4: Figures 4.3 to 4.6). The volcanic clasts



are recrystallized, the feldspars are murky from alteration to sericite, and the intermediate to mafic varieties contain a subgreenschist to greenschist metamorphic assemblage. They do not have a metamorphic fabric, however, and the metamorphism is probably a liquid-rich metasomatic type. The high-grade metamorphic clasts often show evidence of a retrograde event. But although alteration is nearly ubiquitous within the clasts, it probably occurred within the source region, not as a result of burial metamorphism. Vitrinite reflectances ( $R_o$ ) of kerogen from Upper Cretaceous siltstones and mudstones range from 0.49% to 0.76%, with four out of five samples ranging from 0.49% to 0.54%. This suggests that these samples have not experienced temperatures exceeding 200° C, or perhaps 300° C for the higher  $R_o$  sample (see Figure 56 and Appendix A for sample locations; Appendix D contains complete  $R_o$  data lists and maturity range chart prepared by G. Demaison). The highest  $R_o$  value is from the stratigraphically lowest sample in the data set—base of the Santa Margarita Lake section—where the highest burial temperature would be predicted. Resedimented vitrinite populations with  $R_o$  values ranging from 0.84% to 1.22% occur in all samples.

In the La Panza Range, Cretaceous through Eocene strata are unconformably overlain by the Oligocene Simmler Formation (Vedder and others, 1982). At Lake Nacimiento, Cretaceous through Paleocene strata are unconformably overlain by the Oligocene Vaqueros Formation (Durham, 1974). And west of Junipero Serra Peak, Cretaceous and Paleocene strata are unconformably overlain by the upper Paleocene to lower Eocene Reliz Canyon and Church Creek Formations (Graham, 1979). All of these unconformities are angular to some degree, showing that compressional events within the upper Paleocene to Oligocene uplifted the Cretaceous to lower Tertiary sequence and exposed it to erosion. Deformation was apparently diachronous between the various localities. For example, uplift near Junipero Serra Peak is bracketed between 55 and 58 m.y.b.p. (Graham, 1979). In contrast, uplift

apparently did not occur until late Eocene in the La Panza Range (Chipping, 1972; Vedder and others, 1982), although more careful study may reveal previously undiscovered unconformities. In addition, the timing of uplift is obscured by differing amounts of subsequent erosion.

In the La Panza Range, where the sequence is most complete, nearly four kilometers of lower Tertiary sediments were deposited on the Upper Cretaceous section (Chipping, 1970, 1972), thus producing depths up to 8 km at the base of the Cretaceous section. With a geothermal gradient of  $30^{\circ}/\text{km}$ , a depth of 8 km would correspond with a temperature of  $240^{\circ}\text{C}$ , a figure consistent with the vitrinite reflectance data.

#### 5.4.1 Sequence Correlations

As discussed previously, correlations within the Salinian Upper Cretaceous sedimentary sections is hampered by the lack of detailed biostratigraphic information, the lack of distinctive marker beds, and the lateral impersistence of stratigraphic units. The correlations shown in Figure 5.4 are based on similar large-scale stratigraphic variations observed within the sections, but an improvement in the biostratigraphy is required to confirm these correlations. Microfaunal data are consistent with the correlations, but macrofaunal data, particularly the late Campanian age from strata at the top of the Santa Margarita Lake sequence (Saul, 1983; Vedder and others, 1986), are less so. The SML date is suspect, however, because of its position in the stratigraphic succession, its inconsistency with other faunal and floral data, and the possibility of resedimentation from older stratigraphic units. I present the correlations in Figure 5.4, using the principle of least astonishment, considering all of the various data types.

The cross section in Figure 5.4 is based on the reconstruction shown in Figure 5.2, wherein the Nacimiento and Santa Margarita Lakes areas are aligned via

the removal of 60 km of dextral displacement on the Rinonada fault and its presumed extensions to the north—the San Marcos, Espinosa, and Reliz faults (Dibblee, 1976). Dibblee (1976) previously suggested 60 km of offset since the early Tertiary based on similar ages of the sedimentary sections, noting that the thick sequence in the La Panza Range was abruptly truncated to the west and that the sequence near Lake Nacimiento was truncated to the east by the Rinconada fault. Durham (1965) suggested at least 18 km of right-lateral movement along the San Marcos segment, based on offsets of Pliocene strata. Graham (1978) used the offset of Miocene paleo-isobaths to suggest about 43 km of displacement across this segment. Hart (1976) presented geomorphic evidence for strike-slip displacement along the Rinconada fault, and suggested at least 50 km of offset, based on correlations within the Vaqueros Formation. And Ross (1978, 1984), although stating his belief that the central Salinian block is a “comagmatic coherent basement framework within which major structural dislocations seem unlikely”, did allow for up to 45 km of displacement along the Rinconada fault. Smith (1977) correlated the Monterey and La Panza granitic masses to obtain 170 km of dextral offset, but this hypothesis has received little credence.

Although distinctive piercing points do not exist within the La Panza and Nacimiento Upper Cretaceous sedimentary successions, the following similarities are observed:

1. Both sequences crop out on a gently southeast-dipping homocline.
2. Paleocurrent directions and facies relationships in both sections show Late Cretaceous sediment dispersal toward the south/southwest.
3. Stratigraphic successions in both areas demonstrate regression followed by transgression.
4. Similar conglomerate clast types occur at both localities.

While not unique, these elements are consistent with the hypothesized correlations.

Ten km of right-lateral offset is also removed on the La Panza fault. This aligns the basement massifs and honors Durham's (1974) assessment of offset on the Huerhuero fault, the northern extension of the La Panza fault. This restoration, however, affects little change in the overall basinal reconstruction. The base of the Junipero Serra Peak section is correlated to the middle part of the Lake Nacimiento section, because of the observed sediment thinning toward the north/northeast, and the inferred sediment onlap in that direction (as in Figure 5.5).

#### **5.4.2 Implications for Extensional or Transcurrent Influences**

Although the affects of strike-slip faulting are readily visible in modern settings such as the recently active San Andreas fault system, recognizing such affects in ancient sequences can be difficult, because unambiguous evidence of lateral motion is seldom preserved (Mitchell and Reading, 1986). Reconstructing the Late Cretaceous Salinian basin is especially complicated, because Tertiary tectonism has rearranged the original stratal configuration and, in general, obscured older relationships. For example, some of the extant faults may have originated in Cretaceous or early Tertiary times, but more recent motions have disguised their original movement sense. In addition, subcrop data are not available from drilled wells or seismic surveys, mainly because the Upper Cretaceous strata have not proven economically viable with respect to petroleum production, as have Tertiary formations within the Salinian terrane.

Nevertheless, some aspects of the Cretaceous basin's configuration can be inferred from the style of the sedimentary fill, as visible in outcrops. The sedimentary facies are conglomeratic, texturally immature, rapidly deposited, and of limited lateral extent, indicating restricted deposition of locally derived material in an area of pronounced topography. But these features are diagnostic of sedimentation in

fault-bounded, rapidly-subsiding grabens, with or without a strike-slip component of motion (Reading, 1980).

Features typical of strike-slip dominated basins are narrow width (less than about 50 km) and extremely rapid sedimentation, resulting in a basin fill that is deep with respect to its width (Christie-Blick and Biddle, 1985). For example, the Hornelen Basin in western Norway is only 25 km x 70 km in lateral dimensions, but is 25 km thick (Gloppen and Steel, 1981). And the Ridge Basin in southern California accumulated 13 km of sedimentary infill in 7 my (Crowell, 1982). In both of these cases, the basinal depocenters migrated laterally through time as a result of strike-slip motion on basin-bounding faults. Although sedimentation was rapid within the Late Cretaceous Salinian basin (probably exceeding 0.5m/1000yr), it was not as rapid as rates reported for strike-slip basins (up to 12m/1000yr—Stow and others, 1985). And its outcrop pattern (see Figure 5.2) measures 130 km in its northwest to southeast dimension and 30 km in its northeast to southwest dimension, somewhat large for a transtensional basin. Its original size, of course, may have been larger. It was certainly more extensive toward the southwest, because only proximal facies are evident in the present-day outcrop belt.

According to Mitchell and Reading (1986), "the essential feature of strike-slip belts which distinguishes them from areas dominated either by extensional tectonics or by compressional tectonics is that both extensional and compressional features are found closely adjacent to each other and are contemporaneous." In addition to a spatial juxtaposition of these features, a temporal juxtaposition is also expected. Because of the vagaries of strike-slip faults, extension is often short lived, and immediately succeeded by a compressional episode (Christie-Blick and Biddle, 1985). Reading (1980) described the strike-slip cycle in three phases:

1. Phase of extension and crustal thinning.
2. Phase of basin filling.

### 3. Phase of transpression leading to uplift and erosion of deformed basin filling.

Exposures of the Upper Cretaceous Salinian sequences are admittedly poor, but unconformities and angularities, the usual indicators of compressional episodes, have not been observed. Although there may be some depositional hiatuses, there is no evidence of synsedimentary folding or uplift until the Paleocene or Eocene in all localities. These elements suggest that extension was the dominant control on Late Cretaceous to early Tertiary basinal development within the Salinian terrane. The sequence at Santa Margarita Lake (Figure 5.6), for example, shoaled from channelled-slope to nonmarine deposits within its lower part, probably the progradational response to normal faulting and a steep topography along the basin margin. The basin filled because of high sedimentary input associated with the erosion of steep slopes, maintained by recurrent activity. A transgressive event succeeded basin filling, rather than an uplift event, as in Reading's (1980) ideal model. Additional subsidence is common, however, following a rifting episode, because of cooling associated with thermal anomalies developed during crustal extension (McKenzie, 1978). So although strike-slip faulting may have been active within the region, it does not seem to have been the dominant influence on sedimentation within this particular basin, at least during the Cretaceous part of its evolution.

## 5.5 Comparison to Other Cretaceous Sequences

### 5.5.1 Great Valley Sequence (GVS)

Uppermost Cretaceous strata are exposed along the western edge of the San Joaquin Valley east of the San Andreas fault (Figure 5.19) and are deeply buried in the subsurface toward the east. The forearc basin within which they were deposited was widening by the growth of the Franciscan subduction complex and the eastward movement of magmatism within the Sierra Nevadan magmatic arc (Ingersoll, 1988). The shoreline was migrating eastward, and a bathymetric high was being

created along the western edge of the basin as the subduction complex was uplifted (Dickinson and Seely, 1979). During the Maastrichtian stage, communication with open-marine waters was restricted because of the outer-arc ridge, and anoxia ensued, resulting in deposition of organic-rich laminated fine-grained sediments along the western margin of the basin (McGuire, 1988).

Upper Cretaceous strata (found only in the subsurface) more similar to the those in the Salinian terrane were deposited along the western edge of the basin, where fan deltas built out from the Sierran front (Reid, 1988). Figure 5.20 is an isopach map of the Late Cretaceous subcrop. In contrast to the 4 km-thick, northeast-thinning Salinian sequence, the Campanian to Maastrichtian sequence in the southern San Joaquin Valley does not exceed 1100 meters, even in the basin center, and thins depositionally toward the south and east, where it laps onto Sierran basement rocks (Reid, 1988). Conglomerates reported from this sequence do not exceed cobble size, and have compositions similar to the local basement rocks—dark metamorphics, quartzites, and diorites (Reid, 1988). Clearly, even if the Salinian terrane was derived from the southern part of the Sierra Nevada Range, the Late Cretaceous basins were not continuous from north to south. A notable consistency exists between these two areas however. The GVS thins toward the southeast and the Salinian sequence thins toward the northeast, implying a basement high oriented perpendicular to the magmatic arc in the vicinity of the present-day Tehachapi Mountains (assuming an original location for the Salinian terrane from the southern Sierran region).

### 5.5.2 Southern California

Fragments of Upper Cretaceous strata are exposed throughout southern California along the southern edge of the Transverse Ranges and the western edge of the Peninsular Range, all west of the San Andreas fault. Relationships are complicated

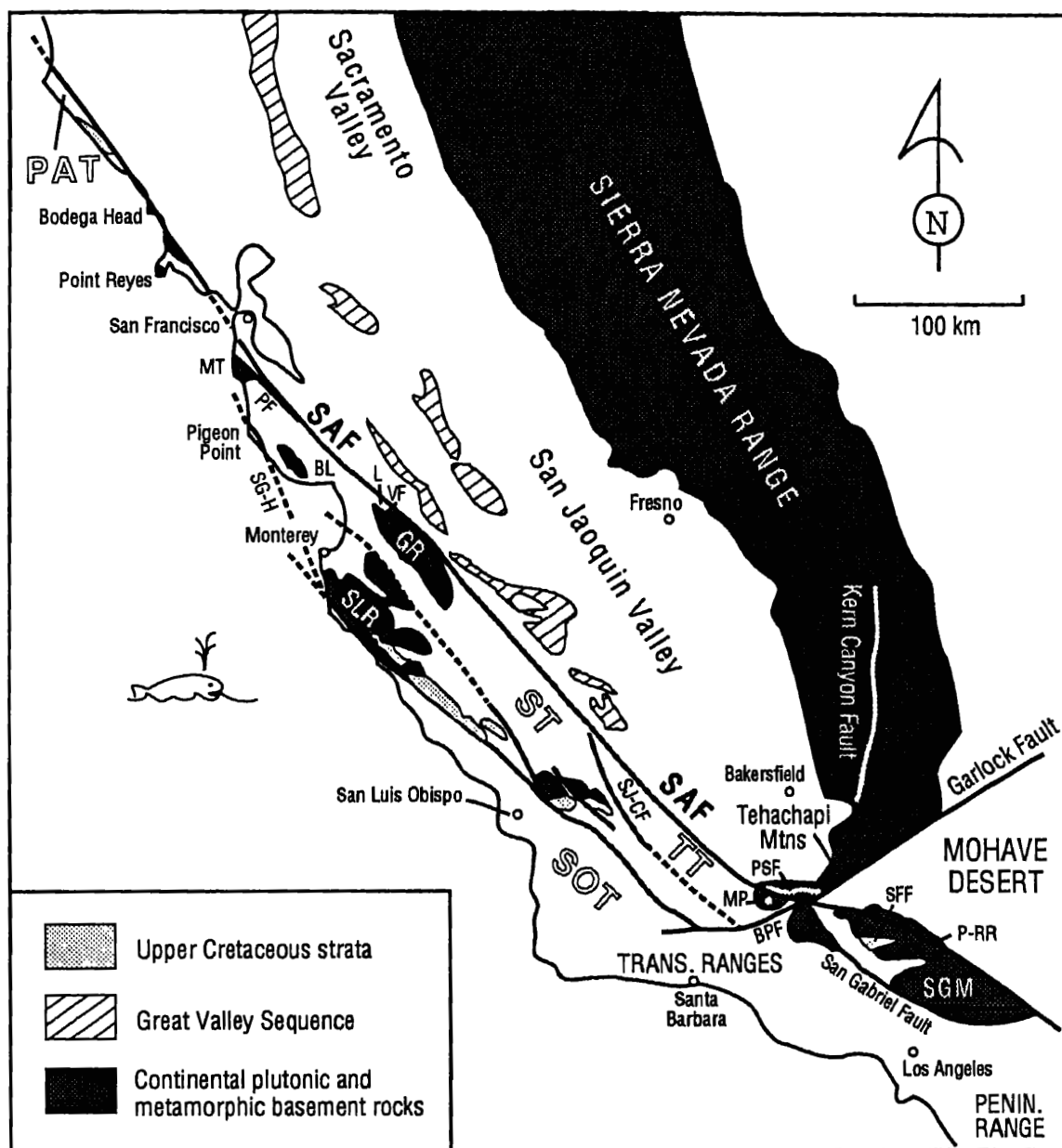


Figure 5.19: Simplified geologic map of central and southern California. Terranes shown: PAT=Point Arena terrane; ST=Salinian terrane; TT=Tujunga terrane; SOT=San Obispo terrane. Faults abbreviations: SAF=San Andreas fault; PF=Pilarcitos fault; SG-H=San Gregorio-Hosgri fault; VF=Vergeles fault; SJ-CF=San Juan/Chimeneas fault; BPF=Big Pine fault; PSF=Pastoria fault. Other abbreviations: MT=Montara; BL=Ben Lomond; SLR=Santa Lucia Range; L=Logan; GR=Gabilan Range; MP=Mount Pinos; SGM=San Gabriel Mountain; SFF=San Francisquito Formation; P-RR=Portal-Ritter Ridge. See Figure ?? for other geographical localities.



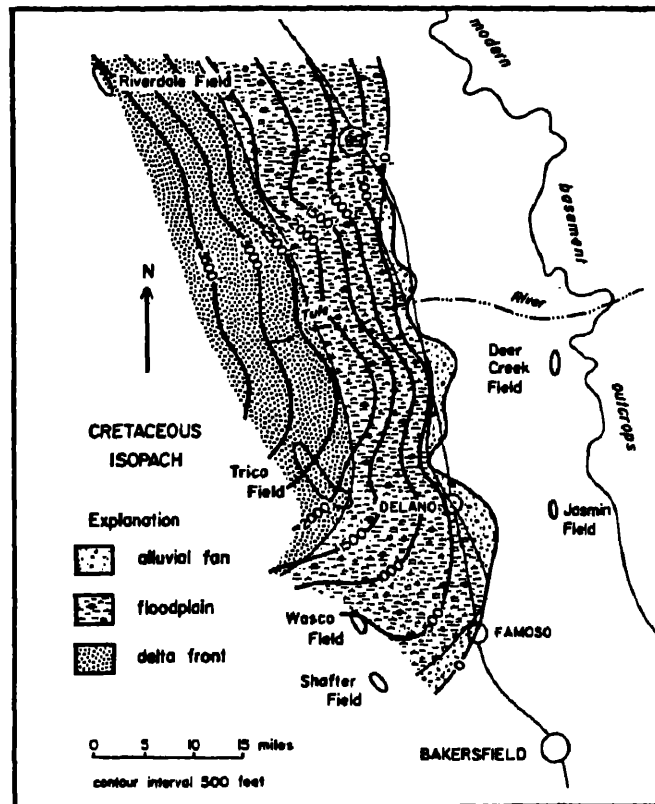


Figure 5.20: Isopach map of Upper Cretaceous strata in the eastern San Joaquin basin with superimposed depositional environments. Note sediment thinning toward the southeast. Diagram from Reid, 1988.

by Neogene rotation and dextral offset, and most of the Transverse Range sections probably formed adjacent to the Peninsular Ranges (Carey and Colburn, 1978; Luyendyk and others, 1980). These sections are generally interpreted as the eastern edge of a forearc basin analogous to the Great Valley Sequence (Bottjer and Link, 1984; Nilsen and Abbott, 1984). Whereas sedimentary facies are similar to those found in Salinian strata, the ages are somewhat different. Some of the Upper Cretaceous sections in southern California demonstrate continuous sedimentation from the Turonian to the Maastrichtian, and all of the sections contain erosional unconformities of latest Cretaceous to lower Paleocene age (Bottjer and Link, 1984). In addition, sequences do not exceed 1.5 km in thickness, and are usually much thinner (Bottjer and Link, 1984). Like the Salinian terrane, these sections were located at least 300 km south of their present location prior to Tertiary dislocation by the San Andreas transform fault.

In contrast to other Upper Cretaceous strata in southern California, the San Francisquito Formation, located inland within the San Gabriel Mountains, is late Maastrichtian to Paleocene in age (Kooser, 1980). The section is nearly 4 km thick, contains south- to southwest-oriented paleocurrent indicators and other evidence of a basin margin to the north and sediment onlap in that direction (Kooser, 1980). Conglomerate clast types are gneiss, quartzite, plutonic, and felsic volcanics (Kooser, 1980) that sound very similar to the Upper Cretaceous Salinian clasts, particularly those in the southeasternmost sections. When Neogene San Andreas dextral offset is restored, the La Panza and San Gabriel Ranges are in close proximity (Figure 5.21). It is tempting to think of the San Francisquito Formation and the Upper Cretaceous Salinian strata as part of the same basin, considering their similarities.

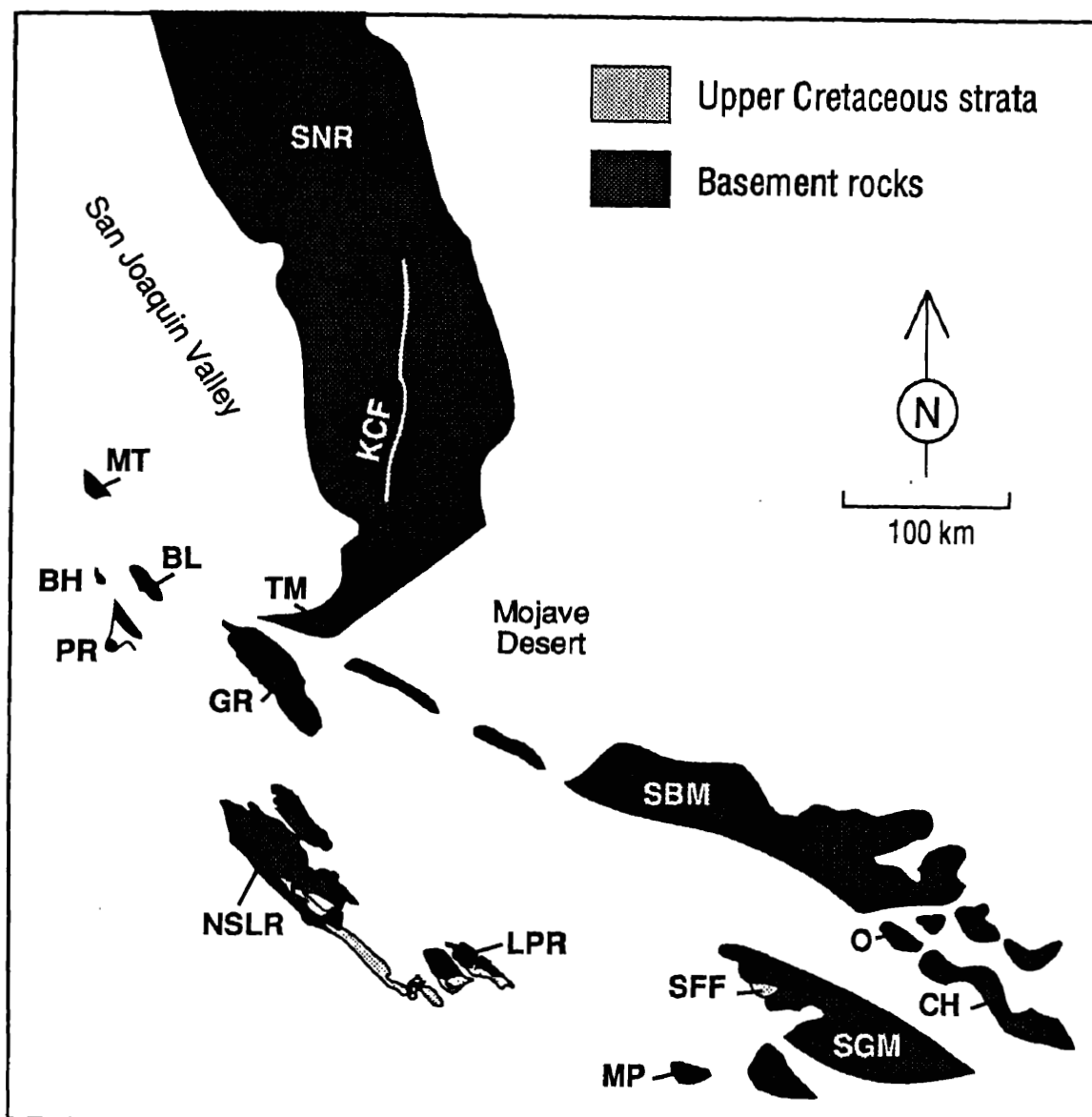


Figure 5.21: Restoration of Salinian terrane to southern California via removal of Neogene fault offsets: San Andreas (central California)=300 km; San Andreas (southern California)=240 km; San Gabriel=60 km; Rinconada=60 km; San Gregorio-Hosgri=135 km (following Ross, 1984). No rotation is restored. Abbreviations: SNR=Sierra Nevada Range; KCF=Kern Canyon fault; MT=Montara; BH=Bodega Head; BL=Ben Lomond; PR=Point Reyes; TM=Tehachapi Mountains; GR=Gabilan Range; SBM=San Bernardino Mountains; O=Orocopia Mountains; CH=Chocolate Mountains; SGM=San Gabriel Mountains; SFF=San Francisco Formation; MP=Mount Pinos; LPR=La Panza Range; NSLR=Northern Santa Lucia Range. See Figures 5.1 and 5.19 for other geographical localities.

### 5.5.3 Sur-Obispo Terrane

A large variety of Upper Cretaceous strata are exposed in the Sur-Obispo terrane, which consists of subduction complex (Franciscan-type) and ophiolitic, rather than plutonic, basement rocks (Figure 5.19). The thickest section (about 3500 km) of Upper Cretaceous strata is exposed in the San Rafael Mountains (Vedder and others, 1967). Vedder and others (1982) inferred the juxtaposition of the Salinian and Sur-Obispo terranes by Late Cretaceous time, based on granitic boulders in the sequence that require a granitic source terrane similar to Salinian basement nearby. Isotopic ages for these boulders are unlike ages from Salinian plutonic rocks (R.W. Kistler, pers. comm., 1988), however, and this model requires further testing.

Tectonically disrupted sequences at Point San Luis, Cambria, and Pfeiffer Beach along the central coast have been interpreted as trench-slope basin fillings (Howell and others, 1977). Other fragments of Upper Cretaceous strata between the coast and the Nacimiento fault are in thrust contact with underlying Franciscan-type rocks (nappes?). Fragments along the Nacimiento fault (Atascadero Formation of Fairbanks, 1904) are similar to the Upper Cretaceous rocks in the Salinian terrane but are generally finer grained and at least in part somewhat older, as the Campanian stage is better represented (Hart, 1976; Page, 1982; Seiders, 1982). Conglomerates from these rocks described by McClure (1969) sound similar to the Salinian conglomerates, but contain higher percentages of metamorphic and mafic volcanic clasts and fewer plutonic clasts. Hall and others' (1979) descriptions of Upper Cretaceous rocks west of the Nacimiento fault also imply greater abundances of mafic volcanic as well as chert clasts. Taliaferro (1944) grouped all of the Upper Cretaceous strata west of the San Andreas fault together as the Ascuncion Formation, but this name has been dropped because of the uncertain relationships east and west of the Nacimiento fault (see Durham, 1974; Dibblee, 1971). The somewhat older ages and finer-grained lithologies described for the strata west of the

Nacimiento fault are consistent with the relationships seen in the Salinian terrane of onlapping through time to the east and of more distal sedimentary facies toward the west, but more study is required to understand the relationships between these sequences.

#### **5.5.4 Pigeon Point and Gualala Formations**

The Pigeon Point Formation has been considered as part of the Salinian terrane, although it lies west of the San Gregorio fault zone and has an uncertain basement type. Restoration of 115 km on the San Gregorio fault (Graham and Dickinson, 1978) matches the Pigeon Point Formation with Upper Cretaceous rocks in the Northern Santa Lucia Range (Figure 5.19). However, restoration of 150 km on the same fault (Clark and others, 1984) places the Pigeon Point Formation west of the Nacimiento fault, matching it with Upper Cretaceous strata of the Sur-Obispo terrane. Campanian ages (Hall and others, 1959) and conglomerate compositions (see Chapter 4) of the Pigeon Point Formation are more compatible with strata of the Sur-Obispo terrane, and it is herein considered a part of that block.

The Gualala Formation is part of the Point Arena terrane (Blake and others, 1982), which has been separated from the Salinian terrane because of its uncertain basement type. The Gualala Formation structurally overlies metabasaltic rocks that are similar to lithologies found within the Franciscan Complex (Wentworth, 1966). Graham and Dickinson's (1978) reconstruction aligns the Point Arena terrane with a sliver between the San Andreas and Pilarcitos faults, which consists of Franciscan basement rocks. Clark and others' (1984) restoration questions this correlation, however, and the original location of the Point Arena terrane remains uncertain.

## 5.6 Southern California Reconstruction

### 5.6.1 Basement Rocks

Geologic investigators of basement rocks within the Salinian terrane, noting the general similarities between these rocks and those in the western Mojave region, the southern Sierra Nevada, Transverse, and Peninsular Ranges, have long suggested a Late Cretaceous–early Tertiary restoration of Salinia to southern California (e.g., Hill and Dibblee, 1953; Weibe, 1970; Ross, 1972; Kistler and Peterson, 1978, Page, 1981; Ross, 1984; Silver and Mattinson, 1986; James and Mattinson, 1988). Specific correlations include the following features (E refers to east of the San Andreas fault, and W refers to west of the San Andreas fault; localities are shown in Figure 5.19). Ross and others (1973) correlated gabbroic clasts in the Gualala Formation of the Point Arena terrane (W) with gabbroic bodies at Logan (W) and near Eagle Rest Peak in the Tehachapi Mountains (E). James (1986) obtained a slightly different age for the Gualala clasts, but accepted the Eagle Rest Peak–Logan correlation put forth by Ross (1970). Ross (1976) correlated the Sierra de Salinas schist (W) and the schist of Portal–Ritter Ridge (E). Ross (1984) correlated the Vergeles fault (W) with the Pastoria fault (E), and also pointed out similarities between assorted plutonic bodies in the Gabilan Range (W) and the Tehachapi Mountains (E), and the general east–west structural grain in the basement rocks of both areas. Kistler and others (1973) and Doe and Delevaux (1973) noted similarities in strontium and lead isotopic compositions between Salinian and Sierran plutonic rocks.

Silver and Mattinson (1986) and James and Mattinson (1988) correlated Salinian and southern Californian basement rocks based on age similarities in both the plutonic and metamorphic lithologies, and on similar trends in both age and metamorphic grade. For example, Salinian plutons were emplaced between 120 and 75 my (based on U/Pb analyses of zircon), with progressively younger ages toward the southeast (Mattinson and James, 1985). Ages derived from K–Ar isotopes (Comp-

ton, 1966; Everdon and Kistler (1970); Hart, 1976), U/Pb data from sphene and apatite (Mattinson and others, 1971; Mattinson, 1978), and fission-track analyses of apatite (Naeser and Ross, 1976) generally range from 60–90 Ma and reflect postintrusive cooling, probably during rapid uplift (Mattinson and James, 1985). These relationships are similar to the eastward-younging and uplift ages found in the southern Sierras (Bateman, 1981; Sams and Saleeby, 1988). And 1.7 b.y. old original and inherited components for metamorphic and plutonic Salinian rocks agree with the ages of Precambrian rocks extensively exposed east of the San Andreas fault and in the San Gabriel Mountains (James and Mattinson, 1988). Ross (1984), although he found problems with the Salinian–Sierran connection in the past (Ross, 1977, 1978), has most recently stressed the similarities after completing a study in the southern Sierras.

Admittedly, some of these correlations are questionable and most are nonunique. But, taken together, these features question the likelihood of pure serendipity juxtaposing two areas with such similar histories, and justify attempts to fit the Salinian story into the southern Californian story.

Believably unique correlations between basement rocks of the San Gabriel Mountains in the Transverse Ranges and the Chocolate and Orocopia Mountains at the western edge of the Mojave region are well established (Crowell, 1962; Ehlig, 1981), so that any major Late Cretaceous or early Tertiary suture must be located east of the San Andreas fault, within the Mojave Desert. In both areas, schists (Pelona and Orocopia) are structurally overlain (Vincent and Chocolate Mountain thrusts) by Precambrian gneisses and Mesozoic intrusive rocks. These relationships extend north of the Big Pine fault into the Mount Pinos area (Haxel and Dillon, 1978), and caused Blake and others (1982) to group these areas together, referring to the underlying plate as the Baldy terrane and the overlying plate as the Tujunga terrane.

Bits of Precambrian gneiss are stretched out along the San Juan-Chimeneas (SJC) fault (Ross, 1978; Mattinson, 1983), and part of the La Panza Range west of the SJC fault is also underlain by gneiss, although it has not been dated (Ross, 1984). Ehlig and Joseph (1977) link the La Panza Range with the Tujunga terrane because of distinctive "polka dot" granites and similar isotopic compositions of basement rocks. So even though the SJC now juxtaposes somewhat different rock types, it is probably not a candidate for a major suture zone, as implied by the reconstruction of Vedder and others (1982). They infer the amalgamation of the Tujunga, Salinian, and Sur-Obispo terranes (Santa Lucia-Orocopia allochthon) by Late Cretaceous time and their subsequent megatransport northward, with accretion to the California margin sometime in the Paleogene, associated with movement on the Vincent-Chocolate Mountains thrust. Most recent work suggests, however, that previous Paleogene metamorphic ages obtained from Pelona schist are uplift ages, and that the metamorphism (induced by movements along the thrust) actually occurred during the Late Cretaceous (Jacobson and others, 1988).

Thus, the problem becomes finding a major suture along which to juxtapose incoming exotic terranes. The relationships outlined above require that the suture be located east of the San Andreas fault zone, in the western Mojave. But workers there find extensions of the Paleozoic miogeoclinal sequence of cratonal North America, and no location to place the suture (Miller and Carr, 1978; Powell, 1982). Silver and Chappell (1988) described the Sierra Nevada, Salinia, western Mojave Desert, and Peninsular Range regions as Cenozoic tectonic fragments of a continuous Mesozoic batholithic belt that extended from northern California to southern Baja California ("California Batholith" of Silver, 1983).



### 5.6.2 Model for Salinian Reconstruction

I suggest that the Late Cretaceous basin within the Salinian terrane may have formed as an east-west-trending intra-arc graben at the southern end of the Sierra Nevada Range. North-south extension could have been produced by the following structural elements (Figure 5.22):

1. North-south-trending dextral faults within the Sierran magmatic arc caused part of the arc massif to move northward, producing extension in a widening gap to the south. Busby-Spera and Saleeby (1988) proposed Late Cretaceous dextral displacement along such a structure—the Kern Canyon fault (Figure 5.19). And a dextral shear zone (“Walker’s Lane”) located east of the Sierran eastern scarp, was probably active within the Cretaceous, although the timing is uncertain (Stewart, 1988).
2. Rapid uplift of the southern Sierran arc, producing gravitational collapse to the south. Sams (1986) and Sams and Saleeby (1988) documented a southward increase in the depth of batholithic exposure within the Sierran range, with uplift commencing in the Late Cretaceous following magmatic cessation.

The Late Cretaceous period was a time of plate reorganization and tectonic transition. The Kula plate, a fast-moving plate with a large component of northward motion relative to the craton, came into existence about 85 Ma (Woods and Davies, 1982). The Laramide orogeny began about 75 Ma, probably induced by acceleration and shoaling of the subducting oceanic plate beneath North America (Coney, 1978; Dickinson and Snyder, 1978). This event coincided with a dramatic increase in the rate of convergence of the Farallon plate (Page and Engebretson, 1984; Engebretson and others, 1985). As North America rapidly overrode the shallow slab, the lower portion of the continental plate may have been tectonically eroded and underplated with oceanic rocks, now exposed in uplifts as the Pelona–Orocopia and

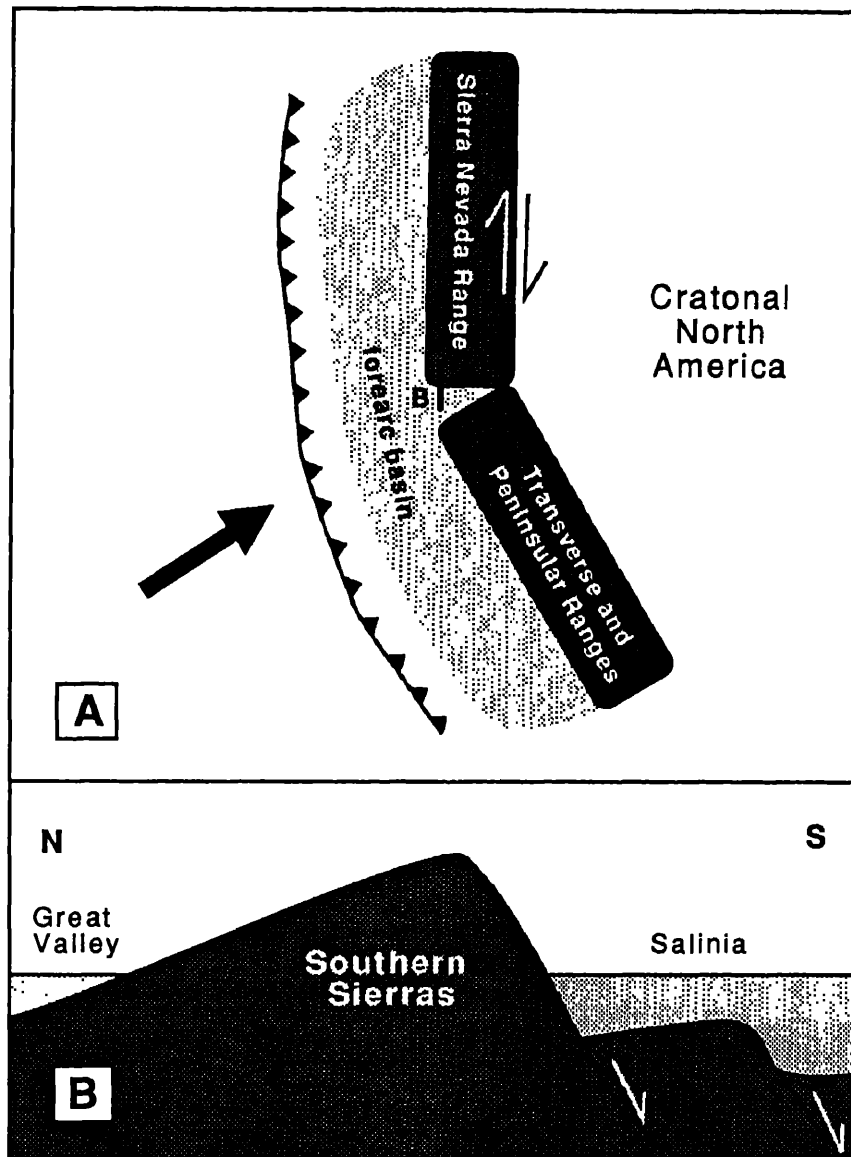


Figure 5.22: Model for extension within the Late Cretaceous Salinian basin. A) Oblique subduction (direction of relative motion shown by large arrow) produces dextral faulting within the Sierran magmatic arc, and an intra-arc graben transverse to the arc. Line labeled B is location of N-S cross section in B. B) Uplift of the magmatic arc produces block faulting within the massif.

related schists (Hamilton, 1988). Magmatism migrated inland, resulting in magmatic cessation along the western arc and isostatic uplift as the batholithic rocks cooled (Snyder and others, 1976; Lipman and others, 1972). The Great Valley forearc basin was also uplifted, progressively west to east (Moxon and Graham, 1987). Compression affected the entire width of the southern Cordillera, reaching far inland to the Rocky Mountain region (Dickinson and Snyder, 1978).

Regional thrusting occurred in southern California, and affects are visible within the Sierra Nevada (Sharry, 1981), Transverse (Powell, 1981; Jacobson, 1983; May, 1986), and Peninsular Ranges (Todd and others, 1988), and in the Mojave Desert region (Burchfiel and Davis, 1981). Thrusting was accompanied by extensive mylonitization and metamorphism from greenschist to lower amphibolite facies (Haxel and Dillon, 1978; Ehlig, 1981; Jacobson and others, 1988). May (1986) found extensive evidence in the San Gabriel Mountains for mylonitization around 81–85 Ma associated with a left-lateral ductile shear zone, which juxtaposed disparate metamorphic terranes and accompanied Late Cretaceous thrusting. He proposed westward tectonic escape of the Salinian–San Gabriel–western Mojave region during the Late Cretaceous as the Peninsular Range converged from the south (see Figure 5.23). This model is appealing because it explains several aspects of Salinian terrane geology:

1. Lateral displacement could explain the juxtaposition of different basement types within the Salinian terrane along the San Juan–Chimeneas and Palo Colorado fault zones prior to Late Cretaceous sedimentation.
2. Westward thrusting could explain relocation of Salinian basement rocks, which are most similar to *eastern* Sierran plutons (Ross, 1972; Silver, 1982), to a forearc position.

3. Westward thrusting would expose the western flank of the Salinian terrane to subduction erosion or transcurrent offset, thus explaining its disappearance (Page, 1982).
4. The extrusion model could explain extension within the Salinian terrane, an escaping crustal fragment (see Figure 5.23).

Nevertheless, although the existence of a regional thrusting event within southern California is well documented, the specific style of this event is much more speculative. Alternatively, Silver (1982, 1983) proposed the westward placement of the Salinian and Mojave regions by 125–150 km of west-directed overthrusting within the late Paleogene. Hall (1988) also proposed Paleogene thrusting—180 km toward the northwest—of a large area which he termed the “Southern California Allochthon”. Detailed mapping by Hall (1988) showed that Salinian basement rocks and Upper Cretaceous and Paleocene strata form the hanging wall of the Sur thrust, and overlie Franciscan-type accretionary complex rocks and other Upper Cretaceous strata in the foot wall. This episode of compression must therefore be post-early Paleocene in age. Hall (1988), based on missing section in the Santa Cruz Mountains, suggests a late Paleocene to early Eocene age for the event.

The Farallon plate maintained its rapid convergence with respect to the North American margin until about 45 Ma (Engelbreton and others, 1985), so it is not surprising that compressional structures are observed throughout the 75–45 Ma time period. The Salinian Upper Cretaceous strata do not throw much light on this subject, but understanding how other Upper Cretaceous rocks relate to the Salinian ones would be enlightening. For example, it is important to know when the Sur-Obispo terrane was juxtaposed next to the Salinian terrane. By Vedder and others' (1982) model, this juxtaposition occurred prior to Late Cretaceous sedimentation and megatransport northward. By Hall's (1988) model, alternatively, the juxtaposition occurred in the late Paleocene during thrusting. Page (1982), on

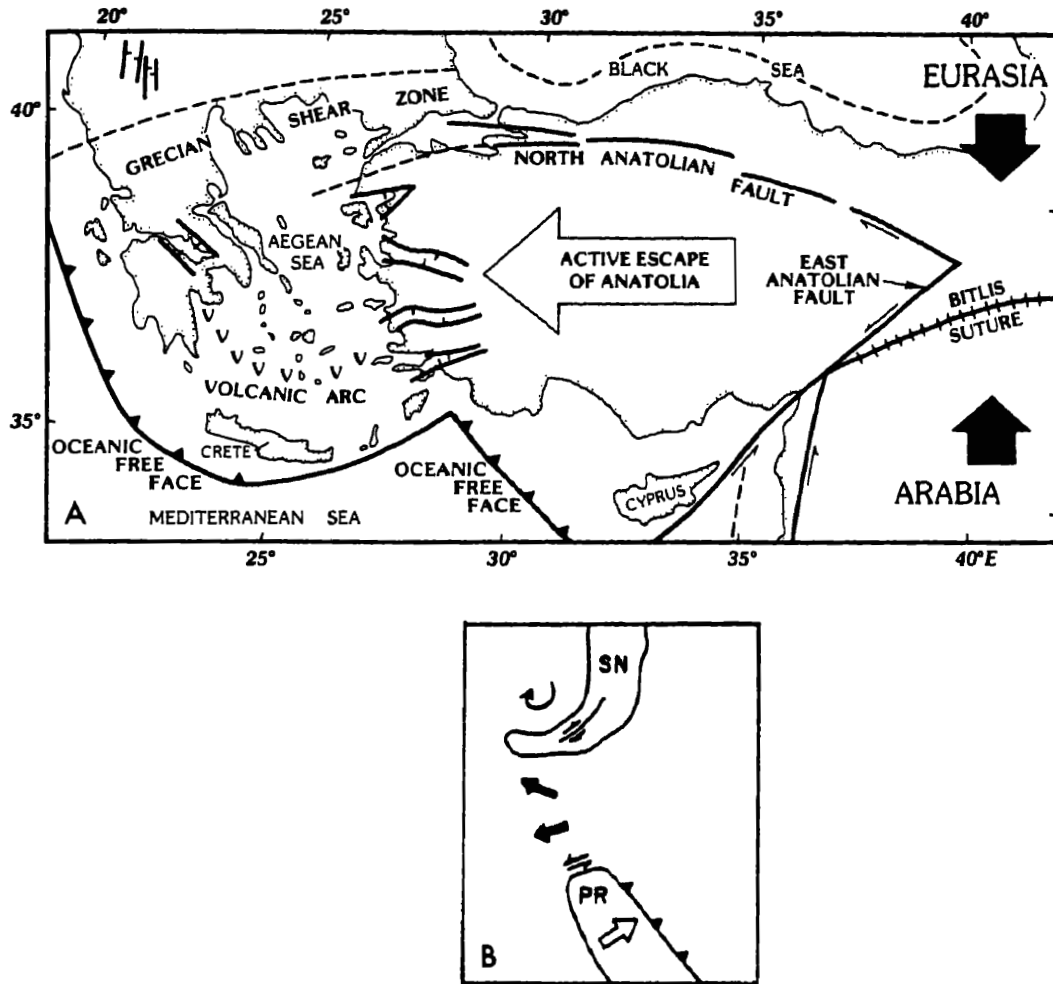


Figure 5.23: Tectonic escape model for the westward thrusting of the Salinian terrane (May, 1986). A) Modern example: Turkey is experiencing compression from the collision of Arabia and Eurasia. Anatolia is "escaping" westward. The area is bounded by strike-slip faults and extension is occurring toward the west (from Burke and Şengör, 1986). B. The model applied to southern California in the Late Cretaceous: the Peninsular Range is moving northeast, creating compression and causing the western escape of the Salinian and western Mojave regions (from May, 1986).

the basis of thrust truncations along the Nacimiento fault and lack of Paleocene strata in the Sur-Obispo terrane as compared to the Salinian terrane, also inferred a post-Cretaceous juxtaposition. Future work geared at understanding the relationships between the various Upper Cretaceous and early Tertiary strata should clarify this issue.

Late Cretaceous to early Tertiary compression was accompanied by rapid uplift. Cooling curves constructed from fission track ages suggest rapid and intensive cooling of the San Gabriel terrane (upper plate of Vincent thrust) between 70 Ma and 57 Ma (Mahaffie and Dokka, 1986). And K-Ar cooling ages from lower plate schists range from 35 to 60 m.y. (Dillon, 1986). Batholithic rocks in both the Sierra Nevada and Peninsular Ranges were uplifted and unroofed in latest Cretaceous and early Tertiary time (Sams and Salleby, 1988; Todd and others, 1988). Sams and Saleeby (1988) suggest that uplift was accompanied by rotation (Kanter and McWilliams, 1982; McWilliams and Li, 1985) and tilting toward the north, thereby exposing floor levels of the batholith in the southern Tehachapi "tail". May's (1986) model also suggests that some rotation occurred in the Late Cretaceous as the Salinian and Mojave regions were extruded westward. These models are in contrast to Hall's (1988), wherein flexure of the southern Sierras, as well as northwesternmost Salinia, did not occur until the Neogene, associated with dextral drag along the San Andreas fault zone.

As with the thrusting episodes, clockwise rotation of the southern Sierras may have been a multi-stage process. Rotation is only poorly constrained between 80 and 20 Ma (Kanter and McWilliams, 1982; McWilliams and Li, 1985), although the work of Plescia and Calderone (1982) suggests that at least some of the bending is post 25 Ma, and S. Graham (unpublished data) suggests that it is all Tertiary. It is not clear whether or not any rotation occurred within the central Salinian terrane. Magnetostratigraphy by Khan and Coe (1987) showed no rotation since the

Miocene. But similar east-west basement trends in the Tehachapi Mountains and in the Gabilan and Northern Santa Lucia Range might point to at least some rotation prior to Upper Cretaceous sedimentation. In the reconstruction of Figure 5.21, only translation was restored along faults. However, a post-Late Cretaceous clockwise rotation of about  $25^{\circ}$  would juxtapose the Salinian terrane more closely to the western Mojave region and align the Upper Cretaceous strata along a more east-west trend, consistent with the basin model developed herein. The only paleomagnetic analysis of central Salinian Upper Cretaceous rocks (see Chapter 3) revealed a "primary" component, after removal of a present-day overprinting direction, that is consistent with the expected latitude, but rotated  $35^{\circ}$  clockwise. Unfortunately, the results are equivocal, and the primary direction may be a second overprinting direction, but in a reversed polarity field. Nevertheless, it is possible that some rotation of the Salinian terrane was associated with thrusting events during the Late Cretaceous and/or Paleogene.

Some normal faults have also been observed that are apparently Late Cretaceous to early Tertiary in age. A normal fault in southeasternmost California is bracketed between the age of motion on the Chocolate Mountains thrust (about 80 Ma) and 60 Ma (Haxel and others, 1975). Barth (1988) and Jacobson and others (1988) present evidence for the reactivation of a number of Late Cretaceous thrust faults as normal faults within the Late Cretaceous or early Tertiary. This is not surprising, since extensional collapse is a common response to major continental shortening and rapid uplift (Dewey, 1988). For example, east-west extension has been well documented in Tibet, where rapid uplift is a result of compression associated with the collision of India and Eurasia (Mercier and others, 1987). Extension has also been reported in the Peruvian Andes (Dalmayrac, 1981), where compression associated with shallow east-dipping subduction of the oceanic plate (Barazangi and Isacks, 1976), probably similar to the situation that existed along the southern Cordillera of North America

during the Laramide orogeny (Jordan and others, 1983).

A noteworthy feature, considering the amount of verbal and written energy that has been expended on it, is the so-called proto-San Andreas fault. This term, describing pre-Neogene dextral displacement, was coined by Suppe (1970) to explain the residual offset that remained between Salinian and Sierran basement rocks following restoration of 300 km of Neogene San Andreas offset (see Figure 5.21). The concept has been discredited by some workers. Johnson and Normark (1974) hypothesized that extensive slivering along Neogene strike-slip faults could restore the Salinian block to a sufficiently compact piece to tuck south of the Sierran massif; documentation of at least 100 km of offset along the San Gregorio-Hosgri fault has provided some of the suggested slivering (Graham and Dickinson, 1978; Clarke and others, 1984). Silver (1982, 1983) placed the Salinian terrane in a position somewhat north of the southernmost Sierra Nevada Range by westward thrusting over the Great Valley, an untenable scenario because the Great Valley was a marine basin at that time. And Hall (1988) accomplished a similar result by northwestward thrusting and clockwise flexure around the southern end of the Great Valley. Still, the concept persists, used to explain a hypothesized transform margin setting in Late Cretaceous to early Tertiary time (Nilsen and Clarke, 1975; Nilsen, 1978), and extended to accommodate over 2000 km of dextral displacement (Vedder and others, 1982; Champion and others, 1984; Howell and others, 1987). Certainly, some component of dextral displacement may have rearranged crustal pieces in this earlier time frame.

## 5.7 Modern Analogs

Figure 5.24 illustrates two modern-day settings wherein dextral displacement within an oblique subduction zone has instigated an extensional basin trending perpendicular to the trend of the trench and magmatic arc. The Sunda arc is apparently



separating between the islands of Sumatra and Java as a result of right-lateral offset along the Central fault in Sumatra, which is taking up the oblique component of subduction (Hamilton, 1979). Java, on the other hand, is oriented parallel to the subduction zone, in a position more conducive to orthogonal subduction. The Sunda Strait is a zone of extension between the islands that accommodates the transition from orthogonal to oblique subduction (Huchon and Le Pichon, 1984). Like the Late Cretaceous (Great Valley) forearc basin in California, the forearc basin off the coast of Sumatra is a wide, ridged type, with uplifted accretionary complex rocks forming a bathymetric high between the forearc and trench. Foraminiferal assemblages suggest that, like the Java island south of Sumatra, the forearc basin associated with the Peninsular Range and the Salinian terrane, was a more open-marine unridged type (Sliter, 1986).

A similar scenario is found in the Kuril arc of northern Japan (Figure 5.24). Here a large dextral fault associated with oblique subduction is also forming a graben transverse to the subduction zone (Kimura, 1986). But whereas the Sumatran strike-slip fault continues to the north into an extensional area, like the San Andreas transform continues into the extensional Gulf of California, the Kuril arc strike-slip fault ends in a collisional zone, where it is encountering the continental mass of the Eurasian plate (Kimura, 1986).

## 5.8 Comparison with Paleomagnetic Data

The model described herein does not account for paleomagnetic data (reviewed in Chapter 1) that suggest that the Salinian terrane was located at about the latitude of southern Mexico rather than southern California in Late Cretaceous time. The discrepancy between geologic and paleomagnetic data sets might be resolved in one of the following ways:

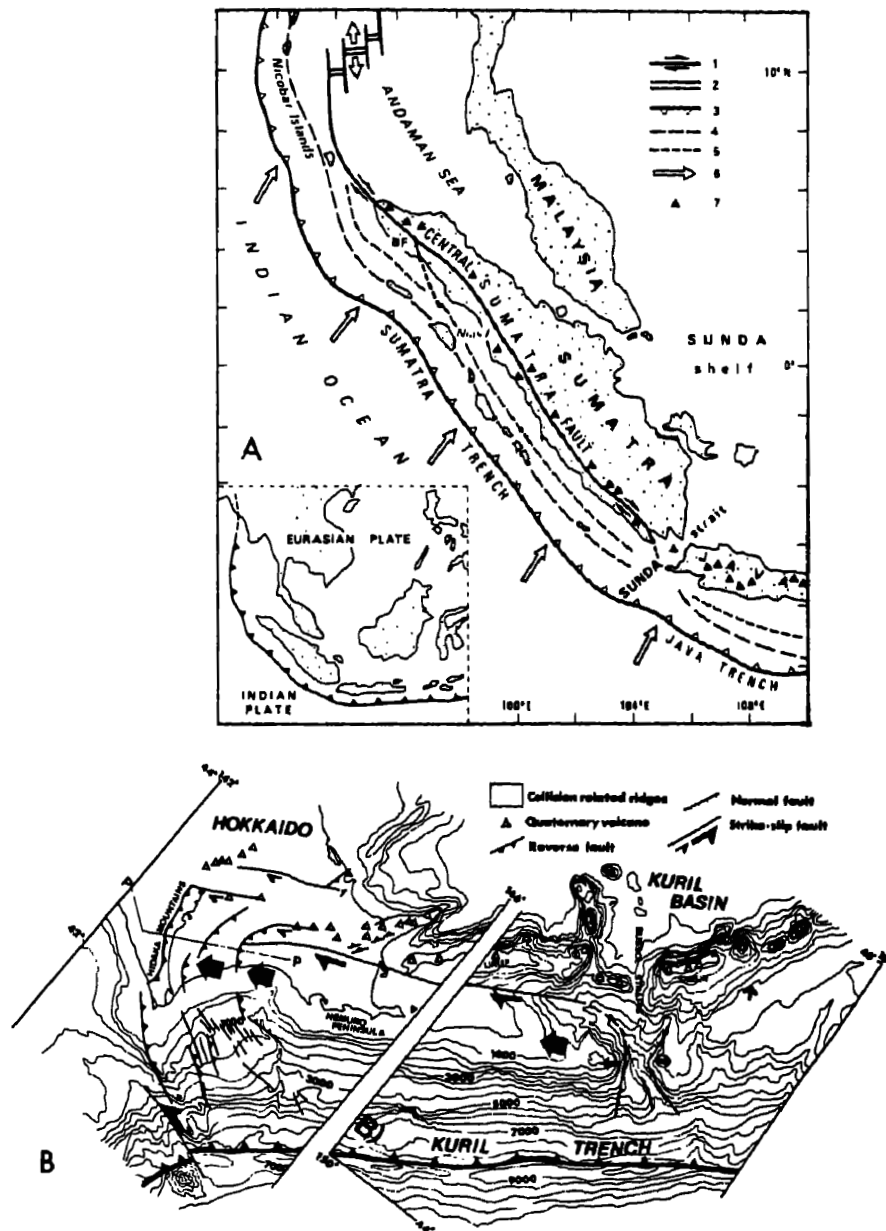


Figure 5.24: Modern analogs for Late Cretaceous basin formation (see Figure 5.22). A) Extension is occurring in the Sunda Strait (Indonesia) as a result of oblique subduction and dextral offset along the Central fault in Sumatra. Extension is also occurring in the Andaman Sea at the other end of the strike-slip fault. 1: Strike-slip fault (BF=Batee fault); 2: spreading center; 3: subduction trench; 4: axis of outer ridge; 5: axis of fore-arc basin; 6: direction of relative motion; 7: active volcano. From Huchon and Le Pichon (1984). B) Extension transverse to the magmatic arc and trench is also occurring within the Kuril arc (between Kamchatka—USSR—and Hakkaido island—Japan) as a result of oblique subduction. Here *compression* is occurring at the other end of the strike-slip fault because of collision with the Eurasian landmass.

1. The similarities between Salinian and southern Californian basement rocks may be coincidental and simply reflect their origin in similar petrotectonic settings. Certainly, subduction and magmatism were occurring along a large portion of the west coast of the Americas during the Cretaceous period. However, basement rocks have been uniquely correlated across the San Andreas fault in southern California, and if the Salinian terrane is tied to these rocks, as many have suggested, then they are also tied to the western Mojave Desert region.
2. The suture between "stable" North American and exotic terranes in southern California is located inland from the San Andreas fault in the Mojave Desert. So far this suture has not been found and workers in the area have correlated stratigraphic sequences found in the continental interior to the western edge of the Mojave region and beyond. In addition, any correlations between the Salinian and Sierran arcs could not be accommodated by this model.
3. The paleomagnetic data have been misinterpreted. This scenario requires some systematic error that is biasing a large region, because various data sets from many different localities consistently suggest low latitudes and clockwise rotations. Inclination error due to sedimentary compaction or batholithic tilting can be ruled out because of consistency between results from both sedimentary and plutonic rocks. A large-scale remagnetization event could have occurred, probably sometime in the Eocene, perhaps diachronously along the continental margin. The Salinian sections, at least, contain angular unconformities, suggesting a deformational event in the late Paleocene to Eocene.
4. Since no robust paleomagnetic data have been obtained from the central Salinian terrane, this area could be related to cratonic North America and the Sur-Obispo and Point Arena terranes could have amalgamated with it

sometime later in the Tertiary. But while the Pigeon Point locality may be related to the Sur-Obispo terrane with removal of San Gregorio-Hosgri fault restoration, the Montara Mountain locality is situated on granitoid basement rocks and is more difficult to dismiss. This option is not considered viable.

Many aspects of the models described in this chapter can be applied to the Upper Cretaceous Salinian basin regardless of its precise location of origin. The models are consistent with an origin in southern California but may not require it. Future investigations are needed, particularly to establish believable correlations between basement rocks and clast types in sedimentary sequences, to more fully comprehend the tectonic setting of the Salinian terrane.

## 5.9 Conclusions

Upper Cretaceous strata on the central part of the Salinian terrane were deposited within a steep-sided, normal-fault-controlled basin that was rapidly and episodically subsiding. The preserved strata are primarily coarse-grained facies of a fan-deltaic system—alluvial fan, delta plain, transition zone (mainly nearshore marine) and delta front and slope. The deposits are interpreted in terms of a slope fan-delta model, wherein coarse-grained sediment-gravity flows are deposited directly seaward of the marine to nonmarine transition zone. This fan type is typical of fault-controlled basins, such as the modern Yallah's fan in Jamaica (Wescott and Ethridge, 1980). It is recognized by the close vertical association of nonmarine and nearshore deposits with submarine gravity-flow and slope deposits.

Facies relationships, paleocurrent indicators, and sedimentary thickness variations show that the sediment source area was toward the north/northeast, and that sediments were dispersed mainly toward the south/southwest. Thus, transverse rather than longitudinal flow was probably dominate within the basin, a typical feature of fan-deltaic sedimentation. The southern and western margins of the

basin are unknown; they have either been tectonically removed or they occur in fragmented form to the west in the Sur-Obispo terrane. However, the relationship between the Upper Cretaceous strata of the central Salinian terrane and those in the Sur-Obispo terrane and to the north at Pigeon Point and Gualala, is uncertain.

Similar lithofacies, vertical successions, and clast types within the central Salinian sections, suggest deposition within a single, laterally continuous basin rather than in a series of sub-basins, as has previously been proposed. Improved biostratigraphy is required, however, to confirm the correlations (Figure 5.4). The Salinian successions record deltaic progradation and basin filling from slope depths, followed by transgression and return to slope depths. Deep-water sedimentation apparently continued into the lower Tertiary. [Note: "Deep water" herein refers to slope depths, probably not exceeding 1000 meters. More distal facies, with greater depths, are not represented in the Salinian sections.]

Conglomerate clast types are similar to what would be expected from a Sierran-western Mojave-Peninsular Range provenance. In addition, the basement rocks from these areas are similar to Salinian basement rocks. Although some of the basement correlations are questionable, the similarities are striking. Considering this, as well as the lack of information from southern Mexico (where paleomagnetic data suggest derivation), I have developed a model based on extraction from the Sierran-Peninsular magmatic arc prior to about 300 km of Neogene offset along the San Andreas fault zone.

By this model, the Upper Cretaceous Salinian sediments were deposited within an east-west-trending intra-arc graben formed by extension associated with right-lateral offset along a north-south-trending fault, such as the Kern Canyon fault. The right-lateral translation was a response to oblique subduction during a time of rapid convergence between the North American and subducting oceanic plates. Both the Kula and Farallon oceanic plates had a dextral component of motion relative to

North America during latest Cretaceous time (Page and Engebretson, 1984). The Kula plate had greater obliquity, but the location of the Kula/Farallon ridge is not known, so it is uncertain which plate was adjacent to California (Engebretson and others, 1985). Busby-Spera and Saleeby (1988) have suggested that dextral motions along the Kern Canyon fault began in response to rapid northward movement of the Kula plate at about 80 Ma.

The scenario resembles the present-day Sunda and Kuril arcs, where grabens are being formed transverse to the trench and magmatic arc in a transition zone between oblique subduction and more orthogonal subduction (Huchon and Le Pichon, 1984; Kimura, 1986). Similarly, I suggest that the Salinian basin may have formed in a transition zone between the Sierran arc, where subduction was oblique, and the Peninsular arc to the south, where subduction may have been more orthogonal.

Extension was also facilitated by uplift throughout southern California as the region cooled following the cessation of magmatism and as compression contracted the area. Batholithic rocks as young as 80 Ma were uplifted and exposed to erosion by the end of the Campanian to early Maastrichtian stages. Very deep batholithic levels exposed within the southern Sierras attest to differential uplift within the Sierran Range even before the most recent uplift that has occurred within the Late Cenozoic (Sams and Saleeby, 1988). This uplift may have led to block faulting within basement rocks. Extension is commonly found in modern compressional settings (e.g., Tibet and the Peruvian Andes), a result of thickened crust and gravitational collapse (Dewey, 1988).

The intra-arc graben model explains certain aspects of Salinian geology. First, it exposes the central to eastern portions of the Sierran/Peninsular plutonic belt, which contain lithologies most similar to Salinian plutonic basement rocks. The progressive younging of Salinian plutonic rocks to the east suggests that an east-west cross-sectional slice has been extracted. And second, the model explains the

sedimentary facies in the Upper Cretaceous sequences, which contain the hallmarks of deposition within a basin that is experiencing rapid vertical movements on structures that are more or less east-west trending. West-vergent thrusting also probably played a role in the extraction of the Salinian fragment from its batholithic home (May, 1986; Silver, 1986; Hall, 1988). This thrusting may have occurred in the Late Cretaceous prior to basinal formation, or sometime within the Paleogene, or both. Clockwise rotation may have accompanied the thrusting episode(s). An important aspect of this issue concerns the timing of the Sur-Obispo's juxtaposition with the Salinian terrane, perhaps following removal of Salinia's western flank (Page, 1982). Strike-slip faulting may have removed this flank after the Salinian terrane was thrust westward, thus vulnerably exposed to fragmentation along a tectonically active plate margin. An improved understanding of the Upper Cretaceous strata on the Sur-Obispo terrane and of the timing of thrusting should clarify these relationships.

It is clear that the Upper Cretaceous to lower Paleocene section was uplifted and exposed to erosion sometime within the Paleocene or Eocene, perhaps diachronously. Nilsen and Clarke (1975) have suggested a borderland-type setting influenced by right-lateral faulting during the early Tertiary in central California. The Salinian fragment was located within a forearc position at least by this time. It has proceeded to move northward, since it was transferred to the Pacific plate, which encountered the North American margin about 30 Ma (Atwater, 1970).

Finally, the model presented herein does not account for discrepant paleomagnetic data that infer a lower-latitude origin for the Salinian crustal block. Although discrepant data have not been obtained from the central Salinian terrane, data from the northern part of the terrane (at Pigeon Point and near Montara Mountain—Champion and others, 1984), from the Point Arena terrane (Kanter and Debiche, 1985), and the Sur-Obispo terrane (McWilliams and Howell, 1982; Fones and oth-

ers, in prep.) imply that the entire region west of the San Andreas fault experienced large latitudinal transport. Some problem is inherent, in the geologic correlations, the paleomagnetic interpretations, or both. But as our knowledge of the eastern Pacific region continues to expand, we are likely to find an answer to the current dilemma. Hopefully, this study provides a few useful pieces for the tectonic reconstruction puzzle.



# Appendix      A

## Paleontology

### A.1 Foraminifers

#### A.1.1 Faunal lists

Foraminiferal assemblages collected by K.Grove and analyzed by William Sliter and Mary McGann: U.S. Geological Survey, Menlo Park, California. Maps and descriptions of sample localities follow faunal listings. Samples contain mostly poorly preserved and sparse agglutinated species with rare pyritic casts of calcareous forms. They represent residue assemblages due to dissolution in corrosive marine environments, surface weathering, or both. Calcareous benthic foraminifers occur only rarely, and are poorly preserved (W.R. Sliter, pers.comm., 1986; 1988). Numbers on chart refer to U.S. Geological Survey Mf designations. X=occurrence in sample. Maps with sampled localities are included after the faunal lists and sample descriptions.

**LAKE NACIMIENTO SAMPLES**

<b>Foraminifers</b>	<b>7073</b>	<b>7074</b>	<b>7075</b>	<b>7076</b>	<b>7077</b>	<b>7078</b>
<i>Allomorphina cretacea</i> Reuss						X
<i>Ammodiscus cretaceus</i>		X			X	
<i>Bathysiphon brosgiei</i> Tappan					X	
<i>Bathysiphon vitta</i> Nauss	X	X	X	X	X	X
<i>Cribrostomoides cretaceus</i> Cushman and Goudkoff	X	X	X	X	X	X
<i>Dentalina basiplanata</i> Cushman						X
<i>Dentalina gracilis</i> (d'Orbiny)						X
<i>Dorothia bulletta</i> (Carsey)	X					
<i>Eggerella</i> ? sp. cf. <i>E. obscura</i> Martin	X					
<i>Gaudryina bentonensis</i> (Carman)	X	X	X		X	
<i>Gavelinella</i> ? sp.						X
<i>Gyroidinoides nitidus</i> (Ruess)						X
<i>Haplophragmioides excavatus</i> Cushman and Waters					X	X
<i>Haplophragmoides fraseri</i> Wickenden				X		
<i>Hoeglundina supracretacea</i> (ten Dam)						X
<i>Lenticulina muensteri</i> (Roemer)						X
<i>Neoflabellina pilulifera</i> (Cushman and Campbell)				X		X
<i>Orthokarstenia whitei</i> (Church)				X		X
<i>Praebulimina aspera</i> Cushman and Parker				X		X
<i>Praebulimina kickapooensis</i> (Cole)						X
<i>Praebulimian venusae</i> (Nauss)				X		X
<i>Reophax globosus</i> Sliter						X
<i>Saccammina complanata</i> Franke		X		X		
<i>Silicosigmoilina californica</i> Cushman and Church	X				X	X
<i>Spiroplectammina</i> cf. <i>S. sigmoidina</i> Lalicker	X				X	
<i>Spiroplectammina</i> cf. <i>S. juncea</i> Cushman	X					
<i>Stilistomella impensia</i> (Cushman)				X		
<i>Tritaxia capitosa</i> (Cushman)	X					
<i>Trochammina</i> cf. <i>T. boehmi</i> Franke					X	
<i>Trochammina</i> cf. <i>T. texana</i> Reuss	X	X	X	X		

**LAKE NACIMIENTO SAMPLES (cont)**

Foraminifers	7038	7039	7041	7042	7044
<i>Allomorphina cretacea</i> Reuss		X			
<i>Ammodiscus glabratus</i>		X			
<i>Ammodiscus cretaceus</i>			X		X
<i>Bathysiphon vitta</i> Nauss	X	X	X	X	X
<i>Cribrostomoides cretaceus</i> Cushman and Goudkoff	X	X	X	X	X
<i>Dorothia bulletta</i> (Carsey)			X		
<i>Haplophragmiodes excavatus</i> Cushman and Waters			X	X	X
<i>Haplophragmoides fraseri</i> Wickenden		X			
<i>Gaudryina bentonensis</i> (Carman)		X	X		X
<i>Praebulimina aspera</i> Cushman and Parker				X	
<i>Praebulimina kickapooensis</i> (Cole)		X			
<i>Praebulimian venusae</i> (Nauss)		X			
<i>Silicosigmoilina californica</i> Cushman and Church	X				X
<i>Spiroplectammina sigmoidina</i> Lalicker	X	X	X		X
<i>Trochammina boehmi</i> Franke					X
<i>Trochammina texana</i> Reuss		X			
<i>Trochammina</i> ? sp.	X				

**SANTA MARGARITA LAKE SAMPLES**

Foraminifers	7425	7426	7427	7429	7430	7431
<i>Allomorphina</i> ? sp. cf. <i>A. cretacea</i> Reuss				X		
<i>Bathysiphon</i> sp.	X				X	
<i>Bathysiphon vitta</i> Nauss		X		X		
<i>Cribrostomoides cretaceus</i> Cushman and Goudkoff	X	X	X	X	X	X
<i>Dentalina vistulae</i> Pozaryska					X	
<i>Dorothia bulletta</i> (Carsey)				X		
<i>Dorothia ellisorae</i> Franke				X		
<i>Gaudryina bentonensis</i> (Carman)	X				X	
<i>Gaudryina laevigata</i> Franke				X		
<i>Gavelinella stephensoni</i> (Cushman)				X		
<i>Gavelinella</i> sp. cf. <i>G. velascoensis</i> (Cushman)	X					
<i>Gyroidinoides nitidus</i> (Ruess)						X
<i>Haplophragmiodes excavatus</i> Cushman and Waters	X	X	X	X		X
<i>Haplophragmoides</i> sp.	X					
<i>Hoeglundina supracretacea</i> (ten Dam)						X
<i>Lenticulina almgreni</i> Martin	X	X		X		
<i>Praebulimina aspera</i> Cushman and Parker				X		
<i>Pyramidina proliza</i> (Cushman and Parker)		X				
<i>Nodosaria</i> sp. cf. <i>N. distans</i> Ruess		X		X		
<i>Praebulimian spinata</i> (Cushman and Campbell)				X		
<i>Serovaina orbicella</i> (Bandy)		X				
<i>Silicosigmoilina californica</i> Cushman and Church		X	X	X		X
<i>Spiroplectammina sigmoidina</i> Lalicker				X		
<i>Spiroplectammina chicoana</i> Lalicker					X	
<i>Stilistomella impensia</i> (Cushman)				X		

### A.1.2 Sample descriptions

Ages and environments from Sliter (pers.comm., 1986; 1988).

Mf# 7038 (field #LNS-15). Lime Mountain 7.5" Quad.; section 19, T25S, R10E; 500'W, 250'N of SE corner of section 19, about 725' elevation. Campanian to Paleocene.

Mf# 7039 (field #LNS-19). Lime Mountain 7.5" Quad.; section 20, T25S, R10E, 300'W, 250'N of SE corner of section 20, about 725' elevation. Fauna other than foraminifers: fish debris, crab carapace. Late Campanian to Maastrichtian. Suggestive of low-oxygen or middle bathyal water depths.

Mf# 7040 (field #LNS-32). Lime Mountain 7.5" Quad.; section 36, T25S, R9E; 1780'W, 1200'S of NE corner of section 36, about 750' elevation. Calcispherulids? Age indeterminate.

Mf# 7041 (field #LNN-52). Lime Mountain 7.5" Quad.; section 23, T25S, R9E; 1400'W, 1000'S of NE corner of section 23, about 750' elevation. Fauna other than foraminifers: Bryozoan?, fish debris. Late Campanian to Maastrichtian. Bathyal water depths.

Mf# 7042 (field #LNN-538). Tierra Redonda Mountain 7.5" Quad.; section 13, T25S, R9E; 300'W, 3050'S of NE corner of section 13, about 775' elevation. As for Mf#7041.

Mf# 7043 (field #LNN-848). Tierra Redonda Mountain 7.5" Quad.; section 17, T25S, R10E; 625'W, 2900'S of NE corner of section 17, about 775' elevation. Echinoid debris, agglutinated foraminifers?. Age indeterminate.

Mf# 7044 (field #AQ-70). Adalaida 7.5" Quad.; section 4, T26S, R11E; 125'E, 650'N of SW corner of section 4, about 1000' elevation. Late Campanian to Maastrichtian. Bathyal environment.

Mf# 7073 (field #LNS-16). Lime Mountain 7.5" Quad.; section 20, T25S, R10E; 1750'E, 1100'N of SW corner of section 20, about 750' elevation. Late Campanian to Maastrichtian (similar to faunas from the upper Marlife Formation). Bathyal depositional environment.

Mf# 7074 (field #LNS-20). Lime Mountain 7.5" Quad.; section 21, T25S, R10E; 650'E, 1725'N of SW corner of section 21, about 725' elevation. As for Mf# 7073.

Mf# 7075 (field #LNS-64). Lime Mountain 7.5" Quad.; section 21, T25S, R10E; 650'E, 1725'N of SW corner of section 21, about 725' elevation. As for Mf# 7073.

Mf# 7076 (field #LNN-78). Lime Mountain 7.5" Quad.; section 13, T25S, R9E; 1900'E, 250'N of Sw corner of section 13, about 710' elevation. Other fauna: Ostracodes. Late Maastrichtian (zone C of Goudkoff or stratal equivalent of the Tierra Loma and Marca Shale Members of the Moreno Formation). Elements of this fauna are found commonly associated with low-oxygen environments—middle bathyal depths (500-1500 m) on an open slope or shallower in restricted basins.

Mf# 7077 (field #LNS-100). Lime Mountain 7.5" Quad.; section 20, T25S, R10E; 2700'E, 2250'N of SW corner of section 20, about 700' elevation. Probably Maastrichtian.

Mf# 7078 (field #LNN-545-3). Tierra Redonda Mountain 7.5" Quad.; section 17, T25S, R10E, 2250'E, 3970'S of NW corner of section 17, anout 750' elevation. Other fauna: Ostracod, echinoid debris, fish debris. Late Maastrichtian (zone C of Goudkoff or stratal equivalents of the Tierra Loma and Marca Shale Members fo the Moreno Formation). Environmental interpretation like Mf# 7076.

- Mf# 7425 (field #SM-23). Santa Margarita Lake 7.5" Quad.; 1520' elevation, T30S, R14E; 70m W, 150m N of SE corner of section 23. Collected in thin-bedded turbidite sequence. Maastrichtian age. Bathyal depth.
- Mf# 7426 (field #SM-27). Santa Margarita Lake 7.5" Quad.; 1280' elevation; T30S, R14E; 400m N of SE corner of section 5. Collected in mudstone/siltstone (slope facies). Maastrichtian age.
- Mf# 7427 (field #SM-31). Santa Margarita Lake 7.5" Quad.; 1640' elevation; T29S, R14E; 475m W, 200m N of SE corner of section 27. Collected in mudstone/siltstone (slope facies). Late Cretaceous to Paleocene.
- Mf# 7428 (field #SM-33). Santa Margarita Lake 7.5" Quad.; 1440' elevation; T30S, R14E; 100m E, 300m S of NW corner of section 10. Collected in shelf(?) facies rocks. Barren of microfossils.
- Mf# 7429 (field #SM-41). Santa Margarita Lake 7.5" Quad.; 1320' elevation; T30S, R14E; 75m E, 650m S of NW corner of section 12. Collected in mudstone/siltstone (slope facies). Maastrichtian age; correlated with the Maastrichtian portion of the Uhalde Formation in the Great Valley Sequence.
- Mf# 7430 (field #SM-51). Pozo Summit 7.5" Quad.; 1520' elevation; T30S, R15E; 275m E, 75m S of NW corner of section 25. Collected in thin-bedded turbidites. Maastrichtian age.
- Mf# 7431 (field #SM-56). Pozo Summit 7.5" Quad.; 1720' elevation; T30S, R16E, along a creek in American Canyon; 200m N of American Canyon campground. Collected in thin-bedded turbidites. Late Cretaceous to Paleocene age.

Mf# 7432 (field #SM-59). Pozo Summit 7.5" Quad.; 1840' elevation; T30S, R15E; 200m W, 600m S of NE corner of section 12. Collected in shelf (?) facies rocks. Barren of microfossils.

## A.2 Palynomorphs

Fauna from calcareous concretions and mudstones sampled at Lake Nacimiento. Processed and analyzed by W.R. Evitt and J. Kokinos at Stanford University.

PL 6694 (field #LNN-805). Tierra Redonda Mountain 7.5" Quad.; 100m N, 100m E of SW corner of section 9; about 730' elevation. Collected from fluvial mudstones. Barren of palynomorphs.

PL 6695 (field #LNS-62). Lime Mountain 7.5" Quad.; 100m E, 600m S of NW corner of section 28; about 720' elevation. Calcareous concretion sample extracted from slope facies mudstones. Diverse spore and pollen species, moderately diverse dinoflagellates. Two species (*Alisocysta circumtabulata* and *Deflandrea strita*), occur at the "Maastrichtian-Danian transition" in the Moreno Formation of the Great Valley Sequence. (Ammonites of uncertain species found near this locality indicate a Cretaceous age for this locality, which is probably Latest Maastrichtian).

PL 6696 (field #LNS-16). Lime Mountain 7.5" Quad.; 300m N, 530m E of SW corner of section 20; about 730' elevation. Calcareous concretion sample from thin-bedded turbidite sequence. Common small non-diagnostic dinoflagellates and occasional pollen.

PL 6697 (field #LNN-78). Lime Mountain 7.5" Quad.; 100m N, 580m E of SW corner of section 13; about 725' elevation. Calcareous concretion sample from slope mudstones. Small non-diagnostic dinoflagellates.

PL 6698 (field #LNS-19). Lime Mountain 7.5" Quad.; 100m W, 100m N of SE corner of section 20; about 725' elevation. Calcareous concretion from thin-bedded turbidite sequence. Barren of palynomorphs.

PL 6699 (field #LNN-78). Lime Mountain 7.5" Quad.; 100m N, 580m E of SW corner of section 13; about 725' elevation. Calcareous concretion sample from slope mudstones. Poorly preserved dinoflagellates, spores, and pollen.

Shallow to nonmarine siltstones to mudstones from the Upper Cretaceous to lower Tertiary sequence around Lake Nacimiento were analyzed by Clark Geological Services, Fremont, California. These samples were all barren of palynomorphs.

#7-8-85-1b. Adelaida 7.5" Quad.; 2000'E, 2800' S of NW corner of section 31; about 1000' elevation; from road cut along the west side of Godfrey Road from sediments with an uncertain environmental interpretation.

#LNN-1-4. Tierra Redonda Mountain 7.5" Quad.; 1750'E, 875'N of SW corner of section 21; about 725' elevation.

#LNS-20. Lime Mountain 7.5" Quad.; 650'E, 1725'N of SW corner of section 21; about 725' elevation.

#LNS-32. Lime Mountain 7.5" Quad.; 1780'W, 1200'S of NE corner of section 36; about 750' elevation.

#LNN-703. Tierra Redonda Mountain 7.5" Quad.; 1100'E, 300'S of NE corner of section 16; about 690' elevation.

#LNN-827. Tierra Redonda Mountain 7.5" Quad.; 400'W, 1650' S of NE corner of section 16; about 775' elevation.



## A.3 Megafossils

### A.3.1 Turritellas

Turritella assemblage analyzed by LouElla Saul, Los Angeles County Museum, Los Angeles, California (also see Saul, 1983; 1986).

#LACMIP 10082 (field #LNN-75). Tierra Redonda Mountain 7.5" Quad.; 250m N, 450m E of SW corner of section 13; about 810' elevation. Fauna are transported tests in shelf/slope sandstones—Figure 2.13). Turritellas are *Turritella chaneyi orienda* and *Turritella webbi paynei*. They suggest a Late Maastrichtian age.

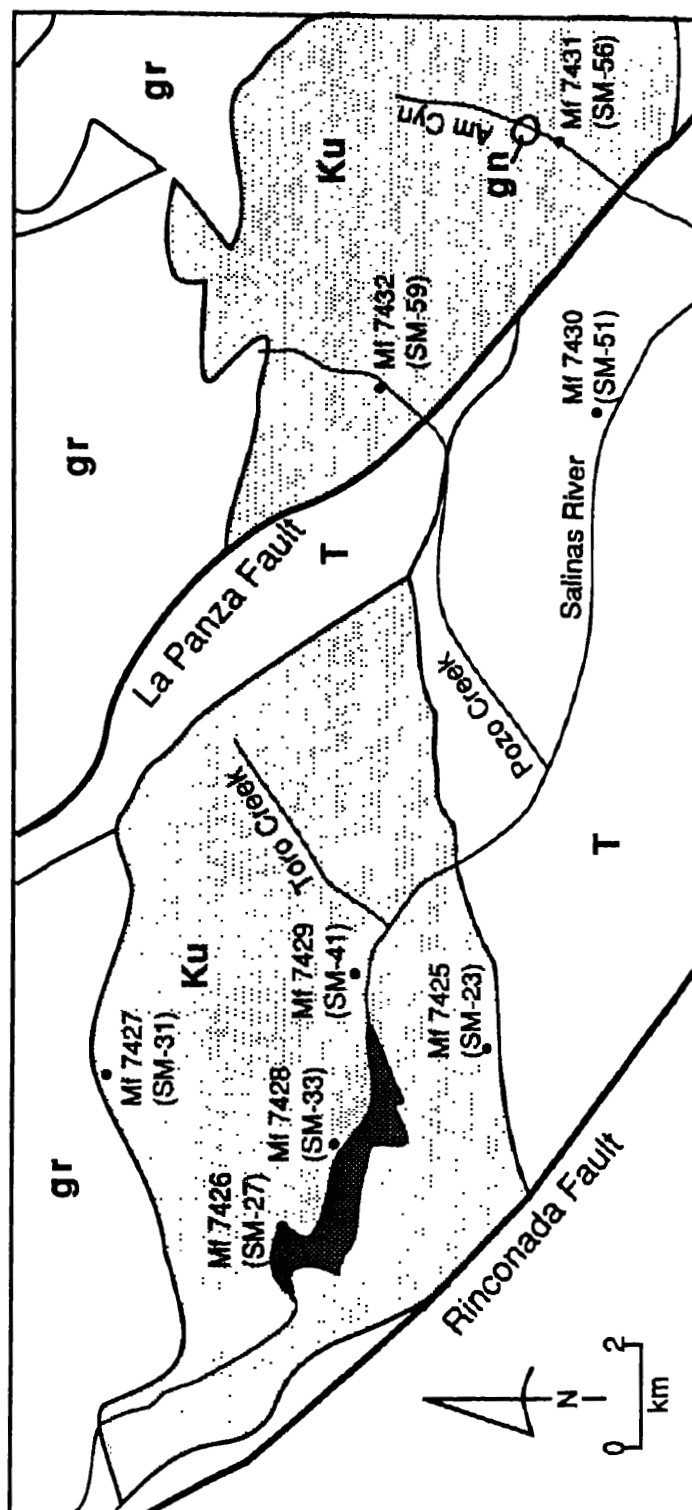
### A.3.2 Ammonites

Ammonite fragments analyzed by Will Elder, U.S. Geological Survey, Menlo Park, California. Fragments too small for certain identification, possibly *Diplomoceras* spp.

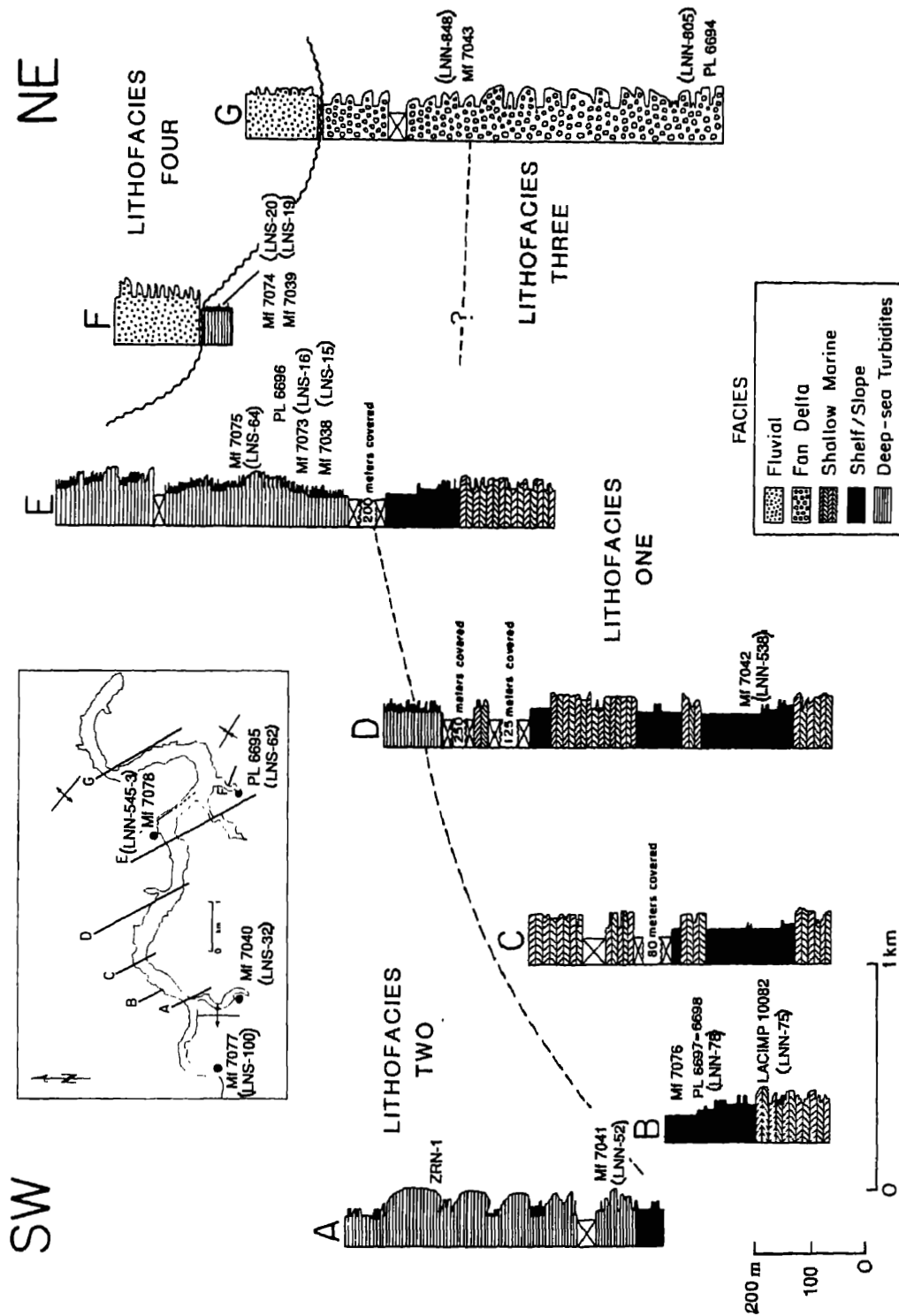
#LNN-75. Tierra Redonda Mountain 7.5" Quad.; 250m N, 450m E of SW corner of section 13; about 810' elevation. Fauna are transported tests in shelf/slope sandstones.

#LNS-16. Lime Mountain 7.5" Quad.; 300m N, 530m E of SW corner of section 20; about 730' elevation. Tests in calcareous concretion sample from thin-bedded turbidite sequence.

**MICROFOSSIL LOCALITIES AT SANTA MARGARITA LAKE, POZO GRADE AREAS**  
(SM-31 and SM-23 are also sampling localities for vitrinite reflectance)



Ku=unnamed Upper Cretaceous strata; T=undifferentiated Tertiary strata;  
gr=granitoid basement; gn=gneissic basement



## Appendix      B

### Paleomagnetic data

#### B.1    Demagnetization measurements

The following list contains stepwise demagnetization measurements for samples from Lake Nacimiento (see Chapter 3 for description of study). Temperatures (in °C) refer to the incremental heating steps that were used to demagnetize the samples. The measured magnetization vectors are given in both uncorrected—(U) and structurally corrected—(S) space. The natural remanent magnetization (NRM) intensity—INT(A/m)—is given for each sample. XYZ refers to the measurement directions; NDM=no demagnetization. During measurement in the cryogenic magnetometer, each sample was subjected to a small magnetic field (5mT) to remove any viscous components that might have been picked up during transfer between magnetometer and oven.

SAMPLE	T(°C)	(U)DEC	(U)INC	(S)DEC	(S)INC	INT(A/m)	DIR	AF(mT)
s16-2	000	23.1	+49.2	34.0	+43.2	8.714E-07	2.2	NDM
s16-2	100	27.3	+68.2	47.2	+60.7	5.217E-07	3.3	XYZ 05.0
s16-2	125	44.4	+69.6	59.8	+59.9	4.411E-07	2.3	XYZ 05.0
s16-2	150	67.0	+68.5	74.4	+57.1	4.078E-07	3.4	XYZ 05.0
s16-2	175	73.8	+68.2	78.8	+56.4	3.370E-07	1.7	XYZ 05.0
s16-2	200	78.9	+72.8	82.9	+61.0	2.100E-07	11.6	XYZ 05.0
s16-2	225	103.7	+69.9	98.5	+58.2	2.926E-07	3.6	XYZ 05.0
s16-2	250	81.7	+63.7	83.7	+51.8	2.552E-07	1.1	XYZ 05.0
s16-2	275	312.3	+65.6	338.8	+72.4	2.373E-07	4.0	XYZ 05.0
s16-2	300	289.5	+67.0	308.3	+77.6	2.279E-07	2.8	XYZ 05.0
s16-2a	000	14.9	+74.8	46.0	+68.3	1.166E-06	3.1	XYZ
s16-2a	050	21.6	+72.5	47.3	+65.4	1.034E-06	2.2	XYZ 05.0
s16-2a	100	19.4	+70.9	44.1	+64.2	8.732E-07	0.9	XYZ 05.0
s16-2a	125	19.4	+69.8	43.0	+63.2	7.582E-07	6.3	XYZ 05.0
s16-2a	150	22.9	+71.3	46.9	+64.1	6.552E-07	1.9	XYZ 05.0
s16-2a	175	30.3	+70.9	51.4	+62.7	5.756E-07	1.0	XYZ 05.0
s16-2a	200	34.9	+71.3	54.7	+62.5	5.133E-07	2.9	XYZ 05.0
s16-2a	225	48.3	+69.6	62.4	+59.5	5.192E-07	1.9	XYZ 05.0
s16-2a	250	44.1	+72.0	61.1	+62.2	4.268E-07	4.1	XYZ 05.0
s16-2a	275	11.5	+73.3	41.9	+67.5	5.350E-07	2.6	XYZ 05.0
s16-2a	300	26.6	+69.3	47.5	+61.7	4.553E-07	3.0	XYZ 05.0
s16-3	000	62.9	+60.8	69.6	+49.7	1.098E-06	1.3	NDM
s16-3	100	52.5	+62.0	62.2	+51.7	7.885E-07	2.3	XYZ 05.0
s16-3	125	64.1	+61.1	70.6	+49.9	6.609E-07	1.1	XYZ 05.0
s16-3	150	70.9	+62.8	75.9	+51.3	5.247E-07	1.9	XYZ 05.0
s16-3	175	62.5	+58.8	68.9	+47.8	4.444E-07	1.9	XYZ 05.0
s16-3	200	75.4	+65.6	79.6	+53.8	4.395E-07	2.6	XYZ 05.0
s16-3	225	29.4	+68.9	49.2	+61.0	3.804E-07	1.9	XYZ 05.0
s16-3	250	64.4	+80.1	77.7	+68.6	2.969E-07	1.9	XYZ 05.0
s16-3	275	238.9	+62.3	221.0	+71.7	2.685E-07	2.7	XYZ 05.0
s16-3	300	217.6	+42.2	207.4	+48.8	2.727E-07	2.6	XYZ 05.0
s16-4	000	356.4	+53.7	12.5	+52.6	7.843E-07	1.7	XYZ
s16-4	050	2.5	+58.4	20.7	+55.8	5.882E-07	4.0	XYZ 05.0
s16-4	100	359.1	+59.0	18.2	+56.9	3.375E-07	2.5	XYZ 05.0
s16-4	125	352.4	+66.2	18.9	+64.8	2.724E-07	9.9	XYZ 05.0
s16-4	150	347.6	+70.5	20.9	+69.4	2.285E-07	4.3	XYZ 05.0
s16-4	175	359.1	+56.2	16.4	+54.3	1.720E-07	7.6	XYZ 05.0
s16-4	200	350.6	+60.1	11.5	+59.7	1.590E-07	12.7	XYZ 05.0
s16-4	225	352.7	+64.9	17.7	+63.5	1.463E-07	10.5	XYZ 05.0
s16-4	250	330.0	+67.5	0.9	+70.5	1.467E-07	2.1	XYZ 05.0
s16-4	275	358.1	+34.2	6.1	+33.5	8.645E-08	6.9	XYZ 05.0
s16-4	300	4.6	+78.2	46.6	+72.4	1.080E-07	6.8	XYZ 05.0
s16-6	000	9.0	+59.7	27.1	+55.7	6.674E-07	1.6	XYZ
s16-6	100	9.7	+62.0	29.2	+57.7	5.270E-07	1.6	XYZ 05.0
s16-6	125	14.4	+62.5	33.3	+57.3	4.054E-07	1.3	XYZ 05.0
s16-6	150	12.9	+63.7	33.0	+58.7	2.506E-07	1.1	XYZ 05.0
s16-6	175	14.1	+62.6	33.2	+57.5	1.985E-07	0.8	XYZ 05.0
s16-6	200	10.2	+65.3	32.2	+60.7	2.169E-07	1.4	XYZ 05.0
s16-6	225	9.8	+64.3	31.1	+59.8	2.116E-07	1.2	XYZ 05.0
s16-6	275	7.9	+67.0	32.0	+62.6	1.264E-07	2.3	XYZ 05.0
s16-6	300	15.2	+63.9	35.0	+58.5	9.258E-08	15.8	XYZ 05.0
s16-7	000	11.2	+58.4	28.2	+54.1	6.594E-07	1.7	XYZ
s16-7	050	15.6	+55.0	30.0	+50.1	5.932E-07	2.2	XYZ 05.0
s16-7	100	14.4	+57.5	30.3	+52.7	3.982E-07	2.5	XYZ 05.0
s16-7	125	8.8	+64.2	30.2	+59.9	3.042E-07	9.5	XYZ 05.0

s16-7	150	6.9	+68.0	32.2	+63.7	2.353E-07	6.1	XYZ	05.0
s16-7	175	9.9	+72.7	39.9	+67.2	1.876E-07	9.6	XYZ	05.0
s16-7	200	7.6	+72.9	38.8	+67.8	1.499E-07	3.1	XYZ	05.0
s16-7	225	6.3	+69.7	33.7	+65.3	1.445E-07	6.5	XYZ	05.0
s16-7	250	316.4	+75.3	8.9	+79.0	9.932E-08	6.9	XYZ	05.0
s16-7	275	276.3	+60.2	280.8	+72.1	8.832E-08	7.3	XYZ	05.0
s16-7	300	348.1	+31.1	355.5	+32.6	5.700E-08	7.6	XYZ	05.0
s17-3	000	10.9	+67.5	43.0	+65.2	7.210E-07	0.9	NDM	
s17-3	100	359.0	+70.9	40.1	+70.5	4.884E-07	0.7	XYZ	05.0
s17-3	125	4.8	+73.5	49.4	+71.1	4.020E-07	0.8	XYZ	05.0
s17-3	150	359.2	+73.1	45.1	+72.0	3.217E-07	2.2	XYZ	05.0
s17-3	175	2.8	+76.1	54.8	+73.1	2.477E-07	0.9	XYZ	05.0
s17-3	200	354.1	+76.1	50.7	+74.9	2.194E-07	3.4	XYZ	05.0
s17-3	225	2.7	+79.1	64.0	+74.8	1.816E-07	6.9	XYZ	05.0
s17-3	250	9.2	+65.4	39.1	+63.9	1.495E-07	2.2	XYZ	05.0
s17-3	275	79.4	+31.7	82.4	+19.2	6.100E-07	4.8	XYZ	05.0
s17-3	300	79.2	+73.3	91.8	+60.3	3.237E-07	5.8	XYZ	05.0
s17-4	000	357.5	+79.7	64.6	+75.9	5.419E-07	2.2	XYZ	
s17-4	100	359.5	+68.7	36.3	+68.7	4.273E-07	2.6	XYZ	05.0
s17-4	125	3.5	+65.0	33.9	+64.8	3.703E-07	3.4	XYZ	05.0
s17-4	150	0.6	+63.4	29.4	+64.1	2.583E-07	1.4	XYZ	05.0
s17-4	175	7.2	+66.2	38.5	+65.0	2.234E-07	2.1	XYZ	05.0
s17-4	200	6.6	+68.5	41.3	+66.9	2.184E-07	8.8	XYZ	05.0
s17-4	225	357.6	+65.8	30.0	+66.8	1.826E-07	6.5	XYZ	05.0
s17-4	250	355.6	+70.3	36.2	+70.8	1.461E-07	2.1	XYZ	05.0
s17-4	275	353.4	+70.2	34.3	+71.3	1.359E-07	1.8	XYZ	05.0
s17-4	300	342.6	+76.6	47.0	+77.5	1.199E-07	2.1	XYZ	05.0
s17-4	325	9.0	+58.6	31.9	+57.9	1.554E-07	10.2	XYZ	05.0
s30-1	000	63.0	+59.9	75.5	+35.1	9.222E-07	1.9	XYZ	
s30-1	100	63.8	+51.9	73.5	+27.3	7.427E-07	1.0	XYZ	05.0
s30-1	125	67.1	+47.5	74.6	+22.5	6.048E-07	2.4	XYZ	05.0
s30-1	150	74.7	+41.1	79.0	+15.2	4.298E-07	2.0	XYZ	05.0
s30-1	175	84.9	+33.8	86.4	+ 7.1	3.674E-07	1.8	XYZ	05.0
s30-1	200	84.7	+34.6	86.2	+ 7.8	3.624E-07	2.6	XYZ	05.0
s30-1	225	85.6	+33.9	86.9	+ 7.1	3.696E-07	1.5	XYZ	05.0
s30-1	250	84.5	+27.5	85.6	+ 0.8	3.339E-07	6.5	XYZ	05.0
s30-1	275	91.3	+20.6	91.4	- 6.3	2.799E-07	5.4	XYZ	05.0
s30-1	300	83.9	+16.9	84.2	- 9.7	2.842E-07	6.8	XYZ	05.0
s30-1	325	93.5	-10.0	93.5	-37.0	3.902E-07	3.5	XYZ	05.0
s30-4	000	34.9	+51.9	54.3	+33.8	9.056E-07	1.5	NDM	
s30-4	100	56.7	+53.6	69.3	+30.2	4.971E-07	1.6	XYZ	05.0
s30-4	125	58.4	+56.9	71.7	+33.0	3.941E-07	2.8	XYZ	05.0
s30-4	150	70.7	+59.0	79.8	+33.2	3.060E-07	2.9	XYZ	05.0
s30-4	175	92.1	+55.0	92.7	+28.0	2.361E-07	2.4	XYZ	05.0
s30-4	200	126.3	+54.9	114.8	+30.6	1.897E-07	10.8	XYZ	05.0
s30-4	225	113.5	+45.5	108.3	+19.6	1.837E-07	7.9	XYX	05.0
s30-4	250	105.2	+35.9	103.1	+ 9.3	1.916E-07	5.4	XYZ	05.0
s30-4	275	82.3	-21.2	77.8	-47.5	1.695E-07	4.6	XYZ	05.0
s30-4	300	59.9	-34.6	41.1	-54.7	1.594E-07	2.7	XYZ	05.0
s30-6	000	8.4	+50.9	36.1	+42.0	7.605E-07	1.5	XYZ	
s30-6	100	15.7	+56.5	45.4	+43.7	7.145E-07	2.1	XYZ	05.0
s30-6	125	22.9	+57.8	50.8	+42.4	5.905E-07	2.5	XYZ	05.0
s30-6	150	27.7	+56.9	52.9	+40.2	4.286E-07	0.9	XYZ	05.0
s30-6	175	33.8	+59.0	58.0	+40.3	3.600E-07	2.5	XYZ	05.0
s30-6	200	28.3	+60.1	55.7	+42.7	3.515E-07	2.2	XYZ	05.0
s30-6	225	32.1	+58.0	56.3	+39.9	3.591E-07	1.1	XYZ	05.0

s30-6	250	36.2	+60.0	60.1	+40.6	3.168E-07	3.2	XYZ	05.0
s30-6	275	50.2	+62.2	69.2	+39.4	2.382E-07	8.0	XYZ	05.0
s30-6	300	84.7	+71.4	89.7	+44.5	2.042E-07	14.6	XYZ	05.0
s30-6	325	320.4	+68.5	40.6	+70.6	1.809E-07	8.5	XYZ	05.0
s32-2a	000	319.0	+79.6	33.3	+70.1	1.007E-06	3.2	XYZ	
s32-2a	050	359.3	+78.4	40.5	+63.0	9.060E-07	1.3	XYZ	05.0
s32-2a	100	7.1	+74.6	38.5	+58.9	7.054E-07	1.6	XYZ	05.0
s32-2a	125	358.3	+74.5	34.7	+60.2	5.253E-07	6.9	XYZ	05.0
s32-2a	150	354.9	+74.4	33.2	+60.8	3.921E-07	6.0	XYZ	05.0
s32-2a	175	342.5	+80.1	38.9	+66.5	2.641E-07	14.0	XYZ	05.0
s32-2a	200	338.3	+79.6	36.9	+66.9	2.489E-07	3.8	XYZ	05.0
s32-2a	225	256.0	+82.7	57.5	+77.1	2.240E-07	5.2	XYZ	05.0
s32-2a	250	239.5	+63.9	225.1	+83.6	1.262E-07	1.2	XYZ	05.0
s32-2a	275	250.0	+48.8	254.7	+68.6	1.119E-07	6.0	XYZ	05.0
s32-2a	300	240.7	+38.6	238.9	+58.5	1.028E-07	3.7	XYZ	05.0
s32-2b	000	327.6	+58.7	358.8	+55.5	3.754E-06	1.9	NDM	
s32-2b	100	325.0	+59.4	357.6	+56.8	2.522E-06	1.8	XYZ	05.0
s32-2b	125	325.9	+59.8	358.8	+56.8	2.325E-06	1.9	XYZ	05.0
s32-2b	150	320.7	+59.5	354.6	+58.2	2.141E-06	2.2	XYZ	05.0
s32-2b	175	320.4	+58.8	353.6	+57.8	2.003E-06	2.2	XYZ	05.0
s32-2b	200	320.8	+57.7	352.6	+56.8	1.924E-06	2.4	XYZ	05.0
s32-2b	225	331.7	+40.8	348.5	+38.7	1.438E-06	99.0	XYZ	05.0
s32-2b	250	317.5	+55.3	347.3	+55.9	1.735E-06	2.2	XYZ	05.0
s32-2b	275	246.3	+48.0	247.9	+68.0	1.581E-06	2.2	XYZ	05.0
s32-2b	300	250.0	+46.8	254.2	+66.6	1.363E-06	2.3	XYZ	05.0
s32-3a	000	49.7	+59.6	54.7	+40.1	1.027E-06	2.3	XYZ	
s32-3a	100	33.1	+61.2	44.3	+43.0	9.262E-07	2.1	XYZ	05.0
s32-3a	125	34.4	+61.7	45.3	+43.4	7.542E-07	1.5	XYZ	05.0
s32-3a	150	40.7	+62.1	49.4	+43.2	5.188E-07	2.8	XYZ	05.0
s32-3a	175	37.0	+62.3	47.1	+43.7	4.374E-07	2.1	XYZ	05.0
s32-3a	200	35.7	+61.6	46.1	+43.1	4.340E-07	2.8	XYZ	05.0
s32-3a	225	40.9	+62.1	49.5	+43.1	4.355E-07	3.3	XYZ	05.0
s32-3a	250	39.3	+62.4	48.6	+43.5	3.701E-07	6.5	XYZ	05.0
s32-3a	275	57.2	+67.7	60.3	+47.7	2.443E-07	5.6	XYZ	05.0
s32-3a	300	75.1	+67.5	70.4	+47.7	2.025E-07	16.8	XYZ	05.0
s32-3a	325	293.6	+43.8	313.6	+54.2	3.281E-07	2.7	XYZ	05.0
s33-2	000	17.0	+41.7	32.9	+28.1	1.208E-06	2.7	XYZ	
s33-2	050	14.5	+42.5	31.5	+29.6	1.149E-06	3.1	XYZ	05.0
s33-2	100	7.5	+43.5	26.8	+33.1	9.540E-07	2.3	XYZ	05.0
s33-2	125	3.6	+37.1	20.1	+29.0	7.890E-07	6.5	XYZ	05.0
s33-2	150	359.5	+39.8	18.4	+33.0	6.564E-07	4.4	XYZ	05.0
s33-2	175	351.4	+36.9	10.1	+33.8	5.633E-07	2.6	XYZ	05.0
s33-2	200	353.3	+37.5	12.1	+33.6	5.511E-07	2.8	XYZ	05.0
s33-2	225	354.8	+36.1	12.5	+31.7	5.181E-07	5.6	XYZ	05.0
s33-2	250	348.5	+36.0	7.2	+34.3	4.391E-07	3.2	XYZ	05.0
s33-2	275	350.1	+36.3	8.7	+33.9	3.865E-07	3.1	XYZ	05.0
s33-2	300	354.6	+33.2	10.5	+29.4	2.974E-07	2.3	XYZ	05.0
s33-2	325	333.5	+23.0	346.2	+29.6	3.700E-07	10.6	XYZ	05.0
s33-2	350	349.3	+30.2	4.4	+28.9	2.864E-07	6.9	XYZ	05.0
s33-4	000	43.3	+42.8	53.1	+21.5	1.492E-06	1.9	XYZ	
s33-4	100	42.5	+46.9	53.9	+25.6	1.165E-06	1.2	XYZ	05.0
s33-4	125	45.7	+49.8	57.2	+27.7	9.636E-07	1.7	XYZ	05.0
s33-4	150	49.1	+48.3	59.1	+25.7	7.565E-07	1.4	XYZ	05.0
s33-4	175	50.6	+49.4	60.5	+26.4	6.954E-07	1.1	XYZ	05.0
s33-4	200	56.0	+50.9	64.7	+27.0	6.817E-07	0.7	XYZ	05.0
s33-4	225	51.1	+50.0	61.0	+26.9	6.680E-07	1.8	XYZ	05.0

s33-4	250	53.7	+46.9	62.0	+23.5	6.277E-07	1.8	XYZ	05.0
s33-4	275	65.1	+46.9	70.2	+21.9	4.716E-07	9.7	XYZ	05.0
s33-4	300	66.5	+48.4	71.5	+23.2	4.266E-07	2.2	XYZ	05.0
s33-4	325	87.8	+ 8.1	88.0	-17.8	4.281E-07	5.9	XYZ	05.0
s34-1	000	34.3	+60.7	51.2	+28.2	2.717E-06	3.4	NDM	
s34-1	100	32.3	+58.4	49.1	+26.5	2.089E-06	3.2	XYZ	05.0
s34-1	125	31.2	+57.2	48.0	+25.7	1.968E-06	3.7	XYZ	05.0
s34-1	150	35.8	+57.7	50.7	+25.2	1.788E-06	3.4	XYZ	05.0
s34-1	175	36.5	+56.7	50.7	+24.1	1.625E-06	4.4	XYZ	05.0
s34-1	200	37.0	+56.9	51.1	+24.2	1.582E-06	5.3	XYZ	05.0
s34-1	225	212.8	+78.7	84.9	+62.2	1.474E-06	4.1	XYZ	05.0
s34-1	250	27.0	+58.9	46.5	+28.1	1.344E-06	4.7	XYZ	05.0
s34-1	275	214.5	+73.7	93.6	+65.6	1.170E-06	3.9	XYZ	05.0
s34-1	300	225.2	+73.8	88.4	+67.8	1.070E-06	3.3	XYZ	05.0
s35-2	000	194.8	+50.5	211.0	+53.9	1.189E-06	2.1	XYZ	
s35-2	100	187.1	+55.1	206.3	+59.9	9.707E-07	2.3	XYZ	05.0
s35-2	125	181.7	+60.5	205.5	+66.1	8.140E-07	2.1	XYZ	05.0
s35-2	150	174.5	+61.2	198.2	+68.2	6.225E-07	1.3	XYZ	05.0
s35-2	175	169.7	+62.5	194.0	+70.4	5.595E-07	1.5	XYZ	05.0
s35-2	200	170.2	+66.5	201.0	+73.8	5.275E-07	1.6	XYZ	05.0
s35-2	225	166.3	+63.9	191.7	+72.3	5.433E-07	2.7	XYZ	05.0
s35-2	250	174.8	+67.1	207.5	+73.3	4.652E-07	6.1	XYZ	05.0
s35-2	275	175.9	+71.1	218.4	+76.2	3.547E-07	7.0	XYZ	05.0
s35-2	300	208.4	+65.3	236.4	+64.4	3.089E-07	7.4	XYZ	05.0
s35-2	325	268.8	+21.4	271.2	+11.1	3.145E-07	4.8	XYZ	05.0
s35-3	000	208.1	+55.3	227.1	+55.4	3.016E-06	6.4	XYZ	
s35-3	050	207.4	+55.7	226.7	+55.9	2.834E-06	4.1	XYZ	05.0
s35-3	100	207.4	+57.4	228.0	+57.5	2.578E-06	1.7	XYZ	05.0
s35-3	125	207.0	+56.0	226.6	+56.4	2.428E-06	3.4	XYZ	05.0
s35-3	150	210.3	+56.8	230.2	+56.3	2.257E-06	1.0	XYZ	05.0
s35-3	175	207.4	+56.1	227.0	+56.3	2.074E-06	1.0	XYZ	05.0
s35-3	200	210.7	+54.7	229.0	+54.3	1.875E-06	1.7	XYZ	05.0
s35-3	225	208.0	+55.2	227.0	+55.3	1.892E-06	1.0	XYZ	05.0
s35-3	250	209.0	+51.0	225.3	+51.3	1.423E-06	1.5	XYZ	05.0
s35-3	275	217.1	+49.9	232.2	+48.4	1.293E-06	1.7	XYZ	05.0
s35-3	300	217.1	+48.3	231.4	+46.9	1.107E-06	1.1	XYZ	05.0
s35-3	325	187.7	+36.9	197.5	+42.6	6.571E-07	1.5	XYZ	05.0
s35-3	350	225.2	+39.8	235.3	+37.0	6.039E-07	7.2	XYZ	05.0
s35-4	000	294.0	+75.9	300.6	+63.1	1.420E-06	2.6	XYZ	
s35-4	050	282.5	+75.2	294.1	+62.9	1.359E-06	3.8	XYZ	05.0
s35-4	100	278.8	+76.5	292.9	+64.4	1.120E-06	2.0	XYZ	05.0
s35-4	125	280.4	+79.8	295.8	+67.5	9.444E-07	3.3	XYZ	05.0
s35-4	150	303.1	+81.6	306.2	+68.6	8.489E-07	1.9	XYZ	05.0
s35-4	175	290.2	+82.4	301.5	+69.7	7.144E-07	3.7	XYZ	05.0
s35-4	200	295.4	+80.9	302.8	+68.0	6.837E-07	3.1	XYZ	05.0
s35-4	225	309.3	+81.9	308.6	+68.9	6.261E-07	3.6	XYZ	05.0
s35-4	250	3.0	+85.7	321.2	+74.1	5.379E-07	2.4	XYZ	05.0
s35-4	275	343.8	+86.0	316.4	+73.6	5.142E-07	2.7	XYZ	05.0
s35-4	300	350.0	+81.8	324.4	+70.2	4.214E-07	3.0	XYZ	05.0
s35-4	350	351.6	+76.3	331.1	+65.2	3.545E-07	2.0	XYZ	05.0
s35-6	000	19.3	+50.1	6.5	+44.5	1.560E-06	1.6	NDM	
s35-6	100	12.0	+48.2	1.0	+41.3	9.734E-07	2.2	XYZ	05.0
s35-6	125	14.0	+49.2	2.3	+42.7	8.543E-07	2.1	XYZ	05.0
s35-6	150	11.5	+48.4	0.5	+41.4	6.751E-07	2.0	XYZ	05.0
s35-6	175	10.2	+48.6	359.3	+41.4	5.599E-07	2.0	XYZ	05.0
s35-6	200	7.6	+46.1	357.9	+38.5	5.321E-07	4.8	XYZ	05.0



s35-6	225	6.1	+46.5	356.5	+38.6	4.010E-07	5.2	XYZ	05.0
s35-6	250	0.5	+39.8	353.5	+31.2	4.082E-07	3.0	XYZ	05.0
s35-6	275	18.3	+12.8	16.1	+ 8.1	2.848E-07	3.4	XYZ	05.0
s35-6	300	20.9	+26.1	15.4	+21.6	3.393E-07	2.4	XYZ	05.0
s38-3	000	352.7	+64.1	16.2	+58.2	1.405E-06	1.8	XYZ	
s38-3	100	2.7	+70.5	29.0	+62.1	1.060E-06	2.1	XYZ	05.0
s38-3	125	3.7	+71.0	30.2	+62.4	8.684E-07	2.5	XYZ	05.0
s38-3	150	15.5	+77.3	43.6	+66.3	6.331E-07	2.2	XYZ	05.0
s38-3	175	5.7	+74.6	35.3	+65.2	5.225E-07	2.4	XYZ	05.0
s38-3	200	19.6	+77.0	45.3	+65.7	5.182E-07	2.2	XYZ	05.0
s38-3	225	358.8	+75.1	32.3	+66.6	5.033E-07	1.2	XYZ	05.0
s38-3	250	347.3	+75.9	27.7	+69.1	4.240E-07	1.8	XYZ	05.0
s38-3	275	347.5	+79.9	36.4	+71.8	3.056E-07	2.8	XYZ	05.0
s38-3	300	305.9	+71.2	351.3	+74.2	3.877E-07	0.5	XYZ	05.0
s38-3	325	0.2	+20.7	4.4	+15.4	4.745E-07	2.5	XYZ	05.0
s38-5	000	342.7	+45.8	356.4	+43.5	9.510E-07	1.0	NDM	
s38-5	100	357.8	+59.4	16.5	+52.9	7.044E-07	1.4	XYZ	05.0
s38-5	125	3.7	+68.7	27.9	+60.3	5.234E-07	1.0	XYZ	05.0
s38-5	150	4.2	+73.8	33.5	+64.7	3.540E-07	1.1	XYZ	05.0
s38-5	175	14.4	+85.5	57.3	+73.0	2.321E-07	0.8	XYZ	05.0
s38-5	200	27.3	+85.1	59.2	+72.1	1.924E-07	10.9	XYZ	05.0
s38-5	225	189.3	+82.5	103.0	+77.8	1.526E-07	3.6	XYZ	05.0
s38-5	250	319.8	+81.3	33.2	+76.4	1.032E-07	7.2	XYZ	05.0
s38-5	275	109.1	+53.5	100.3	+41.9	8.850E-08	6.7	XYZ	05.0
s38-5	300	124.5	+26.6	120.0	+18.0	9.434E-08	3.1	XYZ	05.0
s39-4	000	5.7	+43.5	26.8	+31.7	7.298E-07	0.9	NDM	
s39-4	100	9.1	+58.9	40.6	+42.9	4.152E-07	1.6	XYZ	05.0
s39-4	125	16.1	+59.5	44.9	+41.2	3.085E-07	1.4	XYZ	05.0
s39-4	150	27.9	+58.3	50.5	+36.8	2.110E-07	3.7	XYZ	05.0
s39-4	175	34.5	+62.4	56.7	+38.8	1.527E-07	3.8	XYZ	05.0
s39-4	200	56.1	+61.4	67.9	+34.2	1.238E-07	6.7	XYZ	05.0
s39-4	225	77.7	+56.3	79.8	+27.4	1.101E-07	6.2	XYZ	05.0
s39-4	250	98.0	+52.2	93.1	+23.8	9.349E-08	6.5	XYZ	05.0
s39-4	275	13.6	+37.4	29.0	+23.4	6.683E-08	8.5	XYZ	05.0
s39-4	300	351.8	+44.8	17.9	+38.6	6.791E-08	5.7	XYZ	05.0
s39-5	000	136.6	+50.6	119.1	+29.5	8.563E-07	3.5	XYZ	
s39-5	050	129.9	+45.2	117.0	+22.7	7.160E-07	2.9	XYZ	05.0
s39-5	100	133.9	+47.0	119.0	+25.5	4.966E-07	1.5	XYZ	05.0
s39-5	125	138.1	+50.8	119.9	+30.1	3.792E-07	3.1	XYZ	05.0
s39-5	150	163.1	+52.4	134.7	+39.8	2.020E-07	9.0	XYZ	05.0
s39-5	175	193.1	+27.1	176.2	+33.0	1.369E-07	19.0	XYZ	05.0
s39-5	200	203.1	+27.1	185.4	+37.9	1.063E-07	16.5	XYZ	05.0
s39-5	225	207.7	+15.7	196.8	+30.1	1.222E-07	16.0	XYZ	05.0
s39-5	250	225.8	+ 5.2	220.2	+27.6	1.168E-07	1.5	XYZ	05.0
s39-5	275	240.2	- 5.4	238.5	+21.3	1.149E-07	5.5	XYZ	05.0
s39-5	300	243.4	+ 5.8	239.5	+32.8	8.384E-08	3.8	XYZ	05.0
s39-8a	000	28.2	+59.7	63.8	+44.7	6.733E-07	1.3	XYZ	
s39-8a	100	14.6	+67.1	66.8	+54.1	5.401E-07	2.3	XYZ	05.0
s39-8a	125	9.1	+67.9	66.1	+56.3	4.623E-07	2.2	XYZ	05.0
s39-8a	150	20.7	+74.0	78.9	+55.7	3.193E-07	1.5	XYZ	05.0
s39-8a	175	33.7	+79.1	89.4	+55.6	2.538E-07	1.9	XYZ	05.0
s39-8a	200	32.4	+78.7	88.5	+55.6	2.510E-07	1.6	XYZ	05.0
s39-8a	225	32.4	+78.1	87.7	+55.3	2.421E-07	2.7	XYZ	05.0
s39-8a	250	104.3	+74.6	106.7	+44.7	1.789E-07	14.0	XYZ	05.0
s39-8a	275	96.2	+67.6	102.4	+37.9	1.490E-07	9.7	XYZ	05.0
s39-8a	300	80.3	+63.3	93.3	+35.2	1.337E-07	4.1	XYZ	05.0
s39-8a	325	81.9	+64.2	94.4	+35.7	1.329E-07	3.3	XYZ	05.0

s40-1	000	62.4	+42.2	67.0	+53.4	6.429E-07	0.9	XYZ	
s40-1	100	48.9	+51.9	50.8	+63.8	5.487E-07	2.0	XYZ	05.0
s40-1	125	44.3	+53.3	44.3	+65.3	4.762E-07	1.5	XYZ	05.0
s40-1	150	52.2	+46.9	54.8	+58.7	3.294E-07	2.0	XYZ	05.0
s40-1	175	54.4	+38.5	56.7	+50.3	2.313E-07	0.2	XYZ	05.0
s40-1	200	57.8	+40.0	61.0	+51.6	2.349E-07	1.9	XYZ	05.0
s40-1	225	54.1	+39.1	56.3	+50.8	2.294E-07	0.9	XYZ	05.0
s40-1	250	58.9	+20.8	60.6	+32.4	1.381E-07	31.9	XYZ	05.0
s40-1	275	59.6	+19.3	61.2	+30.9	9.483E-08	16.9	XYZ	05.0
s40-1	300	60.5	+13.0	61.7	+24.5	6.920E-08	5.4	XYZ	05.0
s40-1	325	58.9	- 2.4	59.1	+ 9.2	9.953E-08	8.2	XYZ	05.0
s40-4	000	356.8	+43.4	346.5	+50.8	8.115E-07	0.7	NDM	
s40-4	100	13.0	+55.6	0.0	+65.1	5.044E-07	0.6	XYZ	05.0
s40-4	125	16.7	+57.2	4.0	+67.3	4.043E-07	1.1	XYZ	05.0
s40-4	150	28.6	+57.4	20.6	+68.8	2.708E-07	1.7	XYZ	05.0
s40-4	175	41.5	+62.5	39.5	+74.5	1.825E-07	1.8	XYZ	05.0
s40-4	200	37.1	+54.9	33.8	+66.8	1.405E-07	7.8	XYZ	05.0
s40-4	225	52.0	+46.8	54.5	+58.7	1.205E-07	16.4	XYZ	05.0
s40-4	250	54.8	+45.5	58.0	+57.2	8.907E-08	12.3	XYZ	05.0
s40-4	275	321.6	+43.9	309.9	+44.3	5.368E-08	5.5	XYZ	05.0
s40-4	300	7.0	+67.0	339.8	+74.8	7.017E-08	7.5	XYZ	05.0
s41-1	000	2.0	+58.4	30.5	+54.3	7.007E-07	0.9	NDM	
s41-1	100	12.5	+71.0	51.7	+61.4	5.529E-07	2.0	XYZ	05.0
s41-1	125	8.6	+73.9	54.5	+64.4	4.897E-07	1.6	XYZ	05.0
s41-1	150	27.3	+79.1	70.1	+64.7	3.917E-07	1.8	XYZ	05.0
s41-1	175	51.3	+81.0	80.2	+63.7	3.220E-07	4.1	XYZ	05.0
s41-1	200	95.6	+83.2	94.6	+64.2	2.719E-07	5.6	XYZ	05.0
s41-1	225	119.6	+83.0	101.2	+64.5	2.441E-07	4.8	XYZ	05.0
s41-1	250	4.1	+41.0	19.9	+38.4	1.584E-07	1.4	XYZ	05.0
s41-1	275	20.0	+39.2	32.7	+31.9	2.081E-07	2.6	XYZ	05.0
s41-1	300	14.2	+67.5	48.2	+58.4	3.990E-07	5.3	XYZ	05.0
s41-5	000	15.1	+57.6	39.4	+49.9	6.237E-07	2.6	XYZ	
s41-5	100	15.3	+62.8	43.9	+54.3	4.887E-07	2.3	XYZ	05.0
s41-5	125	17.9	+63.8	46.5	+54.5	4.255E-07	1.8	XYZ	05.0
s41-5	150	21.4	+62.4	47.6	+52.5	3.106E-07	1.2	XYZ	05.0
s41-5	175	36.7	+60.3	56.2	+47.3	2.289E-07	1.2	XYZ	05.0
s41-5	200	39.8	+60.6	58.4	+46.9	2.265E-07	1.5	XYZ	05.0
s41-5	225	40.6	+59.6	58.4	+45.9	2.172E-07	3.3	XYZ	05.0
s41-5	250	46.6	+48.5	57.9	+34.3	1.275E-07	5.9	XYZ	05.0
s41-5	275	75.1	+62.9	82.1	+44.6	1.104E-07	18.1	XYZ	05.0
s41-5	300	124.3	+77.8	106.4	+59.9	5.210E-07	4.6	XYZ	05.0
s41-5	325	253.1	-62.0	260.6	-43.8	1.688E-06	6.2	XYZ	05.0
s41-7	000	349.1	+68.6	35.4	+65.7	6.449E-07	3.1	XYZ	
s41-7	050	6.7	+70.5	48.0	+62.4	6.084E-07	1.9	XYZ	05.0
s41-7	100	5.9	+68.9	45.3	+61.5	5.515E-07	6.0	XYZ	05.0
s41-7	125	358.6	+72.1	46.8	+65.5	5.026E-07	5.4	XYZ	05.0
s41-7	150	18.7	+70.3	54.0	+59.6	3.602E-07	8.0	XYZ	05.0
s41-7	175	13.9	+74.6	57.9	+63.8	2.960E-07	2.8	XYZ	05.0
s41-7	200	22.2	+72.5	58.6	+60.7	2.670E-07	6.0	XYZ	05.0
s41-7	225	15.2	+79.6	67.6	+66.8	2.521E-07	8.6	XYZ	05.0
s41-7	250	42.2	+66.8	63.8	+52.2	2.580E-07	146.8	XYZ	05.0
s41-7	275	174.9	+83.0	113.7	+68.7	2.667E-07	5.1	XYZ	05.0
s41-7	300	111.5	+69.3	103.8	+50.8	4.471E-07	4.7	XYZ	05.0
s42-1b	000	357.3	+59.6	19.3	+76.8	2.695E-06	2.3	NDM	
s42-1b	100	1.9	+62.5	34.9	+78.3	2.061E-06	2.2	XYZ	05.0
s42-1b	125	359.6	+61.6	28.2	+78.2	1.918E-06	1.9	XYZ	05.0

s42-1b	150	0.1	+61.2	28.1	+77.7	1.680E-06	2.2	XYZ	05.0
s42-1b	175	357.6	+61.4	23.5	+78.4	1.549E-06	4.1	XYZ	05.0
s42-1b	200	1.7	+63.4	37.1	+79.1	1.465E-06	3.3	XYZ	05.0
s42-1b	225	357.9	+59.3	19.9	+76.5	1.363E-06	4.0	XYZ	05.0
s42-1b	250	298.9	+68.1	242.0	+75.2	1.282E-06	2.3	XYZ	05.0
s42-1b	275	299.8	+64.7	253.0	+73.6	1.038E-06	2.4	XYZ	05.0
s42-1b	300	300.5	+66.7	247.7	+75.0	9.886E-07	2.1	XYZ	05.0
s42-2a	000	326.1	+66.2	285.0	+82.7	1.111E-06	1.9	XYZ	
s42-2a	100	330.4	+67.5	288.4	+84.8	7.640E-07	2.4	XYZ	05.0
s42-2a	125	324.8	+70.6	247.4	+84.6	6.289E-07	1.8	XYZ	05.0
s42-2a	150	308.7	+70.3	239.3	+79.3	4.924E-07	1.5	XYZ	05.0
s42-2a	175	288.2	+71.4	224.8	+73.5	3.912E-07	1.1	XYZ	05.0
s42-2a	200	283.9	+70.5	225.1	+71.8	3.881E-07	2.4	XYZ	05.0
s42-2a	225	281.9	+70.6	224.0	+71.3	3.723E-07	1.9	XYZ	05.0
s42-2a	250	283.4	+68.2	231.0	+70.5	2.631E-07	5.7	XYZ	05.0
s42-2a	275	256.8	+60.4	225.4	+56.9	2.535E-07	9.2	XYZ	05.0
s42-2a	300	239.6	+60.0	213.7	+51.8	2.090E-07	8.1	XYZ	05.0
s42-2a	325	235.7	+55.0	214.6	+46.4	2.181E-07	6.2	XYZ	05.0
s42-4b	000	354.2	+66.1	31.4	+83.2	2.275E-06	2.8	XYZ	
s42-4b	050	357.7	+67.2	46.5	+83.0	2.164E-06	3.0	XYZ	05.0
s42-4b	100	3.8	+69.4	69.9	+82.2	1.940E-06	3.0	XYZ	05.0
s42-4b	125	5.8	+69.8	74.8	+81.7	1.827E-06	2.5	XYZ	05.0
s42-4b	150	16.5	+73.3	99.6	+79.1	1.567E-06	1.5	XYZ	05.0
s42-4b	175	15.7	+73.4	100.3	+79.4	1.417E-06	1.8	XYZ	05.0
s42-4b	200	15.6	+72.8	96.8	+79.3	1.392E-06	1.6	XYZ	05.0
s42-4b	225	13.6	+72.6	95.4	+79.9	1.308E-06	1.0	XYZ	05.0
s42-4b	250	12.4	+73.9	103.0	+80.3	1.092E-06	2.4	XYZ	05.0
s42-4b	275	12.9	+71.4	88.3	+79.9	9.807E-07	2.2	XYZ	05.0
s42-4b	300	21.8	+68.9	82.2	+76.2	8.730E-07	2.4	XYZ	05.0
s42-4b	325	33.4	+62.7	75.0	+68.7	8.562E-07	5.2	XYZ	05.0
s42-4b	350	32.4	+63.1	74.8	+69.3	7.850E-07	3.3	XYZ	05.0
s42-6c	000	328.4	+49.5	318.9	+67.7	1.324E-06	1.1	NDM	
s42-6c	100	325.2	+45.1	315.8	+63.0	1.238E-06	1.1	XYZ	05.0
s42-6c	125	324.6	+44.6	315.3	+62.3	1.138E-06	1.1	XYZ	05.0
s42-6c	150	324.1	+46.0	313.8	+63.7	9.703E-07	1.4	XYZ	05.0
s42-6c	175	321.1	+45.5	309.5	+62.7	8.471E-07	1.3	XYZ	05.0
s42-6c	200	321.1	+46.6	308.8	+63.8	8.366E-07	1.2	XYZ	05.0
s42-6c	225	322.8	+48.2	310.6	+65.6	8.054E-07	1.2	XYZ	05.0
s42-6c	250	325.7	+48.2	315.1	+66.0	6.603E-07	2.0	XYZ	05.0
s42-6c	275	322.4	+50.7	308.2	+67.9	5.664E-07	5.2	XYZ	05.0
s42-6c	300	320.9	+52.9	303.9	+69.7	5.494E-07	5.3	XYZ	05.0
s42-6c	325	315.8	+52.9	295.9	+68.6	5.019E-07	8.9	XYZ	05.0
s43-3b	000	18.1	+57.5	56.9	+53.4	2.341E-06	3.6	XYZ	
s43-3b	050	19.7	+55.6	55.7	+51.5	2.155E-06	4.0	XYZ	05.0
s43-3b	100	16.3	+54.6	52.3	+52.1	1.891E-06	4.6	XYZ	05.0
s43-3b	125	10.1	+53.7	47.0	+54.0	1.683E-06	3.0	XYZ	05.0
s43-3b	150	9.2	+52.5	44.9	+53.5	1.452E-06	4.3	XYZ	05.0
s43-3b	175	14.5	+51.2	47.4	+50.4	1.146E-06	0.5	XYZ	05.0
s43-3b	200	16.0	+49.1	46.3	+48.1	1.119E-06	1.6	XYZ	05.0
s43-3b	225	15.7	+48.9	46.0	+48.1	1.040E-06	1.1	XYZ	05.0
s43-3b	250	18.5	+46.5	45.9	+45.1	7.313E-07	4.0	XYZ	05.0
s43-3b	275	21.7	+44.8	47.0	+42.4	7.199E-07	3.1	XYZ	05.0
s43-3b	300	20.4	+48.7	49.3	+46.0	6.767E-07	2.3	XYZ	05.0
s43-4a	000	23.6	+48.8	51.7	+44.8	1.512E-06	1.2	NDM	
s43-4a	100	29.1	+56.7	62.8	+48.8	1.058E-06	1.3	XYZ	05.0
s43-4a	125	28.5	+57.1	62.9	+49.2	9.279E-07	1.5	XYZ	05.0

s43-4a	150	38.5	+54.2	66.5	+43.4	8.085E-07	1.1	XYZ	05.0
s43-4a	175	49.8	+55.0	74.4	+40.4	6.667E-07	1.4	XYZ	05.0
s43-4a	200	46.6	+55.4	72.6	+41.7	5.875E-07	2.8	XYZ	05.0
s43-4a	225	47.6	+55.1	73.1	+41.2	5.014E-07	2.7	XYZ	05.0
s43-4a	250	320.3	+38.3	335.4	+61.4	4.236E-07	1.2	XYZ	05.0
s43-4a	275	322.7	+32.3	335.4	+55.1	4.157E-07	1.5	XYZ	05.0
s43-4a	300	328.3	+31.3	342.4	+52.6	3.987E-07	1.6	XYZ	05.0
s43-4b	000	325.1	+86.8	115.7	+66.8	4.544E-06	1.4	XYZ	
s43-4b	100	338.1	+84.0	108.9	+68.4	4.299E-06	1.8	XYZ	05.0
s43-4b	125	335.7	+84.8	111.0	+68.0	4.147E-06	1.4	XYZ	05.0
s43-4b	150	312.6	+85.8	116.6	+68.1	3.926E-06	1.4	XYZ	05.0
s43-4b	175	312.5	+85.9	116.7	+68.0	3.705E-06	1.4	XYZ	05.0
s43-4b	200	315.5	+86.1	116.3	+67.8	3.573E-06	1.3	XYZ	05.0
s43-4b	225	314.6	+86.5	116.8	+67.4	3.512E-06	1.5	XYZ	05.0
s43-4b	250	229.7	+86.9	126.0	+64.9	3.154E-06	1.7	XYZ	05.0
s43-4b	275	261.1	+88.0	122.3	+65.6	3.017E-06	0.9	XYZ	05.0
s43-4b	300	256.5	+86.7	124.8	+66.3	2.831E-06	0.9	XYZ	05.0
s43-4b	325	238.2	+86.5	126.5	+65.5	2.787E-06	1.9	XYZ	05.0
s43-6	000	3.6	+44.9	32.3	+50.3	2.341E-06	2.2	NDM	
s43-6	100	11.1	+55.0	49.3	+54.5	1.562E-06	2.6	XYZ	05.0
s43-6	125	12.5	+54.1	49.2	+53.3	1.406E-06	1.9	XYZ	05.0
s43-6	150	16.5	+51.0	48.6	+49.4	1.243E-06	1.8	XYZ	05.0
s43-6	175	19.8	+50.4	50.4	+47.6	1.107E-06	0.4	XYZ	05.0
s43-6	200	18.4	+55.1	54.3	+51.6	9.784E-07	3.8	XYZ	05.0
s43-6	225	17.9	+55.2	54.1	+51.9	9.326E-07	5.7	XYZ	05.0
s43-6	250	298.9	+45.2	298.5	+71.2	8.249E-07	1.6	XYZ	05.0
s43-6	275	302.8	+44.0	306.8	+69.9	6.912E-07	1.7	XYZ	05.0
s43-6	300	302.1	+46.5	305.9	+72.4	6.358E-07	1.7	XYZ	05.0
s44-1	000	10.7	+57.8	267.3	+68.2	1.222E-06	1.5	NDM	
s44-1	100	13.0	+59.0	263.1	+68.9	9.045E-07	1.7	XYZ	05.0
s44-1	125	10.9	+54.3	276.4	+69.2	7.983E-07	1.6	XYZ	05.0
s44-1	150	10.0	+50.5	287.3	+69.0	6.244E-07	1.6	XYZ	05.0
s44-1	175	7.1	+46.9	296.3	+66.8	4.721E-07	3.4	XYZ	05.0
s44-1	200	9.2	+53.6	279.0	+68.4	4.155E-07	1.9	XYZ	05.0
s44-1	225	14.6	+50.4	287.4	+72.0	3.535E-07	5.1	XYZ	05.0
s44-1	250	117.5	+64.0	183.3	+45.9	2.507E-07	0.8	XYZ	05.0
s44-1	275	39.1	+53.4	229.8	+82.5	3.081E-07	0.7	XYZ	05.0
s44-1	300	77.9	+74.0	202.9	+57.7	2.171E-07	0.2	XYZ	05.0
s44-2	00	0	31.0	+67.5	231.2	+67.9	1.243E-06	1.2	NDM
s44-2	100	32.0	+60.5	237.8	+74.6	9.224E-07	2.0	XYZ	05.0
s44-2	125	26.9	+62.0	242.9	+72.1	8.186E-07	1.4	XYZ	05.0
s44-2	150	31.2	+64.3	234.0	+70.9	6.236E-07	1.8	XYZ	05.0
s44-2	175	54.6	+62.8	201.3	+71.5	4.951E-07	2.5	XYZ	05.0
s44-2	200	48.9	+55.5	196.4	+79.3	4.177E-07	1.3	XYZ	05.0
s44-2	225	53.3	+45.3	130.6	+81.4	3.222E-07	2.4	XYZ	05.0
s44-2	250	65.5	+67.0	198.2	+65.4	2.592E-07	0.3	XYZ	05.0
s44-2	275	92.2	+60.9	176.6	+57.2	2.414E-07	0.7	XYZ	05.0
s44-2	300	49.5	+48.5	157.1	+83.7	3.099E-07	1.3	XYZ	05.0
s44-3	000	22.6	+58.9	255.0	+73.0	9.209E-07	4.4	XYZ	
s44-3	050	21.2	+58.8	256.7	+72.5	8.918E-07	1.4	XYZ	05.0
s44-3	100	17.4	+57.3	264.4	+71.7	8.366E-07	5.6	XYZ	05.0
s44-3	125	15.4	+55.4	271.4	+71.4	7.458E-07	4.8	XYZ	05.0
s44-3	150	18.3	+53.0	277.1	+73.8	6.098E-07	1.2	XYZ	05.0
s44-3	175	23.9	+50.8	281.6	+77.7	5.015E-07	6.3	XYZ	05.0
s44-3	200	24.2	+49.0	289.9	+78.3	4.832E-07	4.9	XYZ	05.0
s44-3	225	28.5	+50.3	279.1	+80.7	4.367E-07	2.0	XYZ	05.0

s44-3	250	37.8	+53.3	235.6	+82.5	3.479E-07	1.2	XYZ	05.0
s44-3	275	30.4	+54.5	255.8	+79.2	3.389E-07	1.6	XYZ	05.0
s44-3	300	35.8	+71.1	224.9	+64.8	2.713E-07	0.6	XYZ	05.0
s44-3	325	346.9	+64.4	259.3	+55.6	2.822E-07	1.7	XYZ	05.0
s44-6	000	32.4	+70.3	228.0	+65.3	1.276E-06	2.5	XYZ	
s44-6	100	27.5	+64.3	238.4	+70.2	1.179E-06	2.3	XYZ	05.0
s44-6	125	27.6	+62.3	241.4	+72.0	1.087E-06	1.9	XYZ	05.0
s44-6	150	25.7	+62.0	244.3	+71.8	9.414E-07	2.1	XYZ	05.0
s44-6	175	28.1	+61.9	241.4	+72.5	8.239E-07	2.2	XYZ	05.0
s44-6	200	28.0	+61.7	241.9	+72.6	8.137E-07	1.9	XYZ	05.0
s44-6	225	25.3	+61.6	245.6	+71.9	7.950E-07	2.3	XYZ	05.0
s44-6	250	17.2	+59.7	258.3	+70.4	6.272E-07	2.2	XYZ	05.0
s44-6	275	24.9	+64.0	241.8	+69.9	5.848E-07	1.6	XYZ	05.0
s44-6	300	359.7	+61.0	263.8	+61.9	5.338E-07	3.1	XYZ	05.0
s44-6	325	14.2	+63.8	251.3	+66.8	4.772E-07	3.7	XYZ	05.0
s44-7	000	30.5	+64.0	235.3	+71.1	1.228E-06	3.1	XYZ	
s44-7	050	28.1	+65.2	236.5	+69.5	1.116E-06	2.3	XYZ	05.0
s44-7	100	23.6	+65.5	240.6	+68.3	9.670E-07	2.2	XYZ	05.0
s44-7	125	21.7	+65.1	242.9	+68.2	8.812E-07	3.6	XYZ	05.0
s44-7	150	25.6	+63.1	242.4	+70.8	6.929E-07	4.7	XYZ	05.0
s44-7	175	23.7	+64.8	241.7	+69.0	5.293E-07	4.5	XYZ	05.0
s44-7	200	19.4	+65.5	244.2	+67.3	5.175E-07	3.7	XYZ	05.0
s44-7	225	36.9	+67.6	225.3	+68.3	3.777E-07	2.2	XYZ	05.0
s44-7	250	63.0	+51.8	160.8	+74.5	2.825E-07	2.5	XYZ	05.0
s44-7	275	63.6	+60.7	187.1	+70.3	2.820E-07	1.4	XYZ	05.0
s44-7	300	57.8	+79.5	215.6	+55.9	2.288E-07	3.9	XYZ	05.0
s44-7a	000	48.1	+67.8	213.8	+67.9	8.697E-07	1.4	XYZ	
s44-7a	100	33.8	+62.9	232.1	+72.6	7.414E-07	1.7	XYZ	05.0
s44-7a	125	28.0	+61.1	243.1	+73.1	6.741E-07	1.5	XYZ	05.0
s44-7a	150	30.5	+57.4	246.8	+76.9	5.304E-07	2.1	XYZ	05.0
s44-7a	175	26.5	+56.4	256.5	+76.2	4.496E-07	0.9	XYZ	05.0
s44-7a	200	26.5	+56.0	257.9	+76.5	4.319E-07	2.6	XYZ	05.0
s44-7a	225	24.9	+57.4	255.9	+74.9	4.240E-07	1.9	XYZ	05.0
s44-7a	250	20.8	+53.1	275.1	+75.2	3.226E-07	6.6	XYZ	05.0
s44-7a	275	37.4	+46.6	296.1	+87.4	2.486E-07	3.1	XYZ	05.0
s44-7a	300	37.2	+21.0	32.6	+64.9	1.728E-07	7.5	XYZ	05.0
s44-7a	325	46.3	+18.6	51.8	+62.2	1.693E-07	14.4	XYZ	05.0
s44-9	000	4.1	+59.2	266.5	+64.5	1.104E-06	2.7	XYZ	
s44-9	050	2.1	+61.4	262.3	+62.9	1.043E-06	4.4	XYZ	05.0
s44-9	100	2.6	+61.5	261.9	+63.1	9.622E-07	6.5	XYZ	05.0
s44-9	125	357.7	+66.1	254.4	+59.6	8.477E-07	3.7	XYZ	05.0
s44-9	150	5.1	+65.3	253.3	+62.7	6.347E-07	2.5	XYZ	05.0
s44-9	175	350.8	+71.0	247.3	+55.6	5.299E-07	5.0	XYZ	05.0
s44-9	200	343.6	+71.7	247.2	+53.2	4.760E-07	7.1	XYZ	05.0
s44-9	225	357.1	+72.0	244.2	+57.0	3.898E-07	2.2	XYZ	05.0
s44-9	250	12.8	+63.3	253.3	+66.6	3.590E-07	0.8	XYZ	05.0
s44-9	275	54.3	+70.9	211.0	+64.3	3.228E-07	1.8	XYZ	05.0
s44-9	300	20.0	+44.4	309.5	+75.1	1.863E-07	6.5	XYZ	05.0
s45-2	000	358.1	+67.8	291.7	+58.3	7.008E-07	4.1	XYZ	
s45-2	050	4.6	+67.5	293.6	+60.6	6.610E-07	2.5	XYZ	05.0
s45-2	100	15.6	+63.8	303.7	+64.2	5.624E-07	7.6	XYZ	05.0
s45-2	125	25.0	+64.7	302.7	+68.4	4.636E-07	1.6	XYZ	05.0
s45-2	150	33.2	+60.8	315.0	+71.8	3.613E-07	6.3	XYZ	05.0
s45-2	175	27.5	+65.1	301.7	+69.5	2.631E-07	5.6	XYZ	05.0
s45-2	200	11.6	+58.1	313.9	+60.5	3.016E-07	3.8	XYZ	05.0
s45-2	225	40.8	+61.4	313.5	+75.5	2.354E-07	7.5	XYZ	05.0

s45-2	250	35.3	+59.3	320.3	+72.6	1.591E-07	6.6	XYZ	05.0
s45-2	275	34.2	+71.8	280.9	+70.3	1.564E-07	1.0	XYZ	05.0
s45-2	300	85.5	+75.6	236.3	+71.4	1.485E-07	2.1	XYZ	05.0
s16-1a	000	9.3	+62.0	28.9	+57.8	9.745E-07	1.4	NDM	
s16-1a	100	332.2	+73.2	14.5	+74.5	4.715E-07	5.3	XYZ	05.0
s16-1a	150	293.7	+73.5	335.1	+82.6	2.475E-07	11.5	XYZ	05.0
s16-1a	200	270.0	+65.7	270.9	+77.7	2.381E-07	8.8	XYZ	05.0
s16-1a	200	282.2	+75.3	324.0	+85.9	2.441E-07	16.7	XYZ	05.0
s16-1a	250	259.9	+79.0	147.1	+87.9	2.437E-07	7.6	XYZ	05.0
s16-1a	300	230.2	+57.8	213.7	+66.1	1.909E-07	35.6	XYZ	05.0
s16-1a	300	230.5	+66.8	203.3	+74.4	2.092E-07	5.3	XYZ	05.0
s16-1a	300	240.1	+60.3	224.6	+70.0	1.989E-07	28.5	XYZ	05.0
s16-1a	350	267.8	+65.0	266.7	+77.0	2.012E-07	3.5	XYZ	05.0
s16-1a	375	306.0	+68.7	336.5	+76.3	1.425E-07	10.3	XYZ	05.0
s16-1a	400	180.4	+84.9	112.3	+77.1	1.460E-07	8.0	XYZ	05.0
s16-1a	425	122.9	+67.4	112.0	+56.8	1.739E-07	13.4	XYZ	05.0
s16-1a	425	137.7	+71.4	119.7	+62.1	2.095E-07	22.5	XYZ	05.0
s16-1a	425	148.9	+70.7	127.6	+62.7	2.196E-07	27.7	XYZ	05.0
s16-1a	450	315.8	+63.1	339.3	+69.5	1.553E-07	8.0	XYZ	05.0
s16-1a	475	220.3	+71.6	180.5	+76.3	2.151E-07	6.2	XYZ	05.0
s16-1a	500	26.6	+70.7	48.8	+63.0	4.562E-07	5.5	XYZ	05.0
s16-5	000	34.9	+69.7	53.5	+61.0	7.656E-07	2.6	NDM	
s16-5	100	3.4	+70.1	32.1	+66.1	3.471E-07	9.5	XYZ	05.0
s16-5	150	350.9	+65.9	17.3	+64.8	2.282E-07	7.3	XYZ	05.0
s16-5	200	344.5	+68.6	15.5	+68.4	1.783E-07	12.5	XYZ	05.0
s16-5	250	336.7	+64.9	3.6	+66.8	8.918E-08	6.0	XYZ	05.0
s16-5	300	335.0	+77.6	30.0	+76.8	6.826E-08	12.8	XYZ	05.0
s16-5	350	353.6	+69.4	23.8	+67.3	6.787E-08	4.1	XYZ	05.0
s16-5	375	265.5	+79.1	119.3	+88.7	1.256E-07	2.8	XYZ	05.0
s16-5	400	298.6	+69.5	328.2	+78.4	1.228E-07	3.3	XYZ	05.0
s16-5	425	238.8	+77.0	172.8	+83.5	9.039E-08	4.6	XYZ	05.0
s16-5	450	212.6	+55.2	195.2	+60.3	2.113E-07	4.2	XYZ	05.0
s16-5	475	226.6	+84.3	115.6	+81.3	2.111E-07	2.7	XYZ	05.0
s17-1a	000	6.5	+56.9	28.2	+57.0	9.623E-07	15.2	NDM	
s17-1a	100	6.5	+60.3	31.3	+60.1	4.882E-07	17.3	XYZ	05.0
s17-1a	150	11.3	+57.4	33.0	+56.4	3.419E-07	1.0	XYZ	05.0
s17-1a	200	359.3	+53.5	18.9	+55.7	2.261E-07	9.6	XYZ	05.0
s17-1a	250	347.0	+53.1	6.3	+58.3	2.039E-07	2.2	XYZ	05.0
s17-1a	300	313.4	+75.3	24.1	+83.7	3.141E-07	17.4	XYZ	05.0
s17-1a	300	320.3	+66.8	352.4	+76.5	2.652E-07	1.7	XYZ	05.0
s17-1a	350	286.2	+66.0	283.9	+80.0	2.844E-07	4.3	XYZ	05.0
s17-1a	375	326.7	+62.8	353.4	+71.7	3.143E-07	7.8	XYZ	05.0
s17-1a	400	313.9	+66.9	343.1	+77.9	4.258E-07	6.5	XYZ	05.0
s17-1a	425	294.7	+74.6	342.9	+87.8	3.642E-07	6.5	XYZ	05.0
s17-1a	450	279.6	+74.1	235.7	+87.1	3.220E-07	6.6	XYZ	05.0
s17-1a	475	297.5	+85.3	103.2	+80.6	3.223E-07	6.9	XYZ	05.0
s17-5	100	13.3	+67.5	44.9	+64.7	4.710E-07	10.2	XYZ	05.0
s17-5	150	21.7	+65.8	49.0	+61.5	2.855E-07	12.5	XYZ	05.0
s17-5	200	26.4	+61.5	48.7	+56.7	2.029E-07	13.2	XYZ	05.0
s17-5	250	29.2	+70.3	59.4	+63.8	1.340E-07	14.3	XYZ	05.0
s17-5	300	284.8	+20.9	284.4	+34.9	5.264E-07	3.0	XYZ	05.0
s17-5	350	246.6	+57.3	225.9	+66.1	2.768E-07	4.8	XYZ	05.0
s17-5	375	249.5	+37.9	240.5	+48.2	2.404E-07	5.4	XYZ	05.0
s17-5	400	167.5	+61.0	150.8	+52.1	2.344E-07	6.7	XYZ	05.0
s17-5	425	265.0	+66.4	239.0	+78.1	2.522E-07	5.6	XYZ	05.0
s17-5	450	279.6	+68.9	264.4	+82.5	2.981E-07	6.1	XYZ	05.0
s17-5	475	278.8	+84.1	114.7	+81.8	2.850E-07	7.5	XYZ	05.0

s30-2	000	35.1	+50.0	53.4	+32.0	7.534E-07	23.6	NDM	
s30-2	000	36.4	+49.8	54.2	+31.5	7.462E-07	21.4	NDM	
s30-2	100	28.8	+63.0	58.2	+45.0	6.564E-07	11.0	XYZ	05.0
s30-2	150	41.2	+59.9	62.8	+39.2	4.476E-07	2.7	XYZ	05.0
s30-2	150	48.2	+45.8	60.5	+24.6	3.859E-07	32.2	XYZ	05.0
s30-2	150	49.2	+44.1	60.6	+22.8	3.908E-07	30.4	XYZ	05.0
s30-2	200	47.4	+57.6	65.2	+35.8	3.561E-07	6.4	XYZ	05.0
s30-2	250	48.1	+61.4	67.6	+39.1	3.139E-07	11.6	XYZ	05.0
s30-2	300	40.9	+64.5	65.6	+43.4	2.337E-07	4.7	XYZ	05.0
s30-2	350	52.6	+55.8	67.6	+33.1	1.793E-07	5.8	XYZ	05.0
s30-2	375	41.6	+54.5	60.1	+34.4	1.874E-07	10.5	XYZ	05.0
s30-2	400	25.2	+60.3	54.1	+43.8	1.185E-07	41.7	XYZ	05.0
s30-2	400	25.6	+54.7	50.2	+39.0	1.527E-07	22.5	XYZ	05.0
s30-2	400	38.2	+54.0	57.6	+34.7	1.459E-07	23.0	XYZ	05.0
s30-2	425	44.9	+61.3	65.8	+39.7	1.481E-07	4.5	XYZ	05.0
s30-2	450	31.3	+52.0	52.0	+35.0	2.271E-07	6.6	XYZ	05.0
s30-2	475	32.3	+32.1	42.8	+16.8	2.500E-07	8.5	XYZ	05.0
s30-3	100	39.8	+59.2	61.6	+39.0	6.601E-07	2.8	XYZ	05.0
s30-3	150	53.3	+60.6	70.2	+37.3	4.965E-07	2.9	XYZ	05.0
s30-3	175	56.7	+60.9	72.3	+37.0	4.459E-07	3.1	XYZ	05.0
s30-3	225	62.8	+60.1	75.4	+35.4	3.770E-07	4.6	XYZ	05.0
s30-3	300	74.5	+41.6	78.9	+15.7	2.723E-07	4.5	XYZ	05.0
s30-3	325	82.1	+48.3	85.4	+21.6	2.520E-07	1.9	XYZ	05.0
s30-3	350	72.7	+47.0	78.5	+21.2	2.333E-07	3.8	XYZ	05.0
s30-3	375	71.6	+39.3	76.3	+13.8	2.059E-07	5.7	XYZ	05.0
s30-3	400	58.1	+45.8	67.7	+22.4	2.180E-07	7.2	XYZ	05.0
s30-3	425	12.5	+32.2	26.9	+24.6	2.478E-07	19.8	XYZ	05.0
s30-3	425	16.1	+37.2	32.5	+27.5	1.949E-07	20.8	XYZ	05.0
s30-3	450	14.6	+35.7	30.5	+26.8	3.341E-07	11.4	XYZ	05.0
s30-5	000	17.0	+41.7	35.8	+31.0	9.701E-07	3.5	NDM	
s30-5	100	19.4	+48.9	42.1	+36.2	4.625E-07	1.3	XYZ	05.0
s30-5	150	20.7	+33.5	34.1	+22.5	3.386E-07	1.4	XYZ	05.0
s30-5	200	23.4	+23.8	31.7	+12.7	2.624E-07	0.8	XYZ	05.0
s30-5	225	27.7	+19.8	33.6	+ 7.4	2.217E-07	1.8	XYZ	05.0
s30-5	250	31.7	+18.5	36.6	+ 4.7	1.798E-07	2.2	XYZ	05.0
s30-5	300	73.6	+35.2	77.2	+ 9.5	3.536E-07	1.3	XYZ	05.0
s30-5	350	30.2	- 6.0	25.0	-17.1	1.752E-07	10.0	XYZ	05.0
s30-5	400	23.8	+80.4	76.4	+58.5	3.207E-07	6.6	XYZ	05.0
s31-3	000	353.5	+50.8	24.5	+43.0	9.161E-07	5.4	NDM	
s31-3	100	1.2	+37.2	19.7	+28.8	4.518E-07	3.4	XYZ	05.0
s31-3	150	6.5	+32.8	21.3	+22.8	2.860E-07	3.4	XYZ	05.0
s31-3	200	13.2	+16.0	18.4	+ 5.1	1.873E-07	3.0	XYZ	05.0
s31-3	225	359.0	+ 1.0	358.9	- 1.5	1.538E-07	1.5	XYZ	05.0
s31-3	250	7.7	-13.0	359.6	-17.9	1.456E-07	1.8	XYZ	05.0
s31-3	300	2.1	+28.3	15.2	+20.9	5.624E-07	22.8	XYZ	05.0
s31-3	300	9.9	+15.8	15.4	+ 6.4	2.239E-07	3.1	XYZ	05.0
s31-3	350	3.5	- 6.9	359.0	-10.6	1.627E-07	2.2	XYZ	05.0
s31-3	400	318.8	-28.8	310.7	-10.1	4.595E-07	1.6	XYZ	05.0
s32-1	000	343.2	+65.3	16.2	+56.3	1.698E-06	3.1	NDM	
s32-1	100	355.9	+65.7	24.2	+53.6	8.501E-07	3.5	XYZ	05.0
s32-1	150	347.9	+72.2	27.2	+60.5	6.353E-07	2.1	XYZ	05.0
s32-1	200	347.7	+75.5	32.0	+62.8	4.751E-07	0.8	XYZ	05.0
s32-1	225	349.2	+75.9	33.1	+62.8	4.277E-07	1.1	XYZ	05.0
s32-1	250	328.2	+78.5	32.0	+68.1	3.401E-07	1.0	XYZ	05.0
s32-1	300	279.5	+80.3	39.1	+76.7	2.977E-07	2.9	XYZ	05.0
s32-1	350	285.0	+64.3	334.3	+73.6	2.237E-07	1.1	XYZ	05.0
s32-1	400	209.3	+75.8	108.6	+78.4	1.837E-07	6.5	XYZ	05.0

s32-3b	000	32.4	+66.8	45.9	+48.5	3.751E-06	2.6	NDM
s32-3b	100	34.1	+69.4	48.0	+50.9	1.674E-06	1.2	XYZ 05.0
s32-3b	150	39.9	+70.1	51.3	+51.1	1.269E-06	0.8	XYZ 05.0
s32-3b	200	44.3	+71.5	54.1	+52.1	1.041E-06	8.4	XYZ 05.0
s32-3b	250	35.6	+73.3	50.5	+54.5	8.215E-07	6.2	XYZ 05.0
s32-3b	300	63.0	+80.9	63.8	+60.9	7.419E-07	4.3	XYZ 05.0
s32-3b	300	66.3	+75.5	65.1	+55.5	6.442E-07	9.7	XYZ 05.0
s32-3b	350	54.7	+81.3	61.2	+61.3	6.370E-07	3.5	XYZ 05.0
s32-3b	375	34.4	+80.1	54.0	+61.0	5.905E-07	2.3	XYZ 05.0
s32-3b	400	346.8	+83.1	46.3	+67.5	5.413E-07	6.8	XYZ 05.0
s32-3b	425	63.1	+87.1	64.1	+67.2	5.113E-07	4.1	XYZ 05.0
s32-3b	475	253.0	+86.6	62.4	+73.3	4.933E-07	3.5	XYZ 05.0
s33-3	000	21.6	+53.6	42.8	+37.1	1.209E-06	3.0	NDM
s33-3	100	25.5	+50.5	43.6	+33.3	5.687E-07	3.8	XYZ 05.0
s33-3	100	82.1	+40.8	82.5	+14.8	9.158E-07	2.7	XYZ 05.0
s33-3	150	34.0	+40.3	45.2	+21.5	3.352E-07	2.8	XYZ 05.0
s33-3	200	40.0	+35.2	48.0	+15.2	2.186E-07	1.8	XYZ 05.0
s33-3	225	36.5	+31.2	43.8	+12.3	1.795E-07	1.4	XYZ 05.0
s33-3	250	37.4	+19.5	40.8	+ 1.0	1.529E-07	1.9	XYZ 05.0
s33-3	300	9.9	+10.1	12.7	+ 2.3	1.372E-07	3.6	XYZ 05.0
s33-3	350	357.4	+49.5	23.7	+41.9	1.065E-07	5.9	XYZ 05.0
s33-3	400	21.9	+41.9	36.7	+26.7	1.417E-07	3.6	XYZ 05.0
s35-1	000	13.5	+58.0	358.0	+51.0	1.040E-06	4.7	NDM
s35-1	100	30.0	+66.4	4.8	+61.7	5.710E-07	4.1	XYZ 05.0
s35-1	100	335.2	+72.3	324.3	+60.2	5.768E-07	3.8	XYZ 05.0
s35-1	150	60.3	+73.6	14.9	+73.5	3.119E-07	2.8	XYZ 05.0
s35-1	200	80.8	+67.5	47.2	+73.4	1.890E-07	0.9	XYZ 05.0
s35-1	225	73.3	+68.1	38.2	+72.2	1.436E-07	1.9	XYZ 05.0
s35-1	250	92.4	+62.5	69.8	+71.5	1.946E-07	1.2	XYZ 05.0
s35-1	300	114.8	+62.4	104.0	+74.8	1.244E-07	5.3	XYZ 05.0
s35-1	350	85.6	+77.1	17.1	+80.6	2.039E-07	3.3	XYZ 05.0
s35-1	400	145.4	+71.3	176.2	+82.7	8.149E-08	1.6	XYZ 05.0
s35-5	000	342.6	+66.1	331.5	+54.6	1.072E-06	5.8	NDM
s35-5	100	4.4	+63.4	348.1	+54.6	6.660E-07	7.4	XYZ 05.0
s35-5	150	1.4	+62.5	346.4	+53.4	4.178E-07	2.9	XYZ 05.0
s35-5	200	356.2	+63.5	342.1	+53.6	3.142E-07	2.4	XYZ 05.0
s35-5	250	9.8	+75.0	342.2	+66.0	2.044E-07	8.5	XYZ 05.0
s35-5	300	127.0	+30.0	126.8	+43.0	1.003E-07	7.3	XYZ 05.0
s35-5	350	38.7	+59.7	17.6	+57.4	1.439E-07	6.6	XYZ 05.0
s35-5	375	52.0	+69.5	17.3	+68.7	1.879E-07	9.1	XYZ 05.0
s35-5	400	106.6	+57.7	94.5	+69.3	1.622E-07	22.4	XYZ 05.0
s35-5	400	110.0	+62.6	95.7	+74.5	1.621E-07	25.2	XYZ 05.0
s35-5	425	34.2	+79.0	347.4	+72.5	1.846E-07	5.0	XYZ 05.0
s35-5	475	285.2	+87.8	304.8	+74.9	2.286E-07	4.7	XYZ 05.0
s37-4	000	6.8	+66.7	24.7	-13.3	7.483E-07	3.8	NDM
s37-4	100	16.2	+64.8	27.5	-16.7	3.671E-07	2.8	XYZ 05.0
s37-4	150	11.8	+63.3	25.0	-17.3	2.551E-07	5.4	XYZ 05.0
s37-4	200	5.4	+68.4	25.1	-11.6	1.820E-07	1.8	XYZ 05.0
s37-4	225	6.6	+68.7	25.6	-11.6	1.507E-07	1.2	XYZ 05.0
s37-4	250	2.1	+69.9	24.9	- 9.7	1.339E-07	2.7	XYZ 05.0
s37-4	300	45.3	+61.1	40.9	-21.5	1.173E-07	3.0	XYZ 05.0
s37-4	350	76.2	+85.8	38.9	+ 3.8	1.091E-07	8.5	XYZ 05.0
s37-4	400	53.0	+66.1	43.2	-15.9	8.065E-08	6.7	XYZ 05.0
s37-4	450	75.7	+37.3	73.0	-32.4	1.538E-07	3.7	XYZ 05.0



s37-5b	000	237.6	+77.2	31.3	+18.9	7.246E-07	3.1	NDM	
s37-5b	100	237.8	+67.9	27.2	+27.4	3.649E-07	7.5	XYZ	05.0
s37-5b	150	222.9	+56.1	31.3	+40.6	2.261E-07	5.3	XYZ	05.0
s37-5b	200	229.7	+58.8	27.4	+37.2	1.741E-07	6.2	XYZ	05.0
s37-5b	250	224.4	+55.6	30.1	+41.0	1.213E-07	17.7	XYZ	05.0
s37-5b	250	229.7	+67.2	30.3	+29.1	1.162E-07	10.9	XYZ	05.0
s37-5b	300	250.7	+50.0	8.6	+38.3	7.466E-08	11.9	XYZ	05.0
s37-5b	350	225.8	+43.9	24.9	+52.2	7.600E-08	10.5	XYZ	05.0
s37-5b	375	213.1	+65.2	37.7	+31.7	9.831E-08	6.7	XYZ	05.0
s37-5b	400	219.5	+80.7	35.6	+16.2	8.654E-08	5.2	XYZ	05.0
s37-5b	475	164.8	+71.5	51.3	+18.2	6.883E-08	12.7	XYZ	05.0
s38-1	000	169.6	+81.7	103.6	+75.0	1.939E-06	1.8	NDM	
s38-1	100	125.4	+87.4	78.1	+74.4	9.136E-07	5.1	XYZ	05.0
s38-1	150	161.9	+79.6	108.0	+72.9	6.683E-07	2.5	XYZ	05.0
s38-1	200	153.4	+72.4	118.6	+66.4	5.548E-07	12.1	XYZ	05.0
s38-1	250	177.6	+73.2	132.1	+71.8	4.091E-07	12.4	XYZ	05.0
s38-1	300	199.4	+77.5	128.4	+78.6	3.496E-07	2.3	XYZ	05.0
s38-1	350	211.7	+80.6	111.6	+81.2	2.254E-07	4.2	XYZ	05.0
s38-1	375	229.8	+63.4	211.0	+75.7	2.443E-07	9.9	XYZ	05.0
s38-1	375	248.1	+66.9	244.9	+80.9	2.681E-07	16.2	XYZ	05.0
s38-1	400	202.2	+63.0	173.4	+69.7	2.259E-07	18.8	XYZ	05.0
s38-1	400	215.5	+65.3	185.8	+74.7	2.352E-07	14.7	XYZ	05.0
s38-1	400	242.2	+63.9	233.6	+77.6	2.199E-07	17.3	XYZ	05.0
s38-1	450	272.8	+78.0	12.4	+84.6	1.344E-07	3.3	XYZ	05.0
s38-1	450	289.8	+49.9	304.4	+59.6	7.061E-07	72.3	XYZ	05.0
s38-1	475	255.9	+67.4	264.6	+81.2	1.849E-07	4.9	XYZ	05.0
s38-2	100	48.6	+84.8	64.3	+71.1	7.167E-07	2.2	XYZ	05.0
s38-2	150	167.0	+82.7	99.3	+75.0	5.108E-07	4.3	XYZ	05.0
s38-2	175	192.9	+79.4	117.8	+77.9	4.271E-07	3.2	XYZ	05.0
s38-2	200	190.1	+74.6	135.8	+75.3	3.790E-07	4.4	XYZ	05.0
s38-2	225	193.4	+73.1	142.7	+75.2	3.538E-07	4.7	XYZ	05.0
s38-2	275	192.3	+63.7	161.9	+68.0	2.983E-07	5.0	XYZ	05.0
s38-2	300	189.8	+67.3	153.6	+70.3	3.404E-07	7.1	XYZ	05.0
s38-2	325	173.1	+56.8	151.2	+57.3	3.117E-07	3.6	XYZ	05.0
s38-2	350	175.7	+67.6	141.4	+67.2	2.774E-07	4.4	XYZ	05.0
s38-2	375	216.8	+73.4	160.1	+81.0	2.417E-07	4.1	XYZ	05.0
s38-2	400	194.8	+66.8	159.3	+71.0	2.361E-07	5.1	XYZ	05.0
s38-2	425	189.6	+73.6	138.5	+74.7	2.729E-07	11.6	XYZ	05.0
s38-2	450	185.3	+68.1	148.4	+69.8	2.579E-07	11.3	XYZ	05.0
s38-4	000	15.5	+66.5	34.0	+56.5	2.546E-06	2.5	NDM	
s38-4	100	35.1	+49.4	42.1	+37.5	3.134E-07	14.0	XYZ	05.0
s38-4	150	41.4	+48.2	47.0	+35.6	2.751E-07	2.4	XYZ	05.0
s38-4	200	38.7	+48.0	44.7	+35.7	2.588E-07	1.6	XYZ	05.0
s38-4	225	42.7	+43.6	47.2	+30.9	2.702E-07	1.7	XYZ	05.0
s38-4	250	34.6	+42.1	40.1	+30.3	2.734E-07	1.9	XYZ	05.0
s38-4	300	46.1	+45.1	50.3	+32.1	2.789E-07	4.5	XYZ	05.0
s38-4	350	40.0	+49.8	46.1	+37.3	2.685E-07	7.9	XYZ	05.0
s38-4	400	35.1	+51.7	42.6	+39.7	2.834E-07	15.3	XYZ	05.0
s38-4	450	23.1	+44.3	31.0	+34.0	3.943E-07	2.7	XYZ	05.0
s39-2a	000	309.1	+63.9	21.1	+69.0	8.986E-07	17.3	NDM	
s39-2a	100	348.9	+64.8	37.2	+53.7	4.684E-07	4.8	XYZ	05.0
s39-2a	150	0.5	+63.7	41.0	+49.2	1.743E-07	25.6	XYZ	05.0
s39-2a	150	358.4	+71.0	49.5	+54.4	2.258E-07	4.1	XYZ	05.0
s39-2a	200	28.5	+86.1	77.1	+58.6	1.109E-07	8.8	XYZ	05.0
s39-2a	200	90.6	+36.7	89.2	+ 7.9	4.943E-08	75.1	XYZ	05.0

s39-2a	250	229.1	+76.8	105.8	+70.6	6.788E-08	12.3	XYZ	05.0
s39-2a	300	139.1	+25.2	132.3	+ 7.3	2.554E-08	32.3	XYZ	05.0
s39-2a	300	140.2	+23.1	134.1	+ 5.8	3.199E-08	40.1	XYZ	05.0
s39-2a	300	145.6	+25.9	137.3	+10.4	4.670E-08	24.2	XYZ	05.0
s39-2a	350	164.1	- 7.0	168.6	-10.5	5.827E-08	8.3	XYZ	05.0
s39-2a	375	243.6	- 8.4	242.7	+18.9	4.968E-08	33.7	XYZ	05.0
s39-2a	375	266.4	- 9.0	266.6	+20.0	6.203E-08	26.2	XYZ	05.0
s39-2a	375	271.4	- 5.3	272.1	+23.4	7.674E-08	30.2	XYZ	05.0
s39-2a	400	74.8	+33.7	76.2	+ 4.9	1.121E-07	43.7	XYZ	05.0
s39-2a	400	77.7	+23.6	78.1	- 5.3	7.386E-08	58.2	XYZ	05.0
s39-2a	400	84.5	+22.4	84.4	- 6.6	6.238E-08	39.2	XYZ	05.0
s39-2a	425	157.6	+11.0	154.3	+ 2.2	8.715E-08	5.4	XYZ	05.0
s39-2a	450	69.8	+19.9	70.5	- 8.3	5.796E-07	2.8	XYZ	05.0
s39-2a	475	75.2	+47.9	77.5	+19.1	2.470E-08	18.7	XYZ	05.0
s39-3a	000	18.4	+65.9	51.3	+45.6	8.242E-07	3.4	NDM	
s39-3a	100	28.4	+75.4	64.1	+50.9	3.863E-07	4.8	XYZ	05.0
s39-3a	150	93.8	+68.0	88.3	+39.2	1.516E-07	6.9	XYZ	05.0
s39-3a	200	128.9	+44.7	116.5	+22.0	1.095E-07	2.2	XYZ	05.0
s39-3a	225	134.4	+24.4	128.7	+ 4.8	8.855E-08	1.8	XYZ	05.0
s39-3a	250	141.5	+ 2.4	143.8	-12.6	9.331E-08	3.2	XYZ	05.0
s39-3a	300	159.8	- 8.8	165.7	-14.2	1.068E-07	2.1	XYZ	05.0
s39-3a	350	148.3	- 2.1	152.1	-13.6	1.124E-07	11.0	XYZ	05.0
s39-3a	400	156.7	+ 1.2	158.1	- 6.9	1.244E-07	6.4	XYZ	05.0
s39-3a	450	177.1	+31.1	160.1	+28.7	2.584E-07	4.0	XYZ	05.0
s39-9	100	347.2	+65.9	56.2	+63.6	5.621E-07	6.7	XYZ	05.0
s39-9	150	341.7	+72.8	72.0	+66.2	3.698E-07	2.9	XYZ	05.0
s39-9	175	337.9	+73.0	72.8	+67.3	2.666E-07	1.4	XYZ	05.0
s39-9	200	324.9	+78.7	90.0	+68.1	2.308E-07	5.6	XYZ	05.0
s39-9	225	299.8	+77.2	99.8	+72.4	2.497E-07	4.3	XYZ	05.0
s39-9	275	315.5	+81.3	97.7	+67.4	1.546E-07	2.7	XYZ	05.0
s39-9	300	286.9	+84.1	108.5	+65.9	1.941E-07	9.5	XYZ	05.0
s39-9	325	319.0	+75.9	86.0	+70.8	1.317E-07	6.9	XYZ	05.0
s39-9	350	112.6	+72.6	110.0	+42.6	1.566E-07	5.3	XYZ	05.0
s39-9	375	132.9	+58.5	122.8	+30.1	1.313E-07	2.5	XYZ	05.0
s39-9	400	180.4	+67.9	140.7	+48.1	1.287E-07	8.1	XYZ	05.0
s39-9	425	32.2	+75.7	84.2	+54.0	1.839E-07	14.0	XYZ	05.0
s39-9	450	23.9	+85.0	98.4	+59.1	2.217E-07	3.8	XYZ	05.0
s40-2	100	4.9	+64.7	340.8	+72.3	5.032E-07	3.5	XYZ	05.0
s40-2	150	351.5	+70.7	314.2	+74.7	3.080E-07	2.1	XYZ	05.0
s40-2	175	335.0	+74.4	291.2	+74.1	2.172E-07	1.7	XYZ	05.0
s40-2	200	329.0	+74.1	287.8	+72.8	1.849E-07	2.3	XYZ	05.0
s40-2	225	321.0	+71.1	287.9	+69.0	1.443E-07	2.3	XYZ	05.0
s40-2	275	313.0	+63.0	291.0	+60.4	7.810E-08	3.7	XYZ	05.0
s40-2	300	346.1	+50.0	331.7	+55.1	4.863E-08	8.6	XYZ	05.0
s40-2	325	0.3	+70.2	324.7	+76.1	4.348E-08	7.8	XYZ	05.0
s40-2	350	42.7	+47.8	42.2	+59.8	6.835E-08	15.9	XYZ	05.0
s40-2	375	344.3	+50.3	329.7	+55.0	5.072E-08	6.7	XYZ	05.0
s40-2	400	27.2	+13.1	25.9	+24.6	6.692E-08	12.2	XYZ	05.0
s40-2	425	349.3	+21.5	344.6	+28.0	6.118E-08	13.7	XYZ	05.0
s40-2	450	3.6	+28.8	358.2	+37.5	1.534E-07	8.6	XYZ	05.0

s40-3	000	2.0	+62.7	339.7	+70.0	3.007E-06	6.7	NDM	
s40-3	100	5.5	+58.8	348.2	+67.0	1.130E-06	4.0	XYZ	05.0
s40-3	150	7.9	+62.9	347.0	+71.3	8.095E-07	2.3	XYZ	05.0
s40-3	200	9.5	+70.4	335.2	+78.2	6.039E-07	1.6	XYZ	05.0
s40-3	250	25.3	+70.9	359.2	+81.4	5.182E-07	3.1	XYZ	05.0
s40-3	300	58.6	+72.0	83.2	+83.0	3.961E-07	2.6	XYZ	05.0
s40-3	350	21.3	+76.3	321.6	+84.7	3.127E-07	5.5	XYZ	05.0
s40-3	375	348.8	+87.3	236.3	+79.3	2.923E-07	11.4	XYZ	05.0
s40-3	400	210.7	+82.9	219.1	+71.1	2.782E-07	10.4	XYZ	05.0
s40-3	425	320.2	+81.2	263.1	+75.9	2.265E-07	6.9	XYZ	05.0
s40-3	450	114.8	+62.0	138.3	+63.7	7.937E-07	19.9	XYZ	05.0
s40-3	450	128.0	+37.0	137.2	+37.3	4.579E-07	2.4	XYZ	05.0
s40-3	475	311.3	+26.8	305.4	+25.6	3.352E-07	5.5	XYZ	05.0
s40-5	000	195.9	+53.9	201.8	+43.1	1.033E-06	3.0	NDM	
s40-5	110	199.9	+63.1	206.7	+51.9	4.932E-07	4.3	XYZ	05.0
s40-5	150	245.4	+67.3	238.6	+55.9	2.692E-07	2.4	XYZ	05.0
s40-5	200	271.4	+50.7	262.8	+41.9	2.036E-07	2.5	XYZ	05.0
s40-5	225	259.7	+54.9	252.2	+44.6	1.671E-07	1.4	XYZ	05.0
s40-5	250	319.6	+64.3	295.3	+62.9	2.549E-07	3.1	XYZ	05.0
s40-5	300	273.9	+47.2	265.9	+38.7	1.152E-07	11.9	XYZ	05.0
s40-5	350	310.0	+45.9	298.2	+43.8	9.467E-08	13.2	XYZ	05.0
s40-5	400	267.3	+27.2	264.0	+18.2	2.589E-07	14.0	XYZ	05.0
s40-5	400	270.8	+22.5	268.0	+14.0	1.674E-07	5.5	XYZ	05.0
s40-6	000	28.2	+62.2	17.5	+73.4	8.349E-07	3.1	NDM	
s40-6	110	41.6	+57.2	40.2	+69.2	4.666E-07	2.6	XYZ	05.0
s40-6	150	54.2	+50.2	57.9	+62.0	2.623E-07	1.5	XYZ	05.0
s40-6	200	73.8	+56.7	87.0	+66.5	2.377E-07	2.0	XYZ	05.0
s40-6	225	85.2	+40.5	93.7	+49.0	1.367E-07	1.7	XYZ	05.0
s40-6	250	87.7	+28.0	93.2	+36.3	1.177E-07	2.5	XYZ	05.0
s40-6	300	72.5	+27.3	76.4	+37.7	1.360E-07	3.4	XYZ	05.0
s40-6	350	101.1	+12.2	103.9	+18.5	7.290E-08	39.3	XYZ	05.0
s40-6	350	105.8	+23.3	111.1	+28.5	7.619E-08	20.3	XYZ	05.0
s40-6	400	81.8	+45.7	91.6	+54.5	2.623E-08	24.6	XYZ	05.0
s40-6	400	97.7	+46.5	109.9	+52.6	2.451E-08	10.8	XYZ	05.0
s40-7	000	358.3	+59.6	338.7	+66.5	1.033E-06	3.2	NDM	
s40-7	100	3.3	+67.7	333.7	+74.7	4.846E-07	2.8	XYZ	05.0
s40-7	150	3.0	+79.7	282.1	+82.0	2.558E-07	3.0	XYZ	05.0
s40-7	175	43.2	+86.9	224.6	+81.1	1.881E-07	2.5	XYZ	05.0
s40-7	200	150.5	+84.5	202.6	+75.5	1.562E-07	4.1	XYZ	05.0
s40-7	225	146.3	+79.5	187.8	+72.5	1.165E-07	4.6	XYZ	05.0
s40-7	275	176.3	+73.5	195.5	+63.9	8.490E-08	5.6	XYZ	05.0
s40-7	300	104.3	+76.3	157.2	+77.1	4.306E-08	9.4	XYZ	05.0
s40-7	300	121.2	+69.0	152.5	+68.5	6.780E-08	22.7	XYZ	05.0
s40-7	325	198.3	+60.7	204.9	+49.6	8.133E-08	14.6	XYZ	05.0
s40-7	350	194.8	+33.2	197.8	+22.5	4.853E-08	6.5	XYZ	05.0
s40-7	375	194.2	+35.8	197.6	+25.2	5.331E-08	2.2	XYZ	05.0
s40-7	400	183.1	+56.2	192.1	+46.6	4.850E-08	14.2	XYZ	05.0
s40-7	400	189.7	+55.7	197.2	+45.3	4.020E-08	6.8	XYZ	05.0
s40-7	425	146.4	+41.1	155.9	+37.5	7.872E-08	9.8	XYZ	05.0
s40-7	450	177.7	+29.8	181.7	+21.2	1.053E-07	15.0	XYZ	05.0
s40-7	450	194.0	+38.0	197.7	+27.4	1.142E-07	21.3	XYZ	05.0
s41-3	000	48.2	+73.8	72.1	+57.6	8.381E-07	6.3	NDM	
s41-3	100	26.7	+71.7	59.8	+59.2	4.785E-07	13.0	XYZ	05.0
s41-3	150	51.0	+69.7	70.7	+53.6	3.250E-07	14.0	XYZ	05.0
s41-3	200	53.3	+68.4	71.1	+52.0	2.393E-07	2.9	XYZ	05.0

s41-3	250	306.4	+68.4	6.6	+78.7	1.959E-07	18.4	XYZ	05.0
s41-3	250	307.9	+81.4	72.0	+77.3	1.597E-07	13.9	XYZ	05.0
s41-3	250	309.3	+72.7	29.7	+79.1	1.499E-07	21.6	XYZ	05.0
s41-3	300	207.9	+69.1	156.9	+68.4	1.811E-07	8.5	XYZ	05.0
s41-3	350	73.9	+79.2	86.6	+60.6	2.780E-07	5.5	XYZ	05.0
s41-3	375	153.1	+9.0	151.9	-1.0	2.008E-06	1.2	XYZ	05.0
s41-3	400	311.5	+16.6	316.9	+31.3	1.940E-06	7.4	XYZ	05.0
s41-3	425	2.9	+16.1	8.4	+15.6	1.518E-06	3.6	XYZ	05.0
s41-3	450	315.9	+10.6	320.1	+24.4	2.949E-06	2.7	XYZ	05.0
s41-3	475	338.9	+12.2	343.9	+19.6	1.928E-06	3.0	XYZ	05.0
s42-1a	000	34.8	+68.5	89.3	+71.9	1.091E-06	3.7	NDM	
s42-1a	110	11.5	+52.6	33.4	+67.2	5.029E-07	2.9	XYZ	05.0
s42-1a	150	11.9	+48.7	30.3	+63.5	3.511E-07	2.0	XYZ	05.0
s42-1a	200	8.9	+42.0	21.7	+57.9	2.191E-07	0.8	XYZ	05.0
s42-1a	225	8.1	+40.9	20.0	+57.0	1.735E-07	3.5	XYZ	05.0
s42-1a	250	357.1	+33.8	2.9	+51.8	1.382E-07	0.9	XYZ	05.0
s42-1a	300	351.3	+22.0	353.5	+40.7	1.516E-07	5.7	XYZ	05.0
s42-1a	350	22.6	+40.5	38.0	+53.1	1.737E-07	11.7	XYZ	05.0
s42-1a	400	11.6	+30.9	20.4	+46.6	9.744E-08	14.5	XYZ	05.0
s42-3a	000	353.4	+41.6	359.7	+59.9	1.590E-06	4.6	NDM	
s42-3a	100	357.9	+56.3	15.7	+73.6	8.579E-07	2.7	XYZ	05.0
s42-3a	150	358.8	+57.2	18.5	+74.4	5.877E-07	2.3	XYZ	05.0
s42-3a	175	3.6	+58.2	28.7	+74.2	4.772E-07	2.7	XYZ	05.0
s42-3a	200	4.3	+60.9	35.3	+76.4	4.315E-07	3.4	XYZ	05.0
s42-3a	200	57.7	+72.9	112.0	+67.9	2.278E-07	3.0	XYZ	05.0
s42-3a	275	5.0	+61.8	38.7	+76.9	3.761E-07	1.4	XYZ	05.0
s42-3a	300	4.0	+59.7	32.1	+75.4	3.465E-07	7.5	XYZ	05.0
s42-3a	325	6.3	+51.6	24.8	+67.5	2.822E-07	1.4	XYZ	05.0
s42-3a	350	22.2	+69.7	85.4	+76.4	1.920E-07	5.5	XYZ	05.0
s42-3a	375	353.2	+72.8	102.5	+85.9	2.076E-07	4.0	XYZ	05.0
s42-3a	400	349.8	+61.3	5.0	+79.8	2.385E-07	2.0	XYZ	05.0
s42-3a	425	302.3	+68.2	244.1	+76.4	1.741E-07	5.3	XYZ	05.0
s42-3a	450	289.0	+51.1	263.7	+59.5	2.060E-07	11.3	XYZ	05.0
s42-4a	000	40.4	+68.6	93.1	+70.2	1.094E-06	2.1	NDM	
s42-4a	110	24.1	+66.7	76.3	+74.3	4.462E-07	3.5	XYZ	05.0
s42-4a	150	39.1	+61.7	78.1	+66.1	3.014E-07	1.0	XYZ	05.0
s42-4a	200	69.1	+64.7	104.5	+59.3	1.914E-07	2.8	XYZ	05.0
s42-4a	225	75.9	+50.7	96.7	+45.6	1.430E-07	2.5	XYZ	05.0
s42-4a	250	92.7	+47.4	108.2	+38.0	1.371E-07	2.7	XYZ	05.0
s42-4a	300	87.4	+49.0	104.9	+40.9	1.238E-07	7.7	XYZ	05.0
s42-4a	350	58.9	+42.1	76.6	+43.3	1.456E-07	5.2	XYZ	05.0
s42-4a	400	163.7	+80.2	162.1	+61.2	6.142E-08	9.5	XYZ	05.0
s42-5	000	317.9	+71.6	235.9	+82.5	8.975E-07	6.5	NDM	
s42-5	100	337.1	+77.3	169.4	+83.7	5.526E-07	1.4	XYZ	05.0
s42-5	150	187.2	+88.3	163.3	+69.4	3.336E-07	3.3	XYZ	05.0
s42-5	175	174.3	+78.0	166.5	+59.2	2.831E-07	2.9	XYZ	05.0
s42-5	275	250.7	+53.3	227.2	+49.1	1.622E-07	5.6	XYZ	05.0
s42-5	300	193.8	+58.8	183.2	+41.8	1.388E-07	31.1	XYZ	05.0
s42-5	300	198.5	+65.1	183.8	+48.5	1.498E-07	8.0	XYZ	05.0
s42-5	325	178.7	+64.8	171.9	+46.3	1.643E-07	5.8	XYZ	05.0
s42-5	350	187.5	+80.5	170.2	+62.2	1.624E-07	6.4	XYZ	05.0
s42-5	400	201.8	+72.1	181.9	+55.4	1.462E-07	4.3	XYZ	05.0
s42-5	425	62.3	+83.5	141.2	+70.9	1.211E-07	3.1	XYZ	05.0
s42-5	450	116.8	+62.9	133.1	+47.3	1.623E-07	4.3	XYZ	05.0

s42-6a	000	293.4	+40.8	276.8	+51.6	8.182E-07	7.5	NDM	
s42-6a	110	265.4	+40.5	248.4	+42.4	3.173E-07	2.5	XYZ	05.0
s42-6a	150	237.3	+34.6	226.2	+28.2	2.301E-07	1.6	XYZ	05.0
s42-6a	200	211.7	+15.2	209.4	+ 2.8	1.884E-07	1.7	XYZ	05.0
s42-6a	225	214.8	+10.2	213.6	- 1.3	1.806E-07	0.8	XYZ	05.0
s42-6a	250	209.8	+ 7.9	209.4	- 4.7	1.673E-07	1.2	XYZ	05.0
s42-6a	300	182.1	+ 6.3	182.4	-11.5	1.571E-07	16.0	XYZ	05.0
s42-6a	300	183.7	+ 7.9	183.8	- 9.7	1.685E-07	7.8	XYZ	05.0
s42-6a	350	198.5	- 4.0	200.9	-18.9	1.539E-07	5.3	XYZ	05.0
s42-6a	400	224.6	+16.7	221.0	+ 7.6	1.173E-07	5.6	XYZ	05.0
s43-1a	000	20.3	+58.3	59.2	+53.2	1.398E-06	2.7	NDM	
s43-1a	110	56.2	+57.8	80.3	+40.9	5.256E-07	2.2	XYZ	05.0
s43-1a	150	73.1	+49.9	87.0	+29.5	3.839E-07	1.2	XYZ	05.0
s43-1a	200	92.8	+27.7	96.0	+ 4.0	2.707E-07	2.8	XYZ	05.0
s43-1a	225	94.0	+22.8	96.1	- 1.0	2.610E-07	2.4	XYZ	05.0
s43-1a	250	98.7	+18.3	99.7	- 6.2	2.727E-07	1.5	XYZ	05.0
s43-1a	300	111.6	+23.0	112.2	- 2.8	2.300E-07	3.1	XYZ	05.0

## B.2 Demagnetization planes data

Following list is the orientations of poles to demagnetization planes calculated by a least squares method using software at the U.S. Geological Survey, Menlo Park, California.

(U)=prefix refers to inclination (INC) and declination (DEC) without structural corrections.

(S)=prefix refers to inclination (INC) and declination (DEC) with structural corrections.

TEMP RANGE refers to the temperature range for the demagnetization steps that were included in the planes calculations.

SAMPLE	(U)INC	(U)DEC	(S)INC	(S)DEC	TEMP RANGE
s16-1a	-16.5	313.3	-7.7	311.5	000-200
s16-2	20.3	229.5	29.3	225.5	100-175
s16-4	-11.8	291.6	-0.6	291.0	050-150
s16-5	-10.8	286.1	0.7	285.8	150-450
s16-6	-13.3	311.4	-4.1	309.7	125-275
s16-7	-0.2	278.7	11.6	279.0	125-200
s17-1a	-22.7	304.2	-9.3	303.1	200-350
s17-3	1.7	264.7	14.5	264.4	100-225
s17-4	-6.7	283.1	7.2	283.2	225-300
s17-5	17.6	154.0	7.5	151.5	100-200
s30-1	32.4	200.1	35.8	181.6	125-225
s30-2	25.0	184.9	22.6	172.8	100-350
s30-3	29.4	238.4	49.4	222.6	100-225
s30-4	32.2	245.4	54.3	229.9	125-225
s30-5	4.9	114.8	-20.4	116.1	100-200
s30-6	26.5	247.9	49.8	237.0	150-275
s31-3	18.4	107.4	-8.4	106.4	000-200
s32-1	-7.8	284.3	7.5	284.4	100-300
s32-2a	-6.3	290.3	7.6	290.5	125-225
s32-3a	23.1	253.1	42.8	255.3	100-300

SAMPLE	(U)INC	(U)DEC	(S)INC	(S)DEC	TEMP RANGE
s33-2	-41.6	40.3	-56.4	14.9	100-325
s33-3	22.3	145.3	8.4	139.2	000-200
s33-4	40.5	224.7	57.1	200.5	125-300
s35-1	16.7	255.0	8.6	257.3	000-150
s35-6	-34.8	49.9	-30.8	58.7	125-225
s37-4	-10.4	303.2	1.3	295.4	150-250
s37-5b	-3.8	312.1	-6.4	303.1	000-350
s38-1	1.2	250.7	15.1	250.5	100-200
s38-2	2.6	289.6	13.4	290.8	100-275
s38-3	7.5	250.7	21.5	250.9	100-200
s38-4	36.0	183.6	40.2	172.8	100-300
s38-5	0.7	272.1	13.7	272.8	125-225
s39-2a	5.0	248.8	32.9	246.3	100-200
s39-3a	13.8	213.0	37.4	222.6	100-250
s39-4	27.8	219.4	45.8	201.7	100-225
s39-8a	8.1	259.0	33.6	252.8	125-225
s39-9	-9.9	281.2	19.9	280.8	100-225
s40-1	19.0	162.2	15.7	172.0	125-200
s40-2	-16.1	312.9	-16.0	316.1	100-225
s40-3	15.9	246.3	4.7	245.7	100-300
s40-4	32.0	186.9	22.1	190.3	125-250
s40-6	27.9	196.7	17.2	199.0	000-250
s40-7	1.6	269.2	-6.9	269.5	100-275
s41-1	6.4	261.4	24.9	260.2	000-225
s41-5	26.8	190.8	27.4	181.1	100-225
s42-1a	-6.6	93.2	-13.3	90.1	110-225
s42-2a	-18.7	307.0	-2.7	309.0	125-275
s42-3a	27.1	207.8	15.5	211.6	100-250
s42-4a	24.3	208.1	10.8	203.9	110-300
s42-5	7.4	301.5	21.8	298.3	175-250
s43-1a	25.9	197.3	18.2	187.1	110-250
s43-3a	21.0	234.5	34.3	291.9	000-110
s43-4a	33.1	207.8	28.9	192.2	100-225
s43-5a	-8.7	305.5	17.2	305.6	000-150
s43-8	19.6	227.7	25.7	216.9	150-250
s44-1	-8.4	88.9	20.8	92.1	100-175
s44-3	24.6	146.7	7.3	159.5	125-200
s44-5	14.1	141.8	5.6	128.1	000-300
s44-7a	-15.1	91.0	14.2	90.8	100-250
s44-9	-11.1	293.4	-20.1	306.2	000-200
s45-2	22.0	168.4	13.9	178.4	000-150

# Appendix

# C

## Conglomerate Data

**LITHOLOGIC CLAST COUNTS: LAKE NACIMIENTO AREA**

LOCALITIES -->	SC-1	SI-1	LN-1	LN-2	LN-3	LN-4	LN-5	LN-6	LN-7	LN-8
Felsic plutonics*		21	29	22	19	6	6	15	16	8
Intermediate/mafic plutonics	3		5	8	6	10		3	3	5
Light aphanites	8	7	7	2	6	12	24	9	7	4
Dark siliceous aphanites	6		1	3	1	2	1	3	3	
Dark int./mafic aphanites†	12	2	1	4	3	4	1	4	2	3
Light tuffs	3	42	36	19	16	32	32	21	25	23
Dark tuffs	65	4	13	25	20	12	12	29	22	23
Tan/grey porphyries	1	2		8	7	6	14	7	12	12
Green porphyries		1	2	4	7	6		2	4	3
Red/purple porphyries		1		4		2				2
Black/brown porphyries					3	4			1	6
White quartzites		19	6		3		7	4	2	7
Brown/grey quartzites		1		1	3	4	3	3	3	1
Green quartzites										2
Low grade metasediments	2									
Intraclasts					6					1
<b>TOTAL CLASTS</b>	<b>100</b>	<b>100</b>	<b>100</b>	<b>100</b>	<b>100</b>	<b>100</b>	<b>100</b>	<b>100</b>	<b>100</b>	<b>100</b>

\*includes apites and granitic porphyries

†includes fine-grained and porphyritic lithologies

**GROUPED CATEGORIES FOR CHART PLOTTING**

	21	28	22	19	6	14	16	8
Felsic plutonics								
Int./mafic plutonics	3	5	8	6	10	3	3	5
Light siliceous volcanics	12	53	33	33	55	70	39	38
Dark siliceous volcanics	71	4	14	32	27	13	32	35
Int./mafic volcanics	12	2	1	4	3	1	4	3
Quartzites		20	6	1	6	4	7	10
Misc.	2		1					1
<b>TOTAL CLASTS</b>	<b>100</b>	<b>100</b>	<b>100</b>	<b>100</b>	<b>100</b>	<b>100</b>	<b>100</b>	<b>100</b>



**LITHOLOGIC CLAST COUNTS: SANTA MARGARITA LAKE AREA**

LOCALITIES →	SML-1	SML-2	SML-3	SML-4	SML-5	SML-6	SML-7	SML-8	SML-9
Felsic plutonics*	47	54	58	27	10	18	10	20	6
Int./mafic plutonics	2	2	4	3	1	2	4	11	10
Light aphanites	2	1		7	2	5	15	4	8
Dark siliceous aphanites	1		1		3			1	1
Dark int./mafic aphanites†		2	2				1	6	17
Light tuffs	7	8	1	21	41	22	28	31	12
Dark tuffs	26	31	25	12	16	13	8	15	15
Tan/grey porphyries	3	2	3	12	17	19	7	5	7
Green porphyries	1		4	1	2	6	11	2	18
Red/purple porphyries									1
Black/brown porphyries	3		1	6					
White/tan quartzites	8		1	9	8	11	13	5	5
Brown/grey quartzites									
Green quartzites						2			
Phyllites						2			
Low grade metasandstones				2			3		
TOTAL CLASTS	100	100	100	100	100	100	100	100	100

\*includes aplites and granitic porphyries

†includes fine-grained and porphyritic lithologies

**GROUPED CATEGORIES FOR CHART PLOTTING**

Felsic plutonics	47	54	58	27	10	18	10	20	6
Int./mafic plutonics	2	2	4	3	1	2	4	11	10
Light siliceous volcanics	13	11	8	40	57	47	61	42	34
Dark siliceous volcanics	30	31	27	19	24	18	8	16	28
Int./mafic volcanics		2	2				1	6	17
Quartzites	8		1	9	8	13	13	5	5
Misc.				2		2	3		
TOTAL CLASTS	100	100	100	100	100	100	100	100	100

**SML (cont.)**

LOCALITIES →	SML-10	SML-11	SMK-12	SML-13	SML-14	SML-15
Felsic plutonics	13	14	12	10	4	8
Int./mafic plutonics		4	2	4	13	6
Light aphanites	30	13	8	8	3	14
Dark siliceous aphanites		1	2	1		1
Dark int./mafic aphanites		4		4	5	
Light tuffs	32	25	26	20	22	24
Dark tuffs	1	9	34	15	21	20
Tan/grey porphyries	10	15	6	12	7	4
Green porphyries		8	8	5	9	10
Red/purple porphyries					1	
Black/brown porphyries			2	2	1	1
White/tan quartzites	11	5		9	4	3
Brown/grey quartzites	3	1		9	3	8
Green quartzites		1		1	6	1
Phyllites						
Lo grade meta-sandstones					1	
TOTAL CLASTS	100	100	100	100	100	100

Felsic plutonics	13	14	12	10	4	8
Int./mafic plutonics		4	2	4	13	6
Light siliceous volcanics	72	61	48	40	36	52
Dark siliceous volcanics	1	10	38	23	28	22
Int./mafic volcanics		4		4	5	
Quartzites	14	7		19	13	12
Misc.					1	
TOTAL CLASTS	100	100	100	100	100	100

**LITHOLOGIC CLAST COUNTS: AMERICAN CANYON AND POZO GRADE AREAS**

LOCALITIES →	AC-1	AC-2	AC-3	PZ-1	PZ-2	PZ-3	PZ-4
Felsic plutonics*	20	15	22	39	23	13	6
Intermediate/mafic plutonics	6	3		14	17		
Light aphanites					5	5	20
Dark int./mafic aphanites†	3	2	1	10	12		
Light tuffs					1	8	44
Dark tuffs			1				4
Tan/grey porphyries							18
Green porphyries				2	3		5
White/tan quartzites	9	19	16	8	12	29	3
Brown/grey quartzites		3	9	5	8	32	
Green quartzites	3	14	15	5	3		
Pink/purple quartzites	2	5	5				
Meta conglomerates	7	4	2				
Low grade metasediments	8	4	4	14	13	11	
Phyllites	5		5		1	2	
Schists	2	4	6		2		
Gneisses	35	27	14	3			
TOTAL	100	100	100	100	100	100	100

\*includes aplites and granitic porphyries

†includes fine-grained and porphyritic lithologies

**GROUPED CATEGORIES FOR CHART PLOTTING**

Felsic plutonics	20	15	22	39	23	13	6
Int./mafic plutonics	6	3		14	17		
Light siliceous volcanics				2	9	13	83
Dark siliceous volcanics							6
Int./mafic volcanics	3	2	2	10	12		2
Quartzites	14	41	45	18	23	61	3
Gneisses, schists	37	31	25	3	2		
Low grade metasediments	20	8	6	14	14	13	
TOTAL CLASTS	100	100	100	100	100	100	100

**LITHOLOGIC CLAST COUNTS: JUNIPERO SERRA PEAK/SUR COAST AREAS**

LOCALITIES →	JS-1	JS-2	JS-3	JS-4	SCI-1	SCI-2	SCI-3
Felsic plutonics*	22	87	44	22	100	77	17
Intermediate/mafic plutonics	6					6	5
Light aphanites	2		2	7			4
Dark siliceous aphanites			2	1			7
Dark int./mafic aphanites†	3		2	2		5	7
Light tuffs	10			36			20
Dark tuffs			2	3			2
Tan/grey porphyries	2	2	6	11		2	16
Green porphyries			6	5			5
White/tan quartzites	18	4	16	8			2
Brown/grey quartzites	11	2	8	1		2	9
Green quartzites	3		4			2	
Low grade metasediments	7	2	3	4		6	6
Schists	6		2				
Gneisses	6	3					
Intracasts	4		3				
TOTAL CLASTS	100	100	100	100	100	100	100

\*includes aplites and granitic porphyries

†includes fine-grained and porphyritic lithologies

**GROUPED CATEGORIES FOR CHART PLOTTING**

Felsic plutonics	22	87	44	22	100	77	17
Int./mafic plutonics	6					6	5
Light siliceous volcanics	14	2	14	53		2	43
Dark siliceous volcanics			4	10			11
Int./mafic volcanics	3		2	2		5	7
Quartzites	32	6	28	9		4	11
Gneisses, schists	12	3	2				
Low grade metasediments	7	2	3	4		6	6
Misc.	4		3				
TOTAL CLASTS	100	100	100	100	100	100	100

**LITHOLOGIC CLAST COUNTS: GUALALA AREA**

LOCALITIES -->	GF-1	GF-2	GF-3	GF-4	GF-5	GF-6
Felsic plutonics*	11	37	27	24	8	9
Intermediate/mafic plutonics	10	2			29	29
Light aphanites	2	4	2	2		
Dark siliceous aphanites	10		5	10		2
Dark int./mafic aphanites†	15	10		6	31	17
Light tuffs	3	12	21	4		
Dark tuffs	11	4	6	13		2
Tan/grey porphyries		12	12	11		
Green porphyries	8	6	6	11		9
Red/purple porphyries			1	1		
Black/brown porphyries	2			2		5
White quartzites		4	5			
Brown/grey quartzites	3	2	4	5	4	5
Green quartzites	10	3			4	4
Low grade metasandstones	15	4	11	8	20	16
Intraclasts		2		3	4	2
TOTAL CLASTS	100	100	100	100	100	100

\*includes aplites and granitic porphyries

†includes fine-grained and porphyritic lithologies

**GROUPED CATEGORIES FOR CHART PLOTTING**

Felsic plutonics	11	37	27	24	8	9
Int./mafic plutonics	10	2			29	29
Light siliceous volcanics	8	31	38	18		
Dark siliceous volcanics	28	7	15	36		18
Int./mafic volcanics	15	10		6	31	17
Quartzites	13	9	9	5	8	9
Low grade metasediments	15	4	11	8	20	16
Misc.		2		3	4	2
TOTAL CLASTS	100	100	100	100	100	100

**LITHOLOGIC CLAST COUNTS: PIGEON POINT AREA**

LOCALITIES -->	PP-1	PP-2	PP-3	PP-4	PP-5
Felsic plutonics*	13		18	11	12
Intermediate/mafic plutonics	9	15	2	10	4
Light aphanites	6	4		2	3
Dark siliceous aphanites	4	16	10	1	12
Dark int./mafic aphanites†	24	26	18	17	14
Light tuffs	2		4	4	4
Dark tuffs	2	3	10	14	7
Tan/grey porphyries	1	9	11	9	7
Green porphyries	7	4	9	6	17
Red/purple porphyries		3	1	2	2
Black/brown porphyries	3	12	1	3	7
White quartzites			2		
Brown/grey quartzites	3		1	2	
Green quartzites			1		
Low grade metasandstones	23	7	5	9	3
Too weathered to ID	3		5	7	8
Intraclasts		1	2	3	
TOTAL CLASTS	100	100	100	100	100

\*includes aplites and granitic porphyries

†includes fine-grained and porphyritic lithologies

**GROUPED CATEGORIES FOR CHART PLOTTING**

Felsic plutonics	13		18	11	12
Int./mafic plutonics	9	15	2	10	4
Light siliceous volcanics	12	11	19	16	23
Dark siliceous volcanics	13	40	27	25	36
Int./mafic volcanics	24	26	18	17	14
Quartzites	3		4	2	
Low grade metasediments	23	7	5	9	3
Misc.	3	1	7	10	8
TOTAL CLASTS	100	100	100	100	100

## Appendix D

### Vitrinite Reflectance Data

Five surface samples were analyzed in reflected light for evaluation of thermal maturity and organic content by Clark Geological Services, Fremont, California. Description of samples and reflectance histograms that follow are from their report. See Chapter 5 for locations of SML samples from Santa Margarita Lake section. See Appendix A for locations of LNN samples from Lake Nacimiento sections. Sample PP-F is from the Upper Cretaceous Pigeon Point Formation in the Pigeon Point 7.5" Quadrangle, west of California Highway 1, just north of Arroyo de los Frijoles Beach (PP-2 locality in Chapter 4).

Percentage descriptions of kerogen-types follow the convention set forth by the International Handbook of Coal Petrology (1971):

Predominant	60% or more
Abundant	30-60%
Very common	10-30%
Common	05-10%
Rare or trace	05% or less

Maturities are given with respect to the thermal oil generative window where:

IMMATURE	$<0.5 \%R_o$ or $<2.5$ TAI.
MARGINALLY MATURE	$0.5-0.6 \%R_o$ or $2.5-2.6$ TAI.
MATURE	$0.6-1.35 \%R_o$ or $2.6-3.4$ TAI.
OVER MATURE	$>1.35 \%R_o$ or $>3.4$ TAI.

#### D.1 Sample descriptions

CGS8907.159 (field #PP-F). Reflected light analysis: Abundant indige-

nous vitronite. Very common material and resedimented vitrinite. Traces of exinite and inertinite. Pyrite present. MATURITY: 0.49  $R_o\%$  (n=79). Oil generation: IMMATURE. Gas generation: IMMATURE. Resedimented vitrinite population at 1.02  $R_o$ .

CGS8907.160 (field #LNN-51C). Reflected light analysis: Abundant indigenous vitrinite and resedimented vitrinite. Very common amorphous material. Traces of exinite and inertinite. Pyrite present. MATURITY: 0.50  $R_o\%$  (n=75). Oil generation: MARGINALLY MATURE. Gas generation: IMMATURE. Resedimented vitrinite population at 0.93  $R_o$ .

CGS8907.161 (field #LNN-78). Reflected light analysis: Predominantly indigenous vitrinite. Very common resedimented vitrinite. Common amorphous material. Traces of exinite and inertinite. Pyrite present. MATURITY: 0.50  $R_o\%$  (n=83). Oil generation: MARGINALLY MATURE. Gas generation: IMMATURE. Resedimented vitrinite population at 1.01  $R_o$ .

CGS8907.162 (field #SML-23). Reflected light analysis: Abundant indigenous vitrinite and resedimented vitrinite. Common amorphous material and inertinite. Trace of exinite. Macerals fine-grained. Pyrite present. MATURITY: 0.54  $R_o\%$  (n=25). Oil generation: IMMATURE. Gas generation: IMMATURE. Statistical analysis may not be significant due to small number of data points. Resedimented vitrinite population at 0.84  $R_o$ .

CGS8907.163 (field #SML-31). Reflected light analysis: Predominantly resedimented vitrinite. Abundant indigenous vitrinite. Common inertinite. Trace of exinite. Sparse organic matter. Pyrite present. MATURITY: 0.76  $R_o\%$  (n=88). Oil generation: MATURE. Gas

generation: marginally mature. Resedimented vitrinite population at 1.22  $R_o$ .

## D.2 Discussion

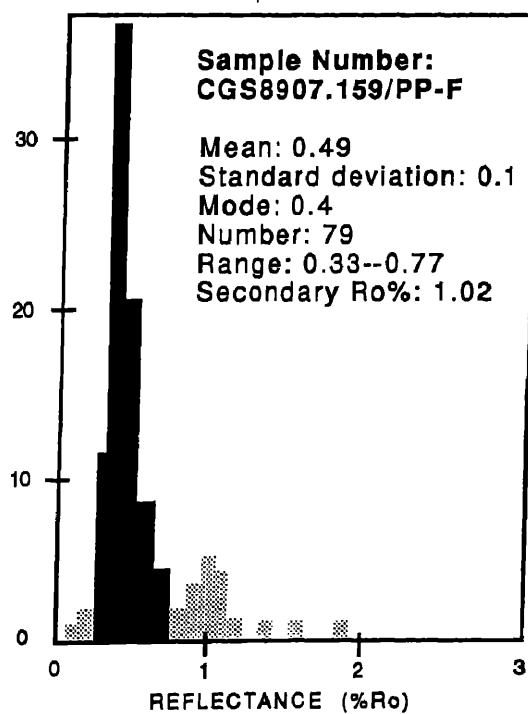
Kerogen in samples PP-F, LNN-51C, LNN-78, and SML-23 is similar in appearance and maturity: it consists mainly of indigenous vitrinite, with slightly lesser amounts of resedimented vitrinite; mean vitrinite reflectances ( $R_o$ ) range from 0.49% to 0.54%. Vitrinite reflectance is considered to be proportional to burial temperature and time, but interpretations are complicated by considerations of heat flow constancy through time and the possibility that some geochemical factors may interfere with the maturation process. A general correlation chart of how reflectances relate to burial temperatures (prepared by G. Demaison, 1980) is included for reference.

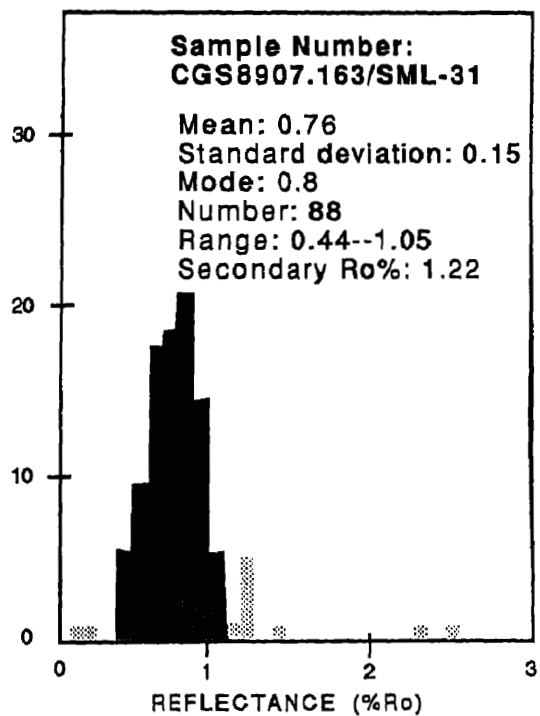
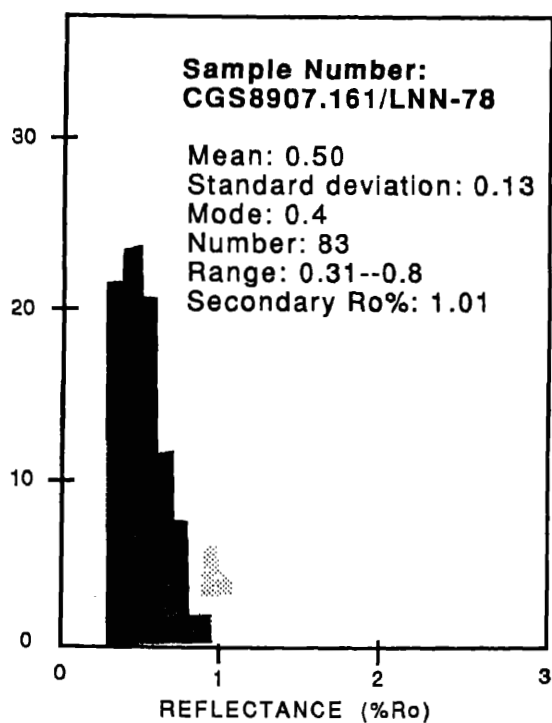
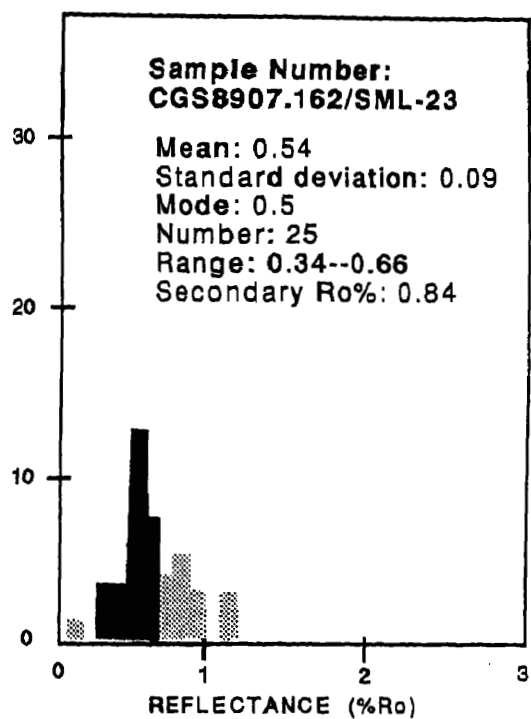
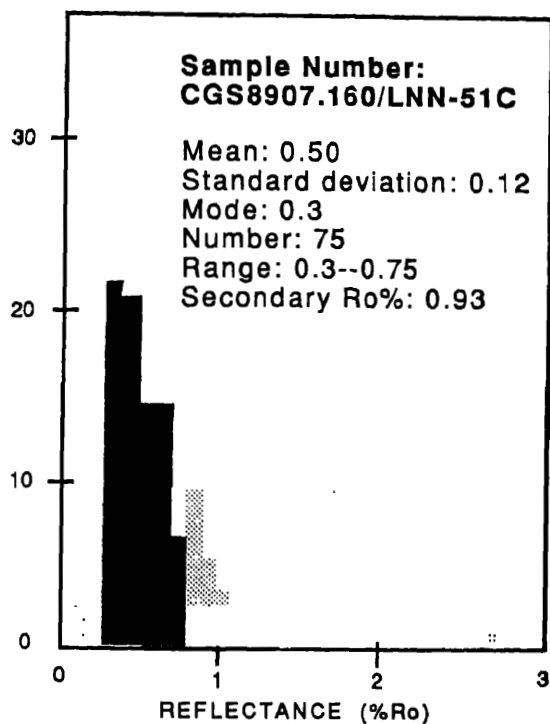
Kerogen in sample SML-31 is different in composition than that of the first four samples. It has a larger percentage of resedimented material and a higher mean  $R_o$  (0.76%). Organic matter is also very sparse in this sample.

Although reflected light analysis for proneness is less accurate than other methods, the analysis suggests that all five samples may be gas prone, based on the predominance of coaly macerals.

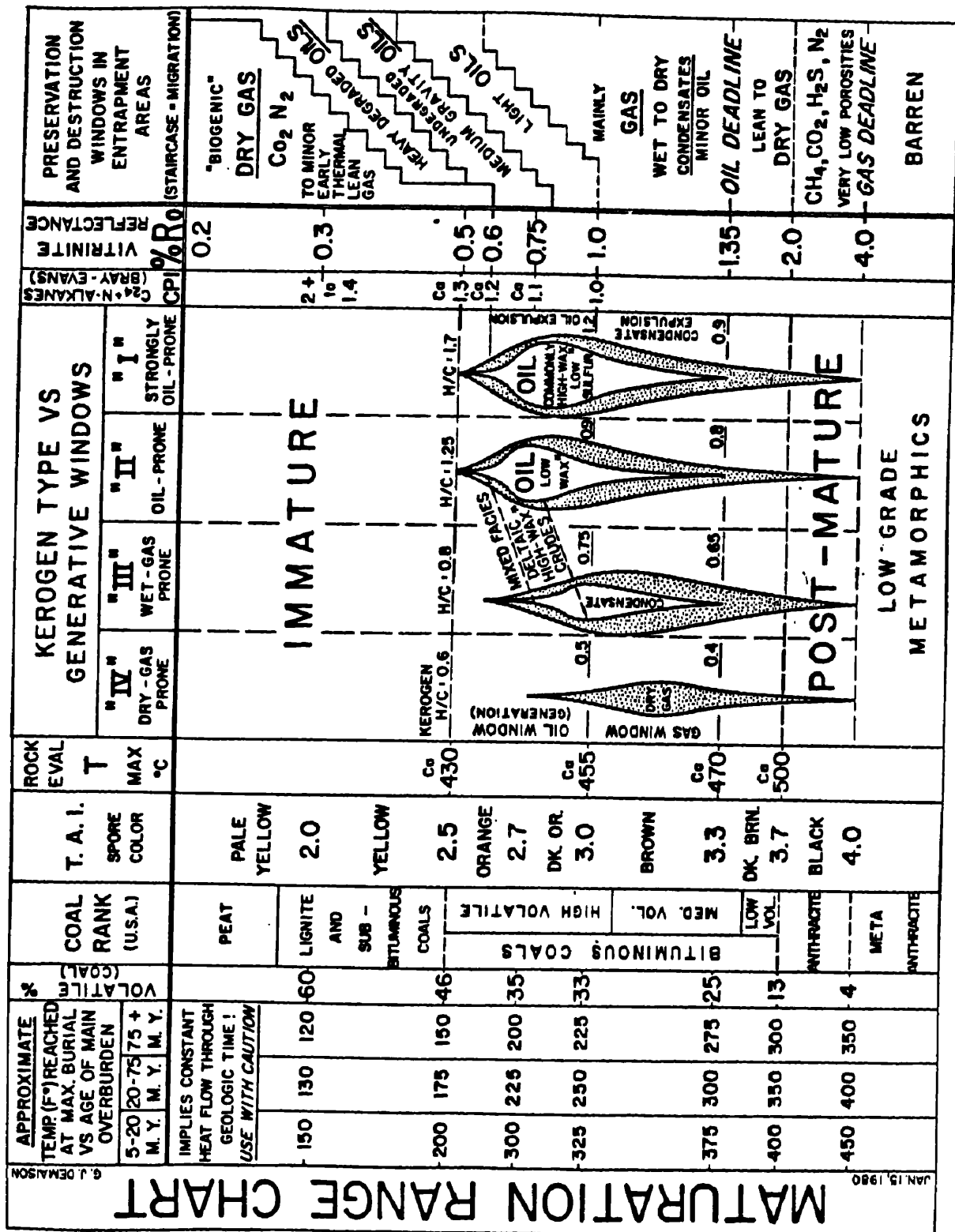
## D.3 Reflectance histograms

Reflection measurements were made on up to one hundred maceral surfaces, using 546 micron incident light on a Zeiss Universal microscope. The histograms present all reflectance data collected from each sample; the reflectance mean is calculated from the population shown in darker shading.









## BIBLIOGRAPHY

- Abbott, P.L., and Peterson, G.L., 1978, Effects of abrasion durability on conglomerate clast populations: examples from Cretaceous and Eocene conglomerates of the San Diego area, California: *Journal of Sedimentary Petrology*, v. 48, p. 31-42.
- Almgren, A.A., and Reay, W.G., 1977, Late Cretaceous and Paleocene(?) foraminifera from the Coast Ranges of central California, in Howell, D.G., Vedder, J.G., and McDougall, K., eds., *Cretaceous Geology of the California Coast Ranges, West of the San Andreas Fault: SEPM Pacific Section, Pacific Coast Paleogeography Field Guide 2*, p. 97-104.
- Atwater, T., 1970, Implications of plate tectonics for the Cenozoic tectonic evolution of western North America: *Geological Society of America Bulletin*, v. 81, p. 3513-3536.
- Bachman, W.R., and Abbott, P.L., 1988, Lower Paleocene conglomerates in the Salinian block, *Paleogene Paleogeography, West Coast of North America: Pacific Coast SEPM*, v. 58, p. 135-150.
- Ballance, P.F., Howell, D.G., and Ort, K., 1983, Late Cenozoic wrench tectonics along the Nacimiento, South Cuyama, and La Panza faults, California, indicated by depositional history of the Simmler Formation, in Anderson, D.W., and Rymer, M.J., eds., *Tectonics and Sedimentation Along Faults of the San Andreas System: SEPM Pacific Section*, p. 1-10.
- Barth, A.P., 1988, Non-exotic model for the Mesozoic San Gabriel terrane, southeasternmost California: *Geological Society of America Abstracts with Programs*, v. 20, p. 275.
- Bateman, P., 1981, Geological and geophysical constraints on models for the origin of the Sierra Nevada batholith, California, in Ernst, W.G., ed., *The*

- Geotectonic Development of California, Rubey Volume I: Englewood Cliffs, N.J., Prentice-Hall, p. 71-86.
- Beck, M.E., 1980, Paleomagnetic record of plate-margin tectonic processes along the western edge of North America: *Journal of Geophysical Research*, v. 85, p. 7115-7131.
- 1986, Model for late Mesozoic-early Tertiary tectonics of coastal California and Western Mexico and speculations on the origin of the San Andreas fault: *Tectonics*, v. 5, p. 49-64.
- Blackmur, R.W., 1978, Late Cretaceous Sedimentation in the La Panza Range, California : M.S. thesis, University of California, Santa Barbara, 85 p.
- Blake, M.C., Howell, D.G., and Jones, D.L., 1982, Map of geologic terranes of California: U.S. Geological Survey Open-file Report 82-593, scale 1:500,000.
- Bottjer, D.J., and Link, M.H., 1984, A synthesis of Late Cretaceous southern California and northern Baja California paleogeography, *in* Crouch, J.K., and Bachman, S.B., eds., *Tectonics and Sedimentation Along the California Margin*: SEPM Pacific Section Volume 38, p. 171-188.
- Bouma, A.H., Normark, W.R., and Barnes, N.E., eds., 1985, *Submarine Fans and Related Turbidite Systems*: New York, Springer-Verlag, 343 p.
- Buck, S.P., and Bottjer, D.J., 1984, Diagenetic carbonate concretions from Late Cretaceous active margin slope deposits, southern California: origin and use in paleoenvironmental reconstruction: *American Association of Petroleum Geologists Bulletin*, v. 68, p. 458.
- 1985, Continental slope deposits from a Late Cretaceous tectonically active margin, southern California: *Journal of Sedimentary Geology*, v. 55, p. 843-855.
- Burchfiel, B.C., and Davis, G.A., 1981, Mohave Desert and environs, *in* Ernst, W.G., ed., *The Geotectonic Development of California, Rubey Volume I*:

- Englewood Cliffs, N.J., Prentice-Hall, Inc., p. 217-252.
- Burke, K., and Sengor, C., 1986, Tectonic escape in the evolution of the continental crust, *in* Barazangi, M., and Brown, L., eds., *Reflection Seismology: The Continental Crust*: American Geophysical Union, Geodynamics Series Volume 14, p. 41-53.
- Busby-Spera, C.J., and Saleeby, J., 1988, An intrabatholithic strike-slip fault: evidence for a Cretaceous movement history of the Kern Canyon fault, southern Sierra Nevada, California: *Geological Society of America Abstracts with Programs*, v. 20, p. 272.
- Butler, P.J., 1984, Upper Cretaceous Turbidites, Southwest Monterey County, California: M.S. thesis, Stanford University, 59 p.
- Carey, S.M., and Colburn, I.P., 1978, Late Cretaceous sedimentation in the Santa Monica Mountains, California, *in* Howell, D.G., and McDougall, K.A., eds., *Mesozoic Paleogeography of the Western United States: Pacific Section SEPM*, p. 547-558.
- Champion, D.E., Gromme, C.S., and Howell, D.G., 1981, Paleomagnetic study of the Upper Cretaceous Pigeon Point Formation, *in* Frizzell, V., ed., *Upper Cretaceous and Paleocene Turbidites, Central California Coast: SEPM Pacific Section, Annual Meeting Field Trip 6*, p. 53-56.
- Champion, D.E., Howell, D.G., and Gromme, C.S., 1984, Paleomagnetic and geologic data indicating 2,500 km of northward displacement for the Salinian and related terranes, California: *Journal of Geophysical Research*, v. 89, p. 7736-7752.
- Champion, D.E., Howell, D.G., and Marshall, M., 1986, Paleomagnetism of Cretaceous and Eocene strata, San Miguel Island, California, borderland and the northward translation of Baja California: *Journal of Geophysical Research*, p. 11557-11570.

- Chipping, D.H., 1970, The petrology and paleogeography of Cretaceous and lower Tertiary strata in the vicinity of Cuyama Valley, California: Ph.D. thesis, Stanford University, 179 p.
- 1972, Early Tertiary paleogeography of central California: American Association of Petroleum Geologists Bulletin, v. 56, p. 480-493.
- Christie-Blick, N., and Biddle, K.T., 1985, Deformation and basin formation along strike-slip faults, *in* Biddle, K.T., and Christie-Blick, N., eds., Strike-slip Deformation, Basin Formation, and Sedimentation: Society of Economic Paleontologists and Mineralogists, Special Publication No. 37, p. 1-34.
- Clark, J.C., Brabb, E.E., Greene, H.G., and Ross, D.C., 1984, Geology of the Point Reyes Peninsula and implications for San Gregorio fault history, *in* Crouch, J.K., and Bachman, S.B., eds., Tectonics and Sedimentation Along the California Margin: SEPM Pacific Section, Volume 38, p. 67-85.
- Clark, S.H., and Nilsen, T.H., 1973, Displacement of Eocene strata and implications for the history of offset along the San Andreas fault, central and northern California, *in* Kovach, R.L., and Nur, A., eds., Proceedings of the Conference on Tectonic Problems of the San Andreas Fault System: Stanford University Publications in the Geological Sciences, v. 13, p. 358-367.
- Clifton, H.E., 1973, Pebble segregation and bed lenticularity in wave-worked versus alluvial gravel: Sedimentology, v. 20, p. 173-187.
- 1981, Progradational sequences in Miocene shoreline deposits, southeastern Caliente Range, California: Journal of Sedimentary Petrology, v. 51, p. 165-184.
- Clifton, H.E., Hunter, R.E., and Phillips, R.L., 1971, Depositional structures and processes in the non-barred high-energy nearshore: Journal of Sedimentary Petrology, v. 41, p. 651-670.
- Clifton, H.E., and Thompson, J.K., 1978, *Macaronichnus segregatis*: a feeding

- structure of shallow marine Polychaetes: *Journal of Sedimentary Petrology*, v. 48, p. 1293-1302.
- Compton, R.R., 1966a, Analysis of Pliocene-Pleistocene deformation and stresses in Northern Santa Lucia Range, California: *Geological Society of America Bulletin*, v. 77, p. 1361-1380.
- 1966b, Granitic and metamorphic rocks of the Salinian block, California Coast Ranges, in Bailey, E., ed., *The Geology of Northern California*: California Division of Mines and Geology Bulletin 190, p. 277-287.
- Compton, R.R., and Dibblee, T.W., 1974, Geologic Map of the Junipero Serra Quadrangle, California: U.S. Geological Survey Open-file Map 74-1021, scale 1:62,000.
- Coney, P.J., 1978, Mesozoic-Cenozoic Cordilleran plate tectonics, Cenozoic tectonics and regional geophysics of western Cordillera: *Geological Society of America Memoir* 152, p. 603-628.
- Crowell, J.C., 1962, Displacement along the San Andreas fault, California: *Geological Society of America Special Paper* 71, p. 61.
- 1974, Sedimentation along the San Andreas fault, California, in Dott, R.H., and Shaver, R.H., eds., *Modern and Ancient Geosynclinal Sedimentation*: Society of Economic Paleontologists and Mineralogists, Special Publication 19, p. 292-303.
- 1982, The tectonics of Ridge Basin, southern California, in Crowell, J.C., and Link, M.H., eds., *Geologic History of Ridge Basin, Southern California*: SEPM Pacific Section, p. 25-42.
- Dalmayrac, B., and Molnar, P., 1981, Parallel thrust and normal faulting in Peru and constraints on the state of stress: *Earth and Planetary Science Letters*, v. 55, p. 473-481.
- Dewey, J.F., 1988, Extensional collapse of orogens: *Tectonics*, v. 7, p. 1123-1139.

- Dibblee, T.W., 1971, Geologic map of the Adelaida, Bradley, and Bryson Quadrangles, California: U.S. Geological Survey Open File Map 71-87.
- 1972, Geological map of the La Panza and Pozo Quadrangles, California: U.S. Geological Survey Open File Map 72-89, scale 1:62,500.
- 1976, The Rinconada Fault and Related Faults in the Southern Coast Ranges, California, and Their Tectonic Significance: U.S. Geological Survey, Professional Paper 981, 55 p.
- Dickinson, W.R., 1982, Compositions of sandstones in circum-Pacific subduction complexes and fore-arc basins: American Association of Petroleum Geologists Bulletin, v. 66, p. 121-137.
- 1983, Cretaceous sinistral strike slip along Nacimiento fault in coastal California: Bulletin of the American Association of Petroleum Geologists, v. 67, p. 624-645.
- Dickinson, W.R., Cowan, D.S., and Schweichert, R.A., 1972, Test of new global tectonics: discussion: Bulletin of the American Association of Petroleum Geologists, v. 56, p. 375-384.
- Dickinson, W.R., and Seely, D.R., 1979, Structure and stratigraphy of forearc regions: American Association of Petroleum Geologists Bulletin, v. 63, p. 2-31.
- Dickinson, W.R., and Snyder, W.S., 1978, Plate tectonics of the Laramide orogeny: Geological Society of America Memoir 151, p. 355-366.
- Dillon, J.T., 1986, Timing of thrusting and metamorphism along the Vincent-Chocolate Mountain thrust system, southern California: Geological Society of America Abstracts with Programs, v. 18, p. 101.
- Doe, B.R., and Delevaux, M.H., 1973, Variations in lead-isotopic compositions in Mesozoic granitic rocks of California: a preliminary investigation: Geological Society of American Bulletin, v. 84, p. 3513-3526.

- Durham, D.L., 1965, Geology of the Jolon and Williams Hill Quadrangles, Monterey County, California: U.S. Geological Survey Bulletin 1181-Q, 27 p.
- 1968, Geology of the Tierra Redonda Mountain and Bradley Quadrangles, Monterey and San Luis Obispo Counties, California: U.S. Geological Survey, Bulletin 1255, 60 p.
- 1974, Geology of the Southern Salinas Valley Area, California: U.S. Geological Survey Professional Paper 819, 111 p.
- Ehlig, P.L., 1981, Origin and tectonic history of the basement terrane of the San Gabriel Mountains, central Transverse Ranges, *in* Ernst, W.G., ed., The Geotectonic Development of California, Rubey Volume I: Englewood Cliffs, N.J., Prentice-Hall, p. 253-283.
- Ehlig, P.L., and Joseph, S.E., 1977, Polka dot granite and correlation of La Panza quartz monzonite with Cretaceous batholithic rocks north of Salton Trough, *in* Howell, D.G., Vedder, J.G., and McDougall, K., eds., Cretaceous Geology of the California Coast Ranges, West of the San Andreas Fault: SEPM Pacific Section, Pacific Coast Paleogeography Field Guide 2, p. 91-96.
- Engelbreton, D.C., Cox, A., and Gordon, R.G., 1985, Relative Motions Between Oceanic and Continental Plates in the Pacific Basin: Geological Society of America Special Paper 206, p. 59.
- Ethridge, F.G., and Wescott, W.A., 1984, Tectonic setting, recognition and hydrocarbon reservoir potential of fan-delta deposits, *in* Koster, E.H., and Steel, R.J., eds., Sedimentology of Gravels and Conglomerates: Canadian Society of Petroleum Geologists, Memoir 10, p. 217-236.
- Everndon, J.F., and Kistler, R.W., 1970, Chronology of emplacement of Mesozoic batholithic complexes in California and western Nevada: U.S. Geological Survey Professional Paper 623, 42 p.



- Fairbanks, H.W., 1904, Description of the San Luis Quadrangle: U.S. Geological Survey, Geological Atlas of the United States, San Luis Folio no. 101, 14 p.
- Fones, M., McWilliams, M., Li, Y., and Clauer, N., in prep.,
- Fry, J.G., Bottjer, D.J., and Lund, S.P., 1985, Magnetostratigraphy of displaced Upper Cretaceous strata in southern California: *Geology*, v. 13, p. 648-651.
- Galloway, W.E., 1976, Sediments and stratigraphic framework of the Copper River fan-delta, Alaska: *Journal of Sedimentary Petrology*, v. 46, p. 726-737.
- Gilbert, W.G., and Dickinson, W.R., 1970, Stratigraphic variations in sandstone petrology, Great Valley Sequence, central California coast: *Geological Society of America*, v. 81, p. 949-954.
- Gloppen, T.G., and Steel, R.J., 1981, The deposits, internal structure and geometry in six alluvial fan--fan delta bodies (Devonian-Norway)--a study in the significance of bedding sequence in conglomerates: *SEPM Special Publication No. 31*.
- Goudkoff, P.P., 1945, Stratigraphic relations of Upper Cretaceous in Great Valley, California: *American Association of Petroleum Geologists Bulletin*, v. 29, p. 956-1007.
- Graham, S.A., 1976, Tertiary Sedimentary Tectonics of the Central Salinian Block of California: Ph.D thesis, Stanford University, 510 p.
- 1978, Role of the Salinian block in the evolution of the San Andreas fault system: *American Association of Petroleum Geologists Bulletin*, v. 62, p. 2214-2231.
- 1979, Tertiary stratigraphy and depositional environments near Indians Ranch, Monterey County, California, in Graham, S.A., ed., *Tertiary and Quarternary Geology of the Salinas Valley and Santa Lucia Range, Monterey County, California*: *SEPM Pacific Section, Pacific Coast*

- Paleogeography Field Guide 4, p. 3-12.
- Graham, S.A., and Dickinson, W.R., 1978, Evidence for 115 kilometers of right slip on the San Gregorio-Hosgri fault trend: *Science*, v. 199, p. 179-181.
- Graham, S.A., Stanley, R.G., Bent, J.V., and Carter, J.B., 1989 , Oligocene and Miocene paleogeography of central California and displacement along the San Andreas fault: *Geological Society of America Bulletin* , v. 101, p. 711-730.
- Grove, K., 1986, Depositional environments of Upper Cretaceous and Lower Tertiary strata near Nacimiento Lake, central California Coast Ranges, *in* Grove, K., and Graham, S., eds., *Geology of Upper Cretaceous and Lower Tertiary Rocks Near Lake Nacimiento, California: SEPM Pacific Section, Book 49*, p. 1-16.
- 1987, Paleomagnetic analysis of Upper Cretaceous rocks from the Salinian terrane, central California: *EOS (American Geophysical Union Transactions)*, v. 68, p. 1253.
- 1989, Upper Cretaceous conglomerates from the Salinian terrane, west-central California, *in* Abbott, P.L., and Colburn, I.P., eds., *Conglomerates and Basin Analysis: SEPM Pacific Section*, p. 143-160.
- Hagstrum, J.T., McWilliams, M.O., Howell, D.G., and Gromme, S., 1985, Mesozoic paleomagnetism and northward translation of the Baja California Peninsula: *Geological Society of America Bulletin*, v. 96, p. 1077-1090.
- Hall, C.A., 1988, Sur megathrust, sole of Southern California Allochthon: *EOS (American Geophysical Union Transactions)*, v. 69, p. 1453.
- Hall, C.A., Ernst, W.G., Prior, S.W., and Wiese, J.W., 1979, Geologic map of the San Luis Obispo-San Simeon region, California: U.S. Geological Survey, Miscellaneous Investigations Series, Map I-1097, scale 1:48,000.
- Hall, C.A., Jones, D.L., and Brooks, S.A., 1959, Pigeon Point Formation of Late

- Cretaceous age, San Mateo County, California: American Association of Petroleum Geologists Bulletin, v. 43, p. 2855-2865.
- Halls, H.C., 1976, A least-squares method to find a remanance direction from converging remagnetization circles: Geophysical Journal of Research of Astronomical Society, v. 45, p. 297-304.
- Hamilton, W., 1979, Tectonics of the Indonesian Region: U.S. Geological Survey Professional Paper 1078, 345 p.
- 1988, Tectonic setting and variations with depth of some Cretaceous and Cenozoic structural and magmatic systems of the western United States, in Ernst, W.G., ed., Metamorphism and Crustal Evolution of the the Western United States, Rubey Volume VII: Englewood Cliffs, N.J., Prentice Hall, p. 1-40.
- Harland, W.B., Cox, A.V., Llewellyn, P.G., Pickton, C.A.G., Smith, A.G., and Walters, R., 1982, A Geological Time Scale: Cambridge University Press, 131 p.
- Hart, E.W., 1976, Basic Geology of the Santa Margarita area, San Luis Obispo county, California: California Division of Mines and Geology Bulletin 199, 45 p.
- Haxel, G., and Dillon, J., 1978, The Pelona-Orocopia schist and Vincent-Chocolate Mountain thrust system, southern California, in Howell, D.G., and McDougall, K.A., eds., Mesozoic Paleogeography of the Western United States : SEPM Pacific Section, Pacific Coast Paleogeography Symposium 2, p. 453-470.
- Haxel, G.B., Tosdal, R.M., and Dillon, J.T., 1975, Tectonic setting and lithology of the Winterhaven Formation: a new Mesozoic stratigraphic unit in souteasternmost California and southwestern Arizona: U.S. Geological Survey Bulletin 1599, p. 19.

- Hill, M.L., and Dibblee, T.W., 1953, San Andreas, Garlock, and Big Pine faults, California: Geological Society of America Bulletin, v. 64, p. 443-458.
- Hill, M.L., and Hobson, H.D., 1968, Possible post-Cretaceous slip of the San Andreas fault zone, *in* Dickinson, W.R., and Grantz, A., eds., Proceedings of Conference on Geological Problems of San Andreas Fault System: Stanford University Publications in the Geological Sciences, v. 11, p. 123-129.
- Hornafius, J.S., 1984, Origin of remanent magnetization in dolomite from the Monterey Formation, *in* Garrison, R.E., Kastner, M., and Zenger, D.H., eds., Dolomites of the Monterey Formation and Other Organic-Rich Units: SEPM Pacific Section, v.41, p. 195-212.
- 1985, Neogene tectonic rotation of the Santa Ynez Range, western Transverse Ranges, California, suggested by paleomagnetic investigation of the Monterey Formation: Journal of Geophysical Research, v. 90, p. 12503-12522.
- Howard, J.D., and Reineck, H.E., 1981, Depositional facies of high-energy beach-to-offshore sequence: comparison with low-energy sequence: American Association of Petroleum Geologists Bulletin, v. 65, p. 807-830.
- Howell, D.G., Champion, D.E., and Vedder, J.G., 1987, Terrane accretion, crustal kinematics, and basin evolution, southern California, *in* Ingersoll, R.V., and Ernst, W.G., eds., Cenozoic Basin Development of Coastal California, Rubey Volume VI: Englewood Cliffs, N.J., Prentice-Hall, p. 242-258.
- Howell, D.G., Crouch, J.K., Greene, H.G., McCulloch, D.S., and Vedder, J.G., 1980, Basin development along the late Mesozoic and Cainozoic California margin: a plate tectonic margin of subduction, oblique subduction and transform, *in* Ballance, P.F., and Reading, H.G., eds., Sedimentation in Oblique-slip Mobile Zones: International Association of Sedimentologists, Special Publication Number 4, p. 43-62.

- Howell, D.G., and Vedder, J.G., 1978, Late Cretaceous paleogeography of the Salinian block, California, *in* Howell, D.G., and McDougall, K.A., eds., Mesozoic Paleogeography of the Western United States, Paleogeography Symposium 2: SEPM Pacific Section, p. 523-534.
- 1981, Structural implications of stratigraphic discontinuities across the southern California borderland, *in* Ernst, W.G., ed., The Geotectonic Development of California, Rubey Volume I: Englewood Cliffs, Prentice-Hall, Inc., p. 535-558.
- Howell, D.G., Vedder, J.G., McLean, H., Joyce, J.M., and Clarke, S.H., 1977, Review of Cretaceous geology, Salinian and Nacimiento blocks, Coast Ranges of central California, *in* Howell, D.G., Vedder, J.G., and McDougall, K., eds., Cretaceous Geology of the California Coast Ranges, West of the San Andreas Fault, Pacific Coast Paleogeography Field Guide 2: SEPM Pacific Section, p. 1-46.
- Huchon, P., and Le Pichon, X., 1984, Sunda Strait and Central Sumatra fault: *Geology*, v. 12, p. 668-672.
- Ingersoll, R.V., 1988, Development of the Cretaceous forearc basin of central California, *in* Graham, S.A., and Olson, H.C., eds., Studies of the Geology of the San Joaquin Basin: SEPM Pacific Section, p. 141-156.
- Jacobson, C.E., 1983, Complex refolding history of the Pelona, Orocopia, and Rand schists, southern California: *Geology*, v. 11, p. 583-586.
- Jacobson, C.E., Dawson, M.R., and Postlethwaite, C.E., 1988, Structure, metamorphism, and tectonic significance of the Pelona, Orocopia, and Rand schists, southern California, *in* Ernst, W.G., ed., Metamorphism and Crustal Evolution of the Western United States: Englewood Cliffs, N.J., Prentice-Hall, p. 976-997.
- James, E.W., 1986, Pre-Tertiary paleogeography along the northern San Andreas

- fault: EOS (American Geophysical Union Transactions), v. 67, p. 1215.
- James, E.W., Kimbrough, D., and Mattinson, J.M., 1986, Evaluation of pre-Tertiary piercing points along the northern San Andreas fault using U/Pb zircon dating, initial Sr and common Pb isotopic ratios: Geological Society of America Abstracts with Programs, v. 18, p. 121.
- James, E.W., and Mattinson, J.M., 1988, Metamorphic history of the Salinian block: an isotopic reconnaissance, *in* Ernst, W.G., ed., Metamorphic and Crustal Evolution of the Western United States, Rubey Volume VII: Englewood Cliffs, N.J., Prentice Hall, Inc., p. 938-952.
- Johnson, J.D., and Normark, W.R., 1974, Neogene tectonic evolution of the Salinian block, central California: *Geology*, v. 2, p. 11-14.
- Jordon, T.E., Isacks, B.L., Allmendinger, R.W., Brewer, J.A., Ramos, V.A., and Ando, C.J., 1983, Andean tectonics related to geometry of subducted Nazca plate: *Geological Society of America Bulletin*, v. 94, p. 341-361.
- Junger, A., 1976, Tectonics of the southern California borderland, *in* Howell, D.G., ed., Aspects of the Geologic History of the California Continental Borderland: American Association of Petroleum Geologists, Pacific Section, Miscellaneous Publication 24, p. 486-498.
- Kanter, L.R., 1983, Paleomagnetic constraints on the motion history of Salinia : Ph.D thesis, Stanford University, 156 p.
- Kanter, L.R., and Debiche, M., 1985, Modeling the motion histories of the Point Arena and central Salinian terranes, *in* Howell, D.G., ed., Tectonostratigraphic Terranes of the Circum-Pacific Region: Circum-Pacific Council for Energy and Mineral Resources, Earth Sciences Series, Number 1, p. 227-238.
- Kanter, L.R., and McWilliams, M.O., 1982, Rotation of the southernmost Sierra Nevada, California: *Journal of Geophysical Research*, v. 87, p. 3819-3830.

- Karig, D.E., Cardwell, R.K., Moore, G.F., and Moore, D.G., 1978, Late Cenozoic subduction and continental margin truncation along the northern Middle America Trench: *Geological Society of America Bulletin*, v. 89, p. 265-276.
- Khan, S.M., and Coe, R.S., 1987, Preliminary paleomagnetic results from the Miocene Monterey Formation, Horse Canyon, Salinas Basin, California: *EOS (American Geophysical Union Transactions)*, v. 68, p. 1254.
- Kies, R.P., and Abbott, P.L., 1983, Rhyolite clast populations and tectonics of the California continental borderland: *Journal of Sedimentary Petrology*, v. 53, p. 461-475.
- Kimura, G., 1986, Oblique subduction and collision: forearc tectonics of the Kuril arc: *Geology*, v. 14, p. 404-407.
- Kirschvink, J.L., 1980, The least-squares line and plane and the analysis of paleomagnetic data: *Geophysical Journal of Research of Astronomical Society*, v. 62, p. 699-718.
- Kistler, R.W., and Peterman, Z.E., 1978, Reconstruction of Crustal Blocks of California on the Basis of Initial Strontium Isotopic Compositions of Mesozoic Granitic Rocks: *U.S. Geological Survey Professional Paper 1071*, 17 p.
- Kistler, R.W., Peterman, Z.E., Ross, D.C., and Gottfried, D., 1973, Strontium isotopes and the San Andreas fault, *in* Kovach, R.L., and Nur, A., eds., *Proceedings of the Conference on Tectonic Problems of the San Andreas Fault System: Stanford University Publications in the Geological Sciences*, p. 339-347.
- Kleinspehn, K.L., Steel, R.J., and Netland, A., 1984, Conglomeratic fan-delta sequences, Late Carboniferous-Early Permian, Western Spitsbergen, *in* Koster, E.H., and Steel, R.J., eds., *Sedimentology of Gravels and Conglomerates: Canadian Society of Petroleum Geologists, Memoir 10*, p. 279-294.

- Kooser, M.A., 1980, Stratigraphy and Sedimentology of the San Francisquito Formation, Transverse Ranges, California: Ph.D thesis, University of California, Riverside, 201 p.
- Kumar, N., and Sanders, J.E., 1976, Characteristics of shoreface storm deposits: modern and ancient examples: *Journal of Sedimentary Petrology*, v. 46, p. 145-162.
- Lajoie, K.R., and Sarna-Wolfcicki, A.M., 1982, Quaternary chronology and rates of crustal deformation in the Ventura area, California, Neotectonics in Southern California: Geological Society of America, Cordilleran Section, 78th Annual Meeting, p. 43-51.
- Lee-Wong, F., and Howell, D.G., 1977, Petrography of Upper Cretaceous sandstones in the Coast Ranges of central California, *in* Howell, D.G., Vedder, J.G., and McDougall, K., eds., *Cretaceous Geology of the California Coast Ranges, West of the San Andreas Fault*: SEPM Pacific Section, p. 47-56.
- Lipman, P.W., Prostka, H.J., and Christiansen, R.L., 1972, Cenozoic volcanism and plate-tectonic evolution of the western United States: I. Early and middle Cenozoic: *Philosophical Transactions of the Royal Society of London*, v. 271, p. 217-278.
- Lowe, D.R., 1979, Stratigraphy and sedimentation of the Pigeon Point Formation, San Mateo County, California, *in* Nilsen, T.H., and Brabb, E.E., eds., *Geology of the Santa Cruz Mountains, California*: Geological Society of America Cordilleran Section field trip guidebook, p. 17-29.
- 1982, Sediment gravity flows: II. Depositional models with special reference to the deposits of high-density turbidity currents: *Journal of Sedimentary Petrology*, v. 52, p. 279-297.
- Luyendyk, B.P., Kamerling, M.J., and Terres, R., 1980, Geometric model for Neogene crustal rotations in southern California: Geological Society of



- America Bulletin, v. 91, p. 211-217.
- Mahaffie, M.J., and Dokka, R.K., 1986, Thermochronology evidence for the age and cooling history of the upper plate of the Vincent thrust, California: Geological Society of America Abstracts with Programs, v. 18, p. 153.
- Manspeizer, W., 1985, The Dead Sea Rift: impact of climate and tectonism on Pleistocene and Holocene sedimentation, *in* Biddle, K.T., and Christie-Blick, N., eds., Strike-slip Deformation, Basin Formation, and Sedimentation: Society of Economic Paleontologists and Mineralogists, Special Publication No. 37, p. 143-158.
- Mattinson, J.M., 1978, Age, origin, and thermal histories of some plutonic rocks from the Salinian block of California: Contributions to Mineralogy and Petrology, v. 67, p. 233-245.
- 1983, Basement rocks of the southeasternmost Salinian Block, California: Geological Society of America Abstracts with Programs, v. 15, p. 414.
- 1986, Nature of granitic crust of the Salinian block, California: isotopic evidence for the recycling of old continental crust: Geological Society of America Abstracts with Programs, v. 18, p. 154.
- Mattinson, J.M., Davis, T.E., and Hopson, C.A., 1971, U-Pb studies in the Salinian block of California: Carnegie Institute and Geophysical Laboratory, Annual Report 1970-71, p. 233-245.
- Mattinson, J.M., and James, E.W., 1985, Salinian block U/Pb age and isotopic variations: implications for origin and emplacement of the Salinian terrane, *in* Howell, D.G., ed., Terranes of the Circum-Pacific Region: Circum-Pacific Council for Energy and Mineral Resources, Earth Science Series, n. 1, p. 215-226.
- May, D.J., 1986, Amalgamation of Metamorphic Terranes in the Southeastern San Gabriel Mountains, California: Ph.D. thesis, University of California,

Santa Barbara, 325 p.

- McClure, D.V., 1969, Late Cretaceous Sedimentation, Southern Santa Lucia Range, California: M.S. thesis, University of California, Santa Barbara, 91 p.
- McGuire, D.J., 1988, Depositional framework of the Upper Cretaceous--lower Tertiary Moreno Formation, central San Joaquin basin, California, *in* Graham, S.A., and Olson, H.C., eds., Studies of the Geology of the San Joaquin Basin: SEPM Pacific Section, p. 173-188.
- McKenzie, D., 1978, Some remarks on the development of sedimentary basins: *Earth and Planetary Sciences*, v. 40, p. 25-32.
- McPherson, J.G., Shanmugam, G., and Moiola, R.J., 1987, Fan-deltas and braid deltas: varieties of coarse-grained deltas: *Geological Society of America Bulletin*, v. 99, p. 331-340.
- McWilliams, M.O., and Howell, D.G., 1982, Exotic terranes of western California: *Nature*, v. 297, p. 215-217.
- McWilliams, M.O., and Li, Y., 1985, Oroclinal bending of the southern Sierra Nevada batholith: *Science*, v. 230, p. 172-175.
- Mercier, J.L., Armijo, R., Tapponnier, P., Carey-Gaithardis, E.C., and Han, T.L., 1987, Change from late Tertiary compression to Quaternary extension in southern Tibet during the India-Asia collision: *Tectonics*, v. 6, p. 275-304.
- Miller, E.L., and Carr, M.D., 1978, Recognition of possible Aztec-equivalent sandstones and associated Mesozoic metasedimentary deposits within the Mesozoic magmatic arc in the southwestern Mojave Desert, California, *in* Howell, D.G., and McDougall, K.A., eds., Mesozoic Paleogeography of the Western United States, Pacific Coast Paleogeography Symposium 2: SEPM Pacific Section, p. 283-290.
- Mitchell, A.H.G., and Reading, H.G., 1986, Sedimentation and tectonics, *in*

- Reading, H.G., ed., *Sedimentary Environments and Facies*: Blackwell Scientific Publications, p. 471-519.
- Moxon, I.W., and Graham, S.A., 1987, History and controls of subsidence in the Late Cretaceous-Tertiary Great Valley forearc basin, California: *Geology*, v. 7, p. 626-629.
- Mutti, E., and Ricci Lucchi, F., 1975, Turbidites of the northern Apennines: introduction to facies analysis: *International Geology Review*, v. 20, p. 127-166.
- Naeser, C.W., and Ross, D.C., 1976, Fission-track ages of sphene and apatite of granitic rocks of the Salinian block, Coast Ranges, California: *U.S. Geological Survey Journal of Research*, v. 4, p. 425-420.
- Nemec, W., and Steel, R.J., 1984, Alluvial and coastal conglomerates: their significant features and some comments on gravelly mass-flow deposits, *in* Koster, E.H., and Steel, R.J., eds., *Sedimentology of Gravels and Conglomerates*: Canadian Society of Petroleum Geologists, Memoir 10, p. 1-32.
- Nilsen, T.H., 1978, Late Cretaceous geology of California and the problem of the proto-San Andreas fault, *in* Howell, D.G., and McDougall, K.A., eds., *Mesozoic Paleogeography of the Western United States*, Pacific Coast Paleogeography Symposium 2: SEPM Pacific Section, p. 559-573.
- Nilsen, T.H., and Abbott, P.L., 1984, Turbidite sedimentology of the Upper Cretaceous Point Loma and Cabrillo Formations, San Diego, California, *in* Abbott, P.L., ed., *Upper Cretaceous Depositional Systems, Southern California--Northern Baja California*: SEPM Pacific Section, p. 3-30.
- Nilsen, T.H., and Clarke, S.H., 1975, Sedimentation and tectonics in the early Tertiary continental borderland of central California: *U.S. Geological Survey Professional Paper* 925, p. 64.

- Page, B.M., 1966, Geology of the Coast Ranges of California, *in* Bailey, E., ed., The Geology of Northern California: California Division of Mines and Geology, Bulletin 190, p. 255-276.
- 1981, The southern Coast Ranges, *in* Ernst, W.G., ed., The Geotectonic Development of California, Rubey Volume I: Englewood Cliffs, Prentice Hall, Inc., p. 329-417.
- 1982, Migration of Salinian composite block, California, and disappearance of fragments: American Journal of Science, v. 282, p. 1694-1734.
- Page, B.M., and Engebretson, D.C., 1984, Correlation between the geologic record and computed plate motions for central California: Tectonics, v. 3, p. 133-155.
- Plescia, J.B., and Calderone, G.J., 1986, Paleomagnetic constraints on the timing and extent of rotation of the Tahachapi Mountains, California: Geological Society of America, Abstracts with Programs, v. 18, p. 171.
- Postma, G., 1984, Mass-flow conglomerates in a submarine canyon: Abrioja fan-delta, Pliocene, southeast Spain, *in* Koster, E.H., and Steel, R.J., eds., Sedimentology of Gravels and Conglomerates: Canadian Society of Petroleum Geologists, Memoir 10, p. 237-258.
- Reading, H.G., 1980, Characteristics and recognition of strike-slip fault systems, *in* Ballance, P.F., and Reading, H.G., eds., Sedimentation in Oblique-skip Mobile Zones: International Association of Sedimentologists Special Publication 4, p. 7-26.
- Reiche, P., 1937, Geology of the Lucia Quadrangle, California: University of California, Department of Geological Sciences Bulletin, v. 7, p. 115-168.
- Reid, S.A., 1988, Late Cretaceous and Paleogene sedimentation along the east side of the San Joaquin basin, *in* Graham, S.A., and Olson, H.C., eds., Studies of the Geology of the San Joaquin Basin: SEPM Pacific Section.

- Ross, D.C., 1970, Quartz gabbro and anorthositic gabbro: markers of offset along the San Andreas fault in the Californian Coast Ranges: Geological Society of America Bulletin, v. 81, p. 3647-3662.
- 1972, Petrographic and Chemical Reconnaissance Study of Some Granitic and Gneissic Rocks near the San Andreas Fault From Bodega Head to Cajon Pass, California: U.S. Geological Survey Professional Paper 698, 92 p.
- 1976, Metagraywacke in the Salinian block, central Coast Ranges, California--and a possible correlative across the San Andreas fault: U.S. Geological Survey Journal of Research, v. 4, no. 6, p. 683-696.
- 1977, Pre-intrusive metasedimentary rocks of the Salinian block, California - a paleotectonic dilemma, in Stewart, J.H., Stevens, C.H., and Fritsche, A.E., eds., Paleozoic Paleogeography of the Western United States, Pacific Section Paleogeography Symposium I: SEPM Pacific Section, p. 371-380.
- 1978, The Salinian block - a Mesozoic granite orphan in the California Coast Ranges, in Howell, D.G., and McDougall, K.A., eds., Mesozoic Paleogeography of the Western United States, Pacific Section Paleogeography Symposium 2: SEPM Pacific Section, p. 509-522.
- 1984, Possible correlations of basement rocks across the San Andreas, San Gregorio-Hosgri, and Rinconada-Reliz-King City faults, California: U.S. Geological Survey Professional Paper 1317, p. 97.
- Ross, D.C., Wentworth, C.M., and McKee, E.H., 1973, Cretaceous mafic conglomerate near Gualala offset 350 miles by San Andreas fault from oceanic crustal source near Eagle Rest Peak, California: U.S. Geological Survey, Journal of Research, v. 1, p. 45-62.
- Ruetz, J.W., 1976, Paleocene Sedimentation in the Northern Santa Lucia Range : M.S. thesis, Stanford University, 104 p.
- Ruiz, J., Patchett, P.J., and Ortega-Gutierrez, F., 1988, Proterozoic and

- Phanerozoic basement terranes of Mexico from Nd isotopic studies: Geological Society of America Bulletin, v. 100, p. 274-281.
- Saleeby, J.B., and Busby-Spera, C., 1986, Fieldtrip guide to the metamorphic framework rocks of the Lake Isabella area, southern Sierra Nevada, California, Mesozoic and Cenozoic Structural Evolution of Selected Areas, East-central California: Geological Society of America Cordilleran Section Annual Meeting Guidebook, p. 81-94.
- Sams, D.B., and Saleeby, J.B., 1988, Geology and petrotectonic significance of crystalline rocks of the southernmost Sierra Nevada, California, in Ernst, W.G., ed., Metamorphism and Crustal Evolution of the Western United States, Rubey Volume VII: Englewood Cliffs, N.J., Prentice Hall, Inc., p. 863-893.
- Saul, L.R., 1983, Turritella zonation across the Cretaceous-Tertiary boundary, California: University of California Publications in the Geological Sciences, v. 125, p. 164.
- 1986, Mollusks of Latest Cretaceous and Paleocene age, Lake Nacimiento, California, in Grove, K., and Graham, S., eds., Geology of Upper Cretaceous and Lower Tertiary Rocks Near Lake Nacimiento, California: SEPM Pacific Section, Book 49, p. 25-31.
- Seiders, V.M., 1982, Geologic Map of an Area Near York Mountain, San Luis Obispo County, California: U.S. Geological Survey Miscellaneous Investigations Series, Map I-1369.
- 1986, Structural geology of Upper Cretaceous and lower Tertiary rocks near the Nacimiento fault, northwest of Lake Nacimiento, California, in Grove, K., and Graham, S.A., eds., Geology of Upper Cretaceous and Lower Tertiary Rocks Near Lake Nacimiento, California: SEPM Pacific Section, Book 49, p. 33-42.

- 1989, Geological Map of the Burnett Peak Quadrangle, Monterey and San Luis Obispo Counties, California: U.S. Geological Survey, Geologic Quadrangle Map, Map GQ-1658.
- Seiders, V.M., and Blome, C.D., 1988, Implications of upper Mesozoic conglomerate for suspect terrane in western California and adjacent areas: Geological Society of America Bulletin, v. 100, p. 374-391.
- Sharry, J., 1981, The Geology of the Western Tehachapi Mountains, California: Ph.D thesis, Massachusetts Institute of Technology, 215 p.
- Silver, E.A., Curray, J.R., and Cooper, A.K., 1971, Tectonic development of the continental margin off central California, in Lipps, J.H., and Moores, E.M., eds., Geologic Guide to the Northern Coast Ranges, Point Reyes Region, California: Geological Society of Sacramento Annual Field Trip Guidebook, p. 1-10.
- Silver, L.T., 1982, Evidence and a model for west-directed early to mid-Cenozoic basement overthrusting in southern California: Geological Society of America Abstracts with Programs, v. 14, p. 617.
- 1983, Paleogene overthrusting in the tectonic evolution of the Transverse Ranges, Mojave and Salinian regions, California: Geological Society of America Abstracts with Programs, v. 15, p. 438.
- Silver, L.T., and Chappell, B.W., 1988, The Peninsular Ranges Batholith: an insight into the evolution of the Cordilleran batholiths of southwestern North America: Transactions of the Royal Society of Edinburgh: Earth Sciences, v. 79, p. 105-11.
- Silver, L.T., and Mattinson, J.M., 1986, "Orphan Salinia" has a home: EOS (American Geophysical Union Transactions), v. 67, p. 1215.
- Sliter, M.V., 1986, Maastrichtian foraminifers from near Lake Nacimiento California---their interpretation and regional correlation, in Grove, K., and

- Graham, S., eds., Geology of Upper Cretaceous and Lower Tertiary Rocks Near Lake Nacimiento, California: SEPM Pacific Section, Book 49, p. 17-24.
- Smith, D.P., 1977, San Juan-St. Francis fault--hypothesized major middle Tertiary right-lateral fault in central and southern California: California Division of Mines and Geology Special Report 129, p. 41-50.
- Snyder, W.S., Dickinson, W.R., and Silberling, M.L., 1976, Tectonic implications of space-time patterns of Cenozoic magmatism in the western United States: Earth and Planetary Science Letters, v. 32, p. 91-106.
- Stewart, J.H., 1988, Tectonics of the Walker Lane Belt, western Great Basin: Mesozoic and Cenozoic deformation in a zone of shear, *in* Ernst, W.G., ed., Metamorphism and Crustal Evolution of the Western United States, Rubey Volume VII: Englewood Cliffs, N.J., Prentice-Hall, p. 683-713.
- Stow, D.A.V., Howell, D.G., and Nelson, C.H., 1985, Sedimentary, tectonic, and sea-level controls, *in* Bouma, A.H., Normark, W.R., and Barnes, N.E., eds., Submarine Fans and Related Turbidite Systems: Springer-Verlag, p. 15-22.
- Suppe, J., 1970, Offset of late Mesozoic basement terrains by the San Andreas fault system: Geological Society of America Bulletin, v. 81, p. 3253-3158.
- Taliaferro, N.L., 1944, Cretaceous and Paleocene of Santa Lucia Range, California: Bulletin of the American Association of Petroleum Geologists, v. 28, p. 449-521.
- Todd, V.R., Erskine, B.G., and Morton, D.M., 1988, Metamorphic and tectonic evolution of the northern Peninsular Ranges batholith, southern California, *in* Ernst, W.G., ed., Metamorphism and Crustal Evolution of the Western United States, Rubey Volume VII: Englewood Cliffs, N.J., Prentice-Hall, p. 894-937.
- Trask, P.D., 1926, Geology of the Point Sur Quadrangle, California: University of California, Department of Geological Sciences Bulletin, v. 6, p. 119-186.



- Vail, P.R., Mitchum, R.M., Jr., and Thompson, S., III, 1977, Seismic stratigraphy and global changes of sea level, part 4: global cycles of relative changes of sea level, *in* Payton, C.E., ed., Seismic Stratigraphy-Applications to Hydrocarbon Exploration: American Association of Petroleum Geologists, Memoir 26, p. 83-98.
- Vedder, J.G., 1977, Preliminary list of Late Cretaceous mollusks from the Pozo district, San Luis Obispo County, California, *in* Howell, D.G., Vedder, J.G., and McDougall, K., eds., Cretaceous Geology of the California Coast Ranges, West of the San Andreas Fault: SEPM Pacific Section, Pacific Coast Paleogeography Field Guide 2, p. 107-109.
- Vedder, J.G., and Brown, R.D., 1968, Structural and stratigraphic relations along the Nacimiento fault in the southern Santa Lucia Range and San Rafael Mountains, California, *in* Dickinson, W.R., and Grantz, A., eds., Proceedings of Conference on Geologic Problems of San Andreas Fault System: Stanford University Publications in the Geological Sciences, v. 11, p. 242-259.
- Vedder, J.G., Gower, H.D., Clifton, H.E., and Durham, D.L., 1967, Reconnaissance geologic map of the central San Rafael Mountains and vicinity, Santa Barbara County, California: U.S. Geological Survey Miscellaneous Investigations Series, Map I-487.
- Vedder, J.G., Howell, D.G., and McLean, H., 1980, Upper Cretaceous redbeds: evidence for early suturing of the Nacimiento and Salinian Blocks, California: Geological Society of America, Abstracts with Programs, v. 12, p. 157-158.
- 1982, Stratigraphy, sedimentation, and tectonic accretion of exotic terranes, southern Coast Ranges, California, *in* Watkins, J.S., and Drake, C.L., eds., Studies in Continental Geology: Tulsa, OK, American Association of

- Petroleum Geologists Memoir No. 34, p. 471-496.
- 1986, Geological map of parts of Lopez Mountain, Santa Margarita Lake, and Pozo Summit Quadrangles, California: U.S. Geological Survey Open File Report 86-635, scale 1:24,000.
- Wentworth, C.M., 1966, The Upper Cretaceous and Lower Tertiary Rocks of the Gualala Area, Northern Coast Ranges, California : Ph.D. thesis, Stanford University, 197 p.
- 1968, Upper Cretaceous and lower Tertiary strata near Gualala, California, and inferred large right slip on the San Andreas Fault, *in* Dickinson, W.R., and Grantz, A., eds., Proceedings of Conference on Geological Problems of San Andreas Fault System: Stanford University Publications in the Geological Sciences, v. 11, p. 130-143.
- Wescott, W.A., and Ethridge, F.G., 1980, Fan-delta sedimentology and tectonic setting--Yallah's Fan Delta, southeast Jamaica: American Association of Petroleum Geologists Bulletin, v. 64, p. 374-399.
- 1982, Bathymetry and sediment dispersal dynamics along the Yallahs fan-delta front, Jamaica: Marine Geology, v. 46, p. 245-260.
- Wiebe, R.A., 1970a, Pre-Cenozoic tectonic history of the Salinian block, western California: Geological Society of America Bulletin, v. 81, p. 1837-1842.
- 1970b, Relations of granitic and gabbroic rocks, northern Santa Lucia Range, California: Geological Society of America Bulletin, v. 81, p. 105-116.
- Woods, M.T., and Davies, G.F., 1982, Late Cretaceous genesis of the Kula plate: Earth and Planetary Science Letters, p. 161-166.
- Zijderveld, J.D.A., 1967, A.C. demagnetization of rocks: analysis of results, *in* Collinson, D.W., Creer, K.M., and Runcorn, S.K., eds., Methods in Paleomagnetism: Amsterdam, Elsevier, p. 254-286.